UNIVERSITY OF CALGARY

Cavity-Induced Synthetic Gauge Potentials

by

Farokh Mivehvar

A THESIS

SUBMITTED TO THE FACULTY OF GRADUATE STUDIES

IN PARTIAL FULFILLMENT OF THE REQUIREMENTS FOR THE

DEGREE OF DOCTOR OF PHILOSOPHY

DEPARTMENT OF PHYSICS AND ASTRONOMY

CALGARY, ALBERTA

January, 2016

UNIVERSITY OF CALGARY

FACULTY OF GRADUATE STUDIES

The undersigned certify that they have read, and recommend to the Faculty of Graduate Studies for acceptance, a thesis entitled "Cavity-Induced Synthetic Gauge Potentials" submitted by Farokh Mivehvar in partial fulfillment of the requirements for the degree of DOCTOR OF PHILOSOPHY.

Supervisor
Dr. David L. Feder
Department of Physics and Astronomy
University of Calgary

Dr. Duncan O'Dell
Department of Physics and Astronomy
McMaster University

Dr. Christoph Simon
Department of Physics and Astronomy
University of Calgary

Dr. Paul Barclay
Department of Physics and Astronomy
University of Calgary

Dr. Dennis Salahub
Department of Chemistry
University of Calgary

Date

Abstract

Abelian and non-Abelian gauge potentials and quantum gauge theories play central roles in our understanding of Nature. Abelian and non-Abelian gauge potentials are also of great significance in condensed matter physics. In fact, minimal coupling of electrons to an Abelian or non-Abelian gauge potential is the essential ingredient for the realization of topological states of matter. Due to the high controllability of ultracold atoms, they are commonly exploited to test fundamental theories of physics, simulate intractable systems, and to realize novel exotic many-body states. Nonetheless, the charge neutrality of atoms places severe constraints on ultracold atomic systems, since neutral particles do not couple to gauge potentials the way charged particles do (via minimal coupling of their center-of-mass momenta to gauge potentials). Topological states of matter, therefore, cannot be directly realized in quantum gases. Likewise, gauge theories cannot be directly tested in ultracold atomic systems. That said, coupling a multi-component quantum gas to laser light can lead to the emergence of artificial Abelian and non-Abelian gauge potentials minimally coupled to the center-of-mass momenta of ultracold neutral atoms, paving the way for realizing topological states of matter and testing gauge theories in quantum gases.

In all previous approaches for inducing gauge potentials in quantum gases, the radiation field is treated classically and the back-action of the atoms on it is ignored, resulting in static gauge potentials. Nevertheless, when the radiation field is confined within a high-finesse cavity the atom-photon interaction is significantly amplified and the back-action of the atoms on the radiation field is no longer negligible, leading to complex coupled dynamics of the matter and radiation fields in which both entities are affected by one another and must be treated on the same footing.

I have developed a two-photon Raman scheme in the strong atom-photon coupling regime, based on two counter-propagating modes of a ring cavity, to induce both synthetic magnetic

field and spin-orbit coupling for a single neutral atom inside the cavity. The spin-orbit interaction is only weakly dependent on the occupation of the cavity modes, whereas the strength of the magnetic field is proportional to the square of the total number of photons in the cavity and can be made arbitrarily large, which is desirable for realizing the quantum Hall phase. I have then extended this single-atom cavity quantum-electrodynamics scheme to many bosons in the weak atom-photon coupling regime. In addition to inducing spin-orbit coupling for the individual atoms, the cavity fields also mediate infinite-ranged interactions between atoms, whose strengths and signs can readily be tuned experimentally. The interplay between these cavity-mediated interactions and the intrinsic two-body interactions determines the many-body ground state and its elementary excitations, with novel consequences such as the stabilization of an attractive Bose-Einstein condensate which otherwise is unstable.

Acknowledgements

I would like to take this opportunity and express my gratitude to individuals and a funding agency who supported me during the course of my Ph.D. It would not be possible to compose this thesis without their intellectual, emotional, and financial supports.

I would like to thank foremost my supervisor, Dr. David Feder, and my supervisory committee members, Dr. Christoph Simon and Dr. Paul Barclay. I am sincerely grateful to you all for your invaluable guidances, priceless advices, and constructive criticisms during my Ph.D. research. My special thanks goes to my supervisor; it was a pleasure and fun to conduct research under your supervision. Besides science and research, you have also given me numerous invaluable advices and supports; thank you basically for every thing.

My family deserves special credits. This includes in particular my parents, my sister, my brothers, and my niece. Words cannot express how thankful I am to you all. Thank you for encouraging me in all of my pursuits and for your continuous supports. Knowing that you have always believed in me was a prime motivation for me to work hard during this long and challenging journey. My deepest gratitude is for my mother who has been my main mentor and inspiration during my entire life.

I would also like to thank all of my colleagues and friends for countless stimulating and exciting discussions that we have had together during the past few years. Thank you for sharing your knowledge and wisdom with me; I have learned a great deal from you all. It was a pleasure to know and/or work with you all. I will remember forever all the fun we had together during the past few years. It would take many pages to name you all. I was also worried that I might fail to name someone, if I would begin to mention names. Therefore, I decided not to mention any name.

At the end, I would like to acknowledge the Alberta Innovates-Technology Futures (AITF) for awarding me a prestigious AITF Doctoral Scholarship. This scholarship significantly

helped me excel and reach my academic goals during the course of my Ph.D.

Table of Contents

List of Figures and Illustrations

List of Symbols, Abbreviations and Nomenclature

Symbol	Definition
U of C	University of Calgary
BEC	Bose-Einstein condensation
GP	Gross-Pitaevskii
QED	quantum electrodynamics
JC	Jaynes-Cummings
SO	spin-orbit
SP	stripe phase
PWP	plane-wave phase
$\mathcal{H}$	Hamiltonian density
H	Hamiltonian
$\hat{\psi}$	field operator
ψ	wavefunction
$\check{\sigma}$	matrix operator acting on internal-state space
$\check{\boldsymbol{\sigma}}$	vector of matrix operators

Chapter 1

Introduction

1.1 Ultracold Atoms and Bose-Einstein Condensation

The experimental realization in 1995 of Bose-Einstein condensation (BEC) in ultracold bosonic atoms marked the beginning of an era of precise and controllable testing of fundamental theories of physics and led to the realization of novel, exotic many-body states with no analog elsewhere. Parallel to this development in bosonic atoms, fermionic atoms have also been cooled down to temperatures on the order of the Fermi temperature. These developments in ultracold atomic gases have made Feynman's revolutionary notion — of simulating an intractable system with another system — a reality, with ultracold atomic gases being the tractable environment [1]. They can readily be manipulated to emulate other physical systems on demand, ranging from strongly interacting condensed matter systems to relativistic particles and gauge theories.

The history of BEC dates back to the 1920s. It started with the groundbreaking work of Satyendra Nath Bose who re-derived the quantum statistical distribution of photons in the black-body radiation, independent of classical electrodynamics and by solely assuming that the elementary cell of radiation phase space has the volume h^3 (with h being the Planck constant). He then obtained the number of possible distributions of photons over elementary cells [2] (the English translation of the paper can be found for instance in Ref. [3]). Having difficulty publishing his results, Bose sent his manuscript to Albert Einstein. After reading it, Einstein immediately recognized its significance. Then he translated it into German and had it published in Bose's name in 1924 with the following comment to the editor: "In my opinion, Bose's derivation of the Planck formula signifies an important advance. The method used here also yields the quantum theory of an ideal gas, as I shall show in details

elsewhere" [3]. By extending Bose's notion into massive particles, Einstein in1924 to 1925 obtained the quantum statistical distribution of a non-interacting gas, now known as "Bose-Einstein statistics" [4, 5] (the English translation of the papers can be found in Ref. [6]).

Bose-Einstein statistics describe the thermal distribution of bosons in discretized energy levels. Einstein immediately realized that according to this distribution a large fraction of particles (i.e., bosons) will occupy the lowest energy state at very low temperature: "A separation is effected; one part condenses, the rest remains a saturated ideal gas," in his own words. This phenomenon is now referred to as "Bose-Einstein condensation." The BEC phase transition happens when the de Broglie wavelength $\lambda_{\rm dB} = \sqrt{2\pi\hbar^2/mk_{\rm B}T}$ (with $\hbar = h/2\pi$, m the mass of the particle, $k_{\rm B}$ the Boltzmann constant, and T the temperature) of the particles becomes comparable with the average inter-particle distance $n^{-1/3}$ (with n being the average particle density); or more precisely when $n\lambda_{\rm dB}^3 \simeq 2.61$ for a homogeneous Bose gas in three dimensions [7]. At this critical transition temperature T_c, the wave packets of individual particles overlap with one another and form a macroscopic condensate wavefunction.

For over a decade the prediction of BEC was overlooked, even by Einstein himself. This was changed in the late 1930s by the work of Fritz London, who attributed the superfluidity of the liquid helium-4 (^{4}He) to BEC [8]. Although Bose-Einstein statistics along with the prediction of BEC at low temperatures had been originally developed for non-interacting bosons, London's theory suggested that BEC could also occur in the strongly interacting bosons, such as liquid ^{4}He. Following London's work, the theory of interacting bosons was developed during the 1940s to 1960s, commencing with the pioneering work of Bogoliubov on formulating quantum field theory of weakly interacting bosons in 1947 [9]. The basic notion due to Bogoliubov was to separate the bosonic field operator $\hat{\psi}$ into two parts: a macroscopically occupied condensate wavefunction $\psi = \langle\hat{\psi}\rangle$ and a quantum fluctuation $\delta\hat{\psi}$. The condensate wavefunction ψ can be envisaged as the BEC order parameter: it vanishes above the critical temperature T_c while it is non-zero below the critical temperature. In the

early 1960s Gross and Pitaevskii independently derived a Schrödinger-like nonlinear equation, now referred to as the Gross-Pitaevskii (GP) equation, for the condensate wavefunction ψ [10, 11, 12]. The GP approach is basically a mean-field approximation, which omits the quantum fluctuations $\delta\hat{\psi}$.

Following these developments, the interest in BEC subsided in the 1970s. Nonetheless with the advance of cooling techniques in the 1980s, such as laser cooling of atoms [13, 14, 15], the hope for the observation of BEC in ultracold bosonic atoms was revived in the mid 1980s and the early 1990s with pioneering works of Thomas Greytak and Dan Kleppner [16]. Laser cooling relies on spontaneous emission of a photon in a random direction by the excited atom and needs a closed optical cycle. Finally in 1995 in two groundbreaking experiments at the University of Colorado and Massachusetts Institute of Technology, BEC was realized for the first time over 70 years after its prediction [17, 18]. Eric Cornell, Carl Wieman, and Wolfgang Ketterle were jointly awarded the Nobel Prize in Physics in 2001 for their efforts.

Following the discovery of BEC, there was an explosion of interest in studying BEC, both theoretically and experimentally [19, 20]. Quickly after the first realization of BEC in rubidium (^{87}Rb) and sodium (^{23}Na) atoms, BEC was also observed in lithium (^{7}Li) and other alkali atoms [21]. The experimental hallmark of BEC was the appearance of a sharp peak in the velocity distribution of the atoms below the critical temperature T_c; see Fig. 1.1 [22]. The typical number of atoms in experiments today ranges from a few thousand to several million, with the BEC diameter on the order of tens or hundreds of μm depending on confining trap potentials. These yield densities in the range of $\sim 10^{20}$ to 10^{21} m^{-3} (cf. the density of air $\sim 10^{25}$ m^{-3}). The critical BEC transition temperature T_c ranges between ~ 100 nK and 1 μK for typical experiments [23].

At such low densities as $n \sim 10^{20} - 10^{21}$ m^{-3}, three-body collisions are highly suppressed and are rare, allowing the system to stay in a gaseous state [19]. Furthermore, at such low energies as $T \sim 100 - 1000$ nK, the two-body interactions can be described by a single

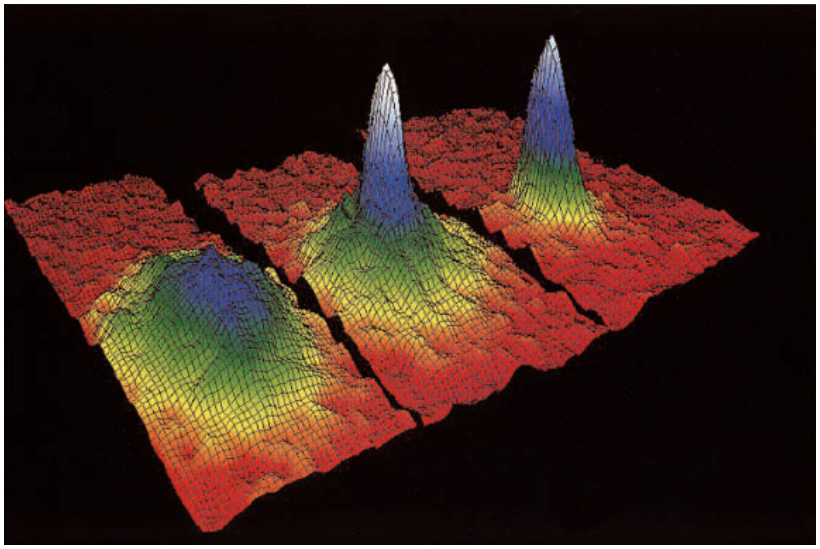

Figure 1.1: Velocity distribution of the Rb atoms just above the critical temperature T_c (left), just below T_c (center), and well below T_c after further cooling (right). Reproduced from Ref. [22] under the courtesy of the Creative Common (Public Domain) license.

parameter a_s, the s-wave scattering length, independent of details of the two-body potential [19]. In other words, it is a good approximation to replace two-body interactions with $V(\mathbf{r}-\mathbf{r}') = (4\pi\hbar a_s/m)\delta(\mathbf{r}-\mathbf{r}')$, where $\delta(\mathbf{r}-\mathbf{r}')$ is the Dirac delta function and a_s solely determines the strength (and sign) of the two-body interactions. In typical experiments in BEC, the ratio of the s-wave scattering length a_s to the average particle spacing $a \sim n^{-1/3}$ is much smaller than one, that is, $n^{1/3}a_s \ll 1$, implying that even two-body interactions are weak in these systems. This makes atomic Bose condensates attractive systems to study theoretically, since the well-known mean-field theory of Gross and Pitaevskii as well as the Bogoliubov theory are well-suited for this weakly interacting regime. In fact, the depletion of the condensate (i.e., the non-condensate fraction) due to two-body interactions is proportional to $\sqrt{na_s^3}$ from the Bogoliubov theory. That is, separating the bosonic field operator into a macroscopically occupied condensate wavefunction and a small quantum fluctuation part is valid in the regime where $\sqrt{na_s^3} \ll 1$ [24].

Although two-body interactions are very weak in dilute Bose condensates, they play a significant role in these systems due to very low temperatures. Not only do they affect the

static properties of condensates, such as the density distribution, they also have fundamental consequences for the dynamics of condensates. The condensate is enlarged due to the interactions and becomes macroscopic, allowing one to study it directly via optical techniques. Therefore, observed densities of interacting Bose condensates at the center of traps are generally one to two orders of magnitude smaller than those predicted for ideal Bose condensates in identical traps. However, the most far-reaching consequences of the interactions are in the dynamics of condensates, with the most prominent example being the appearance of phonon-like (i.e., linear sound-like) dispersion at long wavelengths in elementary excitations of interacting uniform condensates.

Low-energy elementary (or sometimes called collective) excitations — also known as quasi-particles — play an essential role in many-body systems [25], specifically in Bose fluids as will be described below. In the context of BEC, they can be envisaged as small-amplitude fluctuations of the condensate wavefunction ψ (i.e., the BEC order parameter) around its equilibrium, which then propagate in the system [26]. Such elementary excitations have a clear interpretation in a non-interacting homogenous Bose condensate: an elementary excitation is the addition of a boson into a non-zero momentum $\mathbf{p} \neq 0$ (i.e., an excited) state. (Recall that bosons are condensed into the lowest energy state which is the zero momentum $\mathbf{p} = 0$ state in the absence of any spin-orbit coupling.) Then the excitation has the energy dispersion $\epsilon(\mathbf{p}) = \mathbf{p}^2/2m$, which is quadratic (i.e., free-particle like) and implies that the excitation propagates in the system as a free particle with no collective effect. The two-body interactions completely change this simple picture of elementary excitations. Roughly speaking, elementary excitations in the interacting case can be conceived to be composed of a particle and hole. Bogoliubov illustrated that the energy dispersion of such excitations at long wavelengths has the linear form $\epsilon(\mathbf{p}) = c_s p$, with c_s being the speed of sound in the Bose fluid. In other words, the elementary excitations at long wavelengths in an interacting homogenous Bose condensate are phonon-like with a collective nature, analogous to phonon

excitations of a solid crystal.

As mentioned above, superfluidity was first tied to the existence of BEC in a system by London in 1938. It was then generalized by Laszlo Tisza later in the same year to a two-component fluid, comprised of a normal and a superfluid component with corresponding densities ρ_n and ρ_s, respectively, which intimately depend on temperature [27, 28]. Tisza identified the superfluid component with Bose-condensed atoms and the normal component with non-condensed atoms. The superfluid component can then flow without dissipation, while there is a finite viscosity associated with the normal component. These hypotheses could qualitatively explain most observed effects in superfluid ^{4}He at that time, such as the phase transition temperature $T_\lambda = 2.18$ K (which is not very far from the predicted BEC transition temperature $T_c = 3.13$ K of ^{4}He atoms), super-leak and torsional oscillation experiments, where the superfluid component passes through a capillary without viscosity and the normal component is dragged by disk-shaped oscillators, respectively [29]. The postulated connection between superfluity and BEC can be understood by expressing the condensate wavefunction as $\psi = \sqrt{n}e^{i\theta}$, which leads to the condensate velocity field $\mathbf{v} = \hbar(\psi^*\boldsymbol{\nabla}\psi - \psi\boldsymbol{\nabla}\psi^*)/2mi|\psi|^2 = (\hbar/m)\boldsymbol{\nabla}\theta$. The fact that the condensate velocity is given by the gradient of the condensate phase θ has many far-reaching consequences for the motion of the condensate. First, it follows that the condensate is irrotational $\boldsymbol{\nabla}\times\mathbf{v} = 0$, provided that θ is not singular. Second, it implies that the circulation around a closed contour is quantized $\oint \mathbf{v}\cdot d\mathbf{r} = (h/m)l$ (with l being an integer), meaning that vortices in the condensate are quantized provided there are any. These two properties are also well-known indications of superfluidity.

It should be nevertheless underlined that there is a subtle difference between superfluidity and BEC. That is, not all BECs are superfluid and a system may exhibit superfluid behaviour in the absence of BEC. An example of the former is the ideal Bose condensate and an example of the latter is a lower-dimensional system. Furthermore, at very low temperatures close to

absolute zero, where liquid ^{4}He is almost completely superfluid (i.e., $\rho = \rho_n + \rho_s \simeq \rho_s$), the condensate density $\rho_c = |\psi|^2$ is depleted due to strong inter-atomic interactions and it is only about 10% of the total density ρ [7]. Therefore, the superfluid density ρ_s is generally different than the condensate density ρ_c, implying that Tisza's description was not completely correct.

Lev Landau re-introduced the two-fluid model based on his phenomenological phonon-roton description of the superfluidity in 1941 [30] and modified it later in 1947 [31]. Landau postulated that at zero temperature, the fluid is completely superfluid, that is, $\rho = \rho_s$. As the temperature increases, photon and roton quasi-particles are excited from the background superfluid, forming the normal component ρ_n, where now $\rho = \rho_s + \rho_n$. Phonons are low-energy linear excitations, while rotons are higher-energy elementary excitations with an energy gap Δ; see Fig. 1.2. The contribution of rotons becomes more appreciable as the temperature rises (above ~ 0.8 K). Landau's theory has successfully explained many properties of the superfluid ^{4}He, including the temperature dependence of second sound (i.e., entropy waves driven by a temperature gradient, in contrast to density waves driven by a pressure gradient and characterized by first ordinary sound). This indicates that elementary excitations (especially phonons) play a fundamental role in superfluidity, the ingredient missing in London's and Tisza's descriptions.

The aforementioned counter-intuitive example that an ideal Bose condensate is not superfluid follows also directly from the Landau criterion for superfluidity. Consider an object moving through a quantum fluid (such as a Bose gas), which then experiences friction through the creation of elementary excitations in the fluid. Conservation of energy and momentum throughout this process leads to the Landau critical velocity $v_c = \min(\epsilon(\mathbf{p})/\mathbf{p})$, the minimum velocity at which the object can create low-energy excitations in the quantum fluid [32]. Recalling that the elementary-excitation spectrum of an ideal Bose condensate is just free-particle-like $\epsilon(\mathbf{p}) = \mathbf{p}^2/2m$, the Landau critical velocity for the ideal Bose condensate is then just zero, $v_c = 0$. It means that the object experiences friction and drag as soon as it starts

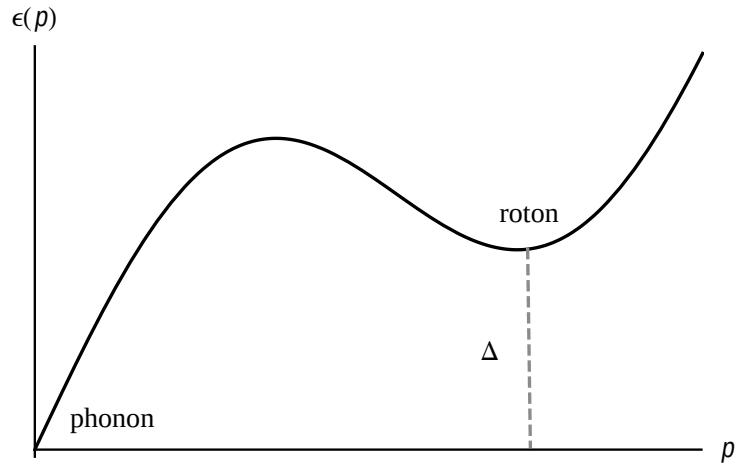

Figure 1.2: Elementary-excitation spectrum of superfluid ^{4}He, as proposed by Landau. The low-lying excitations are linear and phonon-like. There is an energy gap Δ for higher-energy excitations, known as rotons.

moving (i.e., $v \neq 0$), even with an exceedingly small velocity $v \to 0$. This is in complete contrast to an interacting Bose condensate, where the Landau critical velocity is equal to the velocity of sound: $v_c = \min(c_s\mathbf{p}/\mathbf{p}) = c_s$.

Alkali atoms in their ground state have a single electron in an s orbital, implying that their total electronic angular momentum $\mathbf{J} = \mathbf{L} + \mathbf{S}$ (with $\mathbf{L}$ and $\mathbf{S}$ being the angular momentum and spin of the electron) is $J = S = 1/2$. Although their nuclear spin $\mathbf{I}$ depends on the atomic and isotopic species, the total angular momentum $\mathbf{F} = \mathbf{J} + \mathbf{I}$ of the atom can only take two values $F = I \pm 1/2$ for a nonzero nuclear spin I and a single value $F = J = S = 1/2$ for $I = 0$. In the context of BEC, F is identified as the atomic spin and is used, along with its projection $m_F = -F, \cdots, F$, to label atomic state manifolds $\{|F, m_F\rangle\}$. In the original achievement of BEC, atoms were trapped only in one specific spin state $|F, m_F\rangle$, indicating that the spin projection was frozen. Then the field operator $\hat{\psi}$ and the corresponding wavefunction (or the order parameter) ψ of the condensate are single-component "scalar" fields, independent of the spin state.

With the subsequent development of purely optical traps, it then became feasible to simultaneously trap atoms in more than one spin state and study the spin dynamics [33, 34].

Atoms can undergo spin exchange collisions, in which two atoms are scatted into spin states different from their initial ones (with the constraint of the conservation of the angular momentum), and consequently the population of atoms in each spin state is not conserved. Atoms can then condense in multiple spin states with variable densities due to spin exchange collisions, forming "spinor" Bose condensates [35, 36]. Spinor condensates are generically unstable in magnetic traps due to spin flipping processes. This is because only atoms in one specific spin state can be confined in a given magnetic trap and spin flipping processes lead to a severe loss of atoms from the trap. That said, there are exceptions such as ^{87}Rb where the spin exchange interactions are suppressed and the density of each spin component is therefore conserved, referred to as "multi-component" (or "mixture") BEC. In early experiments, ^{87}Rb atoms were simultaneously trapped in spin states $|F = 2, m_F = 2\rangle$ and $|F = 1, m_F = -1\rangle$ in a magnetic trap [37]. It should be emphasized that mixture Bose condensates can also be achieved by trapping and cooling different isotopes of the same species, or different atomic species. In such mixtures collisions cannot change one isotope (or atom) into another, guaranteeing the fixed density of each component.

Loading and confining ultracold atoms in periodic optical lattices was a crucial step in ultracold atomic experiments, opening the possibility for directly simulating solid-state and condensed-matter physics in a controllable manner in atomic systems [38, 39, 40, 41]. Optical lattices with various geometries can be readily generated in a laboratory by interfering laser beams. The simplest configuration is two counter-propagating identical laser beams which results in a one-dimensional standing wave pattern, simulating a somewhat artificial one-dimensional crystal. More complicated laser configurations can be utilized to mimic desired realistic crystals. Lasers are tuned such that they are off-resonant from any atomic transition. The atoms then only experience a position-dependent shift on their ground state energy due to virtual transitions (known as the ac Stark shift) and are attracted to minima or maxima of the potential, depending on the sign of the detuning between laser and atomic frequencies.

Interacting ultracold atoms in optical lattices are reminiscent of interacting electrons in a crystalline solid, which is described by the celebrated Hubbard model [42]. The model describing interacting ultracold bosons in optical lattices is somewhat different than the original Hubbard model for electrons (i.e., fermions) due to bosonic statistics, and is referred to as the Bose-Hubbard model. Unlike fermions in the Hubbard model, in the Bose-Hubbard model more than one boson in the same internal state can occupy the same orbital of a lattice site thanks to Bose-Einstein statistics. Therefore, it is feasible to have a single-component Bose-Hubbard model, in complete contrast to the (Fermi-)Hubbard model. It is well-known that a variety of quantum phases and quantum phase transitions can be realized in the Hubbard and Bose-Hubbard models and its extended versions, the most notable being the quantum phase transition between the superfluid and the Mott insulator. In the very weak interacting regime the ground state of both Hubbard and Bose-Hubbard model is superfluid, while it undergoes the Mott-insulator phase transition in the strongly interacting limit at integer fillings. The superfluid–Mott-insulator phase transition was realized in ultracold bosonic atoms in 2002, pushing the frontier of ultracold atoms further into the strongly interacting regime [43]. In the strongly interacting regime, the two-component Bose-Hubbard model (and of course the Hubbard model) can be mapped into a spin-1/2 model. The two-component Bose-Hubbard model can be realized with a two-component ultracold bosonic gas in an optical lattice, allowing one to engineer various spin-1/2 models and investigate their magnetic orders in ultracold atoms [44, 45]. In addition to these significant examples, many other fundamental questions can also be addressed by studying ultracold atoms in appropriate optical lattice geometries and parameter regimes. They include lower-dimensional systems, higher spin models, interplay between disorder (i.e., Anderson localization) and interactions, etc. [39].

1.2 Synthetic Gauge Fields

Although ultracold atoms can be readily manipulated to simulate other systems, a wide class of condensed matter states such as quantum Hall states and topological insulator states cannot be directly realized in ultracold atoms, since they are charge neutral and do not couple to gauge fields (such as the electromagnetic fields) the way charged particles (such as electrons) do. A recent focus of interest in the ultracold-atom community is to induce Abelian and non-Abelian gauge potentials in these charge-neutral systems. This interest stems from developments in topological states of matter in condensed matter physics [46, 47, 48]. The first known topological state of matter is the quantum Hall state, discovered by Klaus von Klitzing in 1980, who was awarded the Nobel Prize in Physics in 1985 for this discovery [49]. The quantum Hall effect is the quantum analogue of the classical Hall effect, where a two-dimensional (non-interacting) electronic system is subject to a strong magnetic field at low temperatures. Coupling of the electron to the magnetic field is accounted for by replacing the momentum $\mathbf{p}$ with the canonical momentum $\mathbf{p}-q\mathbf{A}$ in the single particle Hamiltonian, where $q=-e$ is the charge of the electron and $\mathbf{A}(\mathbf{r})$ is the Abelian vector potential associated with the magnetic field $\mathbf{B}=\boldsymbol{\nabla}\times\mathbf{A}$. In contrast to the classical Hall effect, the Hall conductance is quantized in the quantum Hall effect, $\sigma_{\mathrm{H}}=(e^2/h)\nu$, where ν is an integer [50]. The quantum Hall state exhibits another remarkable feature: although the bulk of the system is an insulator, there exist conducting edge states which their number is equal to ν. In other words, each edge state carries precisely a quantum of the conductance e^2/h. The edge states are conducting states, exponentially localized on the edges of the system. They are topologically protected and hence are robust against perturbations.

Recently a new class of topological states possessing intrinsic "spin-orbit" (SO) couplings was proposed, which do not need a strong external magnetic field and/or low temperatures [51, 52, 53]; and they were subsequently observed [54]. This new state of matter has been coined the (Z_2) topological insulator, or the quantum spin Hall insulator in two dimen-

sions. In solid state physics, the SO interaction is referred to as the coupling of an electron's center-of-mass momentum to its spin degrees of freedom. Examples of linear SO coupling in two-dimensional electronic systems include Rashba $\propto \check{\sigma}_x p_y - \check{\sigma}_y p_x$ [55] and Dresselhaus $\propto -\check{\sigma}_x p_y - \check{\sigma}_y p_x$ [56] SO couplings, where $\check{\boldsymbol{\sigma}} = (\check{\sigma}_x, \check{\sigma}_y, \check{\sigma}_z)$ are the Pauli matrices[1]. In general, a linear SO coupling can be recast as a non-Abelian vector gauge potential $\check{\boldsymbol{\mathscr{A}}}(\mathbf{r}, \check{\boldsymbol{\sigma}})$ whose components do not commute with each other $[\check{\mathscr{A}}_i, \check{\mathscr{A}}_j] \neq 0$. In topological insulators the SO coupling plays the role of the external magnetic field in the quantum Hall effect; and specifically the quantum spin Hall insulator in its simplest form can be imagined as two copies of the quantum Hall states with two opposite spin projections threaded with opposite magnetic fields, hence the name quantum spin Hall effect. Analogous to the quantum Hall state, there exist topologically protected conducting edge (surface) states in the edge (surface) of two- (three-) dimensional topological insulators. Note that in the quantum Hall state the spin is frozen and edge states are spin polarized due to the large magnetic field, whereas in the quantum spin Hall state edge states come in 2ν pairs, with ν edge states for each spin projection. The emergence of conducting edge states in bulk-insulator materials is a characteristic of all topological states. It has been predicted that elementary excitations of fractional quantum Hall liquids and topological superfluids are anyons with fractional statistics, obeying neither Fermi-Dirac nor Bose-Einstein statistics. It has been proposed to implement fault-tolerant topological quantum computations in these (non-Abelian) anyons [58].

Motivated by these developments in condensed matter physics, over the past decade numerous theoretical schemes have been put forward to induce Abelian and non-Abelian synthetic gauge potentials in ultracold neutral atomic gases mostly via atom-light interactions [59, 57, 60]. Most of these schemes rely on the Berry phase (also known as the geometric phase) to simulate the gauge potentials. Consider a Hamiltonian $\mathcal{H}(X)$, which depends on a parameter X (not necessarily position), with local eigenvectors $\{|m(X)\rangle\}$ and

[1] Throughout this thesis, I will use the "check" notation to distinguish matrix operators $\check{O}$ acting on the internal-state space (when there is an ambiguity), following Ref. [57].

corresponding eigen-energies $\{\varepsilon_m(X)\}$. Sir Michael Berry noticed that a local eigenvector $|n(X)\rangle$ of the Hamiltonian $\mathcal{H}(X)$ moving adiabatically in the parameter space X (such that there is no transition into other states $\{|n'(X)\rangle\}$, as required by the adiabaticity) may acquire a non trivial geometric phase $e^{i\gamma_n}$ when its path encloses a closed circuit[2] [61]. This phase is different than the usual dynamical phase $e^{-i\varepsilon_n(X)t/\hbar}$ and does not depend on elapsed time, but only on the geometry of the circuit [62]. Analogous to the Aharonov-Bohm phase which is related to a vector potential $\mathbf{A}(\mathbf{r})$, the Berry phase can be associated with an emergent geometric vector gauge potential $\boldsymbol{\mathcal{A}}_n(X) = i\,\langle n(X)|\,\boldsymbol{\nabla}_X\,|n(X)\rangle$, also known as the Berry connection [63]. The dynamics of internal states of an atom dressed by the laser light depend parametrically on the center-of-mass position $\mathbf{R}$ of the atom (via atom-light interaction terms). By properly engineering an $\mathbf{R}$-dependent atom-field interaction Hamiltonian (i.e., properly choosing the number of internal states and lasers, their mutual couplings, and laser configurations), the atom can then acquire a non-trivial geometric phase and hence an Abelian or a non-Abelian synthetic gauge potential minimally coupled to the center-of-mass momentum of the atom [64]. Not only does this open up the possibility of inducing solid-state-like gauge potentials in quantum gases, it also provides the opportunity of engineering exotic gauge potentials for bosons and fermions beyond those encountered in conventional solid-state materials.

In a series of pioneering experiments at the National Institute for Standards and Technology, Ian Spielman's group engineered a synthetic magnetic field [65], electric field [66], and SO coupling [67] for neutral atoms using a two-photon Raman scheme. By making the two-photon Raman scheme position dependent in the transverse direction, the same group subsequently realized the spin Hall effect in a Bose condensate of ^{87}Rb atoms [68]. In the two-photon Raman scheme employed to induce the SO-coupling, two internal ground states of an atom are coupled to an excited state in the Λ scheme via two counter-propagating laser beams. Both transitions to the excited state are far off-resonant while the two-photon tran-

[2] See Appendix A for a short review of the Adiabatic Theorem and Berry phase.

sition between the two ground states is almost resonant, resulting in the virtual population of the excited state that allows the adiabatic elimination of its dynamics. After doing so, the atom is formally equivalent to a pseudospin-1/2 particle (boson or fermion depending on the atomic species), where its center-of-mass motion experiences a pseudospin-dependent synthetic gauge potential $\pm\hbar k_R$ (with $k_R = k_1 \simeq k_2$ being the wavenumber of the two Raman lasers) due to the momentum transfer from the radiation fields. This can be recast as a non-Abelian synthetic gauge potential $q^*\check{\mathcal{A}}_x = \hbar k_R \check{\sigma}_z$, with q^* being a synthetic charge, minimally coupled to the center-of-mass momentum P_x of the atom. This non-Abelian synthetic gauge potential can be envisaged to stem from an equal contribution of the Rashba and Dresselhaus SO couplings: $\mathcal{H}_{\rm R} + \mathcal{H}_{\rm D} \propto -\check{\sigma}_y P_x$, which is $\propto -\check{\sigma}_z P_x$ after a pseudospin rotation. The synthetic gauge potential $q^*\check{\mathcal{A}}_x = \hbar k_R \check{\sigma}_z$ (or equivalently the equal Rashba-Dresselhaus SO coupling $H_{\rm RD} = -2\hbar k_R \check{\sigma}_z P_x$) changes the single-particle energy dispersion $\mathbf{P}^2/2M$ of a free atom in an interesting way. The single-particle energy dispersion is modified as $[(P_x - \hbar k_R \check{\sigma}_z)^2 + P_y^2 + P_z^2]/2M$, implying that the energy dispersion has now two minima located at $\mathbf{P}_0 = (\pm\hbar k_R, 0, 0)$. This is in total contrast to the single-particle energy dispersion of a free atom, which has a single minimum at $\mathbf{P}_0 = 0$.

The properties of multi-component Bose condensates in the presence of artificial Abelian and non-Abelian gauge potentials have been the subject of intensive research in the past few years [69]. Inducing synthetic magnetic fields in ultracold atoms has opened the possibility for the realization of the Hofstadter band structure, which would require enormous magnetic fields in conventional crystals. Almost 40 years ago, Douglas Hofstadter predicted that the band structure of a non-interacting electron gas pierced with a strong magnetic field exhibits a fractal structure, known as the Hofstadter butterfly [70]. This prediction has remained elusive since magnetic fields on the order of a billion gauss is required. Therefore, the race for inducing strong synthetic magnetic fields in quantum gases began. In a few recents experiments, Immanuel Bloch's and Wolfgang Ketterle's groups have induced strong

synthetic magnetic fields for ultracold atoms in optical lattices via laser-assisted tunnelling, paving the way for the observation of the Hofstadter butterfly [71, 72, 73].

The single-particle energy dispersion of an equal Rashba-Dresselhaus SO-coupled pseudospin-1/2 atom is a momentum-space double well (as discussed above) in appropriate parameter regimes, which is two-fold degenerate in the symmetric (i.e., two-photon resonant Raman) case. In a Bose condensate the two-body interactions lift this degeneracy and the ground state is either a stripe state, where the continuous translational symmetry is spontaneously broken, or a plane-wave state, depending on the strength and sign of the two-body intra- and inter-species interactions [74, 75, 76, 77]. In the plane-wave state, all atoms condense into one of the two single-particle energy minima (i.e., all atoms condense into one plane-wave state), while the stripe state is a superposition state of the two minima (i.e., atoms condense simultaneously into two plane-wave states) and the total condensate density exhibits faint fringes [78]. When an SO-coupled quantum Bose gas is confined in an optical lattice, the ground state of the system is expected to exhibit a variety of magnetic orders in the Mott-insulator regime, such as spin spiral, vortex and antivortex crystals, and skyrmion crystal phases, in addition to the ferromagnetic and antiferromagnetic orders [79, 80, 81]. The superfluid to Mott-insulator phase transition of quantum Bose gases in the presence of a SO coupling has also been investigated [79, 82].

1.3 Cavity Quantum Electrodynamics

The quantum nature of radiation was first discovered by Max Planck in 1900. He obtained the correct energy distribution of black-body radiation over the whole frequency range by assuming that the energy of a harmonic oscillator is quantized: $\varepsilon_n = n\hbar\omega$, where n is an integer and ω is the frequency of the oscillator [83]. This discovery was the begining of (old) quantum mechanics. In 1905, Albert Einstein provided further evidence regarding the quantized nature of light. He explained the photoelectric effect by assuming that the energy

of light is discrete and light solely exchanges energy with matter in discrete packets [84]. The name "photon" was coined by Gilbert Lewis in 1926 for these discrete energy packets [85]. Planck and Einstein were both awarded the Nobel Prize in Physics in 1918 and 1921, respectively, for their discoveries. It was then Paul Dirac who second quantized light field formally in 1927 and combined wave and particle aspects of light into the same picture [86]. The second-quantized nature of the radiation field is essential in accounting for some fundamental phenomena, such as spontaneous emission due to vacuum fluctuations [87]. The quantum vacuum $|0\rangle$ is the state with lowest energy and has exotic features. Although all field expectation values $\langle 0|\,\hat{X}\,|0\rangle$ vanish in the quantum vacuum state, the field fluctuations $\langle 0|\,\hat{X}^2\,|0\rangle$ are non-zero and give rise to observable effects such as the Casimir effect.

Closed or semi-closed hollow bodies with almost perfect reflective boundaries play an important role in quantum optics — the quantum theory of radiation — as well as classical optics. They are utilized to store radiation fields and are commonly referred to as optical or microwave resonators or cavities, depending on frequency of the confined radiation field. A completely closed cavity with a small hole in it can be envisaged as a blackbody, since it absorbs almost completely an incident radian on the hole without re-emitting it. There exist a wide variety of cavities, including planar-mirror and spherical-mirror Fabry-Perot (also known as linear or standing-wave) resonators, ring-mirror resonator, rectangular cavity, fiber-ring cavity, micro-disk, photonic-crystal micro-cavities, etc. [88]. For instance, a linear (ring) cavity is formed with two (usually three) highly reflective mirrors (see Fig. 1.3), while a photonic-crystal micro-cavity is an engineered defect inside a photonic crystal. Cavities, regardless of their geometries, are generically characterized by two quantities: mode volume V and dimensionless quality factor Q. The mode volume represents the volume occupied by the electromagnetic field and the quality factor is related to the storage time of field energy, considered respectively as degrees of the spatial and temporal confinement of the field within a cavity.

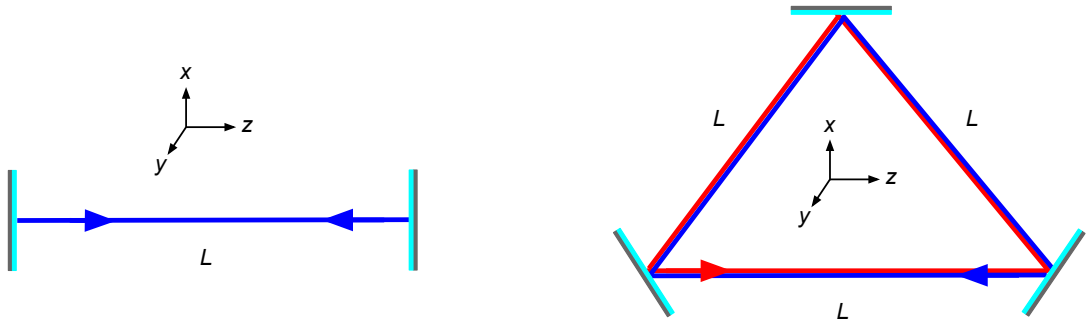

(a) (b)

Figure 1.3: Schematics of a (a) two-mirror linear and (b) three-mirror ring cavities. The mode functions of the linear (ring) cavity are standing (traveling) waves.

Consider the perfect linear cavity shown in Fig. 1.3(a). The time-independent parts of electromagnetic fields satisfy the Helmholtz equation $(\boldsymbol{\nabla}^2+\omega^2/c^2)\mathbf{u}(\mathbf{r})=0$ inside the cavity, where $\nu=\omega/2\pi$ is the frequency [89]. Due to the boundary conditions, solutions of the Helmholtz equations are transverse electromagnetic (TEM) fields $\mathbf{u}(\mathbf{r})=u(\mathbf{r})\mathbf{e}\propto\sin(kz)\mathbf{e}$ with $kL=(\omega/c)L=m\pi$, where $\mathbf{e}$ is a unit polarization vector in the xy plane, L is the linear dimension of the cavity, and m is an integer. Consequently, the wavenumber $k\equiv|\mathbf{k}|$ and frequency ν take discrete values $ck_m=\omega_m=2\pi\nu_m=(c\pi/L)m$. The set of allowed discrete wavenumbers k_m (and resonance frequencies ν_m) can also be obtained by noting that after a round trip of length $2L$ within the cavity a wave should reproduce itself, that is, $k(2L)=2\pi m$, yielding again $k_m=(\pi/L)m$ (the phase shift of 2π imparted by mirrors is ignored since it is immaterial) [88]. The function $\mathbf{u}_m(\mathbf{r})$ is referred to as a mode function.

The resonance frequencies ν_m are equally spaced in frequency. Free spectral range, the frequency spacing between two adjacent modes, is $\Delta\nu=\Delta\omega/2\pi=\nu_m-\nu_{m-1}=c/2L$. The free spectral range $\Delta\nu$ is inversely proportional to the linear dimension L of the cavity and it therefore increases as L decreases. For instance, for a Fabry-Perot cavity of linear dimension $L=3$ μm, the free spectral range is $\Delta\nu\simeq 50$ THz, implying that there exist only a few

modes within the optical-frequency range of $\sim 430 - 770$ THz. The density of modes $\rho(\nu)$ is the number of modes per unit frequency, per unit length of the cavity (including both orthogonal polarizations) and is given by $\rho(\nu) = 2(1/\Delta\nu)/L = 4/c$ [88]. The number of modes within the cavity in the frequency interval $d\nu$ is therefore $(4/c)Ld\nu$, which is directly proportional to the linear dimension L of the cavity and decreases as L reduces.

There are losses associated with cavity mirrors. These losses can be divided into two main categories [90]. First, the cavity mirrors are not perfect. That is, they are not completely reflective and there is a minor transmission of the radiation through them as well as some absorption of radiation. Second, mirrors have finite sizes and the confined radiation may be diffracted out of the cavity by edges of the mirrors. The stored electromagnetic energy I therefore leaks out of the cavity and is dissipated: $dI/dt = -\kappa I = -I/\tau_p$, where τ_p (κ) is the photon lifetime (decay rate). If α is the photon loss per trip, then $\kappa = (c/L)\alpha$ is the photon loss per unit time (or the photon decay rate), yielding $\tau_p = L/c\alpha$. The quality factor is defined as $Q \equiv -\omega I/(dI/dt) = \omega\tau_p = \omega/\kappa$ [90]. Therefore, the quality factor Q (or photon life time τ_p or photon decay rate κ) indicates how well the radiation is temporally stored inside a cavity. Nowadays in experiments, the Q factor on the order of 10^{10} is attainable [91]. The finite lifetime of the stored radiation field inside the cavity leads to broadening of resonance frequencies due to time-frequency uncertainty relation [88].

Likewise, the resonance frequencies of the three-mirror ring cavity shown in Fig. 1.3(b) can be determined by the self-reproducing constraint. That is, after a complete trip of length $3L$ within the ring cavity, the wave should reproduce itself: $k(3L) + 3\pi = 2\pi m$, where 3π is the phase introduced by reflections of light in three mirrors [88]. The resonance modes are then $ck_m = \omega_m = 2\pi\nu_m = (2m-1)c\pi/3L$. The corresponding mode functions are plane waves $u_m(\mathbf{r}) \propto e^{\pm i\mathbf{k}_m\cdot\mathbf{r}}$. Note that each mode is doubly degenerate, because for each wavenumber k_m there are two possible wavevector $\pm\mathbf{k}_m$, associated with two counter-propagating waves.

When the radiation field is confined within a cavity, its mode structure, mode density,

and resonance frequencies change drastically due to the boundary conditions and become significantly different than corresponding ones in free space. In 1946, Purcell predicted that these changes have significant effects on properties of a trapped atom inside the cavity and, in particular, modify spontaneous emission rates of atomic excited states [92]. The Purcell effect can be qualitatively understood by noting that cavity mirrors create many images of the atom, which leads to a faster dissipation of the atomic energy and therefore enhancement of the spontaneous emission rate [87]. It became possible by the end of 1960s to load atoms inside high-quality (high-Q) tiny cavities. This opened the possibility for realizing a single (two-level) atom interacting with a single mode of a second-quantized electromagnetic field (i.e., a single bosonic degree of freedom), known as the Jaynes-Cummings (JC) model [93]. These subjects and related phenomena fall into the realm of cavity quantum electrodynamics (QED) [94].

In free space, atoms couple very weakly to the radiation field and the rate of dissipative and irreversible processes (such as the decay of atomic excited states) Γ is much larger than the coherent atom-field coupling rate Ω; that is, $\Omega \ll \Gamma$. This is the classical (extremely weak-coupling) regime where fluctuations on the order of few in the number of atoms and/or photons are not significant [91]. Nevertheless, this situation can be drastically altered when the radiation field is confined within an extremely small high-Q cavity. In this system, the coherent atom-photon coupling rate $\mathscr{G}$ can well exceed the decay rates of the cavity field $\kappa \propto 1/Q$ [95] and atomic excitation γ. In some modern experiments in cavity environments, the atom-photon coupling on the order of $\mathscr{G}/2\pi \sim 10 - 100$ MHz can be reached, while the decoherence rates are in the order of $\kappa/2\pi \sim 1 - 10$ and $\gamma/2\pi \sim 1$ MHz [91, 96, 97]. These parameter values result in critical atom $N_c \equiv 2\gamma\kappa/\mathscr{G}^2$ and photon $n_c \equiv 4\gamma^2/3\mathscr{G}^2$ numbers in the order of $\sim 10^{-2}$ and $\sim 10^{-4}$ [91], respectively, meaning that even a single atom and/or photon plays a significant role. This is the so-called strong atom-photon coupling regime, where the atoms and photons can coherently exchange energy and momentum [98, 99].

In the JC model, an atom couples strongly to a single mode of a second-quantized field and they coherently exchange energy, which is a reversible process. This is in sharp contrast to free space where the atom interacts with a large number of electromagnetic modes and there are irreversible processes involved (such as the decay of an atomic excited state due to spontaneous emission). An example of a coherent reversible process in cavity QED is the vacuum-field Rabi oscillations, where the atom is initially in an excited state with no photon in the cavity; the atom spontaneously emits a photon into a cavity mode and re-absorbs it later and the process continues in principle forever [100, 101]. In a pioneering experiment, quantum vacuum Rabi oscillation was observed, which provided a direct evidence for second-quantization of the intra-cavity field and the realization of the JC model [102]. Serge Haroche, jointly with David Wineland, was awarded the 2012 Nobel Prize in Physics for his efforts in this field.

Entanglement is one the peculiarities of quantum mechanics with no analogue in a classical world. An entangled state cannot be expressed as a tensor product of constituent states, with the simplest and the most well-known example being Bell states [103]. Such entangled states are at the core of quantum information and quantum computers. Atoms trapped inside or passing slowly through a high-Q cavity can form entangled states with each other or with cavity fields in the strong coupling regime [98]. Such entangled states of matter and quantized fields (i.e., photons) have been realized with Rydberg atoms (i.e., highly excited atoms with the principal quantum number n in order of 50) passing slowly through a microwave superconducting cavity [102]. They are commonly referred to as polariton states.

Laser light in free space has been used to cool and trap alkali atoms for decades, as well as some molecules more recently [104]. Laser cooling has limitations however, and is not applicable to every atom or molecule. The more complex the internal structure of a particle (atom or molecule), the more difficult it becomes to apply laser cooling. This is because when such a particle is excited, there are more allowed transitions where the particle can

spontaneously emit a photon and decay into a dark state. The particle is therefore removed from the cooling cycle and more pumping lasers are required to pump the particle back into the cooling cycle. An alternative approach for cooling atoms and molecules is cavity cooling, which relies on dissipating energy through cavity loss channels (i.e., photon leakage of the cavity) rather than spontaneous emission [105, 106]. The kinetic energy of a particle (atom or molecule) is extracted and transferred into cavity fields due to optical friction forces. This energy is subsequently dissipated by photons leaking out of the cavity. This opens the possibility for cooling any sufficiently polarizable particle, without a need for a closed optical cycle [107].

Unlike in free space, the back-action of the atoms on the intra-cavity radiation field is not negligible, leading to complex coupled dynamics of the matter and radiation fields in which both entities are affected by one another and must be treated on the same footing [107]. As a consequence cavity fields mediate long-ranged interactions between atoms [96, 108]. This can be intuitively understood by noting that due to presence of an atom a cavity resonance frequency and the corresponding field mode are modified with respect to the empty cavity [107]. These modifications are dynamic in the sense that they depend on atomic position and motion. These motion-induced frequency and field changes react back and in turn affect the atomic motion and position. Consider that many atoms are loaded inside the cavity [97]. The motion of a single atom leads to a dynamical change of the resonance frequency and the corresponding mode, which in turn then affect the motion and position of all atoms. Equivalently, the motion and position of a single atom depends on local field which is affected by all atoms. This is the origin of cavity-induced long-range interactions between atoms.

The cavity-mediated long-range interactions give rise to collective phenomena in atomic systems. The most interesting example is the quantum Dicke phase transition from superfluid to a self-organized state in a transversely pumped Bose condensate in a linear cavity [109,

110, 111]. The Bose condensate is loaded inside a linear cavity, whose intra-cavity field is in the vacuum state, and is then driven by a transverse pump laser. Both pump and cavity resonance frequencies are far red-detuned from atomic transitions, but closely detuned from each other. The condensate atoms then scatter photons from the pump laser into the cavity mode and serve as sources of the intra-cavity photons. For a uniform Bose condensate, the accumulation of intra-cavity photons is suppressed due to the destructive interference of sources [110]. Above some critical pumping power, quantum fluctuations in the condensate density nevertheless leads to a small buildup of the intra-cavity field. This results in the formation of a 2D optical lattice (formed by the pump and cavity fields) which in turn attracts the atoms into its odd or even sites (minima), further increasing coherent scattering of the pump field into the cavity mode. The Bose condensate then spontaneously breaks the translational symmetry and self-organizes itself into a checkerboard pattern to maximize cooperative scattering of pump photons into the cavity mode [112]. This collective behavior can be envisaged as cavity-mediated long-ranged interaction between condensate atoms. Other example of cooperative phenomena in cavity QED includes the collective atomic recoil laser [113, 114, 115].

1.4 Outline of the Thesis

In all previous proposals for inducing gauge potentials, the radiation field is treated classically and the back-action of the atoms on it is omitted. This is a fair assumption since all of these proposals are based on laser light interacting with atoms in free space. Therefore, all laser-based schemes result in static synthetic gauge potentials for neutral atoms, where the emergent gauge potentials are only additional terms in the atomic Hamiltonian [57]. In other words, the emergent gauge potentials are background potentials. In a cavity QED environment, the back-action of atoms on the quantized intra-cavity field is no longer negligible and this is the origin of many intriguing dynamical and collective phenomena.

These peculiarities of cavity QED attracted my attention in the early stage of my Ph.D. and exploiting it to induce synthetic gauge potentials in ultracold atomic gases with novel consequences has been the focus of my Ph.D. research. I developed a two-photon Raman scheme in the strong atom-photon coupling regime, based on two counter-propagating modes of a ring cavity, to induce both synthetic magnetic field and SO coupling for a single neutral atom inside the cavity [116]. The SO interaction is only weakly dependent on the occupation of the cavity modes, whereas the strength of the magnetic field is proportional to the square of the total number of photons in the cavity and can be made arbitrary large, which is desirable for realizing fractional quantum Hall phases and the Hofstadter butterfly.

I then extended this single-atom cavity QED scheme to many bosons in the weak atom-photon coupling regime [117]. In addition to inducing SO coupling for the individual atoms, the cavity fields also mediate infinite-ranged interactions between atoms, whose strengths and signs can readily be tuned experimentally. The interplay between these cavity-mediated long-ranged and the two-body contact interactions determines the many-body ground state and its elementary excitations, with novel consequences such as the stabilization of an attractive Bose condensate which otherwise is unstable and collapses. The ground state is either a stripe phase or plane-wave phase. In the stripe phase, atoms condense in both minima of the single-particle energy dispersion, and consequently the translational symmetry is spontaneously broken and the total density exhibits fringes. This is in contrast to the plane-wave phase and conventional Bose condensates where all atoms Bose condense into a single state. The positive cavity-mediated interactions, which can be readily tuned experimentally, favor the stripe phase. Thus, the ring-cavity environment provides an experimentally convenient framework for exploring exotic ground states of SO-coupled Bose condensates. This might have possible applications when the common Feshbach resonance techniques for tuning the two-body interactions are impractical to implement due to the drastic atom losses or not feasible at all [118, 119, 120, 121, 122].

At the same time, a few other schemes were proposed to induce Abelian and non-Abelian gauge potentials in ultracold atoms via cavity QED [123, 124, 125] and to couple a laser-induced SO-coupled Bose condensate to the cavity field [126]. These schemes exhibit a wealth of physics, including strong synthetic magnetic fields, intriguing instabilities, a cavity-mediated Hofstadter spectrum, and a variety of magnetic orders. Furthermore, the cavity QED setting can also open the possibility for engineering dynamical gauge potentials which have their own Hamiltonians and evolve according to their own Hamiltonians [57], since cavity fields are naturally dynamic.

This thesis is comprised of five chapters and four appendices. The introduction is presented in Chapter 1. I have reviewed in the current chapter the related historical development of BEC and cavity QED. These include the emergent research areas of synthetic gauge fields in ultracold atomic gases and collective phenomena in many-body cavity QED.

Chapter 2 is devoted to the theoretical framework used in the rest of the thesis. It is divided into three main sections: Bose-Einstein condensation, gauge theories and gauge fields, and the atom-field interaction. In Sec. 2.1, I review concepts associated with BEC in the context of ideal and interacting Bose gases. I discuss the ground state and elementary excitations of a single- and two-component Bose condensate. In particular, the GP mean-field and Bogoliubov theories are introduced in this section. The notion of gauge theory and gauge fields is introduced in Sec. 2.2, where I illustrate the electromagnetic fields and SO coupling are examples of Abelian $U(1)$ and non-Abelian $SU(2)$ gauge fields which emerge as a natural consequence of local gauge invariance. Finally in Sec. 2.3, I discuss atom-field interaction using both semi-classical and fully quantum mechanical approaches. In particular, cavity QED is introduced in the framework of the fully quantum mechanical approach. I also illustrate in an abstract way how synthetic gauge potentials can emerge in atom-field interaction Hamiltonians and discuss in detail a specific, important example.

In Chapter 3, which is our published work [116], I illustrate how to induce a synthetic

magnetic field and SO coupling for a single pseudospin-1/2 neutral atom in a ring cavity. The calculations are carried out analytically in the strong atom-photon coupling regime. After introduction and literature review in Sec. 3.1, the model of a single atom interacting with two counter-propagating modes of a ring cavity is described in Sec. 3.2 and then the governing Hamiltonian is derived. In Sec. 3.3, this Hamiltonian is expressed in terms of polaritons and diagonalized to yield the energy dispersion spectrum. Section 3.4 describes the circumstances under which a synthetic SO interaction and a magnetic field emerge in this model. A discussion of the results and concluding remarks are presented in Sec. 3.5.

Chapter 4 is dedicated to our published work [117] and is a generalization of Chapter 3 to the many-atom case. Nonetheless, the weak-coupling regime is assumed in this chapter to allow a full analytical treatment of the system. After a survey of the literature in Sec. 4.1, I start in Sec. 4.2 from the full atom-photon Hamiltonian density for a lossy but pumped cavity, to derive an effective many-body atomic Hamiltonian with the photon fields eliminated. The ground state of this effective Hamiltonian is explored in Sec. 4.3 using both a variational method and by solving the generalized Gross-Pitaevskii equations. The remainder of this section is devoted to the analysis of elementary excitations. A discussion of the results and conclusions are found in Sec. 4.4.

Concluding remarks are presented in the last chapter, that is, Chapter 5. I also discuss possible extensions and future directions related to this thesis.

Since the adiabatic evolution and adiabatic elimination are important parts of this thesis, Appendix A is dedicated to the Adiabatic Theorem and Berry's phase. The notion of adiabatic elimination is also illustrated in this appendix for a simple two-level atom interacting with a monochromatic electromagnetic field. Appendices B and C provide details of the adiabatic elimination of the atomic excited state in a Λ scheme in the strong- and weak-coupling regimes, respectively. The adiabatic elimination of the cavity modes in the weak-coupling regime is detailed in Appendix D. Appendix B is taken from the appendix

of our published work in Ref. [116], and Appendices C and D from the appendices of our published work in Ref. [117].

Chapter 2

Theoretical Background

This chapter is comprised of three main sections and in each section I shall present theoretical frameworks which are prerequisites for the next chapters. Section 2.1 is devoted to Bose-Einstein condensation. I will review the concept of Bose-Einstein condensation in ideal and interacting quantum degenerate Bose gases in Secs. 2.1.1 and 2.1.2, respectively. The notion of gauge potentials will be introduced in Sec. 2.2. Two specific classes of gauge potentials, namely Abelian and non-Abelian gauge potentials, will be considered in detail in Secs. 2.2.1 and 2.2.2, respectively. Section 2.3 is dedicated to the atom-field interaction. The semi-classical theory of the atom-field interaction will be presented in Sec. 2.3.1, while the full quantum mechanical (i.e. cavity quantum electrodynamics) approach to the atom-field interaction will be discussed in Sec. 2.3.2. I shall finally illustrate in Sec. 2.3.3 in an abstract way how synthetic gauge potentials can emerge in a (semi-classical) atom-field interaction Hamiltonian and then present a specific example.

2.1 Bose-Einstein Condensation

In this section, I introduce the concept of Bose-Einstein condensation in ideal and interacting quantum degenerate Bose gases.

2.1.1 Non-Interacting Bosons

An ideal gas of N non-interacting, identical bosons is described by the many-body Hamiltonian density

$$\mathcal{H}_0 = \sum_{j=1}^{N} \mathcal{H}_{\mathrm{s},j} = \sum_{j=1}^{N} \left[\frac{\mathbf{p}_j^2}{2m} + V_{\mathrm{ext}}(\mathbf{r}_j) \right], \tag{2.1}$$

where $\mathbf{p}_j = -i\hbar\boldsymbol{\nabla}_j$ is the momentum operator of the jth particle, m is the mass, and $V_{\rm ext}(\mathbf{r}_j)$ is an external potential acting at the position of the jth particle. Since the many-body Hamiltonian density $\mathcal{H}_0$ is a sum of individual single-particle Hamiltonian densities $\mathcal{H}_{\rm s}$, the non-interacting many-body bosonic wavefunction is merely a symmetrized state of single-particle product states,

$$\mathbf{\Phi}^{(0)}_{\boldsymbol{\tau}}(\mathbf{r}_1, \mathbf{r}_2, ..., \mathbf{r}_N) = \frac{1}{\sqrt{N!}} \sum_P P \left(\prod_{j=1}^{N} \phi_{{\rm s},\tau_j}(\mathbf{r}_j) \right), \tag{2.2}$$

where the single-particle state $\phi_{{\rm s},\tau}(\mathbf{r})$ satisfies the single-particle Schrödinger equation,

$$\mathcal{H}_{\rm s}\phi_{{\rm s},\tau}(\mathbf{r}) = \varepsilon_\tau \phi_{{\rm s},\tau}(\mathbf{r}), \tag{2.3}$$

with ε_τ being the single-particle energy. Here τ labels quantum states of the single-particle Hamiltonian density and $\boldsymbol{\tau} = (\tau_1, \tau_2, ..., \tau_N)$ is a collective quantum number. Note that the sum on the permutation operator P runs over all $N!$ elements of the permutation group of N identical particles.

At finite temperature, the average boson occupation of the single-particle state $\phi_{{\rm s},\tau}$ is determined by the Bose-Einstein distribution function [127],

$$N_\tau = \frac{1}{e^{\beta(\varepsilon_\tau - \mu)} - 1}, \tag{2.4}$$

where $\beta = 1/k_{\rm B}T$ is the inverse temperature (with T being the temperature and $k_{\rm B}$ the Boltzmann constant) and μ is the chemical potential. The strict positivity of the occupation number N_τ imposes the constraint $\mu < \varepsilon_\tau$ for all single-particle states τ; and in particular $\mu < \varepsilon_0$, where ε_0 is the ground-state eigenenergy. In thermal gases, the chemical potential is much lower than the ground-state energy (i.e. it has a large negative value) and consequently the average occupation numbers N_τ of all states, including the ground state N_0, are much smaller than one, $N_\tau \simeq e^{-\beta(\varepsilon_\tau - \mu)} \ll 1$. As the temperature T is lowered, the chemical potential μ approaches its upper bound, the ground-state energy ε_0, and the average occupancies of all states but the ground state become vanishingly small. Since the number of particles is

conserved $N = \sum_\tau N_\tau$, the bosons must be then accommodated in the ground state $\phi_{\mathrm{s},0}$. In other words, the single-particle ground state is macroscopically occupied, referred to as "Bose-Einstein condensation" (BEC). The average occupation of the single-particle ground state N_0 becomes on the order of the total particle number N and $N_0/N \lesssim 1$ determines the condensate fraction.

2.1.2 Interacting Bosons

The non-interacting Bose gas is an ideal system and in reality particles interact with one another. The exact form of the interaction potential between particles is required for solving a many-body problem and it can be complicated in general. However, at extremely low densities and low temperatures (such as are found in Bose-condensed gases) the situation can be greatly simplified. As discussed in the preceding chapter, at extremely low densities two-body interactions are the dominant interactions and higher few-body interactions (such as three-body interactions) are highly suppressed and can be therefore omitted. In addition, only the low-energy sector of the two-body interactions is relevant at extremely low temperatures. In this regime therefore, the particle-particle interactions in dilute Bose gases at low temperatures can be well approximated by a pseudo-potential $V(\mathbf{r}_j - \mathbf{r}_l) = g\delta(\mathbf{r}_j - \mathbf{r}_l)$, which is a two-body contact interaction [32]. The strength of the two-body contact interaction g is related to the s-wave scattering length a_s via $g = 4\pi\hbar^2 a_s/m$ [7]. Hereafter, the temperature is restricted to absolute zero, $T = 0$. This guarantees the validity of the low-energy assumption and replacing of the full two-body interactions with the contact interactions. Furthermore, the thermal component of the Bose gas becomes irrelevant. Then the Hamiltonian density of a dilute, weakly interacting Bose gas at $T = 0$ reads,

$$\mathcal{H} = \mathcal{H}_0 + g \sum_{l>j=1}^{N} \delta(\mathbf{r}_j - \mathbf{r}_l), \tag{2.5}$$

where $\mathcal{H}_0$ is the non-interacting Hamiltonian density, Eq. (2.1).

The Mean-Field Ground State: Gross-Pitaevskii Equation

In order to proceed further and find the many-body ground state and energy, one may adopt the Hartree mean-field theory, in which the many-body bosonic wavefunction is assumed to be a symmetrized product of single-particle states, similar to the non-interacting case Eq. (2.2). The Hartree ansatz is a mean-field approximation in the sense that it is a product of single-particle states and does not contain any correlation due to the two-body contact interactions. In a perfectly condensed state where all bosons are in the single-particle ground state, the many-body Hartree-Fock wavefunction reduces to [7],

$$\mathbf{\Phi}_0^{\mathrm{MF}}(\mathbf{r}_1, \mathbf{r}_2, ..., \mathbf{r}_N) = \prod_{j=1}^{N} \phi_0^{\mathrm{MF}}(\mathbf{r}_j) \equiv \prod_{j=1}^{N} \phi_0(\mathbf{r}_j). \tag{2.6}$$

Note that the mean-field single-particle state $\phi_0 \equiv \phi_0^{\mathrm{MF}}$ is completely different than the single-particle state $\phi_{s,0}$ and in particular does not satisfy the single-particle Schrödinger equation (2.3).

The expectation value of the total Hamiltonian density (2.5) with respect to the Hartree-Fock ansatz (2.6) yields the mean-field total energy,

$$E_0^{\mathrm{MF}} = \left\langle \mathbf{\Phi}_0^{\mathrm{MF}} \right| \mathcal{H} \left| \mathbf{\Phi}_0^{\mathrm{MF}} \right\rangle = N \int d\mathbf{r} \left[\frac{\hbar^2}{2m} |\boldsymbol{\nabla} \phi_0(\mathbf{r})|^2 + V_{\mathrm{ext}}(\mathbf{r}) |\phi_0(\mathbf{r})|^2 + \frac{(N-1)}{2} g |\phi_0(\mathbf{r})|^4 \right], \tag{2.7}$$

where the last term is due to the two-body contact interactions (recall that there are $N(N-1)/2$ ways of pairing N identical objects). In the absence of the two-body interactions, the mean-field single-particle state ϕ_0 coincides exactly with the single-particle state $\phi_{\mathrm{s},0}$ and the Hartree-Fock ansatz becomes exact, yielding $E_0^{\mathrm{MF}} = N\varepsilon_0$ for the energy functional (2.7), which is the total energy of N ideal bosons in the single-particle ground state $\phi_{\mathrm{s},0}$. For a uniform Bose gas the ground-state wavefunction is $\phi_0 = 1/\sqrt{V}$, where V is the volume. The total mean-field energy then becomes $E_0^{\mathrm{MF}} = gN(N-1)/2V \simeq gN^2/2V$ (ignoring the term of order $1/N$ under the assumption that $N \gg 1$), yielding the chemical potential $\mu = \partial E_0^{\mathrm{MF}}/\partial N = gn$ for a canonical ensemble [127], where $n = N/V$ is the particle density.

Introducing the condensate wavefunction $\psi(\mathbf{r}) = \sqrt{N}\phi_0(\mathbf{r})$ and omitting terms in the order of $1/N$, the mean-field total energy (2.7) can be re-expressed as,

$$E_0^{\mathrm{MF}} = \int d\mathbf{r} \left[-\frac{\hbar^2}{2m}\psi^*(\mathbf{r})\boldsymbol{\nabla}^2\psi(\mathbf{r}) + V_{\mathrm{ext}}(\mathbf{r})|\psi(\mathbf{r})|^2 + \frac{1}{2}g|\psi(\mathbf{r})|^4 \right], \tag{2.8}$$

where the first (i.e., kinetic-energy) term has been recast using integration by parts. The condensate wavefunction $\psi(\mathbf{r})$ must be determined in a self-consistent manner such that it minimizes the energy functional E_0^{MF}, with the constraint that the total number of particles is conserved, $N = \int |\psi(\mathbf{r})|^2 d\mathbf{r} = \int n(\mathbf{r}) d\mathbf{r}$. This amounts to minimizing the grand potential $\Omega = E_0^{\mathrm{MF}} - \mu N$ with respect to the independent variations of ψ and ψ^* at fixed μ, where the chemical potential μ is the Lagrange multiplier fixing the total mean number of particles. Taking a functional derivative from the grand potential with respect to ψ^* and equating it to zero, $\delta\Omega/\delta\psi^* = 0$, yields the non-linear Schrödinger equation,

$$\left[-\frac{\hbar^2}{2m}\boldsymbol{\nabla}^2 + V_{\mathrm{ext}}(\mathbf{r}) + g|\psi(\mathbf{r})|^2 \right] \psi(\mathbf{r}) = \mu\psi(\mathbf{r}), \tag{2.9}$$

which is also known as the time-independent Gross-Pitaevskii (GP) equation. The non-linear term $g|\psi(\mathbf{r})|^2$ in the GP equation is the mean-field interaction potential a boson experiences due to the rest of the bosons. For a uniform Bose gas the GP equation reduces to $\mu = g|\psi|^2 = gn$, consistent with the chemical potential obtained above in the canonical framework for a uniform Bose gas using the energy functional and the thermodynamic relation $\mu = \partial E_0^{\mathrm{MF}}/\partial N$.

Elementary Excitations: Bogoliubov Theory

The many-body (quantum-field theoretical) Hamiltonian is obtained from the many-body Hamiltonian density [128],

$$\begin{aligned} H &= \int d\mathbf{r}\ \hat{\psi}^\dagger(\mathbf{r})\mathcal{H}_{\mathrm{s}}\hat{\psi}(\mathbf{r}) + \frac{1}{2}g\int d\mathbf{r}d\mathbf{r}'\ \hat{\psi}^\dagger(\mathbf{r})\hat{\psi}^\dagger(\mathbf{r}')\delta(\mathbf{r}'-\mathbf{r})\hat{\psi}(\mathbf{r}')\hat{\psi}(\mathbf{r}) \\ &= \int d\mathbf{r}\ \hat{\psi}^\dagger(\mathbf{r}) \left[-\frac{\hbar^2}{2m}\boldsymbol{\nabla}^2 + V_{\mathrm{ext}}(\mathbf{r}) + \frac{1}{2}g\hat{\psi}^\dagger(\mathbf{r})\hat{\psi}(\mathbf{r}) \right] \hat{\psi}(\mathbf{r}), \end{aligned} \tag{2.10}$$

where $\hat{\psi}(\mathbf{r})$ and $\hat{\psi}^\dagger(\mathbf{r})$ are the bosonic field annihilation and creation operators[1], respectively, and they obey the bosonic commutation relation $[\hat{\psi}(\mathbf{r}), \hat{\psi}^\dagger(\mathbf{r}')] = \delta(\mathbf{r}-\mathbf{r}')$. The time evolution of the field operator can be obtained from the Heisenberg equation of motion $i\hbar\partial_t\hat{\psi} = [\hat{\psi}, H]$ using the Hamiltonian (2.10),

$$i\hbar\frac{\partial\hat{\psi}(\mathbf{r},t)}{\partial t} = \left[-\frac{\hbar^2}{2m}\boldsymbol{\nabla}^2 + V_{\text{ext}}(\mathbf{r}) + g\hat{\psi}^\dagger(\mathbf{r},t)\hat{\psi}(\mathbf{r},t)\right]\hat{\psi}(\mathbf{r},t). \tag{2.11}$$

The Gross-Pitaevskii approach discussed in the preceding section is equivalent to omitting the quantum fluctuation of the field and treating it as a classical field, which is accomplished by virtue of replacing the field operator with its expectation value $\hat{\psi} \to \psi \equiv \langle\hat{\psi}\rangle$. This is a good approximation provided that quantum fluctuations of the field operator is small compared to its expectation value, which will be further justified in the following. Then the Hamiltonian H, Eq. (2.10), reduces to the energy functional E_0^{MF}, Eq. (2.8); and the Heisenberg equation of motion (2.11) becomes the time-dependent Gross-Pitaevskii equation

$$i\hbar\frac{\partial\psi(\mathbf{r},t)}{\partial t} = \left[-\frac{\hbar^2}{2m}\boldsymbol{\nabla}^2 + V_{\text{ext}}(\mathbf{r}) + g|\psi(\mathbf{r},t)|^2\right]\psi(\mathbf{r},t). \tag{2.12}$$

Note that replacing the time-dependent condensate wavefunction with $\psi(\mathbf{r},t) = e^{-i\mu t/\hbar}\psi(\mathbf{r})$ in the time-dependent GP equation (2.12) yields the time-independent GP equation (2.9).

The condensate wavefunction $\psi \equiv \langle\hat{\psi}\rangle$ can be envisaged as the order parameter for the BEC transition: it is zero above the BEC transition temperature T_{BEC}, while it is macroscopically occupied below T_{BEC} (in particular at zero temperature $T = 0$). It is a classical field in the sense that it is macroscopically occupied and the particle-number fluctuation in it due to quantum effects is negligible when the number of condensed particles is large. This is the philosophy behind replacing the field operator $\hat{\psi}$ with its expectation value, the condensate wavefunction ψ. The fluctuations in the condensate wavefunction can

[1] Throughout this thesis, I will only use the "hat" notation for operators when there is a possibility of confusion, such as here where I use the hat notation for the field operator $\hat{\psi}$ to distinguish it from the condensate wavefunction ψ.

be most conveniently accounted for by writing it as

$$\psi(\mathbf{r},t) = e^{-i\mu t/\hbar}\left[\psi(\mathbf{r}) + \delta\psi(\mathbf{r},t)\right], \tag{2.13}$$

where $\delta\psi(\mathbf{r},t) \ll \psi(\mathbf{r})$ is the condensate fluctuation [26]. Substituting Eq. (2.13) (and its complex conjugate) into the time-dependent GP equation (2.12) and linearizing it with respect to the fluctuation (i.e. retaining terms only linear in $\delta\psi$ and $\delta\psi^*$) yields the generic equation

$$i\hbar\frac{\partial}{\partial t}\delta\psi(\mathbf{r},t) = \left[-\frac{\hbar^2}{2m}\boldsymbol{\nabla}^2 + V_{\text{ext}}(\mathbf{r}) + 2g|\psi(\mathbf{r})|^2 - \mu\right]\delta\psi(\mathbf{r},t) + g\big[\psi(\mathbf{r})\big]^2\delta\psi^*(\mathbf{r},t), \tag{2.14}$$

for the time evolution of $\delta\psi$, with a similar equation for $\delta\psi^*$. These coupled equations can be solved using the Bogoliubov ansatz for the fluctuations [7],

$$\delta\psi(\mathbf{r},t) = u(\mathbf{r})e^{-i\omega t} + v^*(\mathbf{r})e^{i\omega t}. \tag{2.15}$$

Substituting the Bogoliubov ansatz (2.15) (and its complex conjugate) into Eq. (2.14) and equating the coefficients of $e^{\pm i\omega t}$ separately yields a set of two coupled equations, referred to as the Bogoliubov equations,

$$\begin{aligned}
&\left[-\frac{\hbar^2}{2m}\boldsymbol{\nabla}^2 + V_{\text{ext}}(\mathbf{r}) + 2g|\psi(\mathbf{r})|^2 - \mu\right]u(\mathbf{r}) + g\big[\psi(\mathbf{r})\big]^2 v(\mathbf{r}) = \epsilon u(\mathbf{r}),\\
&\left[-\frac{\hbar^2}{2m}\boldsymbol{\nabla}^2 + V_{\text{ext}}(\mathbf{r}) + 2g|\psi(\mathbf{r})|^2 - \mu\right]v(\mathbf{r}) + g\big[\psi^*(\mathbf{r})\big]^2 u(\mathbf{r}) = -\epsilon v(\mathbf{r}),
\end{aligned} \tag{2.16}$$

where $\epsilon \equiv \hbar\omega$ is the spectrum of elementary (or collective) excitations.

For any trap, these coupled equations can be numerically solved to yield the spectrum of collective excitations. Nonetheless, the excitation spectrum ϵ can be easily obtained analytically in the homogenous case, $V_{\text{ext}}(\mathbf{r}) = 0$. One can assume plane-wave solutions,

$$u(\mathbf{r}) = \frac{1}{\sqrt{V}}\sum_{\mathbf{q}\neq 0} u_{\mathbf{q}} e^{i\mathbf{q}\cdot\mathbf{r}}, \qquad v(\mathbf{r}) = \frac{1}{\sqrt{V}}\sum_{\mathbf{q}\neq 0} v_{\mathbf{q}} e^{i\mathbf{q}\cdot\mathbf{r}}, \tag{2.17}$$

with the coefficients $u_{\mathbf{q}}$ and $v_{\mathbf{q}}$ to be determined, where the quasi-momentum $\mathbf{q} = 0$ is excluded since BEC occurs at the momentum $\mathbf{q} = 0$ for a homogenous Bose gas (in other

words $\mathbf{q} = 0$ corresponds to the condensate wavefunction itself). The Bogoliubov equations (2.16) can then be recast in the matrix form,

$$\begin{pmatrix} \frac{\hbar^2\mathbf{q}^2}{2m} + gn & gn \\ -gn & -\frac{\hbar^2\mathbf{q}^2}{2m} - gn \end{pmatrix} \begin{pmatrix} u_{\mathbf{q}} \\ v_{\mathbf{q}} \end{pmatrix} = \epsilon(\mathbf{q}) \begin{pmatrix} u_{\mathbf{q}} \\ v_{\mathbf{q}} \end{pmatrix}. \tag{2.18}$$

Here I have used the fact that for a uniform gas $n = \psi^2 = N/V$ and $\mu = gn$. The Bogoliubov Hamiltonian (2.18) can be readily diagonalized to yield the spectrum of elementary excitations,

$$\epsilon(\mathbf{q}) = \sqrt{\epsilon_0^2(\mathbf{q}) + 2gn\epsilon_0(\mathbf{q})} = \sqrt{\epsilon_0(\mathbf{q})\big[\epsilon_0(\mathbf{q}) + 2gn\big]}, \tag{2.19}$$

and the relation between the Bogoliubov coefficients,

$$u_{\mathbf{q}} = -\frac{\epsilon(\mathbf{q}) + \xi(\mathbf{q})}{gn} v_{\mathbf{q}}, \tag{2.20}$$

where $\epsilon_0(\mathbf{q}) = \hbar^2\mathbf{q}^2/2m$ is the energy dispersion of a free particle and $\xi(\mathbf{q}) = \epsilon_0(\mathbf{q}) + gn$. The Bogoliubov excitation spectrum $\epsilon(\mathbf{q})$ is depicted in Fig. 2.1. It exhibits a linear, collective sound-like dispersion at long wavelengths (or small momenta $\mathbf{q}$), an indication of the superfluidity; and it becomes quadratic, free-particle like at large momenta $\mathbf{q}$. This is in sharp contrast to non-interacting Bose gases whose excitations are always free-particle like. The speed of sound for small momenta is found by omitting the quadratic term in the Bogoliubov dispersion, $\epsilon(\mathbf{q}) \simeq c_s\hbar q$ with $c_s = \sqrt{gn/m}$ being the speed of sound. Note that the Bogoliubov Hamiltonian (2.18) is not Hermitian and the excitation spectrum can be complex, in contrast to a Hermitian Hamiltonian, which indicates dynamical instabilities. Negative excitations lower the energy of the system, signalling also that the mean-field ground state is not the real ground state of the system.

The approach of treating non-condensate particles as the fluctuation $\delta\psi$ of the condensate wavefunction ψ discussed above is equivalent to Bogoliubov's original approach of writing the field operator as $\hat{\psi} = \psi + \delta\hat{\psi}$, where $\delta\hat{\psi}$ is the quantum fluctuation operator of the field operator $\hat{\psi}$ [19]. One then substitutes $\hat{\psi} = \psi + \delta\hat{\psi}$ in the many-body Hamiltonian (2.10)

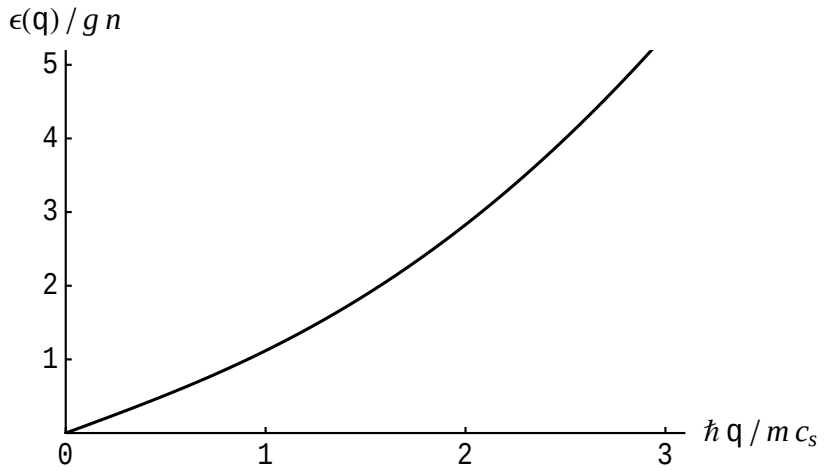

Figure 2.1: The spectrum of elementary excitations $\epsilon(\mathbf{q})$ in unit of gn as a function of the dimensionless quasi-momentum $\hbar\mathbf{q}/mc_s$. The spectrum exhibits a linear sound-like dispersion at small momenta, while it becomes quadratic free-particle like at large momenta.

and retains terms up to second order in fluctuation operators. The resultant Hamiltonian is diagonalized by introducing the Bogoliubov ansatz for the quantum fluctuation operator [26], analogous to the condensate fluctuation (2.15),

$$\delta\hat{\psi}(\mathbf{r},t) = \sum_i \left[u_i(\mathbf{r}) e^{-i\omega t}\hat{\alpha}_i + v_i^*(\mathbf{r}) e^{i\omega t}\hat{\alpha}_i^\dagger \right]. \tag{2.21}$$

Here, $\hat{\alpha}_i$ is the Bogoliubov quasi-particle operator and must satisfy the bosonic commutation relation $[\hat{\alpha}_i, \hat{\alpha}_j^\dagger] = \delta_{ij}$, which is ensured provided that

$$|u_i|^2 - |v_i|^2 = 1. \tag{2.22}$$

The diagonalized Hamiltonian yields the spectrum ϵ of elementary excitations, which for instance is identical with Eq. (2.19) for a uniform Bose gas.

The underlying assumption of the Bogoliubov approach is that the condensate or quantum fluctuations are small compared to the condensate wavefunction, that is, $\delta\psi \ll \psi$ or equivalently $\langle\delta\hat{\psi}\rangle \ll \psi$. This can be confirmed by calculating the depletion of the condensate wavefunction due to the two-body interactions [7],

$$n_{\rm ex} = \frac{1}{(2\pi\hbar)^3}\int |v_{\mathbf{q}}|^2 d\mathbf{q}. \tag{2.23}$$

Using the normalization constraint (2.22), the coefficients $u_{\mathbf{q}}$ and $v_{\mathbf{q}}$ can be readily obtained from Eq. (2.20) as,

$$u_{\mathbf{q}}^2 = \frac{1}{2}\left[\frac{\xi(\mathbf{q})}{\epsilon(\mathbf{q})} + 1\right], \qquad v_{\mathbf{q}}^2 = \frac{1}{2}\left[\frac{\xi(\mathbf{q})}{\epsilon(\mathbf{q})} - 1\right]. \tag{2.24}$$

The ratio of the condensate depletion to the condensate density n is then obtained [7],

$$\frac{n_{\rm ex}}{n} = \frac{8}{3\sqrt{\pi}}(na_s^3)^{1/2}. \tag{2.25}$$

Noting that $n \sim 1/a^3$, where a is the average particle spacing, one has $n_{\rm ex}/n \sim (a_s/a)^{3/2}$. In most experiments, the average particle spacing a is much larger than the s-wave scattering length a_s and the depletion of the condensate is therefore of the order of one percent [7].

Two-Component Bose Condensates

Consider a spinor-1/2 Bose gas where spin exchange interactions are suppressed and the particle density of each spin component is therefore conserved under collisions. This is formally equivalent to a two-component Bose gas. The two desired internal states of the atoms are referred to as the pseudospin states in analogy to two possible spin projections of a spin-1/2. These internal states can be for example the two hyperfine states $|F = 2, m_F = 2\rangle$ and $|F = 1, m_F = -1\rangle$ of ^{87}Rb atoms [37]. The single-component many-body Hartree-Fock wavefunction (2.6) can readily be generalized to a two-component condensate [7],

$$\mathbf{\Phi}_0^{\rm MF}(\mathbf{r}_1, \mathbf{r}_2, ..., \mathbf{r}_{N_1}; \mathbf{r}'_1, \mathbf{r}'_2, ..., \mathbf{r}'_{N_2}) = \prod_{j=1}^{N_1}\prod_{l=1}^{N_2}\phi_0^{(1)}(\mathbf{r}_j)\phi_0^{(2)}(\mathbf{r}'_l), \tag{2.26}$$

where $\phi_0^{(1)}$ ($\phi_0^{(2)}$) is the corresponding mean-field single-particle wavefunction for pseudospin state $|\tau\rangle = |1\rangle$ ($|2\rangle$). The many-body Hamiltonian density (2.5) can be generalized in a similar straightforward manner,

$$\mathcal{H} = \sum_{\tau=1,2}\left[\mathcal{H}_{0,\tau} + g_\tau \sum_{j'_\tau > j_\tau = 1}^{N_\tau}\delta(\mathbf{r}_{j_\tau} - \mathbf{r}_{j'_\tau})\right] + g_{12}\sum_{j=1}^{N_1}\sum_{l=1}^{N_2}\delta(\mathbf{r}_j - \mathbf{r}_l), \tag{2.27}$$

where $\mathcal{H}_{0,\tau}$ is the non-interacting Hamiltonian density (2.1) for pseudospin τ, and g_τ (g_{12}) is the two-body intra- (inter-) species interaction strength. The many-body Hamiltonian then

reads

$$H = \int d\mathbf{r} \left\{ \hat{\mathbf{\Psi}}^\dagger(\mathbf{r}) \left[-\frac{\hbar^2}{2m}\boldsymbol{\nabla}^2 + V_{\rm ext}(\mathbf{r}) \right] \hat{\mathbf{\Psi}}(\mathbf{r}) + \frac{1}{2} g_1 \hat{n}_1^2(\mathbf{r}) + \frac{1}{2} g_2 \hat{n}_2^2(\mathbf{r}) + g_{12} \hat{n}_1(\mathbf{r}) \hat{n}_2(\mathbf{r}) \right\}, \tag{2.28}$$

where $\hat{\mathbf{\Psi}} = (\hat{\psi}_1, \hat{\psi}_2)^{\mathsf{T}}$ is the two-component field operator and $\hat{n}_\tau = \hat{\psi}_\tau^\dagger \hat{\psi}_\tau$ is the density operator for pseudospin τ. The field operators again obey the bosonic commutation relation $[\hat{\psi}_\tau(\mathbf{r}_j), \hat{\psi}_{\tau'}^\dagger(\mathbf{r}_{j'})] = \delta_{\tau,\tau'}\delta(\mathbf{r}_j - \mathbf{r}_{j'})$.

The Heisenberg equations of motion for the field operators $\hat{\psi}_\tau(\mathbf{r}, t)$ can be easily obtained using the many-body Hamiltonian (2.28), analogous to the single-component case (2.11). Replacing the field operators $\hat{\psi}_\tau(\mathbf{r}, t)$ with the corresponding condensate wavefunctions $\psi_\tau(\mathbf{r}, t) \equiv \langle \hat{\psi}_\tau(\mathbf{r}, t) \rangle$ yields a set of two coupled time-dependent GP equations,

$$\begin{aligned} i\hbar \frac{\partial \psi_1(\mathbf{r}, t)}{\partial t} &= \left[-\frac{\hbar^2}{2m}\boldsymbol{\nabla}^2 + V_{\rm ext}(\mathbf{r}) + g_1 n_1(\mathbf{r}, t) + g_{12} n_2(\mathbf{r}, t) \right] \psi_1(\mathbf{r}, t), \\ i\hbar \frac{\partial \psi_2(\mathbf{r}, t)}{\partial t} &= \left[-\frac{\hbar^2}{2m}\boldsymbol{\nabla}^2 + V_{\rm ext}(\mathbf{r}) + g_2 n_2(\mathbf{r}, t) + g_{12} n_1(\mathbf{r}, t) \right] \psi_2(\mathbf{r}, t). \end{aligned} \tag{2.29}$$

Now in addition to the intra-species mean-field interaction potential $g_\tau n_\tau$, each boson experiences an inter-species mean-field interaction potential $g_{12} n_{\tau'}$, where $\tau' = 2$ (1) for $\tau = 1$ (2).

For small fluctuations of the condensates, one can write $\psi_\tau(\mathbf{r}, t) = e^{-i\mu_\tau t/\hbar}[\psi_\tau(\mathbf{r}) + \delta\psi_\tau(\mathbf{r}, t)]$. Substituting these expressions into the time-dependent coupled GP equations (2.29) and linearizing them yields the time-independent coupled GP equations for the stationary condensate wavefunctions $\psi_\tau(\mathbf{r})$,

$$\begin{aligned} \left[-\frac{\hbar^2}{2m}\boldsymbol{\nabla}^2 + V_{\rm ext}(\mathbf{r}) + g_1 n_1(\mathbf{r}) + g_{12} n_2(\mathbf{r}) \right] \psi_1(\mathbf{r}) &= \mu_1 \psi_1(\mathbf{r}), \\ \left[-\frac{\hbar^2}{2m}\boldsymbol{\nabla}^2 + V_{\rm ext}(\mathbf{r}) + g_2 n_2(\mathbf{r}) + g_{12} n_1(\mathbf{r}) \right] \psi_2(\mathbf{r}) &= \mu_2 \psi_2(\mathbf{r}), \end{aligned} \tag{2.30}$$

and a set of two time-dependent coupled equations for the fluctuations $\delta\psi_\tau(\mathbf{r},t)$,

$$\begin{aligned}
i\hbar\frac{\partial}{\partial t}\delta\psi_1(\mathbf{r},t) &= \left[-\frac{\hbar^2}{2m}\boldsymbol{\nabla}^2 + V_{\rm ext}(\mathbf{r}) + 2g_1|\psi_1(\mathbf{r})|^2 + g_{12}|\psi_2(\mathbf{r})|^2 - \mu_1\right]\delta\psi_1(\mathbf{r},t) \\
&\quad + g_1\psi_1^2(\mathbf{r})\delta\psi_1^*(\mathbf{r},t) + g_{12}\psi_1(\mathbf{r})\psi_2^*(\mathbf{r})\delta\psi_2(\mathbf{r},t) + g_{12}\psi_1(\mathbf{r})\psi_2(\mathbf{r})\delta\psi_2^*(\mathbf{r},t), \\
i\hbar\frac{\partial}{\partial t}\delta\psi_2(\mathbf{r},t) &= \left[-\frac{\hbar^2}{2m}\boldsymbol{\nabla}^2 + V_{\rm ext}(\mathbf{r}) + 2g_2|\psi_2(\mathbf{r})|^2 + g_{12}|\psi_1(\mathbf{r})|^2 - \mu_2\right]\delta\psi_2(\mathbf{r},t) \\
&\quad + g_2\psi_2^2(\mathbf{r})\delta\psi_2^*(\mathbf{r},t) + g_{12}\psi_1^*(\mathbf{r})\psi_2(\mathbf{r})\delta\psi_1(\mathbf{r},t) + g_{12}\psi_1(\mathbf{r})\psi_2(\mathbf{r})\delta\psi_1^*(\mathbf{r},t). \quad (2.31)
\end{aligned}$$

After assuming a Bogoliubov ansatz for each condensate fluctuation $\delta\psi_\tau(\mathbf{r},t)$, Eqs. (2.30) and (2.31) in principle can be solved numerically for any trap to yield the ground-state density distributions (i.e. wavefunctions) and collective excitations around these ground states.

Similar to the single-component case, these equations nevertheless admit analytical solutions in the homogenous case $V_{\rm ext}(\mathbf{r}) = 0$. The density distributions can be readily obtained from the coupled GP equations (2.30),

$$n_1 = \frac{g_2\mu_1 - g_{12}\mu_2}{g_1g_2 - g_{12}^2}, \qquad n_2 = \frac{g_1\mu_2 - g_{12}\mu_1}{g_1g_2 - g_{12}^2}. \quad (2.32)$$

Assuming that the fluctuations are plane waves,

$$\delta\psi_\tau(\mathbf{r},t) = \sum_{\mathbf{q}\neq 0}\left[u_{\tau,\mathbf{q}}e^{i(\mathbf{q}\cdot\mathbf{r}-\omega t)} + v_{\tau,\mathbf{q}}^*e^{-i(\mathbf{q}\cdot\mathbf{r}-\omega t)}\right], \quad (2.33)$$

the time-dependent coupled equations for the fluctuations (2.31) can then be recast as

$$\begin{pmatrix}
\epsilon_0(\mathbf{q}) + g_1n_1 & g_1\psi_1^2 & g_{12}\psi_1\psi_2^* & g_{12}\psi_1\psi_2 \\
-g_1\psi_1^{*2} & -\epsilon_0(\mathbf{q}) - g_1n_1 & -g_{12}\psi_1^*\psi_2^* & -g_{12}\psi_1^*\psi_2 \\
g_{12}\psi_1^*\psi_2 & g_{12}\psi_1\psi_2 & \epsilon_0(\mathbf{q}) + g_2n_2 & g_2\psi_2^2 \\
-g_{12}\psi_1^*\psi_2^* & -g_{12}\psi_1\psi_2^* & -g_2\psi_2^{*2} & -\epsilon_0(\mathbf{q}) - g_2n_2
\end{pmatrix}\begin{pmatrix} u_{1,\mathbf{q}} \\ v_{1,\mathbf{q}} \\ u_{2,\mathbf{q}} \\ v_{2,\mathbf{q}} \end{pmatrix} = \epsilon(\mathbf{q})\begin{pmatrix} u_{1,\mathbf{q}} \\ v_{1,\mathbf{q}} \\ u_{2,\mathbf{q}} \\ v_{2,\mathbf{q}} \end{pmatrix}, \quad (2.34)$$

where the chemical potentials μ_τ have been eliminated using the GP equations. Note that for uniform gases, the condensate wavefunctions are real, that is, $\psi_\tau^* = \psi_\tau$. The Bogoliubov

Hamiltonian can then be diagonalized to yield the spectrum of elementary excitations,

$$\epsilon_{\pm}(\mathbf{q}) = \sqrt{\epsilon_0^2(\mathbf{q}) + \epsilon_0(\mathbf{q}) \left[(g_1 n_1 + g_2 n_2) \pm \sqrt{(g_1 n_1 + g_2 n_2)^2 - 4(g_1 g_2 - g_{12}^2) n_1 n_2} \right]}. \quad (2.35)$$

The spectrum of elementary excitations consists of two branches and is illustrated in Fig. 2.2 as dimensionless $\epsilon_{\pm}(\mathbf{q})/gn$ versus $\hbar\mathbf{q}/mc_-$, where $c_- = \sqrt{gn/m}$ is the speed of sound in the negative branch. Both branches are gapless and exhibit linear sound-like behavior at long wavelengths (or small momenta $\mathbf{q}$). Elementary excitations must be strictly positive; negative or complex excitations signal an instability in the system. This imposes the constraint

$$g_1 g_2 \geqslant g_{12}^2, \quad (2.36)$$

on the intra- and inter-species interactions strengths. Note that when $g_{12}^2 = g_1 g_2$ the negative excitation branch ϵ_- reduces to the free-particle dispersion, $\epsilon_-(\mathbf{q}) = \epsilon_0(\mathbf{q})$; and in particular when $g \equiv g_{12} = g_1 = g_2$ (which also implies $g_{12}^2 = g_1 g_2$) the positive excitation branch ϵ_+ coincides exactly with the single-component excitation spectrum (2.19), upon identifying $n = n_1 + n_2$ as the total density.

2.2 Gauge Theories and Gauge Fields

Gauge freedom was first discovered in classical electromagnetic theory. The Maxwell equations describe classical electromagnetic theory and in the vacuum (and in the absence of any charge and current densities) they read [129],

$$\begin{aligned}
\boldsymbol{\nabla} \cdot \mathbf{E}(\mathbf{r}, t) &= 0, \\
\boldsymbol{\nabla} \cdot \mathbf{B}(\mathbf{r}, t) &= 0, \\
\boldsymbol{\nabla} \times \mathbf{E}(\mathbf{r}, t) &= -\frac{\partial}{\partial t} \mathbf{B}(\mathbf{r}, t), \\
\boldsymbol{\nabla} \times \mathbf{B}(\mathbf{r}, t) &= \frac{1}{c^2} \frac{\partial}{\partial t} \mathbf{E}(\mathbf{r}, t),
\end{aligned} \quad (2.37)$$

where $\mathbf{E}$ ($\mathbf{B}$) is the electric (magnetic) field and $c = 1/\sqrt{\mu_0 \varepsilon_0}$ is the speed of light in the vacuum with ε_0 (μ_0) being the electric permittivity (magnetic permeability). The electro-

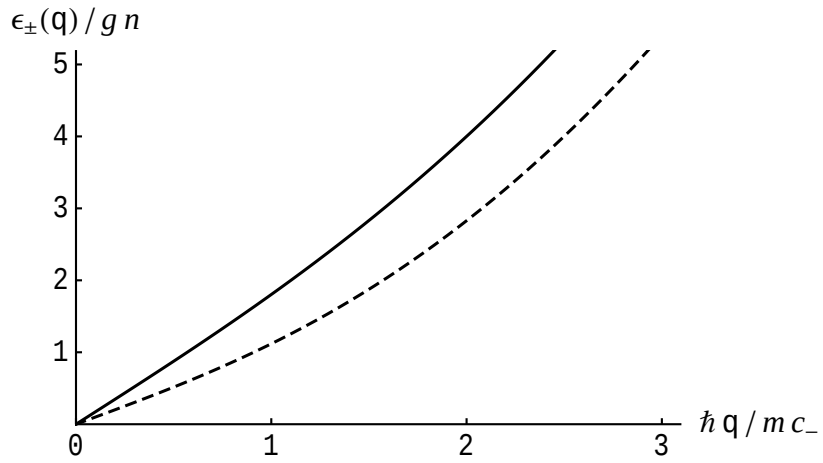

Figure 2.2: The spectrum of elementary excitations $\epsilon_\pm(\mathbf{q})$ in unit of gn (solid and dashed curves respectively) of a two-component uniform Bose condensate as a function of the dimensionless quasi-momentum $\hbar\mathbf{q}/mc_-$. The parameters are set to $g \equiv g_1 = g_2 = 2g_{12}$ and $n/2 = n_1 = n_2$ (with $n = n_1 + n_2$ being the total density). The spectrum consists of two branches and both exhibit linear sound-like dispersion at small momenta, while they become quadratic free-particle like at large momenta. The speed of sound in the positive branch c_+ is related to the speed of sound in the negative branch $c_- = \sqrt{gn/m}$ via $c_+ = \sqrt{3}c_-$.

magnetic fields $\{\mathbf{E}, \mathbf{B}\}$ can be expressed in terms of a scalar $\varphi(\mathbf{r}, t)$ and a vector $\mathbf{A}(\mathbf{r}, t)$ potential

$$\begin{aligned} \mathbf{E}(\mathbf{r}, t) &= -\boldsymbol{\nabla}\varphi(\mathbf{r}, t) - \frac{\partial}{\partial t}\mathbf{A}(\mathbf{r}, t), \\ \mathbf{B}(\mathbf{r}, t) &= \boldsymbol{\nabla} \times \mathbf{A}(\mathbf{r}, t). \end{aligned} \tag{2.38}$$

The electromagnetic potentials $\{\phi, \mathbf{A}\}$ are not unique, that is, the gauge transformation of these potentials,

$$\begin{aligned} \varphi(\mathbf{r}, t) \to \varphi'(\mathbf{r}, t) &= \varphi(\mathbf{r}, t) - \frac{\partial}{\partial t}\chi(\mathbf{r}, t), \\ \mathbf{A}(\mathbf{r}, t) \to \mathbf{A}'(\mathbf{r}, t) &= \mathbf{A}(\mathbf{r}, t) + \boldsymbol{\nabla}\chi(\mathbf{r}, t), \end{aligned} \tag{2.39}$$

under any arbitrary gauge function $\chi(\mathbf{r}, t)$ leaves the electromagnetic fields (2.38) invariant [130]. Rather, the electromagnetic fields are gauge independent, as expected since they are the physically measurable quantities. This allows the gauge to be chosen for a given problem in order to simplify calculations, a procedure known as gauge fixing. The Coulomb

(or radiation) gauge is such a suitable gauge for problems in vacuum,

$$\boldsymbol{\nabla} \cdot \mathbf{A}(\mathbf{r}, t) = 0, \tag{2.40}$$

which also implies that $\varphi(\mathbf{r}, t) = 0$ [130]. By substituting the electric field with Eq. (2.38) in the first Maxwell equation (2.37) and then using the Coulomb gauge (2.40), one obtains

$$\boldsymbol{\nabla}^2 \varphi(\mathbf{r}, t) = 0. \tag{2.41}$$

By imposing the boundary condition that the scalar potential must vanish at infinity, this equation has the solution $\varphi(\mathbf{r}, t) = 0$ in the absence of any charge. Then in the Coulomb gauge the electromagnetic fields (2.38) are determined solely by the vector potential $\mathbf{A}$. I will demonstrate in Sec. (2.3.2) how to second-quantize the electromagnetic fields in the Coulomb gauge.

Quantum mechanics is also invariant under a different kind of gauge transformation, the global phase transformation. This gauge freedom of quantum mechanics leads to the the continuity equation (i.e., conservation of probability) $\partial_t \rho + \boldsymbol{\nabla} \cdot \mathbf{j} = 0$, where ρ is the probability density and $\mathbf{j}$ the probability current[2] [131]. It was further postulated that the invariance of quantum fields (actions or Lagrangians, to be more accurate) under a wider class of gauge transformation, the local gauge transformation, would yield the fundamental interactions (i.e., forces) of the nature and the corresponding conservation laws [133]. Gauge invariance has now become a cornerstone of modern physics, namely quantum field and gauge field theories. This will be elaborated in the following sections, Sec. 2.2.1 and 2.2.2.

[2] This is obtained by demanding the Lagrangian density of the Schrödinger field, Eq. (2.42), to be invariant under an infinitesimal global gauge transformation, that is, $\delta\mathcal{L} = 0$ [131]. The continuity equation can also be obtained directly from the Schrödinger equation [132].

2.2.1 Local $U(1)$ Gauge Invariance and Abelian Gauge Fields

Consider the non-relativistic Lagrangian density of the Schrödinger field for a single charged particle (with charge q) in some external static potential $V_{\text{ext}}(\mathbf{r})$ [134],

$$\mathcal{L} = i\hbar\psi^*\partial_t\psi - \frac{\hbar^2}{2m}\boldsymbol{\nabla}\psi^*\cdot\boldsymbol{\nabla}\psi - V_{\text{ext}}\psi^*\psi, \tag{2.42}$$

where the Euler-Lagrange equation

$$\frac{\partial\mathcal{L}}{\partial\psi^*} = \partial_t\frac{\partial\mathcal{L}}{\partial(\partial_t\psi^*)} + \boldsymbol{\nabla}\cdot\frac{\partial\mathcal{L}}{\partial(\boldsymbol{\nabla}\psi^*)}, \tag{2.43}$$

yields the Schrödinger equation

$$i\hbar\frac{\partial\psi}{\partial t} = -\frac{\hbar^2}{2m}\boldsymbol{\nabla}^2\psi + V_{\text{ext}}\psi. \tag{2.44}$$

Here $\psi = \psi(\mathbf{r},t)$ is the Schrödinger field (or wavefunction) and $\partial_t = \partial/\partial t$. The global gauge transformation of the Schrödinger field $\psi \to \psi' = e^{iq\chi/\hbar}\psi$, where χ is a constant (and the coefficient $q/\hbar$ is included solely for convenience), leaves the Schrödinger Lagrangian (2.42) invariant. Nevertheless, the Schrödinger Lagrangian in the current form is not invariant under a local gauge transformation $\psi \to \psi' = e^{iq\chi(\mathbf{r},t)/\hbar}\psi$, where $\chi(\mathbf{r},t)$ depends on both position and time [128]. The potential energy term transforms as desired $\psi^*\psi \to (\psi^*\psi)' = \psi^*\psi$, while extra terms appear in terms involving the temporal and spatial derivatives, e.g.,

$$\boldsymbol{\nabla}\psi(\mathbf{r},t) \to \boldsymbol{\nabla}'\psi'(\mathbf{r},t) = \boldsymbol{\nabla}\left[e^{iq\chi(\mathbf{r},t)/\hbar}\psi(\mathbf{r},t)\right] = e^{iq\chi(\mathbf{r},t)/\hbar}\left[\frac{iq}{\hbar}\psi(\mathbf{r},t)\boldsymbol{\nabla}\chi(\mathbf{r},t) + \boldsymbol{\nabla}\psi(\mathbf{r},t)\right]. \tag{2.45}$$

This problem can be reconciled by substituting the derivatives with the covariant derivatives in the Lagrangian (2.42) [29],

$$\begin{aligned}\partial_t \to D_t &= \partial_t + \frac{iq}{\hbar}\varphi(\mathbf{r},t),\\ \boldsymbol{\nabla} \to \mathbf{D} &= \boldsymbol{\nabla} - \frac{iq}{\hbar}\mathbf{A}(\mathbf{r},t),\end{aligned} \tag{2.46}$$

with the following gauge transformation laws for $\varphi(\mathbf{r},t)$ and $\mathbf{A}(\mathbf{r},t)$,

$$\begin{aligned}\varphi(\mathbf{r},t) &\to \varphi'(\mathbf{r},t) = \varphi(\mathbf{r},t) - \partial_t\chi(\mathbf{r},t),\\ \mathbf{A}(\mathbf{r},t) &\to \mathbf{A}'(\mathbf{r},t) = \mathbf{A}(\mathbf{r},t) + \boldsymbol{\nabla}\chi(\mathbf{r},t).\end{aligned} \tag{2.47}$$

It is straightforward to check that the covariant derivatives transform as the field itself, e.g.,

$$\begin{aligned}\mathbf{D}\psi(\mathbf{r},t) \to \mathbf{D}'\psi'(\mathbf{r},t) &= e^{iq\chi(\mathbf{r},t)/\hbar}\left\{\boldsymbol{\nabla}\psi(\mathbf{r},t) - \frac{iq}{\hbar}\left[\mathbf{A}'(\mathbf{r},t) - \boldsymbol{\nabla}\chi(\mathbf{r},t)\right]\psi(\mathbf{r})\right\}\\ &= e^{iq\chi(\mathbf{r},t)/\hbar}\mathbf{D}\psi(\mathbf{r},t).\end{aligned} \tag{2.48}$$

The "minimally coupled" Lagrangian density of the the Schrödinger field [131]

$$\mathcal{L}_{\rm mc} = i\hbar\psi^*\partial_t\psi - \frac{\hbar^2}{2m}\left(\boldsymbol{\nabla} - \frac{iq}{\hbar}\mathbf{A}\right)\psi^* \cdot \left(\boldsymbol{\nabla} - \frac{iq}{\hbar}\mathbf{A}\right)\psi - (V_{\rm ext} + q\varphi)\psi^*\psi, \tag{2.49}$$

is therefore invariant under the local gauge transformation.

The set of all gauge functions $e^{iq\chi/\hbar}$ (with χ either being a constant or position- and/or time-dependent) form a $U(1)$ gauge symmetry group [131]. Furthermore, this gauge symmetry group is Abelian, since the gauge functions are just phase factors and commute with each other $e^{iq\chi_1/\hbar}e^{iq\chi_2/\hbar} = e^{iq\chi_2/\hbar}e^{iq\chi_1/\hbar}$. Requiring the Schrödinger Lagrangian density (2.42) to be invariant under the local $U(1)$ gauge transformation, therefore, leads to appearance of the gauge potentials $\{\varphi, \mathbf{A}\}$ and the minimal-coupling Schrödinger Lagrangian density $\mathcal{L}_{\rm mc}$, Eq. (2.49). Comparing the gauge transformation properties of these gauge potentials (2.47) with those of the electromagnetic potentials in Eq. (2.39), it is obvious that the gauge potentials $\{\varphi, \mathbf{A}\}$ are nothing but the electromagnetic scalar and vector potentials. The minimal-coupling Lagrangian density $\mathcal{L}_{\rm mc}$ (2.49) yields therefore the Schrödinger equation of a (non-relativistic) charged particle coupled to an external electromagnetic field through the electromagnetic (gauge) potentials $\{\varphi, \mathbf{A}\}$,

$$i\hbar\frac{\partial\psi}{\partial t} = -\frac{\hbar^2}{2m}\left(\boldsymbol{\nabla} - \frac{iq}{\hbar}\mathbf{A}\right)^2\psi + (V_{\rm ext} + q\varphi)\,\psi, \tag{2.50}$$

and the associated quantum-mechanical minimal-coupling Hamiltonian density is given by

$$\mathcal{H}_{\rm mc} = -\frac{\hbar^2}{2m}\left(\boldsymbol{\nabla} - \frac{iq}{\hbar}\mathbf{A}\right)^2 + V_{\rm ext} + q\varphi. \tag{2.51}$$

It is also instructive to construct the minimal-coupling Hamiltonian directly from the minimal-coupling Lagrangian density (2.49) of the Schrödinger field via [134],

$$H_{\rm mc} = \int d\mathbf{r}\left(\pi_\psi \partial_t \psi + \pi_{\psi^*}\partial_t\psi^* - \mathcal{L}_{\rm mc}\right). \tag{2.52}$$

Here, π_ψ and π_{ψ^*} are the canonically conjugate momentum densities associated with ψ and ψ^*, respectively [134]:

$$\pi_\psi = \frac{\partial \mathcal{L}_{\rm mc}}{\partial(\partial_t\psi)} = i\hbar\psi^*, \qquad \pi_{\psi^*} = \frac{\partial \mathcal{L}_{\rm mc}}{\partial(\partial_t\psi^*)} = 0. \tag{2.53}$$

The minimal-coupling Hamiltonian (2.52) then reads,

$$\begin{aligned} H_{\rm mc} &= \int d\mathbf{r}\left[\frac{\hbar^2}{2m}\left(\boldsymbol{\nabla} - \frac{iq}{\hbar}\mathbf{A}\right)\psi^* \cdot \left(\boldsymbol{\nabla} - \frac{iq}{\hbar}\mathbf{A}\right)\psi + (V_{\rm ext} + q\varphi)\psi^*\psi\right] \\ &= \int \psi^*\left[-\frac{\hbar^2}{2m}\left(\boldsymbol{\nabla} - \frac{iq}{\hbar}\mathbf{A}\right)^2 + V_{\rm ext} + q\varphi\right]\psi d\mathbf{r}, \end{aligned} \tag{2.54}$$

where the last equality has been obtained after integrating by parts. The quantum-mechanical minimal-coupling Hamiltonian density is therefore identical with Eq. (2.51), as expected.

It is worth briefly mentioning how to second-quantize the Schrödinger field. This is attained by promoting canonically conjugate variables into operators and imposing the usual quantum mechanical commutation relation [134]. This procedure is referred to as the canonical quantization and will be also exploited later in Sec. 2.3.2 to second-quantize the electromagnetic fields. Here, $\psi(\mathbf{r},t)$ and $\pi_\psi(\mathbf{r},t) = i\hbar\psi^*(\mathbf{r},t)$ are the canonically conjugate variables. They are then promoted into operators $\hat{\psi}(\mathbf{r},t)$ and $\hat{\pi}_{\hat{\psi}}(\mathbf{r},t) = i\hbar\hat{\psi}^\dagger(\mathbf{r},t)$ with the following commutation relation:

$$[\hat{\psi}(\mathbf{r},t), \hat{\pi}_{\hat{\psi}}(\mathbf{r}',t)] = i\hbar[\hat{\psi}(\mathbf{r},t), \hat{\psi}^\dagger(\mathbf{r}',t)] = i\hbar\delta(\mathbf{r}-\mathbf{r}'), \tag{2.55}$$

which resembles the commutation relation $[\hat{a}_i, \hat{a}_j^\dagger] = \delta_{i,j}$ of harmonic oscillators. Substituting ψ and ψ^* with the corresponding field operators $\hat{\psi}$ and $\hat{\psi}^\dagger$ in the total Hamiltonian of the

classical Schrödinger field [i.e., Eq. (2.54) with $\mathbf{A} = \varphi = 0$], one obtains the quantum-field theoretical Hamiltonian

$$H = \int \hat{\psi}^\dagger(\mathbf{r}', t) \left[-\frac{\hbar^2}{2m} \boldsymbol{\nabla}^2 + V_{\text{ext}} \right] \hat{\psi}(\mathbf{r}', t) d\mathbf{r}, \tag{2.56}$$

which has been introduced before in the context of interacting Bosons.

2.2.2 Local $SU(2)$ Gauge Invariance and non-Abelian Gauge Fields

In the preceding section, the field (or wavefunction) ψ is treated as a complex scalar field. Now let me assume that the field is a two-component Pauli spinor [131],

$$\psi = \begin{pmatrix} \psi_1 \\ \psi_2 \end{pmatrix} \tag{2.57}$$

where each component $\psi_\tau = \psi_\tau(\mathbf{r}, t)$ is a complex scalar field. Consider the gauge transformation $\psi \to \psi' = e^{ig\check{\chi}/\hbar}\psi$, where g is a constant introduced in analogy to the charge q in the preceding section and $\check{\chi}$ is a two-by-two matrix which can be expressed as $\check{\chi} = \sum_a \chi^a \check{\sigma}^a/2 = (\chi^1\check{\sigma}^1 + \chi^2\check{\sigma}^2 + \chi^3\check{\sigma}^3)/2$ in terms of generators of the $SU(2)$ group (i.e., the Pauli matrices),

$$\check{\sigma}^1 = \check{\sigma}_1 = \begin{pmatrix} 0 & 1 \\ 1 & 0 \end{pmatrix}, \qquad \check{\sigma}^2 = \check{\sigma}_2 = \begin{pmatrix} 0 & -i \\ i & 0 \end{pmatrix}, \qquad \check{\sigma}^3 = \check{\sigma}_3 = \begin{pmatrix} 1 & 0 \\ 0 & -1 \end{pmatrix}. \tag{2.58}$$

Here $\{\chi^a\}$ are the gauge transformation parameters; they can be position and time independent or dependent, leading to a global or local gauge transformation, respectively. The gauge functions in this case do not necessarily commute with one another, that is, $e^{ig\check{\chi}_1/\hbar}e^{ig\check{\chi}_2/\hbar} \neq e^{ig\check{\chi}_2/\hbar}e^{ig\check{\chi}_1/\hbar}$. This stems from the fact that the generators of the $SU(2)$ group, Eq. (2.58), do not commute with one another. The set of all gauge functions $e^{ig\check{\chi}/\hbar}$ therefore form a non-Abelian $SU(2)$ gauge symmetry group [135].

Invoking the local $SU(2)$ gauge transformation $\psi \to \psi' = e^{ig\check{\chi}(\mathbf{r},t)/\hbar}\psi$ and requiring the Lagrangian density

$$\mathcal{L} = i\hbar\psi^\dagger \mathbb{1}_2 \partial_t \psi - \frac{\hbar^2}{2m} \mathbb{1}_2 \boldsymbol{\nabla}\psi^\dagger \cdot \mathbb{1}_2 \boldsymbol{\nabla}\psi - V_{\text{ext}}\psi^\dagger\psi, \tag{2.59}$$

to be invariant under this transformation leads to covariant derivatives [136]

$$\begin{aligned}\mathbb{1}_2\partial_t \to \check{D}_t &= \mathbb{1}_2\partial_t + \frac{ig}{\hbar}\check{\varphi}(\mathbf{r},t),\\ \mathbb{1}_2\boldsymbol{\nabla} \to \check{\mathbf{D}} &= \mathbb{1}_2\boldsymbol{\nabla} - \frac{ig}{\hbar}\check{\boldsymbol{\mathscr{A}}}(\mathbf{r},t).\end{aligned} \tag{2.60}$$

Here $\psi^\dagger = (\psi_1^*, \psi_2^*)$, $\mathbb{1}_2$ is the two-by-two identity matrix (which is omitted when there is no ambiguity), $\check{\varphi}(\mathbf{r},t)$ is a two-by-two matrix $\check{\varphi} = \sum_a \varphi^a\check{\sigma}^a/2$, and $\check{\boldsymbol{\mathscr{A}}}(\mathbf{r},t)$ is a vector of two-by-two matrices with component $\check{\mathscr{A}}_j = \sum_a \mathscr{A}_j^a\check{\sigma}^a/2$. Then $\{\check{\varphi},\ \check{\boldsymbol{\mathscr{A}}}\}$ are referred to as Yang-Mills-type, non-Abelian $SU(2)$ gauge potentials [137] with the following gauge transformation laws [136]:

$$\begin{aligned}\check{\varphi}(\mathbf{r},t) \to \check{\varphi}'(\mathbf{r},t) &= \check{\varphi}(\mathbf{r},t) - \partial_t\check{\chi}(\mathbf{r},t) + \frac{ig}{\hbar}[\check{\chi},\check{\varphi}],\\ \check{\boldsymbol{\mathscr{A}}}(\mathbf{r},t) \to \check{\boldsymbol{\mathscr{A}}}'(\mathbf{r},t) &= \check{\boldsymbol{\mathscr{A}}}(\mathbf{r},t) + \boldsymbol{\nabla}\check{\chi}(\mathbf{r},t) + \frac{ig}{\hbar}[\check{\chi},\check{\boldsymbol{\mathscr{A}}}].\end{aligned} \tag{2.61}$$

In the following section, I will demonstrate that spin-orbit coupling can be envisaged as a non-Abelian $SU(2)$ gauge potential [131, 138].

Intrinsic Spin-Orbit Coupling

In atomic physics, the spin-orbit (SO) interaction is the coupling of an electron's orbital motion to its spin degrees of freedom [139]. Likewise in condensed matter physics, an SO interaction commonly refers to the coupling of an electron's center-of-mass motion to its spin degrees of freedom and it has the same origin as the atomic SO coupling, that is, it is a relativistic effect [140]. Consider an electron moving with velocity $\mathbf{v}$ in an external electric field $\mathbf{E}$. According to the Lorentz transformation up to the first order in $(v/c)^2$ (with c being the speed of light), the electron experiences a magnetic field $\mathbf{B} = \mathbf{E}\times\mathbf{v}/c^2$ in its own rest frame and consequently its magnetic moment $\check{\boldsymbol{\mu}} = -e\hbar\check{\boldsymbol{\sigma}}/2m$ couples to this magnetic field: $\mathcal{H}_{\rm SO} = -\check{\boldsymbol{\mu}}\cdot\mathbf{B} = e\hbar\check{\boldsymbol{\sigma}}\cdot(\mathbf{E}\times\mathbf{p})/2m^2c^2$. A more careful consideration reveals that $\mathcal{H}_{\rm SO}$ must be rescaled by a factor of two,

$$\mathcal{H}_{\rm SO} \to \mathcal{H}_{\rm SO} = \frac{e\hbar}{4m^2c^2}\check{\boldsymbol{\sigma}}\cdot(\mathbf{E}\times\mathbf{p}), \tag{2.62}$$

due to the non-inertial frame of the electron, an effect known as the Thomas precession [141]. Here, $q = -e$ and m are the charge and rest mass of the electron, respectively, $\mathbf{p} = m\mathbf{v}$ is its momentum, and $\check{\boldsymbol{\sigma}} = (\check{\sigma}_1, \check{\sigma}_2, \check{\sigma}_3)$ is a vector of the Pauli matrices (2.58). Depending on the form of the external electric field $\mathbf{E}$, the SO coupling Hamiltonian (2.62) can take different forms. The SO coupling Hamiltonian (2.62) obtained above from simple relativistic considerations can be rigorously derived from the non-relativistic limit of the Dirac equation coupled to an external electromagnetic field through the scalar $\varphi(\mathbf{r}, t)$ and vector $\mathbf{A}(\mathbf{r}, t)$ potentials [141, 142].

The SO coupling Hamiltonian (2.62) is linear in the momentum $\mathbf{p}$ and can be therefore absorbed into the (non-relativistic) kinetic energy term $\mathbf{p}^2/2m$. Using the identity $\mathbf{A} \cdot (\mathbf{B} \times \mathbf{C}) = (\mathbf{A} \times \mathbf{B}) \cdot \mathbf{C}$, the SO coupling Hamiltonian can be recast as

$$\mathcal{H}_{\mathrm{SO}} = -\frac{\hbar q}{4m^2c^2}(\check{\boldsymbol{\sigma}} \times \mathbf{E}) \cdot \mathbf{p}. \tag{2.63}$$

Combining the kinetic energy and SO coupling (2.63) terms yields

$$\frac{\mathbf{p}^2}{2m}\mathbb{1}_2 - \frac{\hbar q}{4m^2c^2}(\check{\boldsymbol{\sigma}} \times \mathbf{E}) \cdot \mathbf{p} = \frac{1}{2m}\left(\mathbf{p}\mathbb{1}_2 - \frac{\hbar q}{4mc^2}\check{\boldsymbol{\sigma}} \times \mathbf{E}\right)^2 - \frac{\hbar^2 q^2}{32m^3c^4}(\check{\boldsymbol{\sigma}} \times \mathbf{E})^2, \tag{2.64}$$

where the two-by-two identity matrix $\mathbb{1}_2$ has been included for clarity and use has been made of $\boldsymbol{\nabla} \times \mathbf{E} = 0$. The kinetic energy momentum $\mathbf{p}\mathbb{1}_2 - \hbar q\check{\boldsymbol{\sigma}} \times \mathbf{E}/4mc^2$ is now reminiscent of the $SU(2)$ covariant derivatives (2.60) with the non-Abelian gauge potential,

$$g\check{\boldsymbol{\mathcal{A}}}(\mathbf{r}) = \frac{\hbar q}{4mc^2}\check{\boldsymbol{\sigma}} \times \mathbf{E}(\mathbf{r}). \tag{2.65}$$

As mentioned earlier, depending on the form of the electric field $\mathbf{E}(\mathbf{r})$, the SO coupling term can take different forms. Let me consider a specific case where the electric field is homogeneous and along the z direction; $\mathbf{E} = E\mathbf{z}$. Then the SO coupling Hamiltonian takes the form,

$$\mathcal{H}_{\mathrm{SO}} = \frac{\hbar qE}{4m^2c^2}\left(\check{\sigma}_x p_y - \check{\sigma}_y p_x\right), \tag{2.66}$$

which is the well-known Rashba SO coupling [55]. The corresponding non-Abelian gauge potential is [131, 138],

$$g\check{\mathcal{A}} = \frac{\hbar q E}{4mc^2}\left(\check{\sigma}_y, -\check{\sigma}_x, 0\right). \tag{2.67}$$

2.3 Atom-Field Interaction

In Sec. 2.2.1, I derived the minimal coupling Hamiltonian (2.51), which describes the interaction between a (non-relativistic) charged particle and an electromagnetic field, from the local gauge invariance principle. In this section, I will show using the minimal coupling Hamiltonian how to describe the atom-field interaction in both the semiclassical and fully quantum mechanical limits. In the semi-classical limit the atom is treated quantum mechanically, while the electromagnetic field is treated classically (Sec. 2.3.1). In contrast, in the quantum mechanical limit, both atom and electromagnetic field are treated on the same footing via quantum mechanics (Sec. 2.3.2). For the sake of simplicity, only single-electron atoms are considered; generalization to many-electron atoms is straightforward in principle. I shall illustrate in Sec. 2.3.3 in an abstract way how geometric gauge potentials can emerge in (semi-classical) atom-field interaction Hamiltonians. As a specific and important example, I will then review the emergent SO coupling in the semi-classical Λ scheme.

2.3.1 Semi-Classical Approach

Consider the minimal coupling Hamiltonian density,

$$\mathcal{H}_{\rm mc} = \frac{1}{2m}\left[\mathbf{p} - q\mathbf{A}(\mathbf{r}, t)\right]^2 + V(\mathbf{r} - \mathbf{R}), \tag{2.68}$$

describing the interaction of a single-electron atom with an electromagnetic field. Here, $\mathbf{p}$ ($\mathbf{r}$) is the momentum (position) operator of the electron, q is the charge of the electron, and $V(\mathbf{r} - \mathbf{R}) = q\varphi_{\rm nuc}(\mathbf{r} - \mathbf{R})$ is the potential energy due to the Coulomb interaction between the electron and nucleus (located at $\mathbf{R}$). Note that the Coulomb gauge is assumed so that the vector potential $\mathbf{A}(\mathbf{r}, t)$ solely determines the external electromagnetic fields.

$\mathbf{p} \cdot \mathbf{A}$ Hamiltonian

Expanding the first term of the minimal-coupling Hamiltonian density (2.68), one obtains

$$\mathcal{H}_{\rm mc} = \frac{\mathbf{p}^2}{2m} - \frac{q}{2m}\left[\mathbf{p}\cdot\mathbf{A}(\mathbf{r},t) + \mathbf{A}(\mathbf{r},t)\cdot\mathbf{p}\right] + \frac{q^2}{2m}\mathbf{A}^2(\mathbf{r},t) + V(\mathbf{r}-\mathbf{R}). \tag{2.69}$$

The terms in the square bracket involving the inner products of the momentum operator and the vector potential can be simplified using the relation,

$$[\mathbf{p},\mathbf{A}] = \mathbf{p}\cdot\mathbf{A}(\mathbf{r}) - \mathbf{A}(\mathbf{r})\cdot\mathbf{p} = -i\hbar\boldsymbol{\nabla}\cdot\mathbf{A}(\mathbf{r}) = 0, \tag{2.70}$$

where the last equality follows from the Coulomb gauge (2.40). Here I made use of

$$[\mathbf{p},C]\phi = (\mathbf{p}C - C\mathbf{p})\phi = (-i\hbar\boldsymbol{\nabla}C)\phi, \tag{2.71}$$

which can be understood by noting that $\mathbf{p}$ is an operator acting on everything standing to its right, in contrast to $\boldsymbol{\nabla}$ which only acts on C [141]. The Hamiltonian (2.69) can then be recast as

$$\mathcal{H}_{\rm mc} = \frac{\mathbf{p}^2}{2m} - \frac{q}{m}\mathbf{p}\cdot\mathbf{A}(\mathbf{r},t) + \frac{q^2}{2m}\mathbf{A}^2(\mathbf{r},t) + V(\mathbf{r}-\mathbf{R}). \tag{2.72}$$

In most practical situations, the length scale over which the electromagnetic fields change is usually much larger than the atomic size. Therefore, one can replace the position operator $\mathbf{r}$ of the electron with that of the nucleus $\mathbf{R}$ in the vector potential, $\mathbf{A}(\mathbf{r},t) \simeq \mathbf{A}(\mathbf{R},t)$. This is the long-wavelength (or sometimes called the dipole) approximation. It basically means that the electromagnetic field is practically constant over the entire extent of the atom. Under this approximation the term proportional to $\mathbf{A}^2(\mathbf{R},t)$ can be also omitted, since it is a spatially constant term with zero matrix elements between different electronic states [143]. Note that $\mathbf{R}$ is the position operator of the nucleus and cannot induce any transition between electronic states. Then the Hamiltonian reads,

$$\mathcal{H}_{\rm mc} \approx \frac{\mathbf{p}^2}{2m} + V(\mathbf{r}-\mathbf{R}) - \frac{q}{m}\mathbf{p}\cdot\mathbf{A}(\mathbf{R},t), \tag{2.73}$$

where the last term accounts for the atom-field coupling in the long wavelength limit. This Hamiltonian is commonly referred to as the $\mathbf{p}\cdot\mathbf{A}$ Hamiltonian [87].

$\mathbf{d}\cdot\mathbf{E}$ Hamiltonian

In the previous section, I obtained the atom-field interaction Hamiltonian (2.73), where the vector potential appears instead of the electromagnetic fields. It is however convenient for later uses to obtain an equivalent atom-field interaction Hamiltonian in which the electromagnetic fields appear themselves. Consider the gauge function

$$\chi(\mathbf{r},t) = -(\mathbf{r}-\mathbf{R})\cdot\mathbf{A}(\mathbf{R},t), \tag{2.74}$$

under which the electromagnetic potentials are transformed as,

$$\begin{aligned}\mathbf{A}(\mathbf{r},t) &\to \mathbf{A}'(\mathbf{r},t) = \mathbf{A}(\mathbf{r},t) - \mathbf{A}(\mathbf{R},t),\\ \varphi(\mathbf{r},t) &\to \varphi'(\mathbf{r},t) = \varphi(\mathbf{r},t) + (\mathbf{r}-\mathbf{R})\cdot\frac{\partial}{\partial t}\mathbf{A}(\mathbf{R},t),\end{aligned} \tag{2.75}$$

according to Eq. (2.39). This is the Göppert-Mayer gauge [143]. Then the minimal coupling Hamiltonian (2.68) takes the form,

$$\begin{aligned}\mathcal{H}_{\mathrm{mc}} &= \frac{1}{2m}\left[\mathbf{p} - q\mathbf{A}'(\mathbf{r},t)\right]^2 + V(\mathbf{r}-\mathbf{R}) + q\varphi'(\mathbf{r},t)\\ &= \frac{1}{2m}\left[\mathbf{p} - q\mathbf{A}'(\mathbf{r},t)\right]^2 + V(\mathbf{r}-\mathbf{R}) + q(\mathbf{r}-\mathbf{R})\cdot\frac{\partial}{\partial t}\mathbf{A}(\mathbf{R},t).\end{aligned} \tag{2.76}$$

Recall that $\varphi(\mathbf{r},t) = 0$ in the original Coulomb gauge.

Defining the electric dipole operator

$$\mathbf{d} = q(\mathbf{r}-\mathbf{R}), \tag{2.77}$$

and using Eq. (2.38), the last term in Hamiltonian (2.76) can be re-expressed as $-\mathbf{d}\cdot\mathbf{E}(\mathbf{R},t)$, which is reminiscent of the interaction of a classical dipole moment with an electric field. As before, it is reasonable to consider the long wavelength limit and replace $\mathbf{r}$ with $\mathbf{R}$ in $\mathbf{A}'(\mathbf{r},t)$. The gauge-transformed vector potential then vanishes identically $\mathbf{A}'(\mathbf{R},t) = 0$ and Hamiltonian (2.76) reduces to,

$$\mathcal{H}_{\mathrm{mc}} = \frac{\mathbf{p}^2}{2m} + V(\mathbf{r}-\mathbf{R}) - \mathbf{d}\cdot\mathbf{E}(\mathbf{R},t). \tag{2.78}$$

This is the $\mathbf{d} \cdot \mathbf{E}$ Hamiltonian [87] and will be used in the subsequent sections to describe the atom-field coupling.

2.3.2 Fully Quantum Mechanical Approach

In the previous section 2.3.1, the atom-field interaction was described semi-classically. In this section, a fully quantum mechanical approach is presented, where both the atom and electromagnetic fields are treated on the same footing.

Second Quantization of the Electromagnetic Fields

My approach for the second quantization of the electromagnetic fields is the canonical quantization inside a finite box with perfectly conducting walls [143]. Maxwell's equations (2.37) can be obtained in the Coulomb gauge (2.40) from the electromagnetic Lagrangian density[3]

$$\mathcal{L}_{\mathrm{EM}} = \frac{\varepsilon_0}{2}\left[\left(\frac{\partial \mathbf{A}}{\partial t}\right)^2 - c^2\left(\boldsymbol{\nabla} \times \mathbf{A}\right)^2\right] = \frac{\varepsilon_0}{2}\left(\mathbf{E}^2 - c^2\mathbf{B}^2\right), \tag{2.79}$$

using the Euler-Lagrange equation

$$\frac{\partial \mathcal{L}_{\mathrm{EM}}}{\partial A_i} = \frac{\partial}{\partial t}\frac{\partial \mathcal{L}_{\mathrm{EM}}}{\partial(\partial A_i/\partial t)} + \sum_j \frac{\partial}{\partial r_j}\frac{\partial \mathcal{L}_{\mathrm{EM}}}{\partial(\partial A_i/\partial r_j)}, \tag{2.80}$$

where r_j are the three components of the position vector $\mathbf{r} = (x, y, z)$ [144]. Here the vector potential $\mathbf{A}$ ($\dot{\mathbf{A}} \equiv \partial\mathbf{A}/\partial t$) is the generalized coordinate (velocity). Defining the associated generalized conjugate momentum

$$\boldsymbol{\Pi} = \frac{\partial \mathcal{L}_{\mathrm{EM}}}{\partial \dot{\mathbf{A}}} = \varepsilon_0 \dot{\mathbf{A}} = -\varepsilon_0 \mathbf{E}, \tag{2.81}$$

the electromagnetic energy (or classical Hamiltonian) density can be obtained using the Legendre transformation $\mathcal{E}_{\mathrm{EM}} = \boldsymbol{\Pi} \cdot \dot{\mathbf{A}} - \mathcal{L}_{\mathrm{EM}}$ as follows

$$\mathcal{E}_{\mathrm{EM}} = \frac{1}{2\varepsilon_0}\left[\boldsymbol{\Pi}^2 + \varepsilon_0^2 c^2\left(\boldsymbol{\nabla} \times \mathbf{A}\right)^2\right] = \frac{\varepsilon_0}{2}\left(\mathbf{E}^2 + c^2\mathbf{B}^2\right). \tag{2.82}$$

Note that $\mathbf{E}^2 = \mathbf{E} \cdot \mathbf{E} = |E|^2$, and similarly for all other vectors.

[3] The electromagnetic Lagrangian density (2.79) can be recast as $\mathcal{L}_{\mathrm{EM}} = -\frac{1}{4\mu_0} F_{\mu\nu}F^{\mu\nu}$ in terms of the field strength tensor $F_{\mu,\nu} = \partial_\mu A_\nu - \partial_\nu A_\mu$, with A_μ being the component of the four-potential $A = (\varphi, -\mathbf{A}) = (0, -\mathbf{A})$.

Recall that the electromagnetic fields and the vector potential all satisfy the wave equation,

$$\left(\boldsymbol{\nabla}^2 - \frac{1}{c^2}\frac{\partial^2}{\partial t^2}\right)\left\{\begin{array}{l}\mathbf{E}(\mathbf{r},t)\\ \mathbf{B}(\mathbf{r},t)\\ \mathbf{A}(\mathbf{r},t)\end{array}\right\} = 0, \tag{2.83}$$

in the absence of any charge and current. These wave equations are obtained from Maxwell's equations (2.37); for instance taking the curl of the third Maxwell's equation and then using the first and last equations yields the wave equation for the electric field $\mathbf{E}$:

$$\begin{aligned}\boldsymbol{\nabla}\times(\boldsymbol{\nabla}\times\mathbf{E}) &= \boldsymbol{\nabla}(\boldsymbol{\nabla}\cdot\mathbf{E}) - \boldsymbol{\nabla}^2\mathbf{E} = -\boldsymbol{\nabla}^2\mathbf{E}\\ &= -\frac{\partial}{\partial t}(\boldsymbol{\nabla}\times\mathbf{B}) = -\frac{1}{c^2}\frac{\partial^2}{\partial t^2}\mathbf{E}.\end{aligned} \tag{2.84}$$

Likewise, substituting the electromagnetic fields with the electromagnetic potentials (2.38) in the last Maxwell equation and utilizing the Coulomb gauge (2.40) yields the wave equation for the vector potential $\mathbf{A}$. Then the vector potential can be expressed as the superposition of the monochromatic plane waves [145],

$$\begin{aligned}\mathbf{A}(\mathbf{r},t) &= \mathbf{A}_+(\mathbf{r},t) + \mathbf{A}_-(\mathbf{r},t)\\ &= \frac{-i}{\sqrt{V}}\sum_{\mathbf{k}}\left[\mathbf{A}_{\mathbf{k}}e^{i(\mathbf{k}\cdot\mathbf{r}-\omega_k t)} - \mathbf{A}^*_{\mathbf{k}}e^{-i(\mathbf{k}\cdot\mathbf{r}-\omega_k t)}\right]\\ &= \frac{-i}{\sqrt{V}}\sum_{\mathbf{k},\lambda}\left[A_{\mathbf{k},\lambda}e^{i(\mathbf{k}\cdot\mathbf{r}-\omega_k t)} - A^*_{\mathbf{k},\lambda}e^{-i(\mathbf{k}\cdot\mathbf{r}-\omega_k t)}\right]\mathbf{e}_\lambda,\end{aligned} \tag{2.85}$$

with the dispersion relation $\omega_k = c|\mathbf{k}| = ck$. Here, V is the volume of a box (with perfectly conducting walls) enclosing the electromagnetic fields and $\mathbf{A}_{\mathbf{k}} = \sum_\lambda A_{\mathbf{k},\lambda}\mathbf{e}_\lambda$ are complex coefficients (amplitudes) of the expansion, with $\mathbf{e}_\lambda$ being two mutually orthogonal unit polarization vectors $\mathbf{e}_1\cdot\mathbf{e}_2 = 0$ and $\mathbf{k}\cdot\mathbf{e}_\lambda = 0$. The latter follows from the Coulomb gauge $\boldsymbol{\nabla}\cdot\mathbf{A} = \mathbf{k}\cdot\mathbf{A}_\pm = 0$, implying that the vector potential is transverse $\mathbf{k}\cdot\mathbf{e}_\lambda = 0$. The

electromagnetic fields then read

$$\mathbf{E}(\mathbf{r},t) = \frac{1}{\sqrt{V}}\sum_{\mathbf{k},\lambda}\omega_k\left[A_{\mathbf{k},\lambda}e^{i(\mathbf{k}\cdot\mathbf{r}-\omega_k t)} + A^*_{\mathbf{k},\lambda}e^{-i(\mathbf{k}\cdot\mathbf{r}-\omega_k t)}\right]\mathbf{e}_\lambda,$$
$$\mathbf{B}(\mathbf{r},t) = \frac{1}{\sqrt{V}}\sum_{\mathbf{k},\lambda}\left[A_{\mathbf{k},\lambda}e^{i(\mathbf{k}\cdot\mathbf{r}-\omega_k t)} + A^*_{\mathbf{k},\lambda}e^{-i(\mathbf{k}\cdot\mathbf{r}-\omega_k t)}\right]\mathbf{k}\times\mathbf{e}_\lambda. \tag{2.86}$$

The total electromagnetic field energy is obtained from the electromagnetic energy density (2.82) as

$$E_{\rm EM} = \int d\mathbf{r}\ \mathcal{E}_{\rm EM}. \tag{2.87}$$

Substituting the electromagnetic fields (2.86) in the electromagnetic energy density $\mathcal{E}_{\rm EM}$ and using the orthonormality of the plane waves $\frac{1}{V}\int d\mathbf{r}e^{i(\mathbf{k}-\mathbf{k}')\cdot\mathbf{r}} = \delta_{\mathbf{k},\mathbf{k}'}$, the total electromagnetic energy $E_{\rm EM}$ then reads,

$$E_{\rm EM} = \varepsilon_0\sum_{\mathbf{k},\lambda}\omega_k^2\left(A^*_{\mathbf{k},\lambda}A_{\mathbf{k},\lambda} + A_{\mathbf{k},\lambda}A^*_{\mathbf{k},\lambda}\right) = 2\varepsilon_0\sum_{\mathbf{k},\lambda}\omega_k^2 A^*_{\mathbf{k},\lambda}A_{\mathbf{k},\lambda}. \tag{2.88}$$

Introducing new real canonical variables [145],

$$Q_{\mathbf{k},\lambda} = \sqrt{\varepsilon_0}(A_{\mathbf{k},\lambda} + A^*_{\mathbf{k},\lambda}),$$
$$P_{\mathbf{k},\lambda} = -i\sqrt{\varepsilon_0}\omega_k(A_{\mathbf{k},\lambda} - A^*_{\mathbf{k},\lambda}), \tag{2.89}$$

the electromagnetic field energy $E_{\rm EM}$ can be recast as

$$E_{\rm EM} = \sum_{\mathbf{k},\lambda}\left(\frac{P^2_{\mathbf{k},\lambda}}{2} + \frac{1}{2}\omega_k^2 Q^2_{\mathbf{k},\lambda}\right). \tag{2.90}$$

This is the sum of energies of uncoupled simple harmonic oscillators with unit masses.

The (canonical) second quantization of the electromagnetic field energy (2.90) basically amounts to promoting $P_{\mathbf{k},\lambda}$ and $Q_{\mathbf{k},\lambda}$ to quantum operators[4],

$$P_{\mathbf{k},\lambda} \to \hat{P}_{\mathbf{k},\lambda}, \qquad Q_{\mathbf{k},\lambda} \to \hat{Q}_{\mathbf{k},\lambda}, \tag{2.91}$$

[4] Here I use the "hat" notation to distinguish quantum operators from classical quantities.

with the commutation relation [145]

$$[\hat{Q}_{\mathbf{k},\lambda}, \hat{P}_{\mathbf{k}',\lambda'}] = i\hbar\delta_{\mathbf{k},\mathbf{k}'}\delta_{\lambda,\lambda'}. \tag{2.92}$$

This yields the second quantized Hamiltonian

$$H_{\mathrm{EM}} = \sum_{\mathbf{k},\lambda}\left(\frac{\hat{P}^2_{\mathbf{k},\lambda}}{2} + \frac{1}{2}\omega_k^2\hat{Q}^2_{\mathbf{k},\lambda}\right). \tag{2.93}$$

Note that E_{EM} has been replaced by H_{EM} to emphasize that Eq. (2.93) is the quantum mechanical Hamiltonian. It is now convenient to introduce operators

$$\begin{aligned}
\hat{a}_{\mathbf{k},\lambda} &= \sqrt{\frac{\omega_k}{2\hbar}}\left(\hat{Q}_{\mathbf{k},\lambda} + \frac{i\hat{P}_{\mathbf{k},\lambda}}{\omega_k}\right) = \sqrt{\frac{2\varepsilon_0\omega_k}{\hbar}}\hat{A}_{\mathbf{k},\lambda}, \\
\hat{a}^\dagger_{\mathbf{k},\lambda} &= \sqrt{\frac{\omega_k}{2\hbar}}\left(\hat{Q}_{\mathbf{k},\lambda} - \frac{i\hat{P}_{\mathbf{k},\lambda}}{\omega_k}\right) = \sqrt{\frac{2\varepsilon_0\omega_k}{\hbar}}\hat{A}^\dagger_{\mathbf{k},\lambda},
\end{aligned} \tag{2.94}$$

where the last equalities in both operators follow from Eq. (2.89), by also promoting $A_{\mathbf{k},\lambda}$ ($A^*_{\mathbf{k},\lambda}$) to an operator $\hat{A}_{\mathbf{k},\lambda}$ ($\hat{A}^\dagger_{\mathbf{k},\lambda}$). The operator $\hat{a}_{\mathbf{k},\lambda}$ ($\hat{a}^\dagger_{\mathbf{k},\lambda}$) is the annihilation (creation) operator of the simple harmonic oscillator; here it destroys (creates) a photon, the quantum of the electromagnetic field, in the mode corresponding to $\{\mathbf{k},\lambda\}$. Substituting Eq. (2.94) in the Hamiltonian (2.93) yields the familiar simple harmonic oscillator Hamiltonian expressed in terms of the ladder operators,

$$H_{\mathrm{EM}} = \sum_{\mathbf{k},\lambda}\hbar\omega_k\left(\hat{a}^\dagger_{\mathbf{k},\lambda}\hat{a}_{\mathbf{k},\lambda} + \frac{1}{2}\right). \tag{2.95}$$

The second quantized electromagnetic fields can be readily obtained by substituting Eq. (2.94) in (2.86), yielding

$$\begin{aligned}
\hat{\mathbf{E}}(\mathbf{r},t) &= \sum_{\mathbf{k},\lambda}\mathcal{E}_k\left[\hat{a}_{\mathbf{k},\lambda}e^{i(\mathbf{k}\cdot\mathbf{r}-\omega_k t)} + \hat{a}^\dagger_{\mathbf{k},\lambda}e^{-i(\mathbf{k}\cdot\mathbf{r}-\omega_k t)}\right]\mathbf{e}_\lambda, \\
\hat{\mathbf{B}}(\mathbf{r},t) &= \sum_{\mathbf{k},\lambda}\frac{\mathcal{E}_k}{\omega_k}\left[\hat{a}_{\mathbf{k},\lambda}e^{i(\mathbf{k}\cdot\mathbf{r}-\omega_k t)} + \hat{a}^\dagger_{\mathbf{k},\lambda}e^{-i(\mathbf{k}\cdot\mathbf{r}-\omega_k t)}\right]\mathbf{k}\times\mathbf{e}_\lambda,
\end{aligned} \tag{2.96}$$

where $\mathcal{E}_k = \sqrt{\hbar\omega_k/2\varepsilon_0 V}$ is the electric field of a single photon.

The time evolution of the ladder operators is given by the Heisenberg equation of motion; for instance,

$$i\hbar\partial_t \hat{a}_{\mathbf{k},\lambda}(t) = [\hat{a}_{\mathbf{k},\lambda}(t), H_{\rm EM}] = \hbar\omega_k \hat{a}_{\mathbf{k},\lambda}(t), \tag{2.97}$$

which yields

$$\hat{a}_{\mathbf{k},\lambda}(t) = \hat{a}_{\mathbf{k},\lambda} e^{-i\omega_k t}, \tag{2.98}$$

and similarly $\hat{a}^\dagger_{\mathbf{k},\lambda}(t) = \hat{a}^\dagger_{\mathbf{k},\lambda} e^{i\omega_k t}$. Nonetheless, the (photon) number operator $\hat{n}_{\mathbf{k},\lambda} = \hat{a}^\dagger_{\mathbf{k},\lambda}(t)\hat{a}_{\mathbf{k},\lambda}(t)$ is constant, which also follows from the fact that the number operator commutes with the Hamiltonian

$$H_{\rm EM} = \sum_{\mathbf{k},\lambda} \hbar\omega_k (\hat{n}_{\mathbf{k},\lambda} + 1/2); \tag{2.99}$$

that is, $[\hat{n}_{\mathbf{k},\lambda}, H_{\rm EM}] = 0$. This implies that the Hamiltonian and number operator have simultaneous eigenvectors. The stationary states of the Hamiltonian $H_{\rm EM}$ are therefore the tensor product (denoted by $\otimes$) of single-harmonic oscillator number states $|n_{\mathbf{k},\lambda}\rangle$,

$$|\{n_{\mathbf{k},\lambda}\}\rangle = \bigotimes_{\mathbf{k},\lambda} |n_{\mathbf{k},\lambda}\rangle = \prod_{\mathbf{k},\lambda} \frac{1}{\sqrt{n_{\mathbf{k},\lambda}!}} \left(\hat{a}^\dagger_{\mathbf{k},\lambda}\right)^{n_{\mathbf{k},\lambda}} |0\rangle\,, \tag{2.100}$$

where $|0\rangle$ is the vacuum. The occupation number state $|\{n_{\mathbf{k},\lambda}\}\rangle$ means that there are $n_{\mathbf{k}_1,\lambda_1}$, $n_{\mathbf{k}_2,\lambda_2}$, ... photons in the corresponding modes $\{\mathbf{k}_1,\lambda_1\}$, $\{\mathbf{k}_2,\lambda_2\}$, ...

Cavity QED: Jaynes-Cummings Model

Having second quantized the electromagnetic field (2.96) within a perfectly conducting box, I now turn my attention to describing the atom-field interaction quantum mechanically. This box can be envisaged to be a high-Q cavity with highly reflective mirrors, such as a Fabry-Perot resonator. The interaction of an atom with a quantized electromagnetic field (2.96) of a cavity is described by the Hamiltonian density [87],

$$\mathcal{H} = \mathcal{H}_{\rm a} + H_{\rm EM} + \mathcal{H}_{\rm I}, \tag{2.101}$$

where

$$\mathcal{H}_{\rm a} = \frac{\mathbf{P}^2}{2M} + \frac{\mathbf{p}^2}{2m} + V(\mathbf{r}-\mathbf{R}), \tag{2.102}$$

is the atomic Hamiltonian density with M, $\mathbf{P}$, and $\mathbf{R}$ being the mass, center-of-mass momentum operator, and center-of-mass position operator of the atom, respectively. Here, $H_{\rm EM}$ is the Hamiltonian of the free electromagnetic fields, Eq. (2.99). The atom-field interaction Hamiltonian in the $\mathbf{d}\cdot\mathbf{E}$ (and Schrödinger) picture and in the long-wavelength approximation reads,

$$\mathcal{H}_{\rm I} = -\sum_{\mathbf{k},\lambda} \mathcal{E}_k \left[\hat{a}_{\mathbf{k},\lambda} f_{\mathbf{k}}(\mathbf{R}) + \hat{a}^\dagger_{\mathbf{k},\lambda} f^*_{\mathbf{k}}(\mathbf{R})\right] \mathbf{d}\cdot\mathbf{e}_\lambda, \tag{2.103}$$

where $f_{\mathbf{k}}(\mathbf{r})$ is the cavity-mode function (which is, for instance, $f_{\mathbf{k}}(\mathbf{r}) = \sin(\mathbf{k}\cdot\mathbf{r})$ for a standing cavity and $f_{\mathbf{k}}(\mathbf{r}) = e^{i\mathbf{k}\cdot\mathbf{r}}$ for a ring cavity).

The first term in the atomic Hamiltonian density $\mathcal{H}_{\rm a}$ (2.102) is the kinetic energy associated with the center-of-mass motion of the atom,

$$\frac{\mathbf{P}^2}{2M}\left|\mathbf{P}\right\rangle = \frac{(\hbar\mathbf{K})^2}{2M}\left|\mathbf{P}\right\rangle, \tag{2.104}$$

where $|\mathbf{P}\rangle$ ($\hbar\mathbf{K}$) is the eigenvector (eigenvalue) of the center-of-mass momentum operator $\mathbf{P}$. The last two terms describe the motion of the electron around the nucleus under the Coulomb potential $V(\mathbf{r}-\mathbf{R})$. They form a simple Hamiltonian for the internal structure of the atom,

$$\left[\frac{\mathbf{p}^2}{2m} + V(\mathbf{r}-\mathbf{R})\right]\left|\tau\right\rangle = \varepsilon_\tau \left|\tau\right\rangle, \tag{2.105}$$

with eigenstates $|\tau\rangle$ and corresponding eigenenergies ε_τ. The complete atomic basis can be then expressed as

$$\left|\mathbf{P},\tau\right\rangle \equiv \left|\mathbf{P}\right\rangle \otimes \left|\tau\right\rangle. \tag{2.106}$$

One possible basis for the entire system is the tensor product of the atomic (2.106) and photonic (2.100) states [143],

$$\left|\mathbf{P},\tau,n_1,n_2,\cdots\right\rangle \equiv \left|\mathbf{P}\right\rangle \otimes \left|\tau\right\rangle \otimes \left|n_1,n_2,\cdots\right\rangle, \tag{2.107}$$

where index j in n_j is a collective index for $\{\mathbf{k}_j, \lambda_j\}$.

In the following, a few simplifying assumptions will be made [143, 146]. Relaxing these assumptions will be the subject of next chapters. First, the atom is assumed to be at rest at $\mathbf{R} = 0$; consequently the center-of-mass motion of the atom is irrelevant. Second, I assume that only one of the cavity modes $\hat{a} \equiv \hat{a}_{\mathbf{k},\lambda}$ (with definite wave number $|\mathbf{k}| = \omega/c$ and polarization λ) is near-resonant with an atomic transition $|g\rangle \leftrightarrow |e\rangle$ (with the transition frequency $\hbar\omega_0 \equiv \varepsilon_e - \varepsilon_g$) and can induce this transition; that is, $\omega \sim \omega_0$ and $\langle g| \mathbf{d} \cdot \mathbf{e}_\lambda |e\rangle \neq 0$. Then all the cavity modes except $\hat{a}$ can be omitted. And finally, cavity mirrors are presumed to be almost perfect; that is, the decay of the cavity mode is negligible. Under these simplifying assumptions, the tensor-product basis (2.107) reduces to

$$|\tau, n\rangle = \{|g\rangle, |e\rangle\} \otimes \{|0\rangle, |1\rangle, |2\rangle, \cdots\}, \tag{2.108}$$

and the atom-field interaction Hamiltonian (2.103) becomes

$$\mathcal{H}_{\mathrm{I}} = -\mathcal{E}_k f_{\mathbf{k}}(0) \mathbf{d} \cdot \mathbf{e}_\lambda \left(\hat{a} + \hat{a}^\dagger\right) = -\mathcal{E}_k f_{\mathbf{k}}(0) \mathbb{1}_{\mathrm{a}} \mathbf{d} \cdot \mathbf{e}_\lambda \mathbb{1}_{\mathrm{a}} \left(\hat{a} + \hat{a}^\dagger\right) = \hbar \mathscr{G}_{ge} \left(\sigma_+ + \sigma_-\right) \left(\hat{a} + \hat{a}^\dagger\right), \tag{2.109}$$

where

$$\hbar \mathscr{G}_{ge} \equiv -\mathcal{E}_k f_{\mathbf{k}}(0) \langle g| \mathbf{d} \cdot \mathbf{e}_\lambda |e\rangle = -\mathcal{E}_k f_{\mathbf{k}}(0) \langle e| \mathbf{d} \cdot \mathbf{e}_\lambda |g\rangle, \tag{2.110}$$

is the single atom-photon coupling strength, $\mathbb{1}_{\mathrm{a}} = |g\rangle\langle g| + |e\rangle\langle e|$ is the identity in the atomic-state space, and $\sigma_+ = \sigma_-^\dagger = |e\rangle\langle g|$ are the atomic transition (or raising and lowering) operators. Note that $\langle g| \mathbf{d} \cdot \mathbf{e}_\lambda |g\rangle = \langle e| \mathbf{d} \cdot \mathbf{e}_\lambda |e\rangle = 0$ due to the parity (atomic states $\{|\tau\rangle\}$ have well-defined parities while the dipole operator $\mathbf{d} \propto \mathbf{r}$ is odd under parity[5]) and I further assumed $f_{\mathbf{k}}(0) = f_{\mathbf{k}}^*(0)$ [146].

The atom-field interaction Hamiltonian (2.109) can be further simplified by noting that the terms $\sigma_+ \hat{a}^\dagger$ and $\sigma_- \hat{a}$ are not energy conserving: the atom is excited from the ground state

[5] The parity operator $\hat{\mathcal{P}}$ commutes with the atomic Hamiltonian $\mathcal{H}_{\mathrm{a}}$ (2.102): $[\hat{\mathcal{P}}, \mathcal{H}_{\mathrm{a}}] = 0$, implying that they have simultaneous eigenstates. This in turn means that atomic states have definite parities. For instance, the atomic s (p) orbital is even (odd) under parity [147].

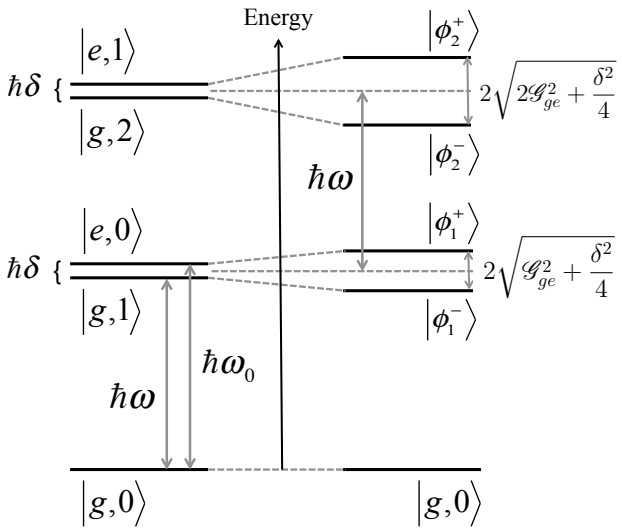

Figure 2.3: The Jaynes-Cummings ladder. The left side depicts the uncoupled states $\{|g,n\rangle, |e,n-1\rangle\}$, Eq. (2.113), and the right side the polariton states $\{|\phi_n^{\pm}\rangle\}$, Eq. (2.116).

$|g\rangle$ into the excited state $|e\rangle$ and meanwhile a photon is also created, and vice versa. Such processes violate energy conservation by an energy on the order of a two-photon energy $2\hbar\omega$ and can therefore be omitted in comparison to the near energy conserving processes $\sigma_+\hat{a}$ and $\sigma_-\hat{a}^\dagger$, where the atom is excited while a photon is annihilated and the opposite process [146]. This is equivalent to the rotating wave approximation [87]. Then the atom-field interaction Hamiltonian (2.109) reduces to

$$\mathcal{H}_{\rm I} \simeq \hbar\mathscr{G}_{ge}\left(\sigma_+\hat{a}+\sigma_-\hat{a}^\dagger\right). \tag{2.111}$$

Dropping constant terms, the total Hamiltonian can be recast as

$$\mathcal{H}_{\rm JC} = \hbar\omega_0\sigma_+\sigma_- + \hbar\omega\hat{a}^\dagger\hat{a} + \hbar\mathscr{G}_{ge}\left(\sigma_+\hat{a}+\sigma_-\hat{a}^\dagger\right), \tag{2.112}$$

which is the celebrated Jaynes-Cummings (JC) Hamiltonian [93].

The JC Hamiltonian (2.112) can be diagonalized in a reduced tensor-product basis (2.108). Other than the ground state $|g,0\rangle$, all states $\{|g,n\rangle, |e,n-1\rangle\}$ are arranged in closely spaced doublet manifolds M_n; see Fig. 2.3. These are the eigenstates of the uncou-

pled atom and field Hamiltonians $\mathcal{H}_{\rm JC} - \mathcal{H}_{\rm I}$,

$$\begin{aligned}\left(\hbar\omega_0\sigma_+\sigma_- + \hbar\omega\hat{a}^\dagger\hat{a}\right)|g,n\rangle &= n\hbar\omega\,|g,n\rangle\,,\\ \left(\hbar\omega_0\sigma_+\sigma_- + \hbar\omega\hat{a}^\dagger\hat{a}\right)|e,n-1\rangle &= \hbar\left[\omega_0 + (n-1)\omega\right]|e,n-1\rangle = \hbar(n\omega-\delta)\,|e,n-1\rangle\,,\end{aligned} \tag{2.113}$$

where $\delta \equiv \omega - \omega_0 \ll \{\omega, \omega_0\}$ is the detuning between the bare cavity and atomic transition frequencies. The atom-field interaction Hamiltonian $\mathcal{H}_{\rm I}$ (2.111) can solely couple states within a single manifold M_n and it is therefore sufficient to diagonalize $\mathcal{H}_{\rm JC}$ in one generic two-dimensional manifold M_n. In this subspace, the JC Hamiltonian in matrix form reads

$$\mathcal{H}_{\rm JC} = \hbar\begin{pmatrix} n\omega & \mathscr{G}_{ge}\sqrt{n} \\ \mathscr{G}_{ge}\sqrt{n} & n\omega-\delta\end{pmatrix}, \tag{2.114}$$

which can be readily diagonalized to yields the eigen-energies

$$\varepsilon_n^{\pm} = \hbar\left[n\omega - \frac{\delta}{2} \pm \sqrt{\mathscr{G}_{ge}^2 n + \frac{\delta^2}{4}}\right], \tag{2.115}$$

and corresponding eigenvectors

$$\begin{pmatrix}|\phi_n^+\rangle \\ |\phi_n^-\rangle\end{pmatrix} = \begin{pmatrix}\cos\theta_n & \sin\theta_n \\ -\sin\theta_n & \cos\theta_n\end{pmatrix}\begin{pmatrix}|g,n\rangle \\ |e,n-1\rangle\end{pmatrix}, \tag{2.116}$$

with the mixing angle

$$\tan 2\theta_n = \frac{2\mathscr{G}_{ge}\sqrt{n}}{\delta}. \tag{2.117}$$

The eigenvectors $|\phi_n^{\pm}\rangle$ are entangled superpositions of atomic and photonic excitations and cannot be decomposed as a tensor product of atomic and photonic states. They are frequently referred to as polariton states in the literature. The polariton states and energies are schematically illustrated in Fig. 2.3 along with uncoupled states and energies.

2.3.3 Emergent Geometric Gauge Potentials

In this section, I will first show in an abstract way how synthetic gauge potentials can emerge in a semi-classical atom-field interaction Hamiltonian following the recent review article by

Goldman *et al.* [57]. Consider the Hamiltonian density of a single atom with $\mathcal{N}$ internal states $\{|m_j\rangle\}$ interacting with electromagnetic fields,

$$\mathcal{H} = \frac{\mathbf{P}^2}{2M}\mathbb{1}_{\mathcal{N}} + \check{\mathcal{H}}_{\text{int}}(\mathbf{R}, t), \tag{2.118}$$

where $\mathbf{P}$ ($\mathbf{R}$) are the center-of-mass momentum (position) operator and $\check{\mathcal{H}}_{\text{int}}(\mathbf{R}, t)$ describes the "internal" dynamics of the atom coupled to the electromagnetic fields (note that it also includes the free internal atomic Hamiltonian) and depends parametrically on the center-of-mass position $\mathbf{R}$. The internal Hamiltonian density $\check{\mathcal{H}}_{\text{int}}$ can be diagonalized to yield dressed states $\{|\phi_j(\mathbf{R}, t)\rangle\}$,

$$\check{\mathcal{H}}_{\text{int}}(\mathbf{R}, t) = \sum_{j,j'=1}^{\mathcal{N}} |m_j\rangle \, \mathcal{H}_{\text{int}}^{jj'}(\mathbf{R}, t) \, \langle m_{j'}| = \sum_{j=1}^{\mathcal{N}} |\phi_j(\mathbf{R}, t)\rangle \, \varepsilon_j(\mathbf{R}, t) \, \langle \phi_j(\mathbf{R}, t)| \,, \tag{2.119}$$

where $\mathcal{H}_{\text{int}}^{jj'} = \langle m_j| \, \check{\mathcal{H}}_{\text{int}} \, |m_{j'}\rangle$ and $\varepsilon_j = \langle \phi_j| \, \check{\mathcal{H}}_{\text{int}} \, |\phi_j\rangle$ is the dressed energy [148]. In other words, the internal Hamiltonian density can be diagonalized by the unitary transformation $\check{\mathscr{U}}(\mathbf{R}, t)$ constructed from the dressed states as $\check{\mathscr{U}}^\dagger \check{\mathcal{H}}_{\text{int}} \check{\mathscr{U}} = \check{\varepsilon}$, where $\check{\varepsilon}$ is a diagonal matrix of the dressed energies. The dressed states are related to the bare atomic states through $|\phi_j(\mathbf{R}, t)\rangle = \check{\mathscr{U}}(\mathbf{R}, t) \, |m_j\rangle$.

Since the dressed states form a complete basis, a general wavevector can be expanded in the dressed-state basis,

$$|\psi\rangle = \sum_j \phi_j(\mathbf{R}, t) \, |\phi_j(\mathbf{R}, t)\rangle = \check{\mathscr{U}} \sum_j \phi_j(\mathbf{R}, t) \, |m_j\rangle = \check{\mathscr{U}} \left|\tilde{\psi}\right\rangle, \tag{2.120}$$

where $\phi_j(\mathbf{R}, t)$ are corresponding wavefunctions for the center-of-mass motion of the atom in jth internal state. Substituting Eq. (2.120) in the Schrödinger equation $i\hbar\partial_t \, |\psi\rangle = \mathcal{H} \, |\psi\rangle$ yields $i\hbar\partial_t \left|\tilde{\psi}\right\rangle = \tilde{\mathcal{H}} \left|\tilde{\psi}\right\rangle$ with

$$\tilde{\mathcal{H}} = \check{\mathscr{U}}^\dagger \mathcal{H} \check{\mathscr{U}} - i\hbar \check{\mathscr{U}}^\dagger \partial_t \check{\mathscr{U}}. \tag{2.121}$$

Recalling that the unitary transformation $\check{\mathscr{U}}$ diagonalizes the internal Hamiltonian density $\check{\mathcal{H}}_{\text{int}}$, it suffices to determine how the center-of-mass momentum $\mathbf{P}$ is transformed under this

unitary transformation. Making use of Eq. (2.71), one obtains

$$[\mathbf{P}, \check{\mathscr{U}}] = \mathbf{P}\check{\mathscr{U}} - \check{\mathscr{U}}\mathbf{P} = -i\hbar\boldsymbol{\nabla}\check{\mathscr{U}}, \tag{2.122}$$

implying that the center-of-mass momentum transforms as $\check{\mathscr{U}}^\dagger \mathbf{P} \check{\mathscr{U}} = \mathbf{P} - i\hbar\check{\mathscr{U}}^\dagger\boldsymbol{\nabla}\check{\mathscr{U}}$. Then the effective Hamiltonian density $\tilde{\mathcal{H}}$ takes the form

$$\tilde{\mathcal{H}} = \frac{1}{2M}\left(\mathbf{P}\mathbb{1}_{\mathcal{N}} - i\hbar\check{\mathscr{U}}^\dagger\boldsymbol{\nabla}\check{\mathscr{U}}\right)^2 + \check{\varepsilon} - i\hbar\check{\mathscr{U}}^\dagger\partial_t\check{\mathscr{U}}, \tag{2.123}$$

which resembles the minimal coupling Hamiltonian (2.51) and (2.60). Then the gauge potentials can be identified as

$$\begin{aligned} q^*\check{\boldsymbol{\mathcal{A}}}(\mathbf{R},t) &= i\hbar\check{\mathscr{U}}^\dagger(\mathbf{R},t)\boldsymbol{\nabla}\check{\mathscr{U}}(\mathbf{R},t) = q^*\sum_{j,j'}|m_j\rangle\,\boldsymbol{\mathcal{A}}_{jj'}\,\langle m_{j'}|\,, \\ q^*\check{\varphi}(\mathbf{R},t) &= -i\hbar\check{\mathscr{U}}^\dagger(\mathbf{R},t)\partial_t\check{\mathscr{U}}(\mathbf{R},t) = q^*\sum_{j,j'}|m_j\rangle\,\varphi_{jj'}\,\langle m_{j'}|\,, \end{aligned} \tag{2.124}$$

with the matrix elements

$$\begin{aligned} q^*\boldsymbol{\mathcal{A}}_{jj'}(\mathbf{R},t) &= i\hbar\,\langle\phi_j(\mathbf{R},t)|\,\boldsymbol{\nabla}\,|\phi_{j'}(\mathbf{R},t)\rangle\,, \\ q^*\varphi_{jj'}(\mathbf{R},t) &= -i\hbar\,\langle\phi_j(\mathbf{R},t)|\,\partial_t\,|\phi_{j'}(\mathbf{R},t)\rangle\,. \end{aligned} \tag{2.125}$$

These gauge potentials can be envisaged as Berry connections; see also Appendix A for a short review of the Adiabatic Theorem and Berry phase. By properly dressing an atom via light, the artificial gauge potentials can therefore emerge for the center-of-mass motion of the atom according to Eq. (2.125).

Synthetic SO Coupling in the Λ Scheme

It is possible in some cases to derive synthetic gauge potentials directly in a Hamiltonian, without the need to obtain dressed states and compute Eq. (2.125). The most common case is when radiation fields are monochromatic plane waves. Consider a three-level atom in the Λ scheme interacting with two counter-propagating laser beams, with positive frequency components $\mathbf{E}_+^{(1)} = E_0^{(1)}e^{i(k_1 z-\omega_1 t)}\mathbf{e}_1$ and $\mathbf{E}_+^{(2)} = E_0^{(2)}e^{i(-k_2 z-\omega_2 t)}\mathbf{e}_2$; see Fig. 2.4. Here $k_j = \omega_j/c$ are the wavenumber of lasers expressed in terms of their frequencies ω_j and $\mathbf{e}_j$ are the

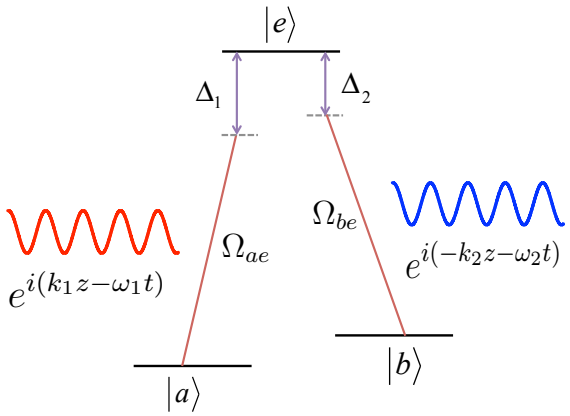

Figure 2.4: Schematic of the Λ scheme. Two low-lying atomic levels $|a\rangle$ and $|b\rangle$ are coupled in the Λ scheme to an excited state $|e\rangle$ by two counter-propagating laser beams $\mathbf{E}_+^{(1)} = E_0^{(1)} e^{i(k_1 z-\omega_1 t)}\mathbf{e}_1$ and $\mathbf{E}_+^{(2)} = E_0^{(2)} e^{i(-k_2 z-\omega_2 t)}\mathbf{e}_2$ with Rabi frequencies Ω_{ae} and Ω_{be}, respectively. The transitions are detuned from resonance by Δ_1 and Δ_2.

polarization vectors. The states $\{|a\rangle, |b\rangle, |e\rangle\}$ are arbitrary internal states of the atom whose energies satisfy the relations $\varepsilon_e > \{\varepsilon_b, \varepsilon_a\}$ and $\{\varepsilon_{ea}, \varepsilon_{eb}\} \gg \varepsilon_{ba}$, where $\varepsilon_{\tau\tau'} \equiv \varepsilon_\tau - \varepsilon_{\tau'}$. For example, the states $|a\rangle$ and $|b\rangle$ might be energy levels in the same hyperfine manifold with an energy separation on the order of MHz while the state $|e\rangle$ could be an excited electronic level with an energy separation on the order of THz. The first (second) laser propagates to the right (left) along z direction and induces solely the $|a\rangle \leftrightarrow |e\rangle$ ($|b\rangle \leftrightarrow |e\rangle$) transition.

Restricting to the z direction, the single-particle Hamiltonian density in the $\mathbf{d}\cdot\mathbf{E}$ picture and the rotating-wave approximation reads [149],

$$\mathcal{H}_\Lambda = \frac{\hbar^2 q_z^2}{2M}\mathbb{1}_3 + \sum_\tau \varepsilon_\tau \sigma_{\tau\tau} + \hbar\Big[\Omega_{ae} e^{i(k_1 z-\omega_1 t)}\sigma_{ea} + \Omega_{be} e^{i(-k_2 z-\omega_2 t)}\sigma_{eb} + \text{H.c.}\Big], \tag{2.126}$$

where $\hbar\Omega_{ae} = E_0^{(1)} \langle a| \mathbf{d}\cdot\mathbf{e}_1 |e\rangle$ and $\hbar\Omega_{be} = E_0^{(2)} \langle b| \mathbf{d}\cdot\mathbf{e}_2 |e\rangle$ are the maximum Rabi frequencies for the corresponding transitions and assumed to be real. Here, $P_z = \hbar q_z$ is the center-of-mass momentum of the atom along the z direction, M the mass of the atom, $\mathbb{1}_3$ the three-by-three identity matrix in the internal-state space, and $\sigma_{\tau\tau'} = |\tau\rangle\langle\tau'|$. It is convenient to set to the

excited-state energy ε_e as the reference and recast the atomic internal energy as

$$\sum_{\tau} \varepsilon_\tau \sigma_{\tau\tau} = \varepsilon_e \mathbb{1}_3 - \hbar\omega_{ea}\sigma_{aa} - \hbar\omega_{eb}\sigma_{bb}, \tag{2.127}$$

where $\hbar\omega_{ea} = \varepsilon_e - \varepsilon_a$ and $\hbar\omega_{eb} = \varepsilon_e - \varepsilon_b$ are the atomic transition frequencies. In order to remove the explicit time dependence in the Hamiltonian $\mathcal{H}_\Lambda$, one can transfer the Hamiltonian (2.126) to the rotating frame of lasers by applying the unitary transformation $\mathscr{U}_\Lambda = \exp\left[-i(\omega_1 t\sigma_{aa} + \omega_2 t\sigma_{bb})\right]$ via the relation[6] $\tilde{\mathcal{H}}_\Lambda = \mathscr{U}_\Lambda \mathcal{H}_\Lambda \mathscr{U}_\Lambda^\dagger + i\hbar(\partial_t \mathscr{U}_\Lambda)\mathscr{U}_\Lambda^\dagger$. Considering that $\mathscr{U}_\Lambda \sigma_{ea} \mathscr{U}_\Lambda^\dagger = e^{i\omega_1 t}\sigma_{ea}$ and $\mathscr{U}_\Lambda \sigma_{eb} \mathscr{U}_\Lambda^\dagger = e^{i\omega_2 t}\sigma_{eb}$, the Hamiltonian in the rotating frame of lasers then reads as,

$$\tilde{\mathcal{H}}_\Lambda = \frac{\hbar^2 q_z^2}{2M}\mathbb{1}_3 + \hbar\Delta_a\sigma_{aa} + \hbar\Delta_b\sigma_{bb} + \hbar\left[\Omega_{ae}e^{ik_1 z}\sigma_{ea} + \Omega_{be}e^{-ik_2 z}\sigma_{eb} + \text{H.c.}\right], \tag{2.128}$$

where $\Delta_a = \omega_1 - \omega_{ea}$ and $\Delta_b = \omega_2 - \omega_{eb}$.

If the laser beams are far off-resonance from atomic transitions then the adiabatic condition holds, and therefore the atomic excited state $|e\rangle$ reaches its steady state quickly and can be adiabatically eliminated. More precisely, the adiabatic condition holds when $|\tilde{\delta}| \ll \Delta$, where $\tilde{\delta} \equiv \Delta_b - \Delta_a$ is the two-photon detuning and $\Delta \equiv (\Delta_a + \Delta_b)/2$ [149]. After adiabatic elimination of the atomic excited state, the effective Hamiltonian for the ground pseudospin states $\{|a\rangle, |b\rangle\}$ then becomes[7] [67],

$$\tilde{\mathcal{H}}_{\text{eff}} = \frac{\hbar^2 q_z^2}{2M}\mathbb{1}_2 + \frac{1}{2}\hbar\delta\check{\sigma}_z + \frac{1}{2}\hbar\Omega_R\left[e^{i(k_1+k_2)z}\sigma_{ba} + \text{H.c.}\right], \tag{2.129}$$

where $\check{\sigma}_z = |b\rangle\langle b| - |a\rangle\langle a|$ is the third Pauli matrix, $\Omega_R = 2\Omega_{ae}\Omega_{be}/\Delta$ the Raman (or two-photon Raman-Rabi) frequency, and

$$\delta = \left(\Delta_b + \frac{\Omega_{be}^2}{\Delta}\right) - \left(\Delta_a + \frac{\Omega_{ae}^2}{\Delta}\right) = \tilde{\delta} + \frac{1}{\Delta}\left(\Omega_{be}^2 - \Omega_{ae}^2\right), \tag{2.130}$$

[6] This relation can be readily proven by considering the time-depend Schrödinger equation. If the wavefunction ψ satisfies the time-depend Schrödinger equation $i\hbar\partial_t\psi = H\psi$, then the transferred wave function $\psi \to \tilde{\psi} = \mathscr{U}\psi$ satisfies the equation $i\hbar\partial_t\tilde{\psi} = \tilde{H}\tilde{\psi}$, with $\tilde{H} = \mathscr{U}H\mathscr{U}^\dagger + i\hbar(\partial_t\mathscr{U})\mathscr{U}^\dagger$.

[7] See Appendix A for a general review of the Adiabatic Theorem. See also Appendix B for details of adiabatic elimination of the atomic excited state in the Λ scheme in the cavity QED framework.

the modified two-photon detuning due to ac Stark shifts $\{\Omega_{ae}^2/\Delta, \Omega_{be}^2/\Delta\}$.

It is evident from Eq. (2.129) that only pseudospin states with momentum difference $\hbar|k_1+k_2|$ can be connected with one another. In other words, the atom acquires momentum $\pm\hbar(k_1+k_2)$ when its internal pseudospin state is flipped due to the two-photon Raman process. In order to make the induced gauge structure explicit, one must apply the unitary transformation $\check{\mathscr{U}} = \exp\left[i(k_1\sigma_{aa} - k_2\sigma_{bb})z\right]$ into the Hamiltonian $\tilde{\mathcal{H}}_{\text{eff}}$, yielding

$$\mathcal{H}_{\text{SO}} = \check{\mathscr{U}}\tilde{\mathcal{H}}_{\text{eff}}\check{\mathscr{U}}^\dagger = \frac{\hbar^2}{2M}\left(\tilde{q}_z\mathbb{1}_2 + k_R\check{\sigma}_z\right)^2 + \frac{1}{2}\hbar\delta\check{\sigma}_z + \frac{1}{2}\hbar\Omega_R\check{\sigma}_x, \tag{2.131}$$

where $\tilde{q}_z = q_z - (k_1-k_2)/2$, $k_R = (k_1+k_2)/2$, and $\check{\sigma}_x = \sigma_{ab} + \sigma_{ba}$ is the first Pauli matrix. The gauge structure is now apparent: the Galilean transferred center-of-mass momentum $\tilde{P}_z = \hbar\tilde{q}_z$ is minimally coupled to the synthetic gauge potential $e^*\check{\mathcal{A}}_z = -\hbar k_R\check{\sigma}_z$, reminiscent of non-Abelian gauge potentials (2.60). Here, e^* is the synthetic charge, which is normally set to unity for convenience. Although the synthetic gauge potential $e^*\check{\mathcal{A}}_z$ acts in the internal pseudospin state and has a structure similar to non-Abelian gauge potentials, it might be interpreted as an Abelian gauge potential since it has only one component and therefore $[\check{\mathcal{A}}_i, \check{\mathcal{A}}_j] = 0$ for any $i,j \in \{x,y,z\}$ [57]. After pseudospin rotation $\check{\sigma}_z \to \check{\sigma}_y \to \check{\sigma}_x \to \check{\sigma}_z$ [57], the synthetic gauge potential transforms to $e^*\check{\mathcal{A}}_z \to e^*\check{\mathcal{A}}_z = -\hbar k_R\check{\sigma}_y$, which is then evident that $e^*\check{\mathcal{A}}_z$ can be interpreted as an equal contribution of the Rashba $\propto \check{\sigma}_x p_y - \check{\sigma}_y p_x$ [55] and Dresselhaus $\propto -\check{\sigma}_x p_y - \check{\sigma}_y p_x$ [56] SO couplings.

The effective SO-coupling Hamiltonian $\mathcal{H}_{\text{SO}}$ can be readily diagonalized to yield the single-particle energy dispersion,

$$\epsilon_\pm(q_z) = E_R\left[\left(\frac{q_z}{k_R}\right)^2 + 1 \pm \frac{1}{2}\sqrt{\left(\frac{4q_z}{k_R} + \frac{\hbar\delta}{E_R}\right)^2 + \left(\frac{\hbar\Omega_R}{E_R}\right)^2}\right], \tag{2.132}$$

where $E_R = \hbar^2k_R^2/2M$ is the recoil energy and I set $\tilde{q}_z = q_z$ for the sake of simplicity of notation[8]. The energy dispersion $\epsilon(q_z)$ is depicted in Fig. 2.5 for different values of the

[8] This substitution is stemmed from the assumption that $k_R \equiv k_1 \simeq k_2$, which is valid when $\omega_1 = \omega_2 + \Delta\omega$ with $|\Delta\omega|/\omega_j \ll 1$, such as in the experiment of Ref. [67].

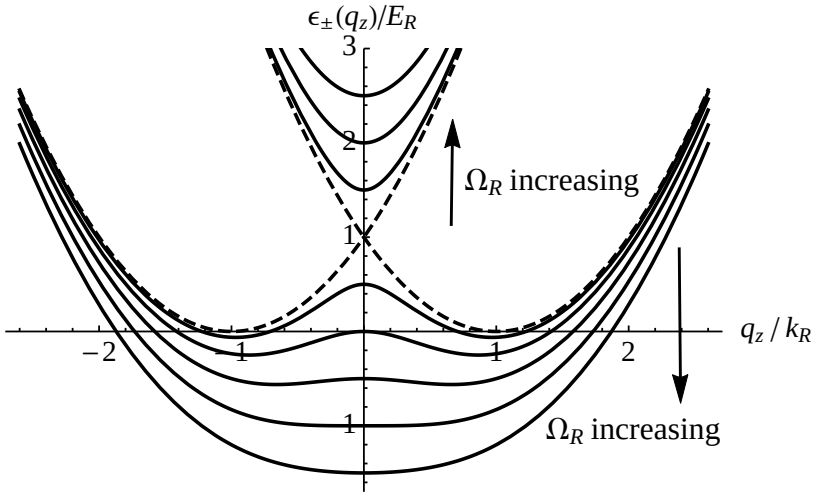

Figure 2.5: The energy dispersion $\epsilon_\pm(q_z)$ is shown for $\delta = 0$ and $\hbar\Omega_R/E_R$ in a range from 0 to 5 in equal increments. Increasing $\hbar\Omega_R/E_R$ (with the dashed curve being correspond to $\Omega_R = 0$) reduces the barrier between the two minima in the energy dispersion.

Raman coupling $\hbar\Omega_R/E_R$ in a range between 0 to 5 in equal increments for the two-photon resonance case, $\delta = 0$. The lower energy dispersion $\epsilon_-(q_z)$ consists of a symmetric double well (for $\delta = 0$) with two minima located at

$$q_z = \pm q_0 = \pm k_R \sqrt{1 - \left(\frac{\Omega_R}{4E_R}\right)^2}, \tag{2.133}$$

when $\Omega_R < 4E_R$. When the two-photon Raman coupling Ω_R is increased slowly from zero, the two dressed pseudospins $|a'\rangle$ and $|b'\rangle$ follow their corresponding minima located at $\pm q_0$. The effect of a small non-zero two-photon detuning (i.e., $|\delta|/\Omega_R \ll 1$) is to distort the energy dispersion.

In the following chapters, I will build upon the two-photon Raman scheme, discussed in the present section, in a cavity QED setting. This is motivated by the quantum-dynamic nature of cavity fields. I will exploit two counter-propagating modes of a ring cavity, instead of two counter-propagating laser beams. Unlike classical laser fields, the cavity fields interact dynamically with atoms and the quantum nature of light plays an essential role, as discussed in Sec. 2.3.2. Then, I shall study this scheme in both single- and many-particle cases. The interplay between the Raman coupling Ω_R, the two-photon detuning δ, and photon

numbers will be thoroughly investigated in the single-particle case in Chapter 3. In the many-particle case presented in Chapter 4, the interplay between cavity-mediated infinite-ranged and contact two-body interactions will be the main theme of the study.

Chapter 3

Synthetic Spin-Orbit Interactions and Magnetic Fields in Ring-Cavity QED

The interactions between light and matter are strongly enhanced when atoms are placed in high-finesse quantum cavities, offering tantalizing opportunities for generating exotic new quantum phases. In this work we show that both spin-orbit interactions and strong synthetic magnetic fields result when a neutral atom is confined within a ring cavity, whenever the internal atomic states are coupled to two off-resonant counter-propagating modes. We diagonalize the resulting cavity polariton Hamiltonian and find characteristic spin-orbit dispersion relations for a wide range of parameters. An adjustable uniform gauge potential is also generated, which can be converted into a synthetic magnetic field for neutral atoms by applying an external magnetic field gradient. Very large synthetic magnetic fields are possible as the strength is proportional to the (average) number of photons in each of the cavity modes. The results suggest that strong-coupling cavity quantum electrodynamics can be a useful environment for the formation of topological states in atomic systems.

3.1 Introduction

The spin-orbit (SO) interaction in solids is the coupling of an electron's spin to its center-of-mass momentum, and is closely related to the SO coupling in atomic systems. In two-dimensional electron gases two kinds of SO coupling have important effects on the electronic band structure: Dresselhaus [56] and Rashba [55, 150] SO interactions. In a groundbreaking paper [51], Kane and Mele showed that including a SO interaction in the Hamiltonian of graphene, while respecting all of the material's symmetries, nevertheless opens up a band gap.

The resulting bands become topologically nontrivial, so that the material supports a pair of robust conducting edge states characterized by a nontrivial Z_2 topological invariant [52]. This new phase of matter is known as a topological insulator, or a quantum spin Hall insulator in two dimensions, and its discovery has opened up a fascinating new research area in condensed matter physics [47]. Determining the conditions under which topological states could arise in condensed matter systems is the subject of continuing investigations [151, 152, 153].

Ultracold atomic gases provide a rich environment for the simulation of condensed matter physics [38, 39, 40]. For example, interacting atoms confined in optical lattices experience a crystalline environment that can mimic strongly correlated superfluid and magnetic states. Over the past decade, many theoretical schemes have been proposed to generate synthetic gauge potentials for neutral ultracold atomic gases via atom-light interactions [59]. In recent years, both synthetic magnetic [65] and electric [66] fields have been realized experimentally. The SO coupling can be interpreted as a non-Abelian gauge field [154], and Lin *et al.* recently realized a scheme to generate a combination of Rashba and Dresselhaus SO couplings in ultracold neutral atoms by means of nearly resonant two-photon Raman transitions [67]. The strength of the gauge field potentials in these experiments is limited by the atomic recoil momentum, though there are recent theoretical proposals that would push these to much higher values [155, 156, 157].

Placing atoms in high-finesse optical cavities strongly enhances atom-photon interactions [99], with numerous potential applications to quantum information science [98]. While much of the early work focused on single atoms, recent investigations of cavity quantum electrodynamics (QED) with multiple trapped ultracold atoms [158] are revealing fascinating new phenomena. The field mode to which atoms are collectively coupled is in turn affected by the atomic states, giving rise to cavity mediated long-range atom-atom interactions [107]. Other examples include the Dicke phase transition [110] and a collective atomic recoil laser [113, 114, 115, 159] in many-atom linear and ring cavity QED, respectively.

The strong coupling of cavity QED therefore offers the tantalizing prospect of enhancing the magnitude of synthetic gauge fields and SO interactions in atomic systems, as well as inducing unique strongly correlated states of both atoms and photons with no analog in condensed matter systems. In this work, we show how to simultaneously engineer a SO interaction and a synthetic magnetic field for a single neutral atom confined inside a ring cavity, as a first step toward generating topological states in ultracold atomic systems. We build on the central ideas of two-photon Raman transitions described in Ref. [67], in which absorption and re-emission of photons from one beam to the other naturally couples the atom's internal states to its center-of-mass momentum. Two propagating modes of a high-finesse ring cavity accomplish the same purpose, but with an enhanced atom-photon coupling strength. This potential advantage comes at the cost of increased mathematical complexity, because unlike the free space Raman case both the atom and photon degrees of freedom need to be treated fully quantum mechanically.

The calculations presented here reveal that the SO interactions and synthetic magnetic fields emerge naturally as the limits of zero two-photon detuning between the atomic and cavity frequencies and large two-photon detuning, respectively. The SO interactions are only weakly dependent on the occupation of the cavity modes, and in fact are robust already at the level of a few photons. That said, the energy barrier between the energy levels split by the SO interactions is greatest when the difference between the occupation of the two modes is largest. In principle, this parameter is adjustable experimentally [160, 161, 162, 163]. The strength of the synthetic magnetic fields is proportional to the square of the total number of photons in the cavity. The cavity QED environment therefore promises huge synthetic magnetic fields, potentially much larger than are currently accessible to ultracold atom experiments. The readiness with which SO interactions and synthetic magnetic fields are manifested in cavity QED should facilitate the production of new strongly correlated states in these systems.

This chapter is organized as follows. The model of the atom interacting with a ring cavity is described in Sec. 3.2, and the governing Hamiltonian is derived. In Sec. 3.3, this Hamiltonian is expressed in terms of polaritons and diagonalized to obtain the spectrum of excitations. Sec. 3.4 describes the circumstances under which synthetic SO interactions and magnetic fields emerge in this model. Sec. 3.5 discusses the results with a view toward future calculations.

3.2 Model and Hamiltonian

Consider a ring cavity with two counter-propagating modes $\hat{A}_1 e^{ik_1 z}$ and $\hat{A}_2 e^{-ik_2 z}$, where $\hat{A}_j$ are field annihilation operators for the photon and $k_j = \omega_j/c$ are the photon wavenumber expressed in terms of their frequencies ω_j. Three atomic levels are coupled via these two cavity modes in the Λ scheme, as depicted in Fig. 4.1(b). The states $\{|a\rangle, |b\rangle, |e\rangle\}$ are arbitrary internal states of an atom whose energies satisfy the relations $\varepsilon_e > \varepsilon_b > \varepsilon_a$ and $\{\varepsilon_{ea}, \varepsilon_{eb}\} \gg \varepsilon_{ba}$, where $\varepsilon_{\tau\tau'} \equiv \varepsilon_\tau - \varepsilon_{\tau'}$. For example, the states $|a\rangle$ and $|b\rangle$ might be energy levels in the same hyperfine manifold with an energy separation on the order of MHz while the state $|e\rangle$ could be an excited electronic level with an energy separation on the order of THz. The mode $\hat{A}_1 e^{ik_1 z}$ ($\hat{A}_2 e^{-ik_2 z}$) propagates to the right (left) and couples solely to the $|a\rangle \leftrightarrow |e\rangle$ ($|b\rangle \leftrightarrow |e\rangle$) transition.

The single-particle Hamiltonian density in the rotating-wave approximation reads

$$\mathcal{H}^{(1)} = \frac{\hbar^2 q_z^2}{2m} I_{3\times 3} + \sum_\tau \varepsilon_\tau \sigma_{\tau\tau} + \hbar \sum_j \omega_j \hat{A}_j^\dagger \hat{A}_j + \hbar \left(\mathscr{G}_{ae}(z) \hat{A}_1 \sigma_{ea} + \mathscr{G}_{be}(z) \hat{A}_2 \sigma_{eb} + \text{H.c.} \right), \tag{3.1}$$

where $\sigma_{\tau\tau'} = |\tau\rangle\langle\tau'|$, $\mathscr{G}_{ae}(z) = \mathscr{G}_{ae} e^{ik_1 z}$, $\mathscr{G}_{be}(z) = \mathscr{G}_{be} e^{-ik_2 z}$ and H.c. stands for Hermitian conjugate. Here $\hbar q_z$ is the center-of-mass momentum of the atom and $I_{3\times 3}$ is the identity matrix in the internal atomic state space. To a first approximation, this Hamiltonian represents an atom with infinite excited-state lifetime and an exceptionally high-finesse cavity,

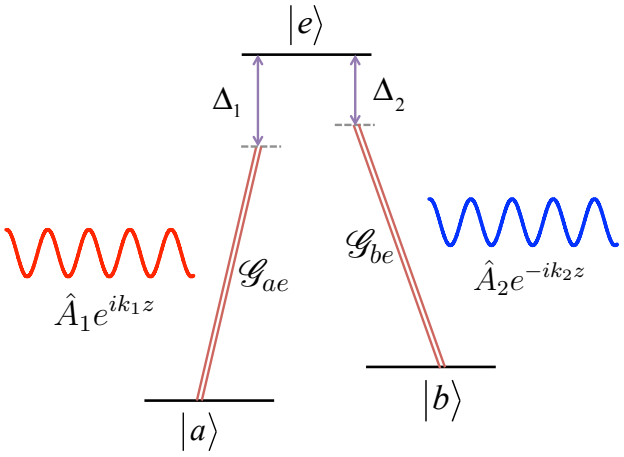

Figure 3.1: Two low-lying atomic levels $|a\rangle$ and $|b\rangle$ are coupled in the Λ scheme to an excited state $|e\rangle$ by two counter-propagating cavity modes $\hat{A}_1 e^{ik_1 z}$ and $\hat{A}_2 e^{-ik_2 z}$ with strength $\mathscr{G}_{ae}$ and $\mathscr{G}_{be}$, respectively. The transitions are detuned from resonance by Δ_1 and Δ_2.

neglecting atomic spontaneous emission and cavity losses by mirror leakage, as well as gains by external pumps. Even with these simplifying assumptions, the analysis of this Hamiltonian is quite involved as can be seen below; relaxing these assumptions will therefore be the focus of future work.

If the cavity modes are far off-resonance from atomic transitions then the adiabatic condition holds. That is, if the frequency detunings $\hbar\Delta_1 \equiv \hbar\omega_1 - \varepsilon_{ea}$ and $\hbar\Delta_2 \equiv \hbar\omega_2 - \varepsilon_{eb}$ are very large compared to ε_{ba} then the excited state $|e\rangle$ can be adiabatically eliminated [164]. Details of the procedure can be found in the Appendix B. The effective Hamiltonian for the ground pseudospin states $\{|a\rangle, |b\rangle\}$ and the cavity modes then becomes

$$\mathcal{H}_{\text{eff}} = \frac{\hbar^2 q_z^2}{2m} I_{2\times 2} + \frac{1}{2}\hbar\tilde{\omega}_0 \sigma_z + \hbar\left(\omega_1 \hat{A}_1^\dagger \hat{A}_1 + \omega_2 \hat{A}_2^\dagger \hat{A}_2\right) + \hbar\Omega_R\left(e^{i(k_1+k_2)z}\hat{A}_2^\dagger \hat{A}_1 \sigma_{ba} + \text{H.c.}\right), \tag{3.2}$$

where $\sigma_z = |b\rangle\langle b| - |a\rangle\langle a|$, and $\hbar\tilde{\omega}_0 = \tilde{\varepsilon}_b - \tilde{\varepsilon}_a > 0$. The $\tilde{\varepsilon}_\tau$ corresponds to the ac Stark-shifted atomic energies (B.5). The $I_{2\times 2}$ operator is the identity matrix in the ground pseudospin state space, and will be implied in the remainder of this work. The two-photon Rabi frequency (B.6) is given by $\Omega_R = \mathscr{G}_{ae}\mathscr{G}_{be}\left(\frac{\Delta_1+\Delta_2}{\Delta_1\Delta_2}\right)$ under the assumption that $\{\mathscr{G}_{ae}, \mathscr{G}_{be}\} \in \mathbb{R}$.

It is useful to perform a Galilean transformation of this Hamiltonian into the frame moving at the momentum transferred to the atom by the interaction with the photons. This is accomplished using the unitary operator $\mathscr{U} = \exp\left[i(k_1\sigma_{aa} - k_2\sigma_{bb})z\right]$:

$$\tilde{\mathcal{H}}_{\text{eff}} \equiv \mathscr{U}\mathcal{H}_{\text{eff}}\mathscr{U}^\dagger = \frac{\hbar^2}{2m}[q_z - (k_1\sigma_{aa} - k_2\sigma_{bb})]^2 + \frac{1}{2}\hbar\tilde{\omega}_0\sigma_z + \hbar\left(\omega_1\hat{A}_1^\dagger\hat{A}_1 + \omega_2\hat{A}_2^\dagger\hat{A}_2\right) + \hbar\Omega_R\left(\hat{A}_2^\dagger\hat{A}_1\sigma_{ba} + \text{H.c.}\right), \tag{3.3}$$

where $\mathscr{U}\sigma_{ba}\mathscr{U}^\dagger = e^{-i(k_1+k_2)z}\sigma_{ba}$ using the Baker-Campbell-Hausdorff formula. One could have applied the unitary transformation $\mathscr{U}' = \exp\left[i(k_1\hat{A}_1^\dagger\hat{A}_1 - k_2\hat{A}_2^\dagger\hat{A}_2)z\right]$ instead; although the first term of the resulting Hamiltonian will be different from that given above, the final results discussed below are independent of the particular choice of a unitary transformation. The last term in Eq. (3.3) resembles the interaction term in the Jaynes-Cummings model [165], but the $\hat{A}$ is replaced by a two-photon $\hat{A}_2^\dagger\hat{A}_1$ operator.

In order to reveal the underlying symmetries of the Hamiltonian (3.3), it is useful to express the operators in the Schwinger representation. Let $\sigma_+ = \sigma_{ba} = \frac{1}{2}(\sigma_x + i\sigma_y) = \frac{1}{\hbar}(s_x + is_y) = \frac{1}{\hbar}s_+$ and $\sigma_- = \sigma_{ab} = \frac{1}{\hbar}s_-$ be the raising and lowering operators for the atom, and $\frac{2}{\hbar}s_z = \sigma_z = \sigma_+\sigma_- - \sigma_-\sigma_+ = |b\rangle\langle b| - |a\rangle\langle a|$. If there are only exactly two modes of the cavity and $\omega_1 > \omega_2$, one can make use of the Schwinger angular momentum operators [166] for the photon field operators $j_x = \frac{\hbar}{2}(\hat{A}_1^\dagger\hat{A}_2 + \hat{A}_2^\dagger\hat{A}_1)$, $j_y = \frac{\hbar}{2i}(\hat{A}_1^\dagger\hat{A}_2 - \hat{A}_2^\dagger\hat{A}_1)$, and $j_z = \frac{\hbar}{2}(\hat{A}_1^\dagger\hat{A}_1 - \hat{A}_2^\dagger\hat{A}_2)$, which satisfy the $SU(2)$ Lie algebra (or angular momentum commutation relation)

$$[j_n, j_m] = i\hbar\varepsilon^{nml}j_l, \tag{3.4}$$

where ε^{nml} is the totally antisymmetric tensor. As in the atomic case, one can define photonic angular-momentum raising and lowering operators $j_+ = j_x + ij_y = \hbar\hat{A}_1^\dagger\hat{A}_2$ and $j_- = j_x - ij_y = \hbar\hat{A}_2^\dagger\hat{A}_1$. The Hamiltonian (3.3) can then be recast as

$$\tilde{\mathcal{H}}_{\text{eff}} = \frac{\hbar^2}{2m}\left\{q_z I_{2\times2} - \left[\frac{\Delta k}{2}I_{2\times2} - k\sigma_z\right]\right\}^2 + \tilde{\omega}_0 s_z + \frac{\hbar}{2}(\omega_1 + \omega_2)\hat{n} + (\omega_1 - \omega_2)j_z + \frac{\Omega_R}{\hbar}(j_-s_+ + j_+s_-), \tag{3.5}$$

where $k = (k_1+k_2)/2$, $\Delta k = k_1-k_2$ and $I_{2\times2} = \sigma_{aa}+\sigma_{bb}$ as before. Here, $\hat{n} = \hat{A}_1^\dagger\hat{A}_1+\hat{A}_2^\dagger\hat{A}_2$ is the total photon number operator with eigenvalues $n = 2j$, where $\hbar^2 j(j+1)$ is the eigenvalue of the total photon spin operator $\mathbf{j}^2$.

The first term in the Hamiltonian (3.5) strongly resembles SO coupling, with equal contributions of Dresselhaus and Rashba terms. Expanding the quadratic operator provides a cross term that explicitly couples the linear momentum to the pseudospin degree of freedom. A more formal mapping will be discussed in detail in the next section.

Aside from the first term, the Hamiltonian (3.5) corresponds to a generalized Jaynes-Cummings model:

$$\mathcal{H}_{\mathrm{GJC}} = \tilde{\omega}_0 s_z + \frac{\hbar}{2}(\omega_1+\omega_2)\hat{n} + (\omega_1-\omega_2)j_z + \frac{\Omega_R}{\hbar}(j_- s_+ + j_+ s_-). \tag{3.6}$$

The components of $\mathbf{j}$ and $\mathbf{s}$ both satisfy the angular momentum commutation relation (3.4), so one can define the total angular momentum operator $\mathbf{J} = \mathbf{j}+\mathbf{s}$. Because $[\mathcal{H}_{\mathrm{GJC}}, \hat{n}] = [\mathcal{H}_{\mathrm{GJC}}, \mathbf{j}^2] = [\mathcal{H}_{\mathrm{GJC}}, J_z] = 0$, it is conventional to represent the eigenstates of $\mathcal{H}_{\mathrm{GJC}}$ and $\tilde{\mathcal{H}}_{\mathrm{eff}}$ in a basis labeled by the eigenstates of s_z, j_z, and $\mathbf{j}$, with eigenvalues $\hbar m_s = \pm\hbar/2$, $\hbar m_j \equiv \hbar(n_1-n_2)/2$, and $\hbar j = (\hbar/2)(n_1+n_2) = (\hbar/2)n$, respectively. For reasons described in detail below, it turns out to be more convenient to instead express the basis in eigenstates of $\mathbf{j}$, s_z, and J_z, where the eigenvalues of the last quantity $\hbar m_z = \hbar(m_j+m_s) = (\hbar/2)(n_1-n_2\pm1)$. Note that the only component of the total angular momentum operator $\mathbf{J}$ that commutes with $\tilde{\mathcal{H}}_{\mathrm{eff}}$ is J_z. Thus, the symmetry of the spin space of the Hamiltonian is reduced to $U(1)$.

3.3 Polariton Mapping

While the first part of the effective Hamiltonian (3.5) indicates that the atoms experience an effective SO coupling through their interactions with the cavity modes, the remainder corresponds to a generalized Jaynes-Cummings model. The natural representation of the quasiparticles in the latter model is that of cavity polaritons (superpositions of atomic and

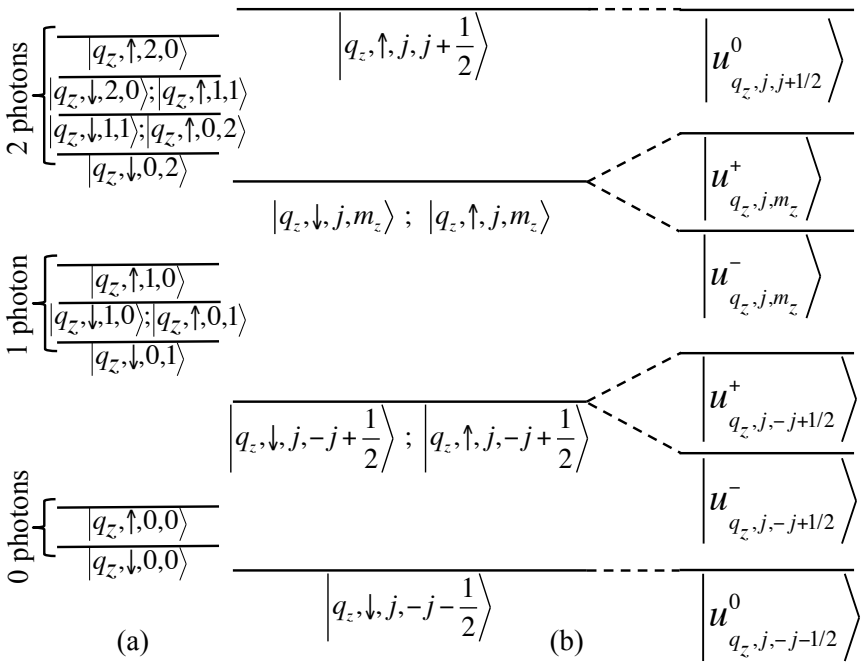

Figure 3.2: The energy manifolds of the atom-cavity system in the uncoupled q_z, s_z, $\hat{n}_1$, and $\hat{n}_2$ basis (i.e. $|q_z, \uparrow\downarrow, n_1, n_2\rangle$) are shown in (a). Shown in (b) is the $2j$-photon manifold and the corresponding sub-manifolds in the uncoupled q_z, s_z, $\mathbf{j}$, and J_z basis (i.e. $|q_z, \downarrow\uparrow, j, m_z\rangle$), and the resulting dressed states of Eq. (3.11) within the manifold. Note that here $\delta = 0$.

photonic excitations). Explicit diagonalization of the full polariton Hamiltonian, performed below, shows that in fact it is the dressed pseudospin states that experience the SO interactions and synthetic magnetic fields.

3.3.1 Diagonalizing the Generalized Jaynes-Cummings Hamiltonian

In order to map the Hamiltonian (3.5) into the polariton basis, we first exactly diagonalize $\mathcal{H}_{\mathrm{GJC}}$. Ignoring the atom-photon coupling $j_+ s_- + j_- s_+$ term, the natural basis states can be represented by $|q_z\rangle \otimes |\downarrow\uparrow\rangle \otimes |n_1\rangle \otimes |n_2\rangle = |q_z, \downarrow\uparrow, n_1, n_2\rangle$, where $|\downarrow\rangle = |a\rangle$, $|\uparrow\rangle = |b\rangle$, and n_1 and n_2 are the number of photons in the first and second cavity modes, respectively. With a total of n photons in the cavity, there are $2(n+1)$ basis states for each value of q_z. These states are depicted in Fig. 3.2. For example, the states for $n = 1$ correspond to $\{|q_z, \downarrow, 0, 1\rangle, |q_z, \downarrow, 1, 0\rangle, |q_z, \uparrow, 0, 1\rangle, |q_z, \uparrow, 1, 0\rangle\}$. The $j_+ s_- + j_- s_+$ term couples basis states $|q_z, \downarrow, n_1, n_2\rangle$ and $|q_z, \uparrow, n_1 - 1, n_2 + 1\rangle$ together within a given n manifold, but the states

$|q_z, \downarrow, 0, n\rangle$ and $|q_z, \uparrow, n, 0\rangle$ will remain uncoupled. For each value of n, the Hamiltonian therefore block diagonalizes into $n+2$ distinct blocks, of which n are two-dimensional and two are one-dimensional.

It is convenient to represent the basis states above in terms of pseudospin quantum numbers: $|q_z, \downarrow\uparrow, j, m_z\rangle = |q_z\rangle \otimes |\downarrow\uparrow\rangle \otimes |j, m_z\rangle$, where $\hbar j = \hbar n/2$ and $\hbar m_z = \hbar(m_j + m_s) = \frac{\hbar}{2}(n_1 - n_2 \pm 1)$ with $m_z = -j - \frac{1}{2}, \ldots, j + \frac{1}{2}$. In this representation, the states $\left|q_z, \downarrow, j, -j - \frac{1}{2}\right\rangle \equiv \left|u^0_{q_z, j, -j-\frac{1}{2}}\right\rangle$ and $\left|q_z, \uparrow, j, j + \frac{1}{2}\right\rangle \equiv \left|u^0_{q_z, j, j+\frac{1}{2}}\right\rangle$ are independent of the others, and have energies

$$\begin{aligned} E^0_{j,-j-\frac{1}{2}} &= -\frac{\hbar\tilde{\omega}_0}{2} + \hbar\omega_2 n_2 = -\frac{\hbar\tilde{\omega}_0}{2} + 2\hbar\omega_2 j; \\ E^0_{j,j+\frac{1}{2}} &= \frac{\hbar\tilde{\omega}_0}{2} + \hbar\omega_1 n_1 = \frac{\hbar\tilde{\omega}_0}{2} + 2\hbar\omega_1 j. \end{aligned} \tag{3.7}$$

The remaining $2n$ states couple in pairs keeping m_z fixed. For example, states with $m_j = \frac{1}{2}(n_1 - n_2)$ and $m_s = -\frac{1}{2}$ (atomic state $|\downarrow\rangle = |a\rangle$) couple with states with $m'_j = \frac{1}{2}(n'_1 - n'_2) = \frac{1}{2}[(n_1 - 1) - (n_2 + 1)] = m_j - 1$ and $m_s = +\frac{1}{2}$; both these have $m_z = \frac{1}{2}(n_1 - n_2 - 1) = m_j - \frac{1}{2}$. The two-dimensional blocks of the Hamiltonian $\mathcal{H}_{\rm GJC}$ are therefore

$$\begin{aligned} \mathcal{H}^{j,m_z}_{\rm GJC} &= \begin{pmatrix} \frac{\hbar\tilde{\omega}_0}{2} + \hbar\omega_1(n_1 - 1) + \hbar\omega_2(n_2 + 1) & \hbar\Omega_R\sqrt{n_1\,(n_2+1)} \\ \hbar\Omega_R\sqrt{n_1\,(n_2+1)} & -\frac{\hbar\tilde{\omega}_0}{2} + \hbar\omega_1 n_1 + \hbar\omega_2 n_2 \end{pmatrix} \\ &= \bar{E}_{j,m_z} I_{2\times 2} + \frac{\hbar}{2}\begin{pmatrix} -\delta & \Omega_R\sqrt{(2j+1)^2 - 4m_z^2} \\ \Omega_R\sqrt{(2j+1)^2 - 4m_z^2} & \delta \end{pmatrix}, \end{aligned} \tag{3.8}$$

where $\bar{E}_{j,m_z} \equiv \hbar\left[(\omega_1 + \omega_2)\, j + (\omega_1 - \omega_2)\, m_z\right]$. Here, the two-photon detuning is defined to be $\delta \equiv (\omega_1 - \omega_2) - \tilde{\omega}_0 \approx \Delta_1 - \Delta_2$ and the number of photons in each mode is written in terms of the pseudospin quantum numbers as $n_1 = j + m_z + \frac{1}{2}$, and $n_2 = j - m_z - \frac{1}{2}$. Defining

$$\Delta_{j,m_z} \equiv \sqrt{\Omega_R^2\left[(2j+1)^2 - 4m_z^2\right] + \delta^2}, \tag{3.9}$$

the eigenvalues of the two-dimensional blocks (3.8) are

$$E^{\pm}_{j,m_z} = \bar{E}_{j,m_z} \pm \frac{1}{2}\hbar\Delta_{j,m_z}. \tag{3.10}$$

Defining the mixing angle $\theta_{j,m_z} \equiv \cos^{-1}(-\delta/\Delta_{j,m_z})$, the dressed states (or polariton states) can be written

$$\begin{pmatrix} \left|u^{+}_{q_z,j,m_z}\right\rangle \\ \left|u^{-}_{q_z,j,m_z}\right\rangle \end{pmatrix} = \begin{pmatrix} \cos\frac{\theta_{j,m_z}}{2} & \sin\frac{\theta_{j,m_z}}{2} \\ -\sin\frac{\theta_{j,m_z}}{2} & \cos\frac{\theta_{j,m_z}}{2} \end{pmatrix} \begin{pmatrix} |q_z,\uparrow,j,m_z\rangle \\ |q_z,\downarrow,j,m_z\rangle \end{pmatrix}. \tag{3.11}$$

Note that this treats $\tilde{\omega}_0$ and therefore δ as a constant independent of j and m_z, which is not strictly correct. Using results found in the Appendix B, the Stark-shifted atomic transition frequency is

$$\begin{aligned} \tilde{\omega}_0 &= \omega_0 + \frac{2\mathscr{G}^2_{be}}{\Delta_2}(j - m_z) - \frac{2\mathscr{G}^2_{ae}}{\Delta_1}(j + m_z + 1) \\ &= \omega_0 - \frac{2\mathscr{G}^2_{ae}}{\Delta_1} + 2j\left(\frac{\mathscr{G}^2_{be}}{\Delta_2} - \frac{\mathscr{G}^2_{ae}}{\Delta_1}\right) - 2m_z\left(\frac{\mathscr{G}^2_{ae}}{\Delta_1} + \frac{\mathscr{G}^2_{be}}{\Delta_2}\right), \end{aligned} \tag{3.12}$$

where $\hbar\omega_0 = \varepsilon_b - \varepsilon_a$. The terms proportional to j and m_z can be ignored to a first approximation. While $2j = n$ is a large number when many photons occupy both modes, for a judicious choice of levels one should be able to ensure that $\mathscr{G}^2_{be}/\Delta_2 \approx \mathscr{G}^2_{ae}/\Delta_1$. Likewise, $m_z = (n_1 - n_2 - 1)/2$, which should be small if $n_1 \sim n_2$. Thus $\tilde{\omega}_0 \approx \omega_0 - 2\mathscr{G}^2_{ae}/\Delta_1$ for each block. In fact, as shown below, synthetic magnetic fields are maximized when $n_1 \sim n_2$. Even if m_z is not small, for sufficiently big frequency detunings Δ_i, the second and the last term in Eq. (3.12) will be negligible and $\tilde{\omega}_0 \approx \omega_0$. Yet the important off-diagonal term in the 2×2 Hamiltonian blocks (3.8) will remain appreciable as long as $j \gg m_z$.

The generalized Jaynes-Cummings Hamiltonian $\mathcal{H}_{\mathrm{GJC}}$ is now diagonal in the dressed state basis

$$\mathcal{H}_{\mathrm{GJC}} = \sum_{j,m_z,\lambda} E^{\lambda}_{j,m_z} P^{\dagger}_{j,m_z,\lambda} P_{j,m_z,\lambda}, \tag{3.13}$$

where $j = 0, \frac{1}{2}, 1, \frac{3}{2}, \ldots$, $m_z = -j - \frac{1}{2}, \ldots, j + \frac{1}{2}$ in integer steps, and $\lambda = \{0, \pm\}$. The energies E^{λ}_{j,m_z} are defined in Eqs. (3.7) and (3.10). The polariton field creation operator is defined as (c.f. Ref. [167, 168])

$$P^{\dagger}_{j,m_z,\lambda} = \left|u^{\lambda}_{q_z,j,m_z}\right\rangle \left\langle u^{0}_{q_z,0,-1/2}\right|, \tag{3.14}$$

where the dependence of the field operator on q_z is suppressed for convenience.

3.3.2 Diagonalizing the Full Hamiltonian

We are now in a position to obtain the matrix elements of the full Hamiltonian (3.5) in the dressed-state basis. It suffices to obtain the coefficients

$$t^{\lambda\lambda'}_{j,m_z} = k \left\langle u^{\lambda}_{q_z,j,m_z} \right| \sigma_z \left| u^{\lambda'}_{q_z,j,m_z} \right\rangle, \tag{3.15}$$

which are

$$t^{\pm\pm}_{j,m_z} = \pm k \cos\theta_{j,m_z}; \qquad t^{\pm\mp}_{j,m_z} = -k \sin\theta_{j,m_z}; \qquad t^{00}_{j,j+\frac{1}{2}} = -t^{00}_{j,-j-\frac{1}{2}} = k. \tag{3.16}$$

With Eqs. (3.7), (3.10), (3.13) and (3.15) and some straightforward algebra, the total Hamiltonian (3.5) becomes:

$$\tilde{\mathcal{H}}_{\text{eff}} = \sum_{j,m_z} \left[\frac{\hbar^2}{2m} \Big(\tilde{q}_z + \sum_{\lambda,\lambda'} t^{\lambda\lambda'}_{j,m_z} P^{\dagger}_{j,m_z,\lambda} P_{j,m_z,\lambda'} \Big)^2 + \sum_{\lambda} E^{\lambda}_{j,m_z} P^{\dagger}_{j,m_z,\lambda} P_{j,m_z,\lambda} \right]. \tag{3.17}$$

in the polariton basis. Here we have introduced the Doppler-shifted center-of-mass momentum $\tilde{q}_z \equiv q_z - \Delta k/2$. The second term in the square brackets can be considered as a Zeeman energy shift for each sub-manifold. The first term contains the essential feature of the SO interaction: a spin-dependent shift of the center-of-mass momentum. This can be made more explicit by introducing the effective spin operators

$$\begin{aligned} \check{X}_{j,m_z} &\equiv P^{\dagger}_{j,m_z,+} P_{j,m_z,-} + P^{\dagger}_{j,m_z,-} P_{j,m_z,+}; \\ \check{Z}_{j,m_z} &\equiv P^{\dagger}_{j,m_z,+} P_{j,m_z,+} - P^{\dagger}_{j,m_z,-} P_{j,m_z,-}, \end{aligned} \tag{3.18}$$

whenever $m_z \neq \pm(j+1/2)$. The Hamiltonian (3.17) can then be written

$$\tilde{\mathcal{H}}^{j,m_z}_{\text{eff}} = \frac{\hbar^2}{2m} \Big[\tilde{q}_z I_{j,m_z} + k \cos\theta_{j,m_z} \check{Z}_{j,m_z} - k \sin\theta_{j,m_z} \check{X}_{j,m_z} \Big]^2 + \frac{1}{2} \hbar \Delta_{j,m_z} \check{Z}_{j,m_z} + \bar{E}_{j,m_z} I_{j,m_z}, \tag{3.19}$$

for some arbitrary $j \neq 0$ and $m_z \neq \pm(j+1/2)$. This equation can be considered to be the main result of the present chapter. The term in brackets corresponds to the Hamiltonian of a particle with a Doppler-shifted center-of-mass momentum $\tilde{q}_z$ subject to a spin-dependent

gauge potential (i.e., the sign and strength of the gauge field depends on the eigenstate of m_s). This takes a particularly simple form when $\cos\theta_{j,m_z} = 0$, or zero two-photon detuning $\delta = 0$. For this case, the kinetic energy term takes the usual SO form $(\hbar^2/2m)[\tilde{q}_z I_{j,m_z} - k\check{X}_{j,m_z}]^2$. The last term is an overall energy shift for each two-dimensional block labeled by m_z. The penultimate term can be considered as a Zeeman splitting for the dressed states.

Eq. (3.19) can be simplified slightly by defining $E_R \equiv \hbar^2 k^2/2m$ as the atomic recoil energy and $p_z \equiv \tilde{q}_z/k$ as the Doppler-shifted center-of-mass momentum in units of k. Ignoring the constant shift for each submanifold labeled by m_z, one obtains

$$\frac{\tilde{\mathcal{H}}_{\text{eff}}^{j,m_z}}{E_R} = \left[p_z I_{j,m_z} + \cos\theta_{j,m_z}\check{Z}_{j,m_z} - \sin\theta_{j,m_z}\check{X}_{j,m_z}\right]^2 + \frac{\hbar\Delta_{j,m_z}}{2E_R}\check{Z}_{j,m_z}. \tag{3.20}$$

This Hamiltonian can then be diagonalized, yielding the dispersion relation

$$\frac{\epsilon_{j,m_z}^{\pm}(p_z)}{E_R} = p_z^2 + 1 \pm \sqrt{4p_z^2 - 2p_z\frac{\hbar\delta}{E_R} + \left(\frac{\hbar\Delta_{j,m_z}}{2E_R}\right)^2}. \tag{3.21}$$

Note that the energy dispersions for the 1D submanifolds $m_z = \pm(j + 1/2)$ are independent of j and m_z and given by

$$\frac{\epsilon_{j,\pm(j+1/2)}^{0}(p_z)}{E_R} = (p_z \pm 1)^2, \tag{3.22}$$

where here also the energy offsets, Eq. (3.7), have been omitted.

3.4 Synthetic SO Interactions and Magnetic Fields

3.4.1 Synthetic SO Interactions

To see the effect of the SO interactions, consider first the lower energy band in the simplest case of zero two-photon detuning, $\delta = 0$. This corresponds to dressed energy levels that are equal superpositions of the original atomic pseudospin states, c.f. Eq. (3.11). The extrema of the dispersion relation $\partial\epsilon_{j,m_z}^{-}/\partial p_z = 0$ are located at

$$p_z^{\text{ex}} = \left\{0, \pm\sqrt{1 - \frac{1}{16}\left[(2j+1)^2 - 4m_z^2\right]\left(\frac{\hbar\Omega_R}{E_R}\right)^2}\right\}. \tag{3.23}$$

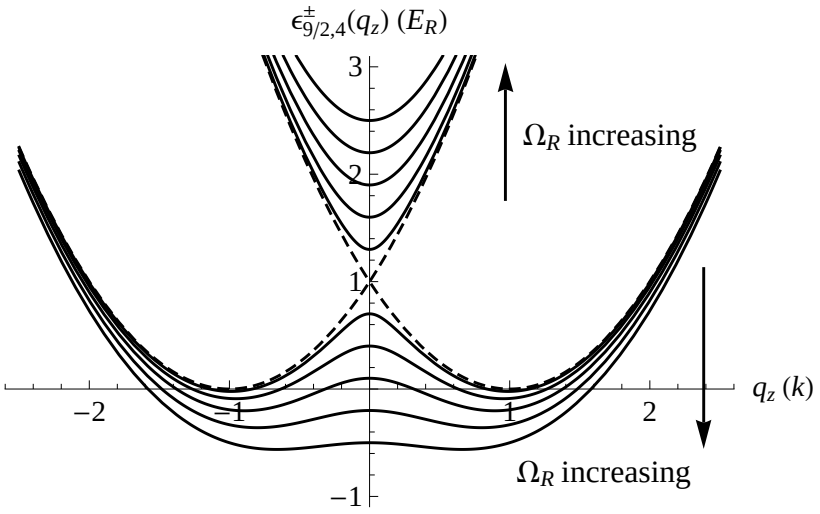

Figure 3.3: The energy dispersion $\epsilon^{\pm}_{9/2,4}(q_z)$ is shown for $\delta = 0$ and $\hbar\Omega_R/E_R$ in a range from 0 to 0.5 in equal increments. Increasing $\hbar\Omega_R/E_R$ (with the dashed curve corresponding to $\Omega_R = 0$) reduces the barrier between the two minima in the energy dispersion.

The non-zero solutions will be real only if

$$\frac{\hbar\Omega_R}{E_R} \leq \frac{4}{\sqrt{(2j+1)^2 - 4m_z^2}}. \tag{3.24}$$

The largest possible value corresponds to $m_z^2 = \left(j - \frac{1}{2}\right)^2$, which yields $\hbar\Omega_R \leq \sqrt{2/j}E_R$. The maximum number of photons in the cavity is therefore $n_{\max} = 2j_{\max} = \lfloor 4(E_R/\hbar\Omega_R)^2 \rfloor$. The value of $n_{\max}$ can be made arbitrarily large by setting $\hbar\Omega_R/E_R \to 0$, which corresponds to big frequency detunings Δ_i of the cavity mode frequencies from the atomic transitions (note that one cannot strictly set $\Omega_R = 0$ unless the number of photons is exactly zero). The curvature at the extremum $p_z^{\text{ex}} = 0$ is given by

$$\left.\frac{\partial^2 \epsilon^-_{j,m_z}}{\partial p_z^2}\right|_{p_z=0} = 2 - \frac{8}{\sqrt{(2j+1)^2 - 4m_z^2}}\left(\frac{E_R}{\hbar\Omega_R}\right), \tag{3.25}$$

which is negative for all $j < j_{\max}$; likewise, the curvature at the other two extrema is strictly positive.

The low-lying excitations for the resonant case, given by the band $\epsilon^-_{j,m_z}(p_z)$ in Eq. (3.21) with $\delta = 0$, therefore consist of a symmetric double-well centered at $\tilde{q}_z = q_z - \Delta k/2 = 0$ whose minima are located at $\tilde{q}_z \simeq \pm k$ in the limit $\hbar\Omega_R/E_R \to 0$. In this same limit the energy

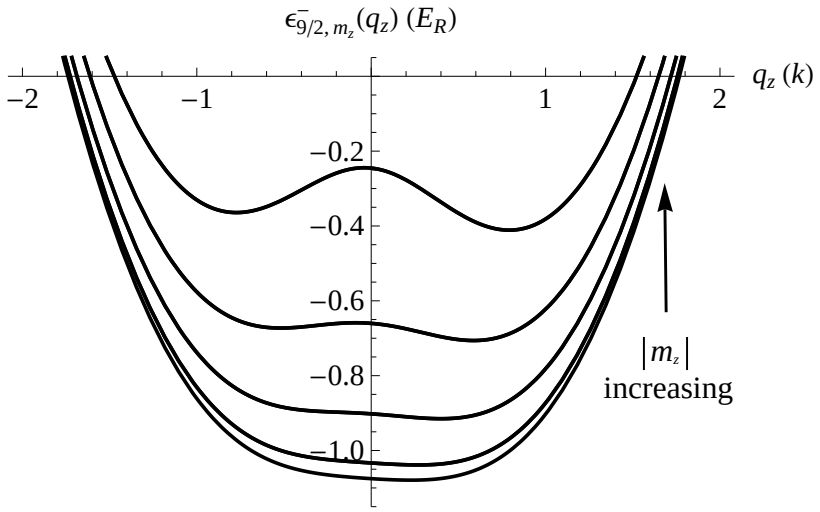

Figure 3.4: The low-lying energy dispersions $\epsilon^{-}_{j,m_z}(q_z)$ are shown for $j = 9/2$ and $|m_z| = 0, ..., 4$. Parameters correspond to $\hbar\Omega_R/E_R = 0.415$ and $\hbar\delta/E_R = -0.06$. The bottommost curve corresponds to $m_z = 0$ and the topmost one to $m_z = \pm 4$. For this choice, only the three topmost energy dispersions correspond to a SO interaction, with an appreciable energy barrier between minima only for $m_z = \pm 4$.

barrier reaches its maximum value of E_R. The exact energy bands $\epsilon^{\pm}_{j,m_z}(q_z)$ are depicted in Fig. 3.3 for the particular case $\delta = 0$, $j = 9/2$, and $m_z = 4$. For concreteness, we have used values for atomic mass and cavity wavenumbers corresponding to an ^{87}Rb atom confined in a ring cavity with nearly degenerate wavelength (i.e., $\Delta k \simeq 0$) $\lambda = 2\pi/k = 804.1$ nm [67]. For large $\hbar\Omega_R/E_R$, the bottom of the dispersion curve is almost flat, but as $\hbar\Omega_R/E_R \to 0$ the minima approach a separation of $2k$ and are separated by a barrier approaching E_R. The existence of such a double well in the energy dispersion is a hallmark of an equal Rashba-Dresselhaus SO interaction.

In the weakly non-resonant case $\delta \neq 0$ but $\hbar\delta/E_R \ll 1$, the double-well dispersion curves become asymmetric. For $\hbar\Omega_R/E_R \ll 1$, the splitting γ of the energy minima is approximately

$$\gamma \approx \left[1 - \frac{(2j+1)^2 - 4m_z^2}{32}\left(\frac{\hbar\Omega_R}{E_R}\right)^2\right]\hbar\delta$$

which is independent of j and m_z only for $\Omega_R \to 0$. The minima are now separated by $2k(\gamma/\hbar\delta)$. Fig. 3.4 depicts the atomic dispersion relations $\epsilon^{-}_{j,m_z}(q_z)$ for $j = 9/2$ and $|m_z| = 0, \ldots, 4$, assuming $\hbar\delta/E_R = -0.06$ and $\hbar\Omega_R/E_R = 0.415$. The bottommost curve

corresponds to $m_z = 0$ and the topmost one to $m_z = \pm 4$. For these parameters with $\hbar\delta/E_R$ small, the dispersion curves qualitatively follow the $\delta = 0$ results above. The uppermost curves with $|m_z| = 2, 3, 4$ now correspond to asymmetric double-wells centered near $\tilde{q}_z = 0$ with well minima slightly less than $2k$ apart and an energy splitting of order $\hbar\delta$ that is only weakly m_z-dependent. Only for the energy dispersion corresponding to $|m_z| = 4$ is the energy barrier appreciable between the two minima. A single well results for $|m_z| = 0, 1$ because the energy difference between the two minima exceeds the barrier height. The analog of Eq. (3.24) for the $\delta \neq 0$ case is

$$\frac{\hbar\Omega_R}{E_R} \leq \frac{4[(2j+1)^2 - 4m_z^2]}{[(2j+1)^2 - 4m_z^2 + \delta^2/\Omega_R^2]^{3/2}}, \tag{3.26}$$

which is equivalent to $m_z\Delta_{j,m_z} \leq 2\hbar k^2 \sin^2\theta_{j,m_z}$. Violating this condition results in a single well. Thus, the SO interaction persists for most values of m_z, but is strongest when there is a large difference between the number of photons in the two cavity modes.

3.4.2 Synthetic Magnetic Fields

In the strongly non-resonant limit $\hbar\delta/E_R \gg 1$, there is only one minimum of the dispersion curve ϵ^-_{j,m_z}, located at

$$p_z^{\text{ex}} \approx -1 + \frac{(2j+1)^2 - 4m_z^2}{2}\frac{\Omega_R^2}{\delta^2}. \tag{3.27}$$

The lowest energy dispersion then consists of a single well, as shown in Fig. 3.5. For the parameters chosen ($j = 9/2$, $m_z = 4$, $k_1 = k_2 = k$, $\hbar\Omega_R = 0.3E_R$, and $\hbar\delta = 3E_R$), the theoretical minimum of the dispersion curve based on the expression above occurs at $q_z = -0.82k$, which is close to the exact result $-0.97k$. These parameters yield a mixing angle $\theta_{\frac{9}{2},4} \approx 0.21\pi$, indicating that the spin mixing is nevertheless appreciable. Note that the $\hbar\delta/E_R \gg 1$ condition is already well-satisfied here for the case $\hbar\delta/E_R = 3$.

Under these circumstances it is reasonable to also assume that $\delta \gg \Omega_R$ so that $\Delta_{j,m_z} \sim \delta$. The effective Hamiltonian (3.20) then becomes

$$\frac{\tilde{\mathcal{H}}^{j,m_z}_{\text{eff}}}{E_R} \approx \left[p_z I_{j,m_z} - \check{Z}_{j,m_z}\right]^2 + \frac{\hbar\delta}{2E_R}\check{Z}_{j,m_z}. \tag{3.28}$$

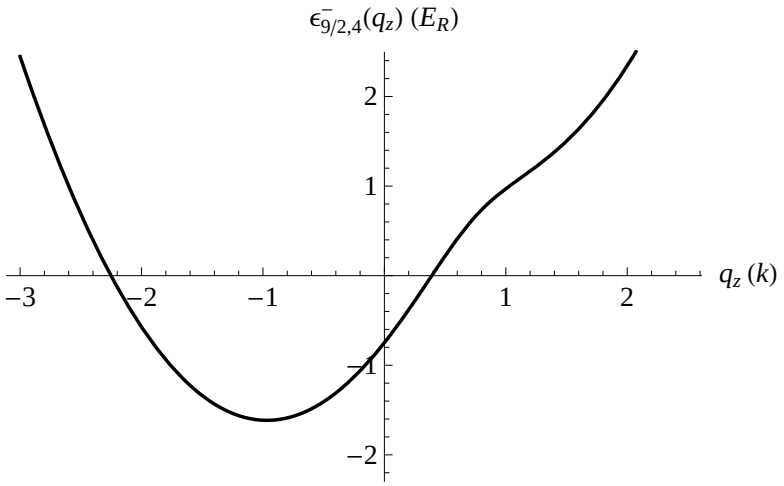

Figure 3.5: The energy dispersion $\epsilon^-_{9/2,4}(q_z)$ is shown for $\hbar\Omega_R = 0.3E_R$ and $\hbar\delta = 3E_R$.

The lower branch has dispersion relation

$$\epsilon^-_{j,m_z}(p_z) \approx E_R\left[(p_z+1)^2 - \frac{\hbar\delta}{2E_R}\right], \tag{3.29}$$

consistent with Eq. (3.27) in the limit $\delta \gg \Omega_R$. In terms of the original atomic momentum the dispersion relation becomes

$$\epsilon^-_{j,m_z} \approx \frac{\hbar^2}{2m}\left(q_z - \frac{\Delta k}{2} + k\right)^2 - \frac{\hbar\delta}{2} = \frac{\hbar^2}{2m}\left(q_z + k_2\right)^2 - \frac{\hbar\delta}{2}. \tag{3.30}$$

Ignoring the overall energy shift $-\hbar\delta/2$, the dispersion relation is equivalent to the minimal coupling energy dispersion $\hbar^2(q_z - q^*\mathcal{A}_z/\hbar)^2/2m$ of a particle with effective charge q^* subject to a synthetic Abelian gauge potential $q^*\mathcal{A}_z/\hbar = -k_2$. This is simply $-k$ in the case $k_1 = k_2$.

Note that in the strongly non-resonant limit for negative two-photon detuning, that is $\hbar\delta/E_R \ll -1$, the minimum of the energy dispersion ϵ^-_{j,m_z} is instead located at

$$p_z^{\text{ex}} \approx 1 - \frac{(2j+1)^2 - 4m_z^2}{2}\frac{\Omega_R^2}{\delta^2}. \tag{3.31}$$

The synthetic gauge potential then becomes $q^*\mathcal{A}_z/\hbar = \Delta k/2 + k = k_1$, which can be considered as the artificial Abelian gauge potential for the other pseudospin dressed state. Thus the difference in the effective gauge potential strengths for the two pseudospin states is set by the maximum two-photon momentum transfer $k_1 + k_2$, consistent with the free space case [65].

The synthetic gauge potential $q^*\mathcal{A}_z$ is position-independent and therefore cannot yield a synthetic magnetic field. Unfortunately it is not possible to make k or Δk depend on position. Instead, one can relax the assumption that $\Omega_R/\delta \approx 0$ and rather make the two-photon detuning δ position-dependent by applying a real external magnetic field gradient transverse to the cavity mode direction. For example, huge magnetic field gradients B' are generated by integrating copper wires in the immediate vicinity of high-finesse optical cavities on microfabricated atom chips [169].

Consider a magnetic field gradient aligned along the **y** direction giving rise to a position-dependent cavity detuning $\delta - \mu B' y/\hbar$, where $\mu/\hbar$ is the atomic gyromagnetic ratio. Taking the curl of Eq. (3.27) then yields the synthetic magnetic field

$$\frac{q^*\boldsymbol{\mathcal{B}}}{\hbar k} = \frac{\mu B'}{\hbar}\left[(2j+1)^2 - 4m_z^2\right]\frac{\Omega_R^2}{(\delta - \mu B' y/\hbar)^3}\mathbf{x} = 4\frac{\mu B'}{\hbar}n_1(n_2+1)\frac{\Omega_R^2}{(\delta - \mu B' y/\hbar)^3}\mathbf{x}, \quad (3.32)$$

which the second equality is written in terms of the cavity occupation numbers. This result shows that the magnitude of the synthetic magnetic field depends not only on the strength of the external magnetic field gradient B' but also on the population of the cavity modes, with the maximum corresponding to $n_1 = (n+1)/2$ where n is the total number of photons in the cavity. The maximum synthetic magnetic field therefore scales as n^2, which implies that much higher synthetic magnetic fields for atoms can be reached in cavities than in the free space. For example, choosing the same parameters as in Fig 3.5, namely $j = 9/2$, $m_z = 4$ (or $n = 9$ photons in the cavity with $n_1 = 9$, $n_2 = 0$, and spin down), $\hbar\delta/E_R = 3$, $\hbar\Omega_R/E_R = 0.3$, $\lambda = 804.1$ nm [65] and $\mu B'/h = 114$ kHz/μm [169], gives a synthetic magnetic field of $|q^*\mathcal{B}_x| \approx 3.8\hbar k/\mu$m at the cavity center. Instead using the optimal value $j = 9/2$, $m_z = 0$ (or $n_1 = 5$, $n_2 = 4$, and spin down) gives $|q^*\mathcal{B}_x| \approx 10\hbar k/\mu$m.

To get a sense of the magnitude of the synthetic magnetic field (3.32), consider the phase φ acquired by the atomic wavefunction for a closed trajectory in the yz-plane. For concreteness, suppose that the path is a rectangle with lengths y_0 and z_0. The accumulated

phase is then

$$\Gamma = \oint \frac{q^*}{\hbar} \boldsymbol{\mathcal{A}} \cdot d\mathbf{r} = 2kz_0 n_1(n_2+1) \left(\frac{\Omega_R}{\delta}\right)^2 \left[\frac{1}{(1-\mu B' y_0/\hbar\delta)^2} - 1\right]. \tag{3.33}$$

A natural choice is $y_0, z_0 = \lambda/2$, corresponding to the length of one unit cell of an external optical lattice generated by external lasers with wavelength λ. Using the parameters above that maximize the synthetic magnetic field, one obtains $\Gamma \approx 0.45\pi$. This is equivalent to almost one quarter of a flux quantum per plaquette. Increasing the number of photons in the cavity to only $n = 15$ increases the effective field to over one flux quantum per plaquette. Comparable magnetic field strengths are impossible to attain in traditional condensed matter systems, requiring applied fields on the order of $B \sim 10^9$ G [170] while the highest non-destructive value so far achieved is just over 10^6 G [171].

It is also instructive to compare the magnetic field (3.32) with its free-space counterpart $q_L^* \mathcal{B}_{Lx}/\hbar k = \hbar\delta_L'/(4E_L - \hbar\Omega_L)$ for low-lying band [172]. Here δ_L' is the detuning gradient related to an applied external magnetic field gradient, Ω_L is the laser two-photon Rabi frequency and the subscript L refers to the laser based scheme. In order to have a consistent comparison, assume that $\delta_L' \approx \mu B'/\hbar$. The ratio between the two magnetic fields at the origin is then $\zeta_{j,m_z} = 4n_1(n_2+1)(4E_L/\hbar - \Omega_L)\Omega_R^2/\delta^3$. For $\hbar\delta = 10\hbar\Omega_R = 3E_R$ and $\hbar\Omega_L = 16E_L$ [172] (note that we have set $E_R = E_L$ for convenience), the absolute value of ζ_{j,m_z} scales as $0.16n_1(n_2+1)$. With only $n_1 = n_2 = 25$ photons in each cavity mode, the artificial magnetic field in the cavity exceeds that in the free space by over two orders of magnitude.

3.4.3 Cavity Coherent States

Strong-Coupling Regime

The foregoing analysis has assumed that the cavity modes are prepared in number (or Fock) states $|n\rangle$. There have been several theoretical proposals for quantum optics schemes that can deterministically prepare such Fock states in cavities [173, 174, 175]. In these schemes, the maximum value of n is restricted by the number of Zeeman sublevels of the atom. In

principle, the ideas can also be extended to the two-mode ring-cavity states on which the present calculations are based.

That said, in the majority of experiments the cavity modes are best described by being occupied by photon coherent states

$$|\alpha_i\rangle = e^{-|\alpha_i|^2/2} \sum_{n_i=0}^{\infty} \frac{\alpha_i^{n_i}}{\sqrt{n_i!}} |n_i\rangle , \quad i = 1, 2, \ldots , \tag{3.34}$$

where $|\alpha_i|^2 = \langle n_i \rangle$ is the average number of photons in the ith cavity mode coherent state. The probability of finding the ith mode in a particular photon number state $|n_i\rangle$ is then found using a Poisson distribution [87]:

$$\mathcal{P}(n_i) = \frac{\langle n_i \rangle^{n_i} e^{-\langle n_i \rangle}}{n_i!}. \tag{3.35}$$

The dispersion curves for coherent states can then be obtained by summing over all the Fock-state low-lying bands (3.21) and (3.22), weighted by their respective probabilities:

$$\overline{\epsilon}(p_z) = \sum_{j,m_z} \sum_{\lambda=\{0,-\}} \mathcal{P}^{\lambda}_{j,m_z} \epsilon^{\lambda}_{j,m_z}(p_z), \tag{3.36}$$

with the associated probabilities given by

$$\mathcal{P}^{0}_{j,-(j+1/2)} = \frac{1}{2} e^{-\langle n_1 \rangle} \frac{\langle n_2 \rangle^{2j} e^{-\langle n_2 \rangle}}{(2j)!}; \qquad \mathcal{P}^{0}_{j,j+1/2} = \frac{1}{2} e^{-\langle n_2 \rangle} \frac{\langle n_1 \rangle^{2j} e^{-\langle n_1 \rangle}}{(2j)!}, \tag{3.37}$$

for $m_z = \pm(j + 1/2)$ and

$$\mathcal{P}^{-}_{j,m_z} = \frac{1}{2} e^{-(\langle n_1 \rangle + \langle n_2 \rangle)} \left[\frac{\langle n_1 \rangle^{j+m_z+1/2} \langle n_2 \rangle^{j-m_z-1/2}}{(j+m_z+\frac{1}{2})!(j-m_z-\frac{1}{2})!} + \frac{\langle n_1 \rangle^{j+m_z-1/2} \langle n_2 \rangle^{j-m_z+1/2}}{(j+m_z-\frac{1}{2})!(j-m_z+\frac{1}{2})!} \right], \tag{3.38}$$

for the remaining states.

The coherent-state dispersion curve $\overline{\epsilon}(p_z)$, Eq. (3.36), is shown as the solid curve in Fig. 3.6 for $\langle n_1 \rangle = 5$, $\langle n_2 \rangle = 4$, $\hbar\Omega_R = 0.215 E_R$ and $\hbar\delta = -0.06 E_R$. The single-manifold Fock-state energy dispersion $\epsilon^{-}_{j,m_z}(p_z)$ with $j = (n_1 + n_2)/2 = 9/2$ and $m_z = (n_1 - n_2 - 1)/2 = 0$ is shown for comparison as the dashed curve. The results clearly show that the dispersion relations for coherent and Fock states are not appreciably different in the regime where

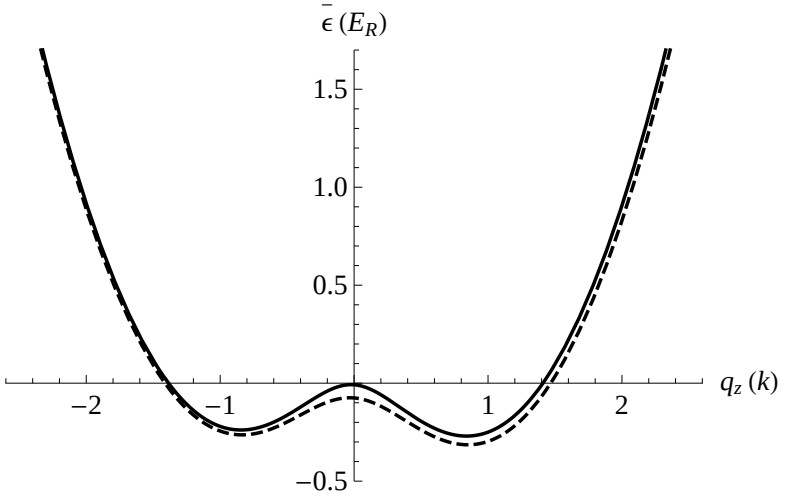

Figure 3.6: The average energy dispersion $\bar{\epsilon}(p_z)$ computed for $\langle n_1\rangle = 5$, $\langle n_2\rangle = 4$, $\hbar\Omega_R = 0.215E_R$ and $\hbar\delta = -0.06E_R$. The dashed curve corresponds to $\epsilon^-_{9/2,0}(p_z)$, see text.

the (exact or mean) occupations of the two cavity modes are comparable. Note that since $m_z = 0$ corresponds to the shallowest SO interaction (see Fig. 3.4), the value of Ω_R has been decreased to $0.215E_R$ in order to yield an appreciable barrier between the two minima.

The coherent-state energy dispersion $\bar{\epsilon}(p_z)$ becomes increasingly distorted from that of a double-well as the average photon numbers in the two cavity modes become more asymmetric, i.e., for $\langle n_1\rangle \gg \langle n_2\rangle \sim 0$ or vice versa, even in the case of zero two-photon detuning. This is because the probabilities $\mathcal{P}^0_{j,\pm(j+1/2)}$ and $\mathcal{P}^-_{j,m_z}$ in Eqs. (3.37) and (3.38) are proportional to $\langle n_i\rangle$. For $\langle n_1\rangle \to 0$, both $\mathcal{P}^-_{j,m_z}, \mathcal{P}^0_{j,j+1/2} \to 0$ which favors the occupation of the $m_z = -j-1/2$ singlet state. As discussed in Sec. 3.3.2, the associated dispersion relation (3.22) corresponds to a single well centered at $\tilde{q}_z = k$. For $\langle n_2\rangle \to 0$ the resulting dispersion relation for coherent states approaches a single well centered instead at $\tilde{q}_z = -k$. For $\langle n_1\rangle \lesssim \langle n_2\rangle$ or vice versa, the double-well dispersion relation with $\delta = 0$ can be made strongly asymmetric. Thus, in the resonant and weakly non-resonant limits, more or less symmetric double-well dispersions can be realized for the coherent-state cavity modes provided that $\langle n_1\rangle \sim \langle n_2\rangle$ and $\hbar\Omega_R \ll E_R$.

Just as was the case for SO interactions, for the analysis of synthetic magnetic fields for coherent-state cavity modes, one should again sum over all Fock states weighted by their

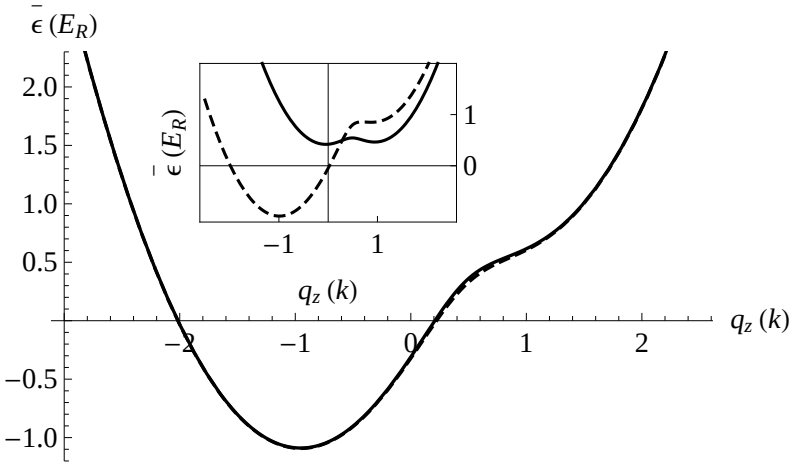

Figure 3.7: The average energy dispersion $\bar{\epsilon}(p_z)$, computed for $\langle n_1\rangle = 8$, $\langle n_2\rangle = 7$, $\hbar\Omega_R = 0.115E_R$ and $\hbar\delta = 1.9E_R$. The dashed curve represents $\epsilon^{-}_{15/2,0}(p_z)$. Inset: $\langle n_1\rangle = 0.1$, $\langle n_2\rangle = 15$, with Ω_R and δ as the main panel.

probabilities, noting that that the singlet manifolds $\epsilon^{0}_{j,\pm(j+1/2)}$ do not contribute in Eq. (3.32). Thus, the average ratio of the cavity to free-space synthetic magnetic fields $\bar{\zeta}$ is now given by

$$\bar{\zeta} = 4\left(\frac{\Omega_R^2}{\delta^3}\right)\left(\frac{4E_L}{\hbar} - \Omega_L\right)\sum_{j,m_z}\mathcal{P}^{-}_{j,m_z}\left(j + m_z + \frac{1}{2}\right)\left(j - m_z + \frac{1}{2}\right), \tag{3.39}$$

recalling that $n_1 = j + m_z + \frac{1}{2}$ and $n_2 = j - m_z - \frac{1}{2}$. When $\langle n_1\rangle \simeq \langle n_2\rangle$, the summation is approximately equals to $\langle n_1\rangle[\langle n_2\rangle + 1]$, and the average ratio $\bar{\zeta}$ is approximately equals to the single-manifold ratio ζ_{j,m_z}. This observation is borne out by numerical calculations for the dispersion curve in the strongly non-resonant limit, as shown in Fig. 3.7. The curves in the main panel correspond to the coherent-state (solid) and the single-manifold Fock-state (dashed) dispersions with $\langle n_1\rangle = 8$, $\langle n_2\rangle = 7$, $\hbar\Omega_R = 0.115E_R$ and $\hbar\delta = 1.9E_R$. As evident from Fig. 3.7, the coherent-state and single-manifold Fock-state dispersions are almost indistinguishable in this limit.

It is interesting that in the strongly non-resonant limit one can restore symmetric single- or double-well dispersions by changing the average photon numbers in the two cavity modes. This is illustrated in the inset of Fig. 3.7, where $\langle n_1\rangle = 0.1$, $\langle n_2\rangle = 15$, with Ω_R and δ set to the same values as the main panel (note that one cannot strictly set $\langle n_i\rangle$ to zero).

The coherent-state energy dispersion (solid) is a shallow double well, with the centre of the double well displaced from the origin $q_z = 0$ and the two minima located some fraction of k apart from each other. For comparison, the dashed curve represents the Fock-state energy dispersion with $n_1 = 0$, $n_2 = 15$ and spin up (i.e., $j = 15/2$ and $m_z = -7$). The change in shape has the same origins as the loss of the (approximately) symmetric double-well dispersion discussed above for the SO case: as $\langle n_1 \rangle \to 0$, the occupations of all but the $m_z = -j - 1/2$ singlet will be strongly suppressed, which will favor the appearance of an additional well in the vicinity of $q_z = k$ and the suppression of the minimum near $q_z = -k$. For very small values of $\langle n_i \rangle$, the synthetic magnetic field (which has its origin strictly in the doublets) will then approach zero.

Weak-Coupling Regime

So far, the strong-coupling limit has been assumed; that is, $(\mathscr{G}_{ae}, \mathscr{G}_{be}) \gg \kappa \sim 0$, where κ is the cavity loss rate for both cavity modes $\hat{A}_1$ and $\hat{A}_2$. In this subsection, we briefly consider the weak-coupling regime $\kappa \gg (\mathscr{G}_{ae}, \mathscr{G}_{be})$ to show how our scheme reduces to the free-space formulation of Lin *et al.* [67]. A deeper and detailed exploration of this limit will be presented in Chapter 4; see also Ref. [117].

In the strong-coupling regime, cavity coherent states can be generated by pumping the cavity modes by monochromatic lasers of frequency ω_{jp} with amplitude η_j for a short period of time. In principle, one could add the pump term

$$\mathcal{H}_{\text{pump}} = \beta(t) i\hbar \sum_{j=1,2} \left(\eta_j \hat{A}_j^\dagger e^{-i\omega_{jp} t} - \text{H.c.} \right), \tag{3.40}$$

to the Hamiltonian (3.1), where $\beta(t)$ is some time-dependent function that defines the time interval over which the lasers are applied. Since the cavity decay is negligible, the mean-cavity photon numbers $\langle n_i \rangle$ would remain almost constant after the pump lasers are turned off and the Hamiltonian (3.1) (or equivalently the Hamiltonian (3.3) after adiabatic elimination of the atomic excited state) well describes the system.

As the cavity decay κ increases, however, one must keep the pumping lasers on (i.e., $\beta(t) = 1$) in order to balance the cavity loss. Otherwise, the cavity modes will decay to their vacuum states, leaving the atom-cavity system in the ground-state energy manifold, that is, the lowest energy manifold of Fig. (3.2a). In order to remove the time dependence in the pump term, one can re-express the Hamiltonian in the rotating frame of the pump lasers (see Appendix C):

$$\begin{aligned}\mathscr{H} = &\frac{\hbar^2 q_z^2}{2m} I_{3\times 3} + \frac{\hbar\tilde{\delta}}{2}\sigma_{aa} - \frac{\hbar\tilde{\delta}}{2}\sigma_{bb} - \frac{\hbar}{2}(\tilde{\Delta}_{\mathrm{a}1} + \tilde{\Delta}_{\mathrm{a}2})\sigma_{ee} + \hbar\left[\mathscr{G}_{ae}(z)\hat{A}_1\sigma_{ea} + \mathscr{G}_{be}(z)\hat{A}_2\sigma_{eb} + \mathrm{H.c.}\right] \\ &- \hbar\left(\tilde{\Delta}_{\mathrm{c}1}\hat{A}_1^\dagger\hat{A}_1 + \tilde{\Delta}_{\mathrm{c}2}\hat{A}_2^\dagger\hat{A}_2\right) + i\hbar\left(\eta_1\hat{A}_1^\dagger + \eta_2\hat{A}_2^\dagger - \mathrm{H.c.}\right), \end{aligned} \tag{3.41}$$

where one can define the atomic and cavity detunings relative to the pump laser frequencies:

$$\begin{aligned} \hbar\tilde{\Delta}_{\mathrm{a}1} = \hbar\omega_{1p} - (\varepsilon_e - \varepsilon_a); \qquad \hbar\tilde{\Delta}_{\mathrm{a}2} = \hbar\omega_{2p} - (\varepsilon_e - \varepsilon_b); \\ \hbar\tilde{\delta} = \hbar(\omega_{1p} - \omega_{2p}) - (\varepsilon_b - \varepsilon_a) = \hbar(\tilde{\Delta}_{\mathrm{a}1} - \tilde{\Delta}_{\mathrm{a}2}); \qquad \tilde{\Delta}_{\mathrm{c}j} = \omega_{jp} - \omega_j, \quad j \in \{1, 2\}. \end{aligned} \tag{3.42}$$

Note that $(\tilde{\delta}, \tilde{\Delta}_{\mathrm{a}\tau})$ reduce to (δ, Δ_τ) when $\tilde{\Delta}_{\mathrm{c}1} = \tilde{\Delta}_{\mathrm{c}2} = 0$. As before, one can adiabatically eliminate the atomic excited state and then apply a unitary transformation to obtain an effective Hamiltonian (see Appendix C):

$$\begin{aligned}\tilde{\mathscr{H}}_{\mathrm{eff}} = &\frac{\hbar^2}{2m}\left[q_z I_{2\times 2} - (k_1\sigma_{aa} - k_2\sigma_{bb})\right]^2 - \frac{\hbar\tilde{\delta}}{2}\check{\sigma}_z + 2\hbar\Big[\frac{\mathscr{G}_{ae}^2}{\tilde{\Delta}_{\mathrm{a}1}}\hat{A}_1^\dagger\hat{A}_1\sigma_{aa} + \frac{\mathscr{G}_{be}^2}{\tilde{\Delta}_{\mathrm{a}2}}\hat{A}_2^\dagger\hat{A}_2\sigma_{bb}\Big] \\ &+ \hbar\tilde{\Omega}_R\left(\hat{A}_2^\dagger\hat{A}_1\sigma_{ba} + \mathrm{H.c.}\right) + \hbar\sum_j\left[-\tilde{\Delta}_{\mathrm{c}j}\hat{A}_j^\dagger\hat{A}_j + i\left(\eta_j\hat{A}_j^\dagger - \mathrm{H.c.}\right)\right], \end{aligned} \tag{3.43}$$

where now the two-photon Rabi frequency is defined as $\tilde{\Omega}_R = \mathscr{G}_{ae}\mathscr{G}_{be}\left(\frac{\tilde{\Delta}_{\mathrm{a}1}+\tilde{\Delta}_{\mathrm{a}2}}{\tilde{\Delta}_{\mathrm{a}1}\tilde{\Delta}_{\mathrm{a}2}}\right)$.

In the presence of cavity loss, the Hamiltonian (3.43) is not conserving and therefore exact diagonalization is not feasible. Instead, the master equation approach should be used to analyze the dynamics of the system [176]. That said, in the weak-coupling regime $\kappa \gg (\mathscr{G}_{ae}, \mathscr{G}_{be})$, the master equation approach amounts to including the dissipation in the Heisenberg equations of motion, that is, $i\hbar\partial_t\hat{A}_j = [\hat{A}_j, \tilde{\mathscr{H}}_{\mathrm{eff}}] - i\hbar\kappa\hat{A}_j$ [107]. In this regime, the cavity fields reach a steady state much more quickly than other operators. Thus they can be adiabatically

eliminated (by setting $\partial_t \hat{A}_j = 0$) to obtain an effective model for the atom (details are given in Appendix D). In the extreme weak-coupling regime $(\mathscr{G}_{ae}/\kappa, \mathscr{G}_{be}/\kappa) \sim 0$ when η_i and κ are the dominant energy scales (i.e., the classical regime), the steady-state cavity fields approach their coherent field amplitudes $|\hat{A}_j| = \alpha_j \sim \eta_j/\kappa$. Substituting this result into Eq. (3.43) and dropping constant terms, one obtains

$$\tilde{\mathscr{H}}_{\text{eff}} \approx \frac{\hbar^2}{2m}\left[\tilde{q}_z I_{2\times 2} + k\check{\sigma}_z\right]^2 - \frac{\hbar\tilde{\delta}}{2}\check{\sigma}_z + \hbar\tilde{\Omega}_R\frac{\eta_1\eta_2}{\kappa^2}\check{\sigma}_x + 2\frac{\hbar}{\kappa^2}\Big[\frac{\mathscr{G}_{ae}^2\eta_1^2}{\tilde{\Delta}_{\text{a1}}}\sigma_{aa} + \frac{\mathscr{G}_{be}^2\eta_2^2}{\tilde{\Delta}_{\text{a2}}}\sigma_{bb}\Big], \tag{3.44}$$

where as before $\tilde{q}_z = q_z - \Delta k/2$, $\Delta k = k_1 - k_2$, $k = (k_1 + k_2)/2$, and $\check{\sigma}_x = (\sigma_{ba} + \sigma_{ab})$. The last term of Eq. (3.44) represents ac Stark shifts for pseudospin states and can be omitted when $\mathscr{G}_{ae} \sim \mathscr{G}_{be}$, $\eta_1 \sim \eta_2$, and $\tilde{\Delta}_{\text{a1}} \sim \tilde{\Delta}_{\text{a2}}$. The structure of the Hamiltonian (3.44) is identical to the semi-classical SO-coupled Hamiltonian of Ref. [67]; thus, our results in the extremely bad-cavity limit reduce to those found previously in the free space.

3.5 Discussion and Conclusions

In this work, we considered three internal atomic states in the Λ scheme coupled to two counter-propagating far off-resonance ring-cavity modes. After adiabatic elimination of the atomic excited state by virtue of the large detunings of the cavity frequencies from the atomic transitions, we obtained the effective Hamiltonian $\tilde{\mathcal{H}}_{\text{eff}}$. This Hamiltonian can be divided into two parts: a generalized Jaynes-Cummings Hamiltonian $\mathcal{H}_{\text{GJC}}$ and a kinetic contribution $\tilde{\mathcal{H}}_{\text{eff}} - \mathcal{H}_{\text{GJC}}$. Diagonalizing $\mathcal{H}_{\text{GJC}}$ yields dressed (i.e., polariton) states, so the total Hamiltonian $\tilde{\mathcal{H}}_{\text{eff}}$ is then naturally expressed in the polariton basis, with $\mathcal{H}_{\text{GJC}}$ essentially a Zeeman shift for the polaritons.

The dispersion relation of the total Hamiltonian $\tilde{\mathcal{H}}_{\text{eff}}$ is found to correspond to a symmetric double-well structure in the limit of zero two-photon detuning δ, which is the hallmark of an induced SO interaction. The energy barrier between degenerate polariton ground states is found to shrink as the Rabi frequency Ω_R increases. Furthermore, the strength of the SO

interactions is enhanced by accentuating the asymmetry in the occupation of the two cavity modes. Assuming Fock states the largest energy barrier occurs for one photon in one mode, and all the other photons in the other mode. For coherent states a strong asymmetry in the average mode occupations destroys the double-well structure, instead yielding single-well dispersion relations. Therefore, a SO coupling (i.e., a double well) with a large barrier requires instead approximately equal average photon numbers in each cavity mode as well as smaller values of Ω_R. In either case, this mode occupation parameter is unique to cavities, with no analog in the free space where atoms interact with many-photon laser fields, and is in practice an experimentally accessible parameter. For small two-photon detunings, the energy dispersions become slightly asymmetric; that is, one of the two energy wells is shifted up or down with respect to the other.

For larger cavity detunings a single well results, corresponding to a uniform vector gauge potential for one pseudospin dressed state. In the presence of a real external magnetic field gradient, this potential becomes position dependent and yields a synthetic magnetic field for the neutral atom. For large occupation asymmetry, the strength of the magnetic field is proportional to the number of photons in one of the modes, but the largest fields result for smallest asymmetry in which case the strength is proportional to the square of the total number of cavity photons. For large magnetic field gradients, which can be generated particularly easily with integrated atom-chip cavity QED, even moderate occupations (on the order of 10-20 photons in the cavity) result in synthetic magnetic fields that can easily exceed one flux quantum per cavity wavelength squared, much larger than is accessible using (fundamentally weak-coupling) laser Raman techniques in the free space.

The present strong-coupling calculations have neglected cavity gain and loss that are non-negligible in many practical situations, such as the presence of cavity pump lasers and loss due to the spontaneous decay into vacuum modes or decay of the cavity modes. Under these conditions, the exact polariton approach that is adopted here is not wholly suitable,

and other approaches such as use of a master equation are required. That said, in the weak-coupling limit it should be possible to adiabatically eliminate the cavity fields to obtain an effective Hamiltonian for the atoms. This regime will be explored in the next chapter.

The natural emergence of the SO interaction and strong synthetic magnetic field for a neutral atom in a ring cavity suggests that exotic quantum phases would result for many atom systems. For example, one might expect topological insulators, including quantum Hall-type states, to result. Cavities provide a unique environment where strong atom-atom correlations could emerge naturally. The dynamic of the atomic field operators depends on the cavity fields and vice versa; in this respect, the system resembles a real material characterized by strong interplay between the electrons and phonons. In the presence of an additional optical lattice, for example, the effective Hamiltonian for the cavity atoms would resemble a SO-coupled Hubbard Hamiltonian [177] locally, but would also enjoy a variety of infinite-range atom-atom interactions. These would include arbitrarily long-range density-density interaction of the form $\hat{N}_{i,\tau}\hat{N}_{j,\tau}$, where $\hat{N}_{i,\tau}$ is the particle number operator for pseudospin state $\tau \in \{a, b\}$ at the lattice site i. The emergence of such infinite-range interactions is a direct consequence of the back-action of the cavity fields in the atomic states and they drastically modify the quantum phases of the original Hubbard model and can give rise to exotic many-body states [178, 179].

Chapter 4

Enhanced Stripe Phases in Spin-Orbit-Coupled Bose-Einstein Condensates in Ring Cavities

The coupled dynamics of the atom and photon fields in optical ring cavities with two counter-propagating modes give rise to both spin-orbit interactions as well as long-ranged interactions between atoms of a many-body system. At zero temperature, the interplay between the two-body and cavity-mediated interactions determines the ground state of a Bose-Einstein condensate. In this work, we find that cavity quantum electrodynamics in the weak-coupling regime favors a stripe-phase state over a plane-wave phase as the strength of cavity-mediated interactions increases. Indeed, the stripe phase is energetically stabilized even for condensates with attractive intra- and inter-species interactions for sufficiently large cavity interactions. The elementary excitation spectra in both phases correspond to linear dispersion relation at long wavelengths, indicating that both phases exhibit superfluidity, although the plane-wave phase also displays a characteristic roton-type feature. The results suggest that even in the weak coupling regime cavities can yield interesting new physics in ultracold quantum gases.

4.1 Introduction

The experimental realization of Bose-Einstein condensation (BEC) has opened many opportunities for realizing new many-body phases [17, 18, 40]. Ultracold atoms trapped in laser-generated optical lattice potentials experience crystalline environments and exhibit a variety of intriguing phenomena [39], most notably the superfluid–Mott-insulator phase transition [43]. There are numerous proposals for inducing gauge fields in quantum gases by means of laser light [59], and recently Abelian [65] and non-Abelian [67] gauge fields have

been realized. In the latter work an equal combination of Rashba and Dresselhaus spin-orbit (SO) couplings were induced via two-photon Raman transitions. These developments have set the stage for realizing topological states in these systems [48].

The single-particle energy dispersion of a (equal Rashba-Dresselhaus) SO-coupled atom is a momentum-space double well, which is two-fold degenerate in the symmetric case [65]. In a Bose-Einstein condensate of atoms, the two-body interactions lift this degeneracy and drive the Bose condensate into either a plane wave phase (PWP) or a stripe phase (SP), depending on the strength and sign of the intra- and inter-species two-body interactions [74, 75, 76, 77]. In the PWP, all atoms condense into one of the two single-particle energy minima, while the SP is a superposition state of the minima and the total condensate density exhibits faint fringes [78]. Additional phases are found for fully three-dimensional SO interactions [180]. When a SO-coupled quantum gas is confined in an optical lattice, the ground state of the system exhibits a variety of magnetic orderings in the Mott-insulator regime, such as ferromagnetic, antiferromagnetic, spin spiral, vortex and antivortex crystals, and skyrmion crystal phases [79, 80, 81]. The superfluid to Mott-insulator phase transition of SO-coupled quantum gases has also been investigated [79, 82].

In laser-based approaches to generating SO couplings, the radiation field is treated classically and one ignores the back-action of the atoms on it. Confining the radiation field to within an optical cavity leads to a coherent exchange of energy and momentum between atoms and photons [91]. The back-action of the atoms on the photon fields is no longer negligible, leading to complex coupled dynamics of the matter and radiation fields in which both entities are affected by one another and must be treated on the same footing [107]. As a consequence, cavity-mediated long-range interactions are induced between atoms, yielding novel collective phenomena in atomic systems [110]. A few schemes have been recently proposed to induce SO coupling in ultracold atoms via cavity quantum electrodynamics [116, 123, 124, 125] and to couple a laser-induced SO-coupled Bose condensate

to the cavity field [126]. These schemes exhibit a wealth of physics, including strong synthetic magnetic fields, a cavity-mediated Hofstadter spectrum, and a variety of magnetic orders.

In this work we investigate the ground state and the elementary excitations of a two-component Bose-Einstein condensate at zero temperature subject to ring-cavity-induced SO interaction [116]. Here we consider lossy cavities where a steady-state photon population is maintained by the application of external pump lasers. The cavity photons mediate infinite-range interactions between atoms, whose strengths can be tuned experimentally by adjusting the amplitudes of the pump lasers. The sign of these interactions can be made positive or negative depending on the cavity detuning, the frequency difference between the applied pump lasers and the cavity. These cavity-mediated interactions compete with the inherent two-body interactions between atoms to determine the ground state of the SO-coupled Bose condensate. In particular, the SP is always favored when positive cavity-mediated interactions dominate the two-body-interactions, even in the case where the intrinsic atomic interactions (both intra- and inter-species) are attractive. Asymmetry in the strength of cavity-mediated interactions for different spin components yields SP states with an arbitrary number of atoms in the left or right minimum of the single-particle dispersion relation, so that the magnetization varies continuously from zero in the SP to unity in the PWP. This behavior allows us to identify a SP order parameter, and to identify its associated mean-field critical exponent.

Consideration of the quantum fluctuations around the mean-field ground states reveals that the particle-hole elementary excitation spectra in both PWP and SP have the usual linear sound-like dispersion relation at long wavelengths, an indication of superfluidity. In the PWP, the dispersion relation also exhibits a roton-type feature at the same wave vector that charactizes the fringe periodicity in the SP, which could be used experimentally as a distinguishing feature. The critical transition between the PWP and SP occurs when the energy of this minimum falls below zero. Unlike for the PWP, in the SP the speed of sound

depends strongly on the cavity-mediated interactions. The speed of sound is found to fall below zero at a critical value of the cavity interactions and inter-species interactions strength, but this appears to signal a phase transition to a phase-separated state. Overall, the ring-cavity environment provides an experimentally convenient framework for exploring exotic ground states of SO-coupled Bose-Einstein condensates.

This chapter is organized as follows. In Section 4.2, we start from the full atom-photon Hamiltonian density for a lossy but pumped cavity, to derive an effective atomic Hamiltonian with the photon fields eliminated. The ground state of this effective Hamiltonian is explored in Section 4.3 using both a variational method and by solving the generalized Gross-Pitaevskii equations. The remainder of this Section is devoted to an analysis of the elementary excitations. A discussion of the results and conclusions are found in Sec. 4.4.

4.2 Model and Hamiltonian

Consider spin-1 bosonic atoms inside a ring cavity with two driven counter-propagating running modes $\hat{A}_1 e^{ik_1 z}$ and $\hat{A}_2 e^{-ik_2 z}$, where $\hat{A}_j$ is the annihilation operator for the photon in jth mode with wave vector $k_j = \omega_j/c$ and z is the direction along the cavity axis; see Fig. 4.1(a). Without loss of generality, one can assume that the wave vectors k_1 and k_2 of the two modes are approximately equal to each other[1], $k_R \equiv k_1 \approx k_2$. The mode $\hat{A}_1 e^{ik_R z}$ ($\hat{A}_2 e^{-ik_R z}$) propagates to the right (left) and solely induces the atomic transition $|a\rangle \to |e\rangle$ ($|b\rangle \to |e\rangle$), where $\{|a\rangle, |b\rangle\}$ are non-degenerate pseudospin states of interest and $|e\rangle$ is an excited state; see Fig. 4.1(b). These ground pseudospin states could be chosen to be the $|a\rangle = |F = 1, m_F = -1\rangle$ and $|b\rangle = |F = 1, m_F = 1\rangle$ hyperfine states of an ^{87}Rb atom in the ground electronic manifold ($5S_{1/2}$) with the Zeeman splitting $\varepsilon_b - \varepsilon_a = \hbar\omega_Z$. With this choice, the $|a\rangle \Leftrightarrow |e\rangle$ and $|b\rangle \Leftrightarrow |e\rangle$ transitions would be driven by right and left circularly

[1] The applied frequencies are assumed to be $\omega_1 = \omega_2 + \Delta\omega$ with $|\Delta\omega|/\omega_j \ll 1$ (implying that $|k_1 - k_2|/k_j \ll 1$). In the general case when $k_1 \neq k_2$, one can define $k_R \equiv \frac{1}{2}(k_1 + k_2)$ and $\Delta k \equiv k_1 - k_2$. All the results still hold, except that the momentum operator p_z is replaced by $p_z - \frac{1}{2}\hbar\Delta k$ after transferring to the co-moving frame of the cavity modes, which is just a Galilean transformation of the momentum; see also Chapter 3.

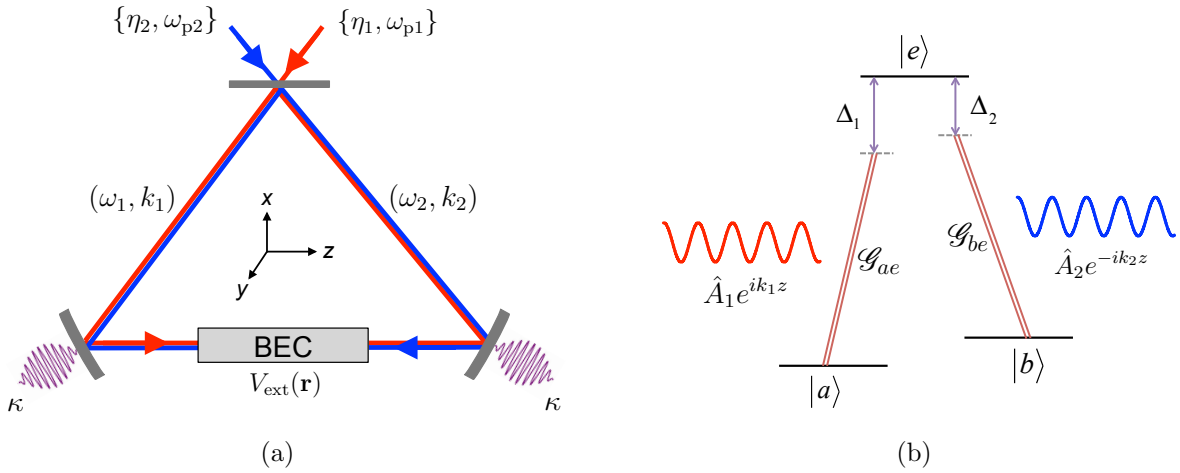

Figure 4.1: (Color online) (a) A schematic of the ring cavity geometry. (b) The atom-photon coupling in the Λ scheme.

polarized cavity modes, respectively, the so-called $\sigma_+ - \sigma_-$ configuration [181, 182]. As discussed further below, no appreciable additional light-shift energies result for suitably chosen parameters. The two cavity modes $\hat{A}_j$ are assumed to be sufficiently populated to justify omitting associated degenerate modes $\hat{A}'_j$, an approximation justified further below.

The single-particle Hamiltonian density in the dipole and rotating-wave approximations is

$$\mathcal{H}^{(1)} = \mathcal{H}^{(1)}_{\rm at} + H_{\rm cav} + \mathcal{H}^{(1)}_{\rm ac}, \tag{4.1}$$

with

$$\begin{aligned}
\mathcal{H}^{(1)}_{\rm at} &= \left[-\frac{\hbar^2}{2m}\nabla^2 + V_{\rm ext}(\mathbf{r})\right] I_{3\times 3} + \sum_{\tau\in\{a,b,e\}} \varepsilon_\tau \sigma_{\tau\tau}, \\
H_{\rm cav} &= \hbar \sum_{j=1,2} \omega_j \hat{A}^\dagger_j \hat{A}_j + i\hbar \sum_{j=1,2} \left(\eta_j \hat{A}^\dagger_j e^{-i\omega_{pj} t} - \text{H.c.}\right), \\
\mathcal{H}^{(1)}_{\rm ac} &= \hbar \left[\left(\mathscr{G}_{ae} e^{ik_R z} \hat{A}_1 \sigma_{ea} + \mathscr{G}_{be} e^{-ik_R z} \hat{A}_2 \sigma_{eb}\right) + \text{H.c.}\right],
\end{aligned} \tag{4.2}$$

where ε_τ are the internal atomic-state energies, $\sigma_{\tau\tau'} = |\tau\rangle\langle\tau'|$, and $I_{3\times 3}$ is the identity matrix in the internal atomic-state space. The atom-photon coupling for the transition $\tau \leftrightarrow \tau'$ is denoted $\mathscr{G}_{\tau\tau'}$, and H.c. stands for the Hermitian conjugate. The cavity mode $\hat{A}^\dagger_j$ is driven

by a pump laser with frequency $\omega_{\mathrm{p}j}$ and amplitude η_j, indicated by the second sum in H_{cav}. Here $V_{\mathrm{ext}}(\mathbf{r})$ is a state-independent external potential imposed to confine atoms inside the cavity. In order to simplify the analytical calculations throughout this work, we consider a box potential where $V_{\mathrm{ext}}(\mathbf{r}) = 0$ except at the boundaries; such a potential has recently been realized experimentally [183, 184, 185]. The transverse dimensions $L_{x,y}$ of this box trap can be assumed to be smaller than the waist w ($1/e^2$) of the radial cavity-mode function $e^{-(x^2+y^2)/w^2}$, so that the plane-wave mode approximation $e^{-(x^2+y^2)/w^2 \pm ik_R z} \simeq e^{\pm ik_R z}$ is reasonable. The waist of the radial mode function in a typical ring-cavity experiment is $w \sim 130$ μm [186], while the transverse dimensions of a box trap with volume $V = L_x L_y L_z \sim 10^{-4}$ mm^3 are $L_x \sim L_y \sim 35$ (with $L_z \sim 70$) μm [184].

After expressing the Hamiltonian (4.1) in the rotating frame of the pump lasers [178] and assuming that the atomic detunings $\Delta_1 = \omega_1 - \varepsilon_{ea}/\hbar$ and $\Delta_2 = \omega_2 - \varepsilon_{eb}/\hbar$ are large compared to $\varepsilon_{ba}/\hbar = (\varepsilon_b - \varepsilon_a)/\hbar$, one can adiabatically eliminate the atomic excited state to obtain an effective Hamiltonian $\mathcal{H}_{\mathrm{SO}}^{\prime(1)}$ for the ground pseudospin states $\{|1\rangle, |2\rangle\} \equiv \{|b\rangle, |a\rangle\}$. The details are presented in Appendix C. One can then transform to the co-moving frame of the cavity modes by applying the unitary transformation $\mathscr{U}_2 = e^{-ik_R z \check{\sigma}_z}$ (where $\check{\sigma}_z = \sigma_{11} - \sigma_{22}$ is the third Pauli matrix, see also Appendix C). The kinetic-energy part of the Hamiltonian density $\mathcal{H}_{\mathrm{SO}}^{\prime\prime(1)} \equiv \mathscr{U}_2 \mathcal{H}_{\mathrm{SO}}^{\prime(1)} \mathscr{U}_2^\dagger$ associated with the momentum p_z, Eq. (C.7), then takes the familiar form of an equal Rashba-Dresselhaus SO coupling: $\frac{1}{2m}(p_z I_{2\times 2} + \hbar k_R \sigma_z)^2$, which is characterized by a double-well energy dispersion [67].

In the presence of dissipation, such as when the decay rate κ of both cavity modes is non-zero, one should in principle numerically solve the associated master equation [176]. That said, in the weak-coupling regime when κ is the dominant energy scale, $\kappa \gg (\mathscr{G}_{ae}, \mathscr{G}_{be})$, the master equation approach is equivalent to including dissipation in the Heisenberg equations of motion for the cavity fields: $\partial_t \hat{A}_j = -i[\hat{A}_j, \mathcal{H}_{\mathrm{SO}}^{\prime\prime(1)}]/\hbar - \kappa \hat{A}_j$ [107]. The cavity fields quickly reach steady states, allowing them to be adiabatically eliminated. Setting $\partial_t \hat{A}_j = 0$ one

obtains steady-state expressions for $\hat{A}_j$ that can be substituted into $\mathcal{H}_{\rm SO}^{\prime\prime(1)}$ to yield an effective atomic Hamiltonian; the details are relegated to Appendix D.

The resulting effective many-body Hamiltonian reads

$$\begin{aligned} H_{\rm eff} = &\int d^3r \left(\hat{\mathbf{\Psi}}^\dagger \mathcal{H}_{\rm SO}^{(1)} \hat{\mathbf{\Psi}} + \frac{1}{2} g_1 \hat{n}_1^2 + \frac{1}{2} g_2 \hat{n}_2^2 + g_{12} \hat{n}_1 \hat{n}_2 \right) \\ &+ \sum_{\tau=1,2} U_\tau \hat{N}_\tau^2 + U_\pm \hat{S}_+ \hat{S}_- + U_\mp \hat{S}_- \hat{S}_+ + 2U_{\rm ds} \hat{N} \hat{S}_x, \end{aligned} \tag{4.3}$$

where $\hat{\mathbf{\Psi}}(\mathbf{r}) = (\hat{\psi}_1(\mathbf{r}), \hat{\psi}_2(\mathbf{r}))^{\mathsf{T}}$ are the bosonic field operators obeying the commutation relation $[\hat{\psi}_\tau(\mathbf{r}), \hat{\psi}_{\tau'}^\dagger(\mathbf{r}')] = \delta_{\tau,\tau'}\delta(\mathbf{r}-\mathbf{r}')$, $\hat{N}_\tau = \int \hat{n}_\tau(\mathbf{r}) d^3r = \int \hat{\psi}_\tau^\dagger(\mathbf{r}) \hat{\psi}_\tau(\mathbf{r}) d^3r$ is the total atomic number operator for pseudospin $\tau \in \{1,2\}$, $\hat{N} = \hat{N}_1 + \hat{N}_2$ is the total atomic number operator, and the x-component of the total spin operator is defined in the usual way $\hat{S}_x = \frac{1}{2}(\hat{S}_+ + \hat{S}_-)$ using the collective pseudospin raising and lowering operators $\hat{S}_+ = \hat{S}_-^\dagger = \int \hat{\psi}_1^\dagger(\mathbf{r}) \hat{\psi}_2(\mathbf{r}) d^3r$. The atoms in this system experience two kinds of interactions, reflected in the effective Hamiltonian $H_{\rm eff}$: the standard two-body contact interactions and the cavity-mediated long-ranged interactions. Here $g_\tau \equiv g_{\tau\tau}$ denotes the two-body intra-species interaction strength and g_{12} the two-body inter-species interaction strength. The strength of the cavity-mediated interactions are found in Appendix D:

$$\begin{aligned} U_{1(2)} &= \frac{4\hbar \mathscr{G}_0^4 \Delta_{\rm c} (\Delta_{\rm c}^2 - 3\kappa^2)}{\Delta^2 (\Delta_{\rm c}^2 + \kappa^2)^3} \eta_{2(1)}^2, \\ U_{\pm(\mp)} &= \frac{4\hbar \mathscr{G}_0^4 \Delta_{\rm c}}{\Delta^2 (\Delta_{\rm c}^2 + \kappa^2)^3} \left[\Delta_{\rm c}^2 - \left(1 + 2\frac{\eta_{2(1)}^2}{\eta_{1(2)}^2} \right) \kappa^2 \right] \eta_{1(2)}^2, \\ U_{\rm ds} &= \frac{4\hbar \mathscr{G}_0^4 \Delta_{\rm c} \left(\Delta_{\rm c}^2 - 3\kappa^2\right)}{\Delta^2 (\Delta_{\rm c}^2 + \kappa^2)^3} \eta_1 \eta_2, \end{aligned} \tag{4.4}$$

where $\mathscr{G}_0 \equiv \mathscr{G}_{ae} = \mathscr{G}_{be}$, $\Delta \equiv \Delta_1 = \Delta_2$, and $\Delta_c \equiv \omega_{{\rm p}j} - \omega_j$. The single-particle part of the effective Hamiltonian density has the familiar form of the equal Rashba-Dresselhaus SO coupling:

$$\mathcal{H}_{\rm SO}^{(1)} = \frac{\hbar^2}{2m} \left[-\nabla_\perp^2 + (-i\partial_z + k_R \check{\sigma}_z)^2 \right] + \hbar \Omega_R \check{\sigma}_x + \frac{\hbar\delta}{2} \check{\sigma}_z, \tag{4.5}$$

with the effective two-photon detuning and Raman coupling given by (see Appendix D)

$$\begin{aligned}\delta &= \frac{2\mathscr{G}_0^2(\Delta_{\rm c}^2-\kappa^2)}{\Delta(\Delta_{\rm c}^2+\kappa^2)^2}(\eta_2^2-\eta_1^2),\\ \Omega_R &= \frac{2\mathscr{G}_0^2(\Delta_{\rm c}^2-\kappa^2)}{\Delta(\Delta_{\rm c}^2+\kappa^2)^2}\left[1-\frac{2\mathscr{G}_0^2\Delta_{\rm c}}{\Delta(\Delta_{\rm c}^2-\kappa^2)}\right]\eta_1\eta_2.\end{aligned} \tag{4.6}$$

Before proceeding further, consider briefly some realistic order-of-magnitude estimates for various parameters used in the theory based on current experiments in ultracold atomic gases and cavity QED. The first experimental realization of a synthetic SO coupling was carried out on ^{87}Rb atoms using two counter-propagating Raman laser beams with wavelength $\lambda_R = 804.1$ nm ($E_R = 2.33\times10^{-30}$ J) [67]; the two-body interaction strengths for the desired pseudospin states of ^{87}Rb atoms are reported to be $g_1 = 5.009\times10^{-51}$ Jm^3 and $g_2 = g_{12} = 4.986\times10^{-51}$ Jm^3. With typical average BEC densities $\bar{n}$ of order $10^{20}-10^{21}$ m^{-3} [18], one obtains $g_\tau\bar{n}/E_R \sim 1$.

One might reasonably expect interesting physics to emerge when the strength of cavity-mediated interactions becomes comparable to the intrinsic inter-particle interactions, i.e. when $VU_\tau/g_\tau \sim 1$. Most experimental work is focused on the strong-cavity limit, where $\mathscr{G} \gg \kappa$; typical atom-cavity coupling and cavity decay rates for ^{87}Rb are $\mathscr{G}_{ae} \sim \mathscr{G}_{be} \sim 10\kappa \sim 2\pi\times10$ MHz [96, 97]. One can attain $VU_\tau/g_\tau \sim 1$ by choosing $\Delta \sim 26$ THz, $\eta_1 = \eta_2 = -\Delta_{\rm c} = 10$ MHz (for example, $\Delta_{\rm c} \approx 28\kappa$ and $\eta \approx 2.2\kappa$ in Ref. [96]), and a gas volume $V = 10^{-4}$ mm^3 [184]; for these parameters one also obtains $\hbar\Omega_R/E_R \sim 4\times10^{-3}$. The weak coupling regime relevant to the present work can be attained by increasing the value of κ, for example by decreasing the reflectivity of the cavity mirrors. Choosing $\kappa \sim 2\pi\times100$ MHz one can nevertheless ensure $VU_\tau/g_1 \sim 1$ by choosing a larger volume $V = 10^{-3}$ mm^3 as well as stronger pump fields and cavity detuning $\eta_1 = \eta_2 = -3\Delta_{\rm c} = 3$ GHz; these choices yield $\hbar\Omega_R/E_R \sim 4\times10^{-2}$. Further increasing the driving field intensities up to $\eta_1 = \eta_2 = 15$ GHz at the fixed $\Delta_{\rm c} = -1$ GHz results in cavity-mediated interactions that are an order of magnitude larger than the two-body interactions $VU_\tau/g_1 \sim 30$ while $\hbar\Omega_R/E_R \sim 1$. Note that for all cases, the light-shift energies $\sim \hbar\Omega_R^2/\Delta \ll 1$ associated with the two coupling

lasers are negligible.

In Appendix D, which discusses the adiabatic elimination of the cavity fields and the origin of the long-ranged cavity interactions, quantities such as $\xi \equiv 2\mathscr{G}_0^2/[\Delta(\Delta_c + i\kappa)]$ and ξN_τ are assumed to be small. Using the weak-coupling values considered above and assuming a typical average BEC particle number $N_\tau \sim 10^5$, it is straightforward to verify that both $|\xi| \ll 1$ and $|\xi| N_\tau \sim 10^{-2} \ll 1$. Making use of $\kappa \ll \Delta_c$ and $\xi \approx 2\mathscr{G}_0^2/\Delta\Delta_c \ll 1$, one can write

$$\begin{aligned} \Omega_R &\approx \frac{\xi}{\Delta_c}\eta_1\eta_2, \qquad & \delta &\approx \frac{\xi}{\Delta_c}\left(\eta_2^2 - \eta_1^2\right); \\ U_{ds} &\approx \frac{\hbar\xi^2}{\Delta_c}\eta_1\eta_2, \qquad & U_{1(2)} &= U_{\mp(\pm)} \approx \frac{\hbar\xi^2}{\Delta_c}\eta_{1(2)}^2. \end{aligned} \tag{4.7}$$

If $\eta_1 = \eta_2$ then $\hbar\delta = 0$ and $U_{ds} = U_{1(2)} = U_{\mp(\pm)}$ with $U_1/\hbar\Omega_R = \xi \ll 1$. Alternatively, if both pump fields are non-zero ($\eta_1, \eta_2 \neq 0$), then defining $\delta U \equiv U_2 - U_1$ one obtains $\delta U/\hbar\delta = U_{ds}/\hbar\Omega_R = \xi \ll 1$. These relations will be important below when choosing parameters for the theoretical calculations.

With these expressions in hand, the average occupation of the cavity modes can be obtained from the steady-state field solutions (D.8), which up to leading order in ξ give $A_{ssj}^* A_{ssj} \approx \eta_j^2/(\Delta_c^2 + \kappa^2)$. Using the weak-coupling values considered above, one obtains $A_{ss1}^* A_{ss1} \sim A_{ss2}^* A_{ss2}$ on the order of 3^2 to 15^2. The probability of scattering a photon into the already-populated modes $\hat{A}_{1/2}e^{\pm ik_R z}$ is therefore one or two orders of magnitude larger than the probability of scattering a photon into empty counter-propagating degenerate modes $\hat{A}'_{1/2}e^{\mp ik_R z}$ [143]. This justifies the omission of these modes in the Hamiltonian (4.1).

4.3 Ground State and Excitations: Mean-Field and Bogoliubov Theories

The above analysis indicates that as long as η_1 and η_2 are not too different from one another then $\delta \ll \Omega_R$; in the following we therefore restrict calculations to $\delta \simeq 0$. The effective single-particle Hamiltonian can be diagonalized and expressed in the form $H_{SO}^{(1)} =$

$\sum_{\mathbf{k},\lambda=\pm} \epsilon_\lambda(\mathbf{k})\hat{\varphi}^\dagger_\lambda(\mathbf{k})\hat{\varphi}_\lambda(\mathbf{k})$, with single-particle energy dispersion relation

$$\tilde{\epsilon}_\pm(\tilde{\mathbf{k}}) \equiv \frac{\epsilon_\pm(\mathbf{k})}{E_R} = \tilde{k}^2 + 1 \pm \sqrt{4\tilde{k}_z^2 + \tilde{\Omega}_R^2}, \tag{4.8a}$$

and spinor eigenstates

$$\boldsymbol{\phi}_-(\mathbf{k}) = \begin{pmatrix} \sin\theta_\mathbf{k} \\ -\cos\theta_\mathbf{k} \end{pmatrix}; \quad \boldsymbol{\phi}_+(\mathbf{k}) = \begin{pmatrix} \cos\theta_\mathbf{k} \\ \sin\theta_\mathbf{k} \end{pmatrix}, \tag{4.8b}$$

where '+' and '−' designate the upper and lower band, respectively, and $\sin 2\theta_\mathbf{k} = \tilde{\Omega}_R/\sqrt{4\tilde{k}_z^2 + \tilde{\Omega}_R^2}$. The unitless parameters $\tilde{\mathbf{k}} = \mathbf{k}/k_R$ and $\tilde{\Omega}_R = \hbar\Omega_R/E_R$ are defined for convenience, where $E_R = \hbar^2 k_R^2/2m$ is the recoil energy.

The energy dispersion with respect to $\tilde{k}_z$ consists of two bands with a band gap of $2\tilde{\Omega}_R$ at the origin $\tilde{\mathbf{k}} = 0$. The lower energy band $\tilde{\epsilon}_-(\tilde{\mathbf{k}})$ is a symmetric double well along the $\tilde{k}_z$ direction with the two minima located at

$$\tilde{k}_z = \pm\tilde{k}_0 \equiv \pm\sqrt{1 - \tilde{\Omega}_R^2/4}, \tag{4.9}$$

for $\tilde{\Omega}_R < 2$, and it has a single minimum at $\tilde{k}_z = 0$ when $\tilde{\Omega}_R > 2$ (the minima along the other two directions always occur at $\tilde{\mathbf{k}}_\perp = 0$). The operators $\hat{\boldsymbol{\Phi}}(\mathbf{k}) = (\hat{\varphi}_+(\mathbf{k}), \hat{\varphi}_-(\mathbf{k}))^\mathsf{T}$ annihilate a boson at momentum $\mathbf{k}$ in the upper and lower bands and are related to the field operators through $\hat{\boldsymbol{\Psi}}(\mathbf{r}) = \sum_{\mathbf{k},\lambda=\pm} e^{i\mathbf{k}\cdot\mathbf{r}}\boldsymbol{\phi}_\lambda(\mathbf{k})\hat{\varphi}_\lambda(\mathbf{k})$. Note that the laboratory-frame bosonic field operators $\hat{\tilde{\boldsymbol{\Psi}}}(\mathbf{r})$ (which gives the observable atomic density distribution) are related to $\hat{\boldsymbol{\Psi}}(\mathbf{r})$ by the unity transformation $\mathscr{U}_2$, i.e. $\hat{\tilde{\boldsymbol{\Psi}}}(\mathbf{r}) = \mathscr{U}_2^\dagger\hat{\boldsymbol{\Psi}}(\mathbf{r})$.

The single-particle ground state of the symmetric double well (i.e. when $\tilde{\Omega}_R < 2$) is two-fold degenerate; the atom is either in the left minimum at $\tilde{\mathbf{k}} = -\tilde{\mathbf{k}}_0 = (0, 0, -\tilde{k}_0)$ or the right minimum at $\tilde{\mathbf{k}} = \tilde{\mathbf{k}}_0 = (0, 0, \tilde{k}_0)$. The non-interacting N-particle ground state, when the cavity-mediated interactions are also absent, is therefore $(N+1)$-fold degenerate (any number of pseudospin-up atoms, up to N, can reside in the left well). Nonetheless, the two-body and cavity-mediated interactions compete with each other to lift this degeneracy.

4.3.1 Variational Approach

To determine the nature of the ground state, consider the ansatz for the Bose condensate wavefunction:

$$\begin{pmatrix}\psi_1(\mathbf{r})\\ \psi_2(\mathbf{r})\end{pmatrix} = \sqrt{\bar{n}}\left[c_1 e^{-ik_0 z}\begin{pmatrix}\cos\theta_{\mathbf{k}_0}\\ -\sin\theta_{\mathbf{k}_0}\end{pmatrix} + c_2 e^{ik_0 z}\begin{pmatrix}\sin\theta_{\mathbf{k}_0}\\ -\cos\theta_{\mathbf{k}_0}\end{pmatrix}\right] \tag{4.10}$$

where $k_0 = k_R\tilde{k}_0$ and $\bar{n} = N/V$ is the average particle density, with N and V being the total particle number and volume, respectively. The variational parameters are c_1 and c_2 with the normalization constraint $|c_1|^2 + |c_2|^2 = 1$. Once they are determined, one can find the relevant ground-state quantities such as the total density $n(\mathbf{r}) = |\psi_1(\mathbf{r})|^2 + |\psi_2(\mathbf{r})|^2$, and the magnetization per particle $s_z(\mathbf{r}) = \left[|\psi_1(\mathbf{r})|^2 - |\psi_2(\mathbf{r})|^2\right]/\bar{n}$:

$$n(\mathbf{r}) = \bar{n}\left[1 + 2|c_1 c_2|\cos(2k_0 z + \gamma)\sin 2\theta_{\mathbf{k}_0}\right], \tag{4.11}$$

$$s_z(\mathbf{r}) = \left(|c_1|^2 - |c_2|^2\right)\cos 2\theta_{\mathbf{k}_0}, \tag{4.12}$$

where γ is the relative phase between c_1 and c_2. Note that the magnetization s_z is homogeneous while the total density $n(\mathbf{r})$ exhibits fringes in the z direction provided that $c_1 c_2 \neq 0$. Constraining $\tilde{\Omega}_R < 2$, one can write $\sin 2\theta_{\mathbf{k}_0} = \tilde{\Omega}_R/2$ and $\cos 2\theta_{\mathbf{k}_0} = \tilde{k}_0$; then these take the simpler form $n(z) = \bar{n}[1 + \tilde{\Omega}_R|c_1 c_2|\cos(2k_0 z + \gamma)]$ and $s_z = \tilde{k}_0\left(2|c_1|^2 - 1\right)$. The energy functional $E[c_1, c_2] = E_0 + E_{\text{int}}$ is obtained from Eq. (4.3) by replacing the field operators $\hat{\psi}_\tau$ with the corresponding condensate wavefunctions ψ_τ. This yields $E_0 = -NE_R\tilde{\Omega}_R^2/4$ and

$$\begin{aligned}E_{\text{int}} = \frac{N^2|g_1|}{4V}\Bigg\{&\operatorname{sgn}(g_1) + \tilde{g}_2 + 4\tilde{U}_1 + 2\delta\tilde{U} - 2\tilde{U}_{\text{ds}}\tilde{\Omega}_R\\ &+ \left[2\tilde{g}_{12} - \operatorname{sgn}(g_1) - \tilde{g}_2 + 4\left(\tilde{U}_{\text{ss}} - \tilde{U}_1\right) - 2\delta\tilde{U}\right]\frac{\tilde{\Omega}_R^2}{8}\\ &+ \frac{1}{2}\left(|c_1|^2 - |c_2|^2\right)\left(4 - \tilde{\Omega}_R^2\right)^{1/2}\left[\operatorname{sgn}(g_1) - \tilde{g}_2 - 2\delta U\right]\\ &- 2|c_1 c_2|^2\Bigg[\operatorname{sgn}(g_1) + \tilde{g}_2 + 4\tilde{U}_1 + 2\delta\tilde{U} - 2\tilde{g}_{12}\\ &\qquad - \left(3\operatorname{sgn}(g_1) + 3\tilde{g}_2 + 8\tilde{U}_1 + 4\delta\tilde{U} - 2\tilde{g}_{12}\right)\frac{\tilde{\Omega}_R^2}{8}\Bigg]\Bigg\},\end{aligned} \tag{4.13}$$

where the two-body interaction strengths are rescaled by $|g_1|$ (for example $\tilde{g}_2 = g_2/|g_1|$) and the cavity-mediated interaction strengths are rescaled by $|g_1|/V$ (for example $\tilde{U}_1 = VU_1/|g_1|$). In the above equations we have defined $2\tilde{U}_{\rm ss} \equiv \tilde{U}_{\pm} + \tilde{U}_{\mp}$ and $\delta\tilde{U} \equiv \tilde{U}_2 - \tilde{U}_1$, and $\mathrm{sgn}(g_1) = g_1/|g_1| = \pm 1$ denotes the sign of g_1. E_0 is the single-particle contribution to the energy and is independent of c_i, as expected. Minimizing $E_{\rm int}$ with respect to c_i determines the ground state of the system. The parameters $\tilde{U}_1$ and $\delta\tilde{U}$ (or $\tilde{U}_2$) are the only cavity-mediated interaction parameters having an effect on the ground state.

Consider first the simplest case where $\tilde{g}_2 = \mathrm{sgn}(g_1)$ and $\delta\tilde{U} = 0$, so that only the last line of Eq. (4.13) contributes to the interaction energy. Then the energy is minimized either with $(c_1, c_2) = (1, 0)$ or $(0, 1)$, or with $c_1 = c_2 = 1/\sqrt{2}$ (neglecting relative phases). The first solution set corresponds to all atoms condensing in a single minimum of the single-particle energy dispersion (i.e. a single plane wave with wave vector $-\mathbf{k}_0$ or $\mathbf{k}_0$), labeled the plane wave phase (PWP). In the PWP the total density is uniform. The magnetization takes the value $s_z = \pm\tilde{k}_0 = \pm(1 - \tilde{\Omega}_R^2/4)^{1/2}$, with the upper (lower) sign corresponding to $c_1 = 1$ ($c_1 = 0$). For small $\tilde{\Omega}_R$ the magnetization approaches unity. Note that the PWP is twofold degenerate; that is, all atoms can condense in the left ($c_1 = 1$) or right minimum ($c_2 = 1$). The second solution set corresponds to atoms condensing into a superposition state of plane waves. It is characterized by the broken translational symmetry and the resulting density $n(z) = n[1 + \frac{1}{2}\tilde{\Omega}_R \cos(2k_0 z + \gamma)]$ exhibits spatial variations in the z (i.e., SO-coupling) direction, so this is referred to as the stripe phase (SP). In this phase the density oscillations have greatest contrast for large $\tilde{\Omega}_R \to 2$. The SP magnetization s_z is zero.

The SP solution yields a lower energy than the PWP solution when the term in square brackets in the last line of Eq. (4.13) is positive. (Recall $\tilde{g}_2 = \mathrm{sgn}(g_1)$ and $\delta\tilde{U} = 0$ so that the middle line vanishes identically.) The cavity interaction strength that favors the SP solution is therefore $\tilde{U}_1 > \tilde{U}_{1\mathrm{c}}^0$, where

$$\tilde{U}_{1\mathrm{c}}^0 \equiv \frac{8\,[\tilde{g}_{12} - \mathrm{sgn}(g_1)] - [\tilde{g}_{12} - 3\,\mathrm{sgn}(g_1)]\,\tilde{\Omega}_R^2}{4(4 - \tilde{\Omega}_R^2)}, \tag{4.14}$$

is the critical cavity interaction for the SP-PWP transition. In the limit of small $\tilde{\Omega}_R$, this becomes $\tilde{U}^0_{1c} \simeq \frac{1}{2}[\tilde{g}_{12} - \mathrm{sgn}(g_1)] + \frac{1}{16}[\tilde{g}_{12} + \mathrm{sgn}(g_1)]\tilde{\Omega}^2_R$. If $\tilde{g}_{12} = \mathrm{sgn}(g_1)$ the SP is favored for any non-zero, positive cavity interaction in the limit $\tilde{\Omega}_R \to 0$. On the other hand when $\tilde{\Omega}_R \to 2$ and $\tilde{g}_{12} \neq -\mathrm{sgn}(g_1)$, the critical cavity interaction $\tilde{U}^0_{1c}$ diverges and SP is only favored for very large positive cavity interaction.

It is important to verify that the total interaction energy, Eq. (4.13), remains positive; the system is stable only if $\partial^2 E_{\mathrm{int}}/\partial N^2 > 0$. Let us examine this first in the SP where $c_1 = c_2 = 1/\sqrt{2}$, for a special case where $\tilde{U}_{\mathrm{ds}} = \tilde{U}_{\mathrm{ss}} = \tilde{U}_1$ (and $\tilde{g}_2 = \mathrm{sgn}(g_1)$ and $\delta\tilde{U} = 0$ as before). One obtains

$$E_{\mathrm{int}} = \frac{N^2|g_1|}{4V}\left\{\frac{1}{8}\left[\tilde{g}_{12} + \mathrm{sgn}(g_1)\right]\left(8 + \tilde{\Omega}^2_R\right) + \frac{1}{2}\tilde{U}_1\left(2 - \tilde{\Omega}_R\right)^2\right\}. \tag{4.15}$$

Surprisingly, the SP is energetically stable for two-component attractive Bose condensates in the presence of SO interactions as long as the inter-species interaction strength is sufficiently large and positive. Substituting the critical cavity interaction $\tilde{U}^0_{1c}$ into Eq. (4.15) yields the constraint

$$\tilde{g}_{12} \geqslant \mathrm{sgn}(g_1)\frac{\tilde{\Omega}_R\left[(2 - \tilde{\Omega}_R)^2 - 12\right]}{\tilde{\Omega}^3_R + 16}. \tag{4.16}$$

In the limit of $\tilde{\Omega}_R \to 0$, for the lowest possible values of the cavity interaction favoring the SP phase $\tilde{U}_1 \gtrsim \tilde{U}^0_{1c} = \frac{1}{2}[\tilde{g}_{12} - \mathrm{sgn}(g_1)]$, the SP is energetically stable as long as $\tilde{g}_{12} \geqslant 0$, with no constraint on the sign of the intra-species interaction strength. Thus, the infinite-range cavity-mediated atom-atom interactions stabilize attractive two-component Bose condensates against collapse, even in the absence of a confining potential. For larger values of $\tilde{U}_1$ even the inter-species interactions can be attractive.

The coefficient of $\tilde{U}_1$ in Eq. (4.15) is strictly positive. Therefore, for a given parameter set $\{\mathrm{sgn}(g_1), \tilde{g}_{12}, \tilde{\Omega}_R\}$ one can choose arbitrary large positive values of the cavity interaction strength to strongly favor SP without compromising stability (i.e. to satisfy $\tilde{U}_1 > \tilde{U}^0_{1c}$ while ensuring that $E_{\mathrm{int}} \geqslant 0$). In other words, the minimal cavity interaction $\tilde{U}_1$ which favors a

stable SP satisfies

$$\tilde{U}_1 > \max\left\{ -\frac{\left[\tilde{g}_{12} + \mathrm{sgn}(g_1)\right]\left(8 + \tilde{\Omega}_R^2\right)}{4\left(2 - \tilde{\Omega}_R\right)^2}, \tilde{U}_{1\mathrm{c}}^0 \right\}. \tag{4.17}$$

The stability of PWP can be investigated in a similar manner. The plane wave phase is favored when $\tilde{U}_1 < \tilde{U}_{1\mathrm{c}}^0$. The positivity constraint of the interaction energy in the PWP

$$E_{\mathrm{int}} = \frac{N^2|g_1|}{2V}\left\{ \mathrm{sgn}(g_1) + \frac{1}{8}\left[\tilde{g}_{12} - \mathrm{sgn}(g_1)\right]\tilde{\Omega}_R^2 + \tilde{U}_1\left(2 - \tilde{\Omega}_R\right) \right\} > 0, \tag{4.18}$$

imposes a lower bound in the cavity interaction

$$-\frac{8\,\mathrm{sgn}(g_1) + \left[\tilde{g}_{12} - \mathrm{sgn}(g_1)\right]\tilde{\Omega}_R^2}{8\left(2 - \tilde{\Omega}_R\right)} < \tilde{U}_1 < \tilde{U}_{1\mathrm{c}}^0, \tag{4.19}$$

beyond which PWP is unstable. Thus, even the PWP becomes energetically stable for attractive SO-coupled two-component Bose condensates if the cavity-mediated interactions are judiciously chosen.

Figure 4.2 depicts the phase diagrams in the $\{\tilde{U}_1, \tilde{\Omega}_R\}$ and $\{\tilde{U}_1, \tilde{g}_{12}\}$ parameter planes. The phase diagrams are comprised of two physical regions: the SP and PWP, denoted by black and white in Fig. 4.2, respectively. The dark (light) grey indicates the regions where the SP (PWP) is energetically unstable. Figure 4.2(a) shows the phase diagram in the $\{\tilde{U}_1, \tilde{\Omega}_R\}$ parameter space for $\mathrm{sgn}(g_1) = \tilde{g}_2 = 1$ and different values of $\tilde{g}_{12}$. The SP is favored over an ever-larger parameter space as $\tilde{U}_1$ increases as long as $|\tilde{\Omega}_R| < 2$ to assure the existence of a double-well single-particle dispersion. This general trend is also evident from Fig. 4.2(b), the phase diagram in the $\{\tilde{U}_1, \tilde{g}_{12}\}$ parameter plane for $\mathrm{sgn}(g_1) = \tilde{g}_2 = -1$ and constant $\tilde{\Omega}_R = 0.1$, where Eq. (4.14) reveals that the phase boundary is linear in $\tilde{g}_{12}$ for fixed $\tilde{\Omega}_R$.

Relaxing the constraint considered above that $\delta\tilde{U} = 0$ in Eq. (4.13), one can prepare any arbitrary superposition state, i.e. arbitrary c_1 and c_2 subject to $|c_1|^2 + |c_2|^2 = 1$. The PWP is no longer degenerate; rather, the minimum favored depends on the sign of $\delta\tilde{U}$. Figure 4.3 shows the dependence of $|c_1|^2$ in the $\{\tilde{U}_{12}, \tilde{\Omega}_R\}$ plane for $\mathrm{sgn}(g_1) = \tilde{g}_2 = \delta\tilde{U} = 1$, and $\tilde{g}_{12} = 2$. Under these conditons the SP with $|c_1| = |c_2|$ is found only for very large $\tilde{U}_1 \gg \tilde{U}_{1\mathrm{c}}$, i.e. far

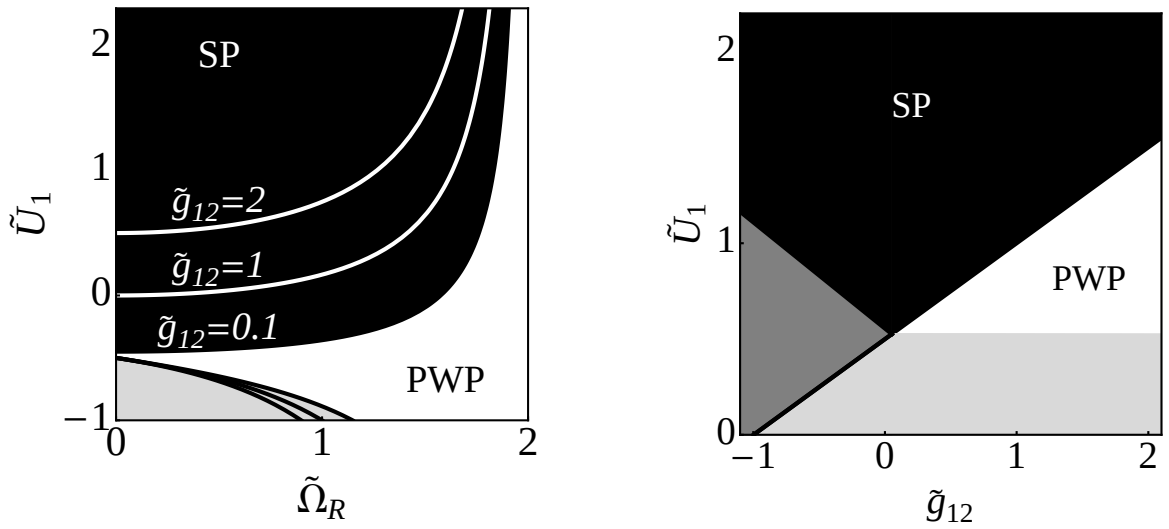

(a) (b)

Figure 4.2: Phase diagrams in the (a) $\{\tilde{U}_1, \tilde{\Omega}_R\}$ and (b) $\{\tilde{U}_1, \tilde{g}_{12}\}$ parameter planes. The stripe and plane-wave phases are denoted by black and white, respectively; dark (light) grey indicates the regions where the SP (PWP) is unstable. (a) Phase diagram for $\mathrm{sgn}(g_1) = \tilde{g}_2 = 1$ and different values of $\tilde{g}_{12} = 0.1$, 1, and 2. (b) Phase diagram for $\mathrm{sgn}(g_1) = \tilde{g}_2 = -1$ and $\tilde{\Omega}_R = 0.1$.

from the SP-PWP phase boundary $\tilde{U}_{1c}$. Whereas for $\tilde{U}_1 \to \tilde{U}_{1c}^+$, $|c_1|$ increases monotonically until the PWP with $|c_1|^2 = 1$ is attained for $\tilde{U}_1 < \tilde{U}_{1c}$ (note that the critical value $\tilde{U}_{1c} \simeq \tilde{U}_{1c}^0$ and is weakly dependent on $\delta\tilde{U}$, as discussed below). The PWP begins to be unstable in the left bottom corner of this figure.

The magnetization $s_z = \tilde{k}_0\,(2|c_1|^2 - 1)$ as a function of $\tilde{U}_1$ is illustrated with the black solid curve in Fig. 4.4 for $\mathrm{sgn}(g_1) = \tilde{g}_2 = \delta\tilde{U} = 1$, $\tilde{g}_{12} = 2$, and $\tilde{\Omega}_R = 0.1$. For contrast, the magnetization when $\delta\tilde{U} = 0$ is also shown (blue dashed curve). Note that while the sign of the magnetization in the PWP is arbitrary for the $\delta\tilde{U} = 0$ case (a spontaneously broken symmetry in the ground state), in the present case the sign of s_z always follows that of $\delta\tilde{U}$. On the PWP side, the magnetization is fixed at its maximal value $s_z = \tilde{k}_0$; for $\tilde{U}_1 \gtrsim \tilde{U}_{1c}$ on the SP side, the magnetization decreases sharply before reaching an asymptotic value deep within the SP phase.

For small $\delta\tilde{U}$ and $\tilde{\Omega}_R$, the SP-PWP phase transition occurs at almost the same value of

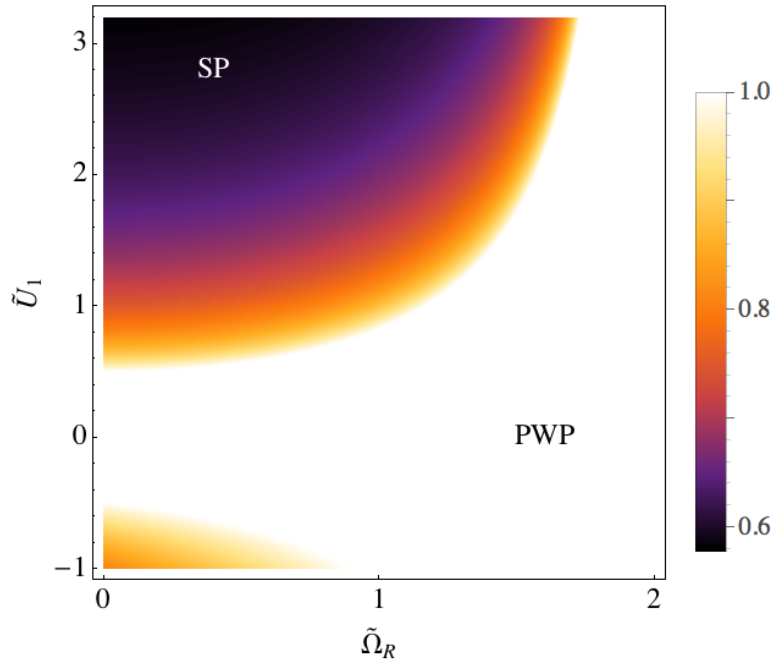

Figure 4.3: (Color online) Density plot of $|c_1|^2$ in the $\{\tilde{U}_1, \tilde{\Omega}_R\}$ parameter plane for $\mathrm{sgn}(g_1) = \tilde{g}_2 = \delta\tilde{U} = 1$, and $\tilde{g}_{12} = 2$. The PWP begins to be unstable in the left bottom corner.

the critical cavity interaction $\tilde{U}_{1c}^0 = 0.5$ obtained using Eq. (4.14) which assumed $\delta\tilde{U} = 0$. Near the phase transition point on the SP side, one can write $c_1 = 1 - x^2$ and $c_2 = \sqrt{2}x$, where $x \ll 1$ and $c_1^2 + c_2^2 \simeq 1 + \mathcal{O}(x^4)$. Setting the term proportional to x^2 in $E_{\mathrm{int}}[c_1 = 1, c_2 = 0] - E_{\mathrm{int}}[c_1 = 1 - x^2, c_2 = \sqrt{2}x]$ equal to zero yields a modified critical cavity interaction

$$\tilde{U}_{1c} = \tilde{U}_{1c}^0 - \left[\frac{2 - (4 - \tilde{\Omega}_R^2)^{1/2} - \frac{1}{2}\tilde{\Omega}_R^2}{4 - \tilde{\Omega}_R^2}\right]\delta\tilde{U}. \tag{4.20}$$

In the small $\tilde{\Omega}_R$ limit this may be simplified to $\tilde{U}_{1c} \simeq \frac{1}{2}[\tilde{g}_{12} - \mathrm{sgn}(g_1)] + \frac{1}{16}[\tilde{g}_{12} + \mathrm{sgn}(g_1) + \delta\tilde{U}]\tilde{\Omega}_R^2$, which is the same critical cavity interaction $\tilde{U}_{1c}^0$ obtained above in the small $\tilde{\Omega}_R$ limit, save for the $\delta\tilde{U}$-dependent correction.

The behavior of the magnetization for $\tilde{U}_1 > \tilde{U}_{1c}$ suggests that one can define the order parameter for the SP to be $P = 1 - s_z/\tilde{k}_0 = 2(1 - c_1^2)$. As desired, this vanishes in the PWP (here we only consider a PWP with momentum $-\mathbf{k}_0$) and takes a nonzero value in SP. The order parameter is shown in the inset of Fig. 4.4. The discontinuity in the derivative of P with $\tilde{U}_1$ suggests that the SP-PWP quantum (zero-temperature) phase transition is

second order. It is therefore of interest to determine the (mean-field) exponent β for the order parameter P in the vicinity of the transition point. Substituting $\tilde{U}_1 = \tilde{U}_{1c} + \chi$ into the energy functional $E_{\rm int}$ and minimizing it with respect to c_1 yields

$$c_1 = \sqrt{\frac{2\delta\tilde{U}\left(4-\tilde{\Omega}_R^2\right)^{1/2} + \chi\left(4-\tilde{\Omega}_R^2\right)}{2\delta\tilde{U}\left(4-\tilde{\Omega}_R^2\right)^{1/2} + 2\chi\left(4-\tilde{\Omega}_R^2\right)}}. \tag{4.21}$$

The order parameter $P = 2(1-c_1^2)$ computed using this expression for c_1 is illustrated as the green dashed curve in the the inset of Fig. 4.4, and is in excellent agreement with the numerical results of the variational approach, shown as the black solid curve. Taylor expanding c_1 in Eq. (4.21) for small χ and $\tilde{\Omega}_R$ up to first and second order, respectively, one obtains $c_1^{\rm MF} \simeq 1 - \chi/2\delta\tilde{U}$ (the term proportional to $\chi\tilde{\Omega}_R^2$ is also omitted). This yields the mean-field order parameter $P_{\rm MF} = 2\chi/\delta\tilde{U} = 2(\tilde{U}_1 - \tilde{U}_{1c})^\beta/\delta\tilde{U}$ and a critical exponent $\beta = 1$. The behavior of the order parameter near the transition point fits well to P, as is shown by the orange dashed curve in the inset of Fig. 4.4.

In principle, it is not valid to consider $\delta\tilde{U} \neq 0$ while at the same time assuming that $\tilde{\delta} \equiv \hbar\delta/E_R = 0$. Rather, if $\eta_1 \neq \eta_2 \neq 0$ but $\eta_1 \sim \eta_2$, then Eqs. (4.7) state that $\tilde{\delta} \sim \delta\tilde{U}$ whenever $\tilde{U}_1 \sim \tilde{\Omega}_R$. That said, in Fig. 4.4 the parameters are chosen so that $\tilde{\Omega}_R = 0.1 \ll \delta\tilde{U} = 1$. One can therefore expect $\tilde{\delta} \ll \delta\tilde{U}$ by a similar ratio, which again justifies neglecting it.

Consider briefly the effect of keeping a non-zero but small value of $\tilde{\delta}$. The single-particle energy dispersion of the spin-orbit Hamiltonian (4.5) becomes

$$\tilde{\epsilon}_\pm(\tilde{\mathbf{k}}) = \tilde{k}^2 + 1 \pm \sqrt{\frac{1}{4}\left(4\tilde{k}_z + \tilde{\delta}\right)^2 + \tilde{\Omega}_R^2}, \tag{4.22}$$

rather than the expressions given in Eq. (4.8a). The associated (orthogonal) spinors have the same form as Eqs. (4.8b) but now $\sin 2\theta_{\mathbf{k}} = \tilde{\Omega}_R/\sqrt{\frac{1}{4}\left(4\tilde{k}_z + \tilde{\delta}\right)^2 + \tilde{\Omega}_R^2}$. For $\tilde{\delta} \neq 0$, the lower double-well dispersion curve $\tilde{\epsilon}_-$ is no longer symmetric; rather, the right well is lower (higher) when $\tilde{\delta} > 0$ ($\tilde{\delta} < 0$). Thus, in the absence of particle interactions a PWP is energetically favored in one well or the other with no ambiguity. The presence of $\tilde{\delta}$ precludes a simple

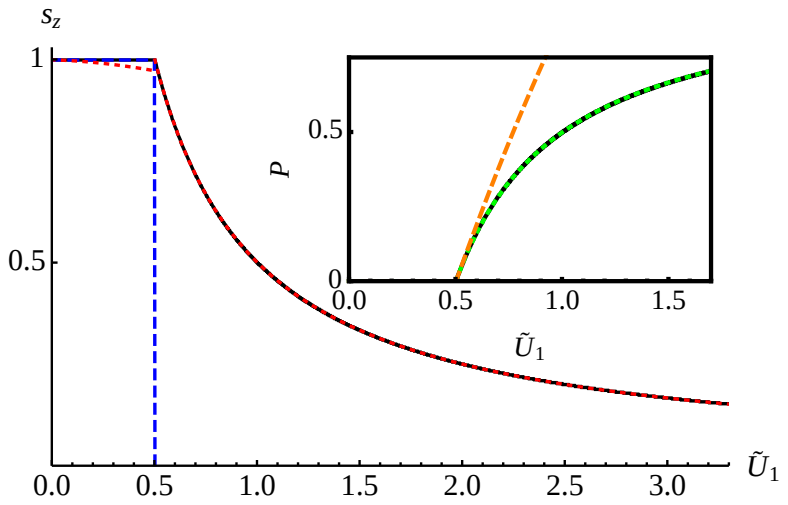

Figure 4.4: (Color online) The magnetization s_z as a function of $\tilde{U}_1$ shown as the black solid curve for $\mathrm{sgn}(g_1) = \tilde{g}_2 = \delta\tilde{U} = 1$, $\tilde{g}_{12} = 2$, and $\tilde{\Omega}_R = 0.1$. The blue dashed curve represents the magnetization when $\delta\tilde{U} = 0$. The red dotted curves are the magnetization computed from solutions of the coupled Gross-Pitaevskii equations in the SP and PWP assuming $\tilde{U}_{\mathrm{ss}} = \tilde{U}_{\mathrm{ds}} = \tilde{U}_1$ for the same parameters as the solid black curve, and $|g_1|\bar{n}/E_R = 1$. Inset: the SP order parameter P is shown as a function of $\tilde{U}_1$ (black curve); an analytical approximation (dashed green curve) and the behavior near the critical point (orange dashed curve) are shown for comparison.

form like Eq. (4.9) for the location of the energy minima, but in the limit when both $\tilde{\Omega}_R \ll 1$ and $\tilde{\delta} \ll 1$ one obtains

$$\tilde{k}_0 \approx 1 - \frac{\tilde{\Omega}_R^2}{8}\left(1 - \frac{\tilde{\delta}}{2}\right). \tag{4.23}$$

The lowest-order contribution of $\tilde{\delta}$ is a correction to the coefficient of the already small $\tilde{\Omega}_R$-dependent term, and therefore the value of $\tilde{k}_0$ is well-approximated by assuming $\tilde{\delta} = 0$. Likewise, the BEC approximation consists of $\tilde{k}_z$ with $\tilde{k}_0$; because $4\tilde{k}_z \to 4\tilde{k}_0 \approx 4 \gg \tilde{\delta}$ in the expressions for the single-particle energies and eigenvectors above, $\tilde{\delta}$ can be similarly neglected in the calculations.

4.3.2 Coupled Gross-Pitaevskii Equations

While the variational calculation discussed in the preceding section has revealed that a ring cavity can stabilize SPs in attractive SO-coupled Bose-Einstein condensates, it is important to verify the results using a more rigorous approach. In this section, the coupled Gross-

Pitaevskii (GP) equations are derived for both PWP and SP states and the ground state properties are obtained from their solutions. The GP equations can be obtained directly from the many-particle Hamiltonian (4.3):

$$\left[\frac{\hbar^2}{2m}\hat{\triangle}_1 + g_1|\psi_1|^2 + g_{12}|\psi_2|^2 + 2U_1N_1 + 2U_{\rm ds}S_x\right]\psi_1 + \left[\hbar\Omega_R + 2U_{\rm ss}S_- + U_{\rm ds}N\right]\psi_2 = \mu\psi_1,$$
$$\left[\frac{\hbar^2}{2m}\hat{\triangle}_2 + g_2|\psi_2|^2 + g_{12}|\psi_1|^2 + 2U_2N_2 + 2U_{\rm ds}S_x\right]\psi_2 + \left[\hbar\Omega_R + 2U_{\rm ss}S_+ + U_{\rm ds}N\right]\psi_1 = \mu\psi_2, \tag{4.24}$$

where $\hat{\triangle}_1 = -\nabla_\perp^2 + (-i\partial_z + k_R)^2$ and $\hat{\triangle}_2 = -\nabla_\perp^2 + (-i\partial_z - k_R)^2$ and the Bose condensate wavefunctions for the two spin components are denoted by $\psi_{1(2)}$ rather than $\psi_{1(2)}(\mathbf{r})$ to save space.

Plane-Wave Phase

The GP equations (4.24) can be simplified in the PWP by assuming homogeneous wavefunctions $\psi_\tau(\mathbf{r}) = e^{\pm ik_0z}\bar{\psi}_\tau$, where the upper (lower) sign corresponds to a condensate in the right (left) minimum. The GP equations are then recast as

$$\frac{|g_1|}{E_R}\left\{\left[\left(\mathrm{sgn}(g_1) + 2\tilde{U}_1\right)|\bar{\psi}_1|^2 + \left(\tilde{g}_{12} + 2\tilde{U}_{\rm ss}\right)|\bar{\psi}_2|^2\right]\bar{\psi}_1 + \tilde{U}_{\rm ds}\left(2|\bar{\psi}_1|^2 + |\bar{\psi}_2|^2\right)\bar{\psi}_2 + \tilde{U}_{\rm ds}\bar{\psi}_1^2\bar{\psi}_2^*\right\}$$
$$= \left[\tilde{\mu} - (\tilde{k}_0 \pm 1)^2\right]\bar{\psi}_1 - \tilde{\Omega}_R\bar{\psi}_2,$$
$$\frac{|g_1|}{E_R}\left\{\left[\left(\tilde{g}_2 + 2\tilde{U}_2\right)|\bar{\psi}_2|^2 + \left(\tilde{g}_{12} + 2\tilde{U}_{\rm ss}\right)|\bar{\psi}_1|^2\right]\bar{\psi}_2 + \tilde{U}_{\rm ds}\left(|\bar{\psi}_1|^2 + 2|\bar{\psi}_2|^2\right)\bar{\psi}_1 + \tilde{U}_{\rm ds}\bar{\psi}_2^2\bar{\psi}_1^*\right\}$$
$$= \left[\tilde{\mu} - (\tilde{k}_0 \mp 1)^2\right]\bar{\psi}_2 - \tilde{\Omega}_R\bar{\psi}_1, \tag{4.25}$$

where again the upper (lower) sign in each equation corresponds to a condensate in the right (left) minimum, and the chemical potential is expressed in recoil energy units, $\tilde{\mu} \equiv \mu/E_R$.

The chemical potential can be obtained from the first of Eqs. (4.25) and then substituted into the second. Under the assumption that both condensate wavefunctions are real, $\tilde{U}_1 = \tilde{U}_{\rm ss} = \tilde{U}_{\rm ds}$, and $\mathrm{sgn}(g_1) = \tilde{g}_2$, one obtains

$$\frac{|g_1|}{E_R}\left[\left(\tilde{g}_{12} - \mathrm{sgn}(g_1)\right)\left(\bar{\psi}_2^2 - \bar{\psi}_1^2\right)\bar{\psi}_1\bar{\psi}_2 + \tilde{U}_1\left(\bar{\psi}_2^4 - \bar{\psi}_1^4\right)\right] \pm 4\tilde{k}_0\bar{\psi}_1\bar{\psi}_2 + \tilde{\Omega}_R\left(\bar{\psi}_2^2 - \bar{\psi}_1^2\right) = 0. \tag{4.26}$$

In the PWP, both $\bar{\psi}_1$ and $\bar{\psi}_2$ are assumed to be constant, so that $\bar{\psi}_1^2 + \bar{\psi}_2^2 = \bar{n}$ and $\bar{\psi}_1^2 - \bar{\psi}_2^2 = \bar{n}s_z$. Inserting these into Eq. (4.26) gives

$$\sqrt{1-s_z^2}\left[\mp 4\tilde{k}_0 + s_z\frac{|g_1|\bar{n}}{E_R}\Big(\tilde{g}_{12} - \mathrm{sgn}(g_1)\Big)\right] + 2s_z\left(\tilde{\Omega}_R + \tilde{U}_1\frac{|g_1|\bar{n}}{E_R}\right) = 0. \tag{4.27}$$

When $\tilde{U}_1 = 0$ and $\tilde{\Omega}_R \approx 0$, this expression is approximately correct when $s_z \approx 1$, consistent with the variational results in this regime. Recall that in the variational approach, the magnetization $s_z = \tilde{k}_0$ is constant [c.f. Eq. (4.12)], solely determined by $\tilde{\Omega}_R$. Unlike the variational result, however, it is immediately apparent from the second term in Eq. (4.27) that the magnetization must decrease monotonically as $\tilde{U}_1$ is increased.

The magnetization s_z obtained via numerical solution of Eq. (4.27) is shown as the red dotted curve in Fig. 4.4 for a condensate in the left well (i.e. choosing the lower sign) of the PWP for $\tilde{U}_1 \leq \tilde{U}_{1c}$. Parameters are $\tilde{U}_1 = \tilde{U}_{ss} = \tilde{U}_{ds}$, $\mathrm{sgn}(g_1) = \tilde{g}_2 = |g_1|\bar{n}/E_R = \delta\tilde{U} = 1$, $\tilde{g}_{12} = 2$, and $\tilde{\Omega}_R = 0.1$. As expected, the magnetization decreases monotonically with $\tilde{U}_1$ from its maximum at $\tilde{U}_1 = 0$. The difference between the results of the two methods has its origins in the fact that the variational ansatz, Eq. (4.10), is a single-particle wavefunction which satisfies the GP equations in PWP only when all the two-body and cavity-mediated interactions are zero. In principle, the variational ansatz could be remedied by allowing both k_0 and $\theta_{\mathbf{k}_0}$ to be variational parameters [76]. The dependence of the solution of GP equations on the two-body and cavity-mediated interactions will be investigated further in Sec. 4.3.3, where we calculate elementary excitations in the PWP.

Stripe Phase

The momentum dependence of the condensate in the SP is not as readily apparent as it is for the PWP. It is therefore convenient to instead construct an effective low energy Hamiltonian by first mapping the complete Hamiltonian (4.3) into the lower band and then deriving the low energy coupled GP equations [78, 187]. This is reasonable because the occupation of the upper band $\epsilon_+(\mathbf{k})$ can be assumed to be small at low temperatures $k_\mathrm{B}T \ll \hbar\Omega_R$. Furthermore, only states in the vicinity of the two minima $\pm\tilde{\mathbf{k}}_0$ will be occupied.

The field operators $\hat{\mathbf{\Psi}}(\mathbf{r})$ can then be expanded in the lower band basis around the two minima (recall that $\boldsymbol{\phi}_-(\mathbf{k})$ is the *two-component* spinor of the lower band):

$$\hat{\mathbf{\Psi}}(\mathbf{r}) \simeq \sum_{\mathbf{q}<\mathbf{q}_c} \left[e^{i(-\mathbf{k}_0+\mathbf{q})\cdot\mathbf{r}} \boldsymbol{\phi}_-(-\mathbf{k}_0+\mathbf{q}) \hat{\varphi}_-(-\mathbf{k}_0+\mathbf{q}) + e^{i(\mathbf{k}_0+\mathbf{q})\cdot\mathbf{r}} \boldsymbol{\phi}_-(\mathbf{k}_0+\mathbf{q}) \hat{\varphi}_-(\mathbf{k}_0+\mathbf{q}) \right], \tag{4.28}$$

where the sum over $\mathbf{q}$ need only be taken up to some maximum $\mathbf{q}_c$. Approximating the spinor $\boldsymbol{\phi}_-(\pm\mathbf{k}_0+\mathbf{q}) \simeq \boldsymbol{\phi}_-(\pm\mathbf{k}_0)$ in the limit $\tilde{\Omega}_R \ll 2$ and defining the new operators $\hat{\varphi}_{1'}(\mathbf{q}) \equiv \hat{\varphi}_-(-\mathbf{k}_0+\mathbf{q})$ and $\hat{\varphi}_{2'}(\mathbf{q}) \equiv \hat{\varphi}_-(\mathbf{k}_0+\mathbf{q})$ [78], the field operators read

$$\hat{\mathbf{\Psi}}(\mathbf{r}) = e^{-i\mathbf{k}_0\cdot\mathbf{r}} \boldsymbol{\phi}_-(-\mathbf{k}_0) \hat{\psi}_{1'}(\mathbf{r}) + e^{i\mathbf{k}_0\cdot\mathbf{r}} \boldsymbol{\phi}_-(\mathbf{k}_0) \hat{\psi}_{2'}(\mathbf{r}), \tag{4.29}$$

where $\hat{\psi}_{\tau'}(\mathbf{r}) = \sum_{\mathbf{q}} e^{i\mathbf{q}\cdot\mathbf{r}} \hat{\varphi}_{\tau'}(\mathbf{q})$. In the small $\tilde{\Omega}_R$ limit and keeping terms only up to second order in $\tilde{\Omega}_R$ and noting that $k_0 \simeq (1-\tilde{\Omega}_R^2/8)k_R$, the field operators can be further simplified to

$$\begin{pmatrix} \hat{\psi}_1(\mathbf{r}) \\ \hat{\psi}_2(\mathbf{r}) \end{pmatrix} \simeq \begin{pmatrix} (1-\frac{\tilde{\Omega}_R^2}{32})e^{-ik_0 z} & \frac{\tilde{\Omega}_R}{4} e^{ik_0 z} \\ -\frac{\tilde{\Omega}_R}{4} e^{-ik_0 z} & -(1-\frac{\tilde{\Omega}_R^2}{32}) e^{ik_0 z} \end{pmatrix} \begin{pmatrix} \hat{\psi}_{1'}(\mathbf{r}) \\ \hat{\psi}_{2'}(\mathbf{r}) \end{pmatrix}. \tag{4.30}$$

Note that the lab-frame pseudospin field operator $\hat{\tilde{\psi}}_\tau$ maps correctly to the corresponding dressed pseudospin field operator $\hat{\psi}_{\tau'}$ in the $\tilde{\Omega}_R \to 0$ limit; recall that $\hat{\tilde{\mathbf{\Psi}}}(\mathbf{r}) = \mathscr{U}_2^\dagger \hat{\mathbf{\Psi}}(\mathbf{r})$. Substituting Eq. (4.30) back into the original Hamiltonian (4.3) and only keeping terms to second order in $\tilde{\Omega}_R$ yields the effective low-energy Hamiltonian:

$$H_{\mathrm{e}} = \int d^3r \left(\hat{\mathbf{\Psi}}'^\dagger H_{\mathrm{e}}^{(1)} \hat{\mathbf{\Psi}}' + \frac{1}{2} g'_1 \hat{n}_{1'}^2 + \frac{1}{2} g'_2 \hat{n}_{2'}^2 + g'_{12} \hat{n}_{1'} \hat{n}_{2'} \right) + \frac{1}{2} U'_1 \hat{N}_{1'}^2 + \frac{1}{2} U'_2 \hat{N}_{2'}^2 + U'_{12} \hat{N}_{1'} \hat{N}_{2'}, \tag{4.31}$$

where $\hat{\mathbf{\Psi}}'(\mathbf{r}) = (\hat{\psi}_{1'}(\mathbf{r}), \hat{\psi}_{2'}(\mathbf{r}))^{\mathsf{T}}$, as before $\hat{N}_{\tau'} = \int \hat{n}_{\tau'}(\mathbf{r}) d^3r = \int \hat{\psi}_{\tau'}^\dagger(\mathbf{r}) \hat{\psi}_{\tau'}(\mathbf{r}) d^3r$ is the total atomic number operator for the dressed pseudospin $\tau' \in \{1', 2'\}$, and we have introduced the

dressed interaction parameters

$$
\begin{aligned}
g'_\tau &\equiv g_{\tau'\tau'} = g_\tau - \frac{1}{8}(g_\tau - g_{12})\tilde{\Omega}_R^2, \\
g'_{12} &\equiv g_{1'2'} = g_{12} + \frac{1}{8}(g_1 + g_2)\tilde{\Omega}_R^2, \\
U'_\tau &\equiv U_{\tau'\tau'} = 2U_\tau - U_{\rm ds}\tilde{\Omega}_R - \frac{1}{4}(U_\tau - U_{\rm ss})\tilde{\Omega}_R^2, \\
U'_{12} &\equiv U_{1'2'} = -U_{\rm ds}\tilde{\Omega}_R + \frac{1}{8}(U_1 + U_2 + 2U_{\rm ss})\tilde{\Omega}_R^2,
\end{aligned} \tag{4.32}
$$

with $\tau \in \{1, 2\}$ and $\tau' \in \{1', 2'\}$.

The single-particle part of the effective low energy Hamiltonian $H_{\rm e}^{(1)} = (-\hbar^2/2m)[\nabla_\perp^2 + (1 - \tilde{\Omega}_R^2/4)\partial_z^2]$ can be easily diagonalized [78], yielding the effective low energy dispersion $\epsilon_{\rm e}(\mathbf{k})/E_R = \tilde{k}_\perp^2 + (1 - \tilde{\Omega}_R^2/4)\tilde{k}_z^2$. It is important to note that the lowest single-particle energy state for both dressed pseudospins is the $\mathbf{k} = 0$ momentum state, not $\mathbf{k} = \pm\mathbf{k}_0$ as it was for the actual pseudospins. Then the effective low energy GP equations for the SP can be obtained from $H_{\rm e}$, Eq. (4.31):

$$
\begin{aligned}
\left[\left(\tilde{g}'_1 + \tilde{U}'_1\right)|\psi_{1'}|^2 + \left(\tilde{g}'_{12} + \tilde{U}'_{12}\right)|\psi_{2'}|^2\right]\psi_{1'} &= \bar{\mu}\psi_{1'}, \\
\left[\left(\tilde{g}'_2 + \tilde{U}'_2\right)|\psi_{2'}|^2 + \left(\tilde{g}'_{12} + \tilde{U}'_{12}\right)|\psi_{1'}|^2\right]\psi_{2'} &= \bar{\mu}\psi_{2'},
\end{aligned} \tag{4.33}
$$

where the dressed pseudospin wavefunctions $\psi_{\tau'}$ are assumed to be homogeneous and unitless parameters have been introduced for convenience: $\tilde{g}'_\tau = g'_\tau/|g_1|$, $\tilde{g}'_{12} = g'_{12}/|g_1|$, $\tilde{U}'_\tau = VU'_\tau/|g_1|$, and $\tilde{U}'_{12} = VU'_{12}/|g_1|$. Here $\bar{\mu} = \mu/|g_1|$ which has units of inverse volume. These algebraic equations have the solution

$$
\begin{aligned}
n_{1'} &= \frac{2\tilde{U}_2 + \tilde{g}'_2 - \tilde{g}'_{12} - \frac{1}{8}\left(\tilde{U}_1 + 3\tilde{U}_2\right)\tilde{\Omega}_R^2}{\tilde{g}'_1 + \tilde{g}'_2 - 2\tilde{g}'_{12} + 2\left(\tilde{U}_1 + \tilde{U}_2\right)\left(1 - \frac{1}{4}\tilde{\Omega}_R^2\right)}\bar{n}, \\
n_{2'} &= \frac{2\tilde{U}_1 + \tilde{g}'_1 - \tilde{g}'_{12} - \frac{1}{8}\left(3\tilde{U}_1 + \tilde{U}_2\right)\tilde{\Omega}_R^2}{\tilde{g}'_1 + \tilde{g}'_2 - 2\tilde{g}'_{12} + 2\left(\tilde{U}_1 + \tilde{U}_2\right)\left(1 - \frac{1}{4}\tilde{\Omega}_R^2\right)}\bar{n},
\end{aligned} \tag{4.34}
$$

where $n_{1'} + n_{2'} = \bar{n}$. Note that although the GP equations for the SP, Eq. (4.33), depend on the cavity parameters $\tilde{U}_{\rm ss}$ and $\tilde{U}_{\rm ds}$, these solutions do not; rather, $\tilde{U}_1$ and $\tilde{U}_2$ are the

only cavity interaction parameters that affect $\psi_{\tau'}$, consistent with the variational approach of Sec. 4.3.1.

The dressed magnetization $s_z' = (n_{1'} - n_{2'})/\bar{n}$ can easily be obtained from Eq. (4.34), and the actual magnetization $s_z = s_z'(1 - \tilde{\Omega}_R^2/8)$ up to $\mathcal{O}(\tilde{\Omega}_R^3)$ is found using Eq. (4.30):

$$s_z = \frac{\left[\tilde{g}_2' - \tilde{g}_1' + 2\delta\tilde{U}\left(1 - \frac{1}{8}\tilde{\Omega}_R^2\right)\right]\left(1 - \frac{1}{8}\tilde{\Omega}_R^2\right)}{\tilde{g}_1' + \tilde{g}_2' - 2\tilde{g}_{12}' + 2\left(\tilde{U}_1 + \tilde{U}_2\right)\left(1 - \frac{1}{4}\tilde{\Omega}_R^2\right)}. \tag{4.35}$$

The SP magnetization s_z is displayed as a function of $\tilde{U}_1 (\geqslant \tilde{U}_{1c})$ in Fig. 4.4 with the red dotted curve for $\mathrm{sgn}(g_1) = \tilde{g}_2 = \delta\tilde{U} = 1$, $\tilde{g}_{12} = 2$, and $\tilde{\Omega}_R = 0.1$. The behavior is indistinguishable from the magnetization obtained from the variational approach, Eq. (4.12). The critical cavity interaction for the SP-PWP phase transition can be obtained from Eq. (4.34) by setting $n_{1'} = \bar{n}$ (or setting $s_z' = 1$):

$$\tilde{U}_{1c}^{\mathrm{L}} = \frac{1}{4(4 - \tilde{\Omega}_R^2)}\Bigg\{ - \left[\tilde{g}_{12} - \mathrm{sgn}(g_1) - 2\tilde{g}_2 - \delta\tilde{U}\right]\tilde{\Omega}_R^2 + 8\left[\tilde{g}_{12} - \mathrm{sgn}(g_1)\right]\Bigg\}, \tag{4.36}$$

for a phase transition from SP to a PWP at the left minimum. Instead setting $n_{1'} = 0$ (or $s_z' = -1$) for a phase transition from SP to a PWP at the right minimum, one obtains

$$\tilde{U}_{1c}^{\mathrm{R}} = \frac{1}{4(4 - \tilde{\Omega}_R^2)}\Bigg\{ - \left[\tilde{g}_{12} - \mathrm{sgn}(g_1) - 2\tilde{g}_2 - 3\delta\tilde{U}\right]\tilde{\Omega}_R^2 + 8\left[\tilde{g}_{12} - \mathrm{sgn}(g_1) - 2\delta\tilde{U}\right]\Bigg\}. \tag{4.37}$$

Note that when $\mathrm{sgn}(g_1) = \tilde{g}_2$ and $\delta\tilde{U} = 0$, the two critical cavity interactions $\tilde{U}_{1c}^{\mathrm{L}}$ and $\tilde{U}_{1c}^{\mathrm{R}}$ become equal to the value $\tilde{U}_{1c}^0$ found using the variational approach, Eq. (4.14).

4.3.3 Elementary Excitations: Bogoliubov Theory

Thus far we have treated the bosons as classical fields, having replaced the field operators with their expectation values $\hat{\psi}_\tau \to \psi_\tau \equiv \langle\hat{\psi}_\tau\rangle$. In this section, we consider the quantum fluctuations of the fields and obtain the elementary excitation spectrum using Bogoliubov theory. This is accomplished by writing the field operators as $\hat{\psi}_\tau = \psi_\tau + \delta\hat{\psi}_\tau$, where $\delta\hat{\psi}_\tau$ is the quantum fluctuation operator. These expressions are substituted into the time-dependent GP equations and the resulting equations are linearized, i.e. terms are retained only up to first order in the fluctuations. One then obtains a set of time-dependent coupled equations for $\delta\hat{\psi}_\tau$ which yields the elementary excitation spectrum after diagonalization.

Plane-Wave Phase

Following the approach taken in Sec. 4.3.2 for the PWP, it is reasonable to define the bosonic field operator

$$\hat{\psi}_\tau(\mathbf{r},t) \equiv e^{\pm ik_0 z}\left[\bar{\psi}_\tau + \delta\hat{\psi}_\tau(\mathbf{r},t)\right], \tag{4.38}$$

where $\bar{\psi}_\tau$ are the time-independent, homogeneous solutions of the coupled GP equations (4.25) in the PWP. To consider time-dependent fluctuations around the equilibrium solutions it is convenient to replace the chemical potential (which is the eigenvalue of the time-independent GP equations) by a time-dependent operator, $\mu \to \mu + i\hbar\partial_t$. The time-dependent fluctuations can then be expressed using the usual Bogoliubov approach in terms of particle and hole excitations with amplitudes $\bar{u}_{\tau,\mathbf{q}}e^{i(\mathbf{q}\cdot\mathbf{r}-\omega t)}$ and $\bar{v}^*_{\tau,\mathbf{q}}e^{-i(\mathbf{q}\cdot\mathbf{r}-\omega t)}$, respectively.

Consider the specific case of a condensate in the left minimum $-\tilde{\mathbf{k}}_0$ of the double-well single-particle dispersion relation; for condensation in the right well one need only replace $\tilde{k}_0$ in what follows with $-\tilde{k}_0$. Substituting Eq. (4.38) into the time-dependent GP equations and keeping only linear terms in the fluctuations, one obtains the following non-Hermitian eigenvalue equation for each value of $\mathbf{q}$:

$$\begin{pmatrix} M_{11}-\hbar\omega(\mathbf{q}) & g_1\bar{\psi}_1^2 & g_{12}\bar{\psi}_1\bar{\psi}_2^* + \hbar\Omega_{\text{eff}} & g_{12}\bar{\psi}_1\bar{\psi}_2 \\ -g_1\bar{\psi}_1^{*2} & -M_{22}-\hbar\omega(\mathbf{q}) & -g_{12}\bar{\psi}_1^*\bar{\psi}_2^* & -g_{12}\bar{\psi}_1^*\bar{\psi}_2 - \hbar\Omega^*_{\text{eff}} \\ g_{12}\bar{\psi}_1^*\bar{\psi}_2 + \hbar\Omega^*_{\text{eff}} & g_{12}\bar{\psi}_1\bar{\psi}_2 & M_{33}-\hbar\omega(\mathbf{q}) & g_2\bar{\psi}_2^2 \\ -g_{12}\bar{\psi}_1^*\bar{\psi}_2^* & -g_{12}\bar{\psi}_1\bar{\psi}_2^* - \hbar\Omega_{\text{eff}} & -g_2\bar{\psi}_2^{*2} & -M_{44}-\hbar\omega(\mathbf{q}) \end{pmatrix} \begin{pmatrix} \bar{u}_{1,\mathbf{q}} \\ \bar{v}_{1,\mathbf{q}} \\ \bar{u}_{2,\mathbf{q}} \\ \bar{v}_{2,\mathbf{q}} \end{pmatrix} = 0, \tag{4.39}$$

where

$$\begin{aligned} M_{11/22} &= E_R\left[\tilde{q}^2 \mp 2(\tilde{k}_0-1)\tilde{q}_z\right] + g_1|\bar{\psi}_1|^2 - \hbar\Omega_{\text{eff}}\frac{\bar{\psi}_2}{\bar{\psi}_1}, \\ M_{33/44} &= E_R\left[\tilde{q}^2 \mp 2(\tilde{k}_0+1)\tilde{q}_z\right] + g_2|\bar{\psi}_2|^2 - \hbar\Omega^*_{\text{eff}}\frac{\bar{\psi}_1}{\bar{\psi}_2}, \\ \hbar\Omega_{\text{eff}} &= \hbar\Omega_R + |g_1|\tilde{U}_{\text{ds}}\bar{n} + 2|g_1|\tilde{U}_{\text{ss}}\bar{\psi}_1\bar{\psi}_2^*. \end{aligned} \tag{4.40}$$

In deriving the Bogoliubov Hamiltonian (4.39), we made use of the fact that $\hat{N}_\tau = \int \hat{\psi}_\tau^\dagger(\mathbf{r},t)\hat{\psi}_\tau(\mathbf{r},t)d\mathbf{r} = \int |\bar{\psi}_\tau|^2 d\mathbf{r} = V|\bar{\psi}_\tau|^2 = N_\tau$, because $\bar{\psi}_\tau$ is homogeneous by assumption and $\int \delta\hat{\psi}_\tau(\mathbf{r},t)d\mathbf{r} = 0$ because the spatial integral of either Bogoliubov amplitude $\bar{u}_{\tau,\mathbf{q}}e^{i(\mathbf{q}\cdot\mathbf{r}-\omega t)}$ or $\bar{v}^*_{\tau,\mathbf{q}}e^{-i(\mathbf{q}\cdot\mathbf{r}-\omega t)}$ is zero for any $\mathbf{q} \neq 0$. A similar argument ensures that $\hat{S}_+ = S_+$ and $\hat{S}_- = S_-$ as well. Note also that the chemical potential in Eq. (4.39) has been eliminated using the coupled GP equations (4.25).

Diagonalizing Eq. (4.39) yields the spectrum $\omega_\pm^{\rm PW}(\mathbf{q})$ of collective excitations. The results are shown in Fig. 4.5(a) for the parameters $\mathrm{sgn}(g_1) = \tilde{g}_2 = |g_1|\bar{n}/E_R = 1$, $\tilde{g}_{12} = 2$, and $\tilde{\Omega}_R = 0.1$, when all the cavity-mediated interaction terms are zero ($\tilde{U}_1 = \tilde{U}_2 = \tilde{U}_{\rm ss} = \tilde{U}_{\rm ds} = 0$), i.e. the system is deep in the PWP. The lower curve exhibits the usual superfluid sound-like linear dispersion around the origin $\tilde{q}_z \equiv q_z/k_R = 0$ (around the left minimum of the single-particle energy dispersion where all the atoms are condensed) and a roton-type minimum around $\tilde{q}_z \simeq 2$. As the cavity interactions are increased, the energy of the roton minimum lowers. For parameters $\tilde{U}_1 = 0.5$, $\delta\tilde{U} = 1.5$, $\tilde{U}_{\rm ss} = \tilde{U}_{\rm ds} = 0$, and the other parameters same as in Fig. 4.5(a), this minimum coincides with zero energy (i.e. the excitation energy at the origin $\tilde{q}_z = 0$); see the black solid curve in Fig. 4.5(b). The red dashed-dotted curve represents the elementary excitation spectrum for the same values of $\tilde{U}_1$ and $\delta\tilde{U}$ but for $\tilde{U}_{\rm ss} = \tilde{U}_{\rm ds} = 0.5$. In this case, $\hbar\Omega_{\rm eff}/E_R$ [cf. Eq. (4.40)] is somewhat bigger than the bare $\tilde{\Omega}_R = 0.1$ for the black solid curve, so the roton minimum lies somewhat above that of the black solid curve around $\tilde{q}_z \simeq 2$.

The energy of the roton minimum near $q_z \simeq 2k_R$ can be reduced below zero by further increasing the cavity interaction strength $\tilde{U}_1$. This signals a dynamic instability toward the formation of the SP; recall from Eq. (4.11) that the density modulation in the SP has wave vector $2k_0 \simeq 2k_R$ for $\tilde{\Omega}_R \to 0$. The critical cavity interactions for the black solid and the red dashed-dotted excitation spectra in Fig. 4.5(b) are $\tilde{U}_{1c} \simeq 0.5$ and 0.53, respectively, and these are in good agreement with that of the variational approach, where Eq. (4.20) predicts

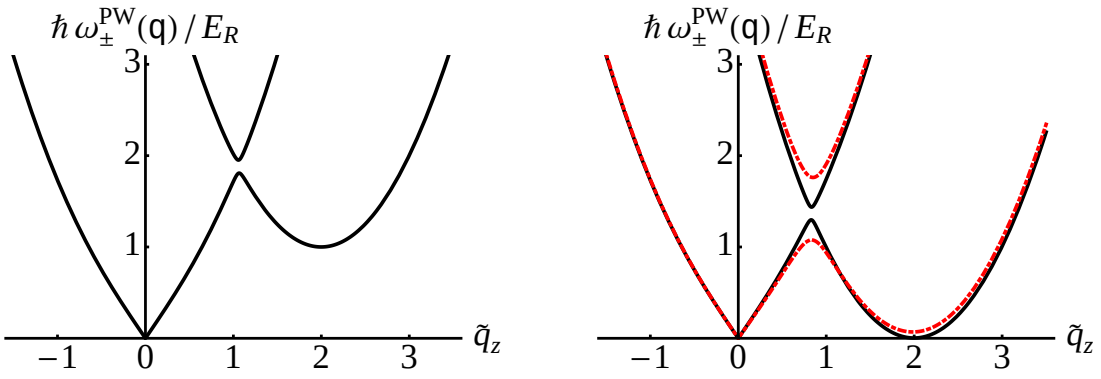

Figure 4.5: (Color online) Elementary excitation spectrum in the PWP for $\mathrm{sgn}(g_1) = \tilde{g}_2 = |g_1|\bar{n}/E_R = 1$, $\tilde{g}_{12} = 2$, and $\tilde{\Omega}_R = 0.1$. $(\tilde{U}_1, \tilde{U}_2, \tilde{U}_{\rm ss}, \tilde{U}_{\rm ds}) = (0, 0, 0, 0)$ in (a), and $(0.5, 1.5, 0, 0)$ and $(0.5, 1.5, 0.5, 0.5)$ in (b) for the black solid and red dashed-dotted curves, respectively.

a phase transition between the PWP and the SP at the critical value $\tilde{U}_{1\rm c} \simeq 0.5$ for the parameters $\mathrm{sgn}(g_1) = \tilde{g}_2 = \delta\tilde{U} = 1$, $\tilde{g}_{12} = 2$, and $\tilde{\Omega}_R = 0.1$ (cf. also Fig. 4.4).

If one hypothetically sets $\tilde{U}_{\rm ss} = \tilde{U}_{\rm ds} = 0$ in the PWP, then the critical cavity interaction $\tilde{U}_{1\rm c}$ obtained from the analysis of the elementary excitations and the variational method would match exactly with each other for any range of parameters. Nevertheless, they begin to deviate from one another as $\tilde{U}_{\rm ss}$ and $\tilde{U}_{\rm ds}$ become larger and larger, because Eq. (4.20) is independent of these cavity interaction parameters while both the coupled GP equations and the Bogoliubov Hamiltonian depend explicitly on them (the latter through $\hbar\Omega_{\rm eff}$). That said, we have compared the critical phase transition point $\tilde{U}_{1\rm c}$ obtained from both the variational approach and the elementary excitation spectrum in the PWP and have found that when $\tilde{U}_1 = \tilde{U}_{\rm ss} = \tilde{U}_{\rm ds}$ they agree with one another within a $\sim 8\%$ error for $\tilde{g}_{12}$ in the range of $\sim 0 - 8$, assuming $\mathrm{sgn}(g_1) = \tilde{g}_2 = |g_1|\bar{n}/E_R = \delta\tilde{U} = 1$ and $\tilde{\Omega}_R = 0.1$.

Stripe Phase

The derivation of the Bogoliubov excitation spectrum begins with the corresponding

time-dependent, effective low energy GP equations in the SP [c.f. Eq. (4.33)]:

$$\begin{aligned} i\hbar\frac{\partial}{\partial t}\hat{\psi}_{1'} =& \Big(H_{\rm e}^{(1)} + g_1'|\hat{\psi}_{1'}|^2 + g_{12}'|\hat{\psi}_{2'}|^2 + U_1'\hat{N}_{1'} + U_{12}'\hat{N}_{2'} - \mu\Big)\hat{\psi}_{1'}, \\ i\hbar\frac{\partial}{\partial t}\hat{\psi}_{2'} =& \Big(H_{\rm e}^{(1)} + g_2'|\hat{\psi}_{2'}|^2 + g_{12}'|\hat{\psi}_{1'}|^2 + U_2'\hat{N}_{2'} + U_{12}'\hat{N}_{1'} - \mu\Big)\hat{\psi}_{2'}. \end{aligned} \tag{4.41}$$

As in the PWP case, the low energy field operators are replaced with $\hat{\psi}_{\tau'}(\mathbf{r},t) = \psi_{\tau'} + \delta\hat{\psi}_{\tau'}(\mathbf{r},t)$ in these equations. Here $\psi_{\tau'}$ are the time-independent, homogeneous solutions of the effective low energy GP equations in the SP, Eq. (4.34), and $\delta\hat{\psi}_{\tau'}(\mathbf{r},t)$ are the quantum fluctuations. Linearizing Eq. (4.41) yields the Bogoliubov Hamiltonian:

$$\begin{pmatrix} M_{11}' - \hbar\omega(\mathbf{q}) & g_1'\psi_{1'}^2 & g_{12}'\psi_{1'}\psi_{2'}^* & g_{12}'\psi_{1'}\psi_{2'} \\ -g_1'\psi_{1'}^{*2} & -M_{22}' - \hbar\omega(\mathbf{q}) & -g_{12}'\psi_{1'}^*\psi_{2'}^* & -g_{12}'\psi_{1'}^*\psi_{2'} \\ g_{12}'\psi_{1'}^*\psi_{2'} & g_{12}'\psi_{1'}\psi_{2'} & M_{33}' - \hbar\omega(\mathbf{q}) & g_2'\psi_{2'}^2 \\ -g_{12}'\psi_{1'}^*\psi_{2'}^* & -g_{12}'\psi_{1'}\psi_{2'}^* & -g_2'\psi_{2'}^{*2} & -M_{44}' - \hbar\omega(\mathbf{q}) \end{pmatrix} \begin{pmatrix} u_{1',\mathbf{q}} \\ v_{1',\mathbf{q}} \\ u_{2',\mathbf{q}} \\ v_{2',\mathbf{q}} \end{pmatrix} = 0, \tag{4.42}$$

where

$$\begin{aligned} M_{11}' &= M_{22}' = \epsilon_{\rm e}(\mathbf{q}) + g_1'|\psi_{1'}|^2, \\ M_{33}' &= M_{44}' = \epsilon_{\rm e}(\mathbf{q}) + g_2'|\psi_{2'}|^2. \end{aligned} \tag{4.43}$$

The Bogoliubov Hamiltonian (4.42) can be diagonalized to give the spectrum of the elementary excitations:

$$\hbar\omega_{\pm}^{\rm SP}(\mathbf{q}) = \sqrt{\epsilon_{\rm e}^2(\mathbf{q}) + \epsilon_{\rm e}(\mathbf{q})\left(D_1 \pm \sqrt{D_1^2 - 4D_2}\right)}, \tag{4.44}$$

with

$$\begin{aligned} D_1 &= g_1'n_{1'} + g_2'n_{2'}, \\ D_2 &= (g_1'g_2' - g_{12}'^2)n_{1'}n_{2'}. \end{aligned} \tag{4.45}$$

We have again used the fact that $\hat{N}_{\tau'} = N_{\tau'}$.

Surprisingly, the Bogoliubov Hamiltonian in the SP does not depend explicitly on the cavity parameters and the form of the excitation spectrum coincides with the quasiparticle

spectrum of a Raman-induced SP Bose condensate [78]. That said, the excitation spectrum implicitly depends on the cavity parameters $\tilde{U}'_\tau$ through $n_{\tau'}$, as can be seen in Eq. (4.34). Both $\omega_\pm^{\rm SP}(\mathbf{q})$ are gapless and exhibit linear dispersion at long wavelengths, the characteristic of superfluidity in this phase; the slope of the dispersion relation at long wavelength corresponds to the speed of sound in the medium. In the transverse direction, one obtains

$$v_\perp^{(\pm)} = \frac{d\omega_\pm^{\rm SP}(\mathbf{q})}{dq_\perp}\Big|_{\mathbf{q}\to 0} = \frac{1}{\sqrt{2m}}\sqrt{D_1 \pm \sqrt{D_1^2 - 4D_2}}, \tag{4.46}$$

and the speed of sound in the z (SO-coupling) direction is nearly the same for small $\tilde{\Omega}$, $v_z^{(\pm)} = v_\perp^{(\pm)}\sqrt{1-\tilde{\Omega}_R^2/4}$.

Figure 4.6 depicts $v_\perp^{(\pm)}$ as a function of $\tilde{U}_2$ for $\tilde{U}_1 = 1/4$ (solid curves) and $\tilde{U}_1 = 5/2$ (dashed curves), with the other parameters fixed to $\mathrm{sgn}(g_1) = \tilde{g}_2 = 1$, $\tilde{g}_{12} = 0.7$, $\tilde{\Omega}_R = 0.4$, and $g_1\bar{n}/E_R = 1$. The mass is assumed to be that of ^{87}Rb. As $\tilde{U}_2$ is increased above zero, the speed of sound in the positive branch $v_\perp^{(+)}$ (the blue curves) first decreases quickly and reaches a minimum around $\delta\tilde{U} = \tilde{U}_2 - \tilde{U}_1 \sim 0$ for both curves, and then gradually approaches its asymptotic value. The speed of sound in the negative branch $v_\perp^{(-)}$ (black curves) has the opposite behavior, first increasing sharply to a maximum again near $\delta\tilde{U} \sim 0$ for both curves, before asymptotically approaching zero. The insets show the behaviour of $v_\perp^{(\pm)}$ close to the origin. The asymptotic behaviour of the speed of sound can be understood by noting that for large positive $\tilde{U}_2 \gg \tilde{U}_1$, $n_{1'}$ approaches $\bar{n}$ and $n_{2'}$ approaches zero [c.f. Eqs. (4.34)]. As a consequence $D_2 \to 0$ and $v_\perp^{(-)} \to 0$ while $v_\perp^{(+)} \to \sqrt{g'_1\bar{n}/m}$. For the solid curves (where $\tilde{U}_1 = 1/4$), the speed of sound in the negative branch $v_\perp^{(-)}$ becomes zero at $\tilde{U}_2 \simeq 37$, consistent with the value at which the dressed magnetization s'_z becomes unity for this choice of parameters. This signifies an instability toward the formation of a different phase.

The condition that the speed of sound must be non-negative imposes the constraint $D_2 \geqslant 0$. This condition marks the onset of a phase transition at the critical point $\tilde{g}_{12}^{\prime(\rm c)} = \sqrt{\tilde{g}'_1\tilde{g}'_2}$, which does not depend on any cavity-mediated interaction parameters and is solely deter-

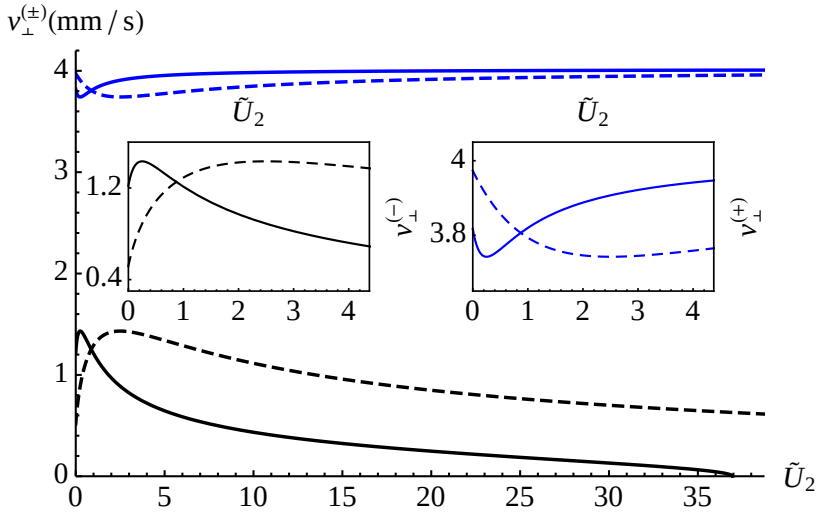

Figure 4.6: (Color online) The speed of sound in the transverse direction $v_\perp^{(\pm)}$ is shown as a function of $\tilde{U}_2$ for $\tilde{U}_1 = 1/4$ (solid curves) and $\tilde{U}_1 = 5/2$ (dashed curves). For all curves: $\tilde{\Omega}_R = 0.4$, $\mathrm{sgn}(g_1) = \tilde{g}_2 = 1$, $\tilde{g}_{12} = 0.7$, $g_1\bar{n}/E_R = 1$, and m is the mass of ^{87}Rb atom. The insets show the results closer to the origin.

mined by the two-body interactions and $\tilde{\Omega}_R$. This critical point is not consistent with the previous results obtained from the variational approach, the effective low-energy GP equations in the SP, or the elementary excitations in the PWP which all consistently predict a critical point for the PWP-SP phase transition that depends on the cavity-mediated interaction parameters. To verify that there was not an error in the calculations, the elementary excitations were computed directly in momentum space by Fourier transforming the effective low-energy Hamiltonian (4.31), and treating the fluctuations around the condensate $\varphi_{\tau'}(\mathbf{q} = 0)$ to second order in $\hat{\varphi}_{\tau'}(\mathbf{q})$ for small momenta $\mathbf{q}$. The results were identical with the real-space analysis, Eq. (4.44). Interestingly, the critical inter-species interaction $\tilde{g}_{12}^{\prime(\mathrm{c})}$ above defines a phase boundary between the SP and a phase-separated state in Raman-induced SO-coupled Bose condensates [78]. It is therefore conceivable that there is another phase between the SP and the PWP induced by the cavity interactions, whose signature is

the observed inconsistency in the critical point.

4.4 Discussion and Conclusions

In this work we have shown that cavity-mediated long-ranged interactions between atoms can profoundly alter the nature of the ground state and the elementary excitations of a cavity-induced SO-coupled two-component Bose-Einstein condensate, for ring-type cavities in the weak-coupling regime. Specifically, experimentally tunable cavity-mediated interactions compete with the standard two-body interactions to yield both PWP and SP ground states. Indeed, positive long-range cavity interactions can stabilize fully attractive Bose-Einstein condensates (condensates where intra-species collisional interactions are negative, independent of the sign of the inter-species interaction) against collapse in the SP. The collective excitations of the PWP ground states are found to have a distinctive roton-type excitation spectrum reminiscent of that of superfluid ^{4}He, which can be used as a signature of the phase. The stripe phase has a standard linear dispersion relation; the associated speed of sound is found to go negative at a critical value of the cavity interaction strength, signalling an instability toward another (likely phase-separated) phase. The results suggest that cavity QED, even in the weak-coupling regime, can yield interesting new physics for SO-coupled Bose-Einstein condensates.

The results raise interesting avenues for future investigations. This work assumed a fictional experimental configuration where the momentum is a good quantum number in the direction of the applied spin-orbit interactions. In reality the condensate would be confined in this direction, and even a weak harmonic potential could change the physics. While the SP would likely remain robust, as it is essentially a weak standing wave superimposed on the background condensate density profile, the PWP has no analog in a confined geometry. Another loose end is the nature of the phase hinted at in the limit of a large difference $\delta\tilde{U}$ between the cavity-mediated interactions between the two kinds of spin components $\tilde{U}_1$ and $\tilde{U}_2$. For large $\delta\tilde{U}$, the sound velocity in the SP was found to go negative, a signature of the

dynamic instability of the phase.

However, a few intriguing issues and questions remain unclear and deserve further investigations. These include the inconsistency in the critical phase transition point, how the combined SO coupling effect, the two-body interactions, and the cavity-mediated long-ranged interactions change the superfluid–Mott-insulator phase transition as well as the nature of magnetic orders in the Mott-insulating regime when an optical lattice imposed inside the cavity. Furthermore, whether it is possible to have a superfluid–Mott-insulator-like phase transition with solely the cavity-mediated long-range interactions, whether there is more interesting physics in strong-coupling regime, and how the cavity fields are affected by the atoms. Some of these questions are the subject of our current works with some promising preliminary results and will be published elsewhere.

Chapter 5

Discussion and Conclusions

Progress in the precise manipulation of ultracold atomic gases has made Feynman's revolutionary notion — of simulating an intractable system with another system — a reality, with ultracold atomic gases being the tractable environments. They can readily be manipulated to emulate other physical systems on demand, ranging from strongly interacting condensed matter to relativistic particles, allowing one to carefully study these systems in detail. A notable example is ultracold atoms trapped in optical lattice potentials, which can be exploited to simulate condensed-matter-like phenomena such as the superfluid–Mott-insulator phase transition.

Abelian and non-Abelian gauge potentials and quantum gauge theories play central roles in our understanding of Nature. Quantum electrodynamics (QED), a relativistic gauge theory describing the coupling of an electron field into the Abelian electromagnetic gauge potentials (i.e., the photon field), is among the most successful and most accurate theories of physics. Abelian and non-Abelian gauge potentials are also of great significance in condensed matter physics, and are in fact the essential ingredients of topological states of matter. Nonetheless, gauge theories and topological states of matter cannot be directly simulated by quantum gases due to their charge neutrality. That said, coupling a multi-component or spinor quantum gas into laser light in an efficient manner can lead to the emergence of artificial Abelian and non-Abelian gauge potentials (such as artificial magnetic fields and SO couplings, respectively) in ultracold neutral atoms.

In this thesis, I have demonstrated how to induce synthetic magnetic fields and SO couplings in the cavity QED environment. Specifically, I have developed a two-photon Raman scheme in the strong atom-photon coupling regime, based on two counter-propagating modes

of a ring cavity, to induce both synthetic magnetic field and SO coupling for a single neutral atom inside the cavity. Although the SO coupling is only weakly dependent on the occupation of the cavity modes and its strength is basically limited by the two-photon momentum transfer, the strength of the magnetic field is proportional to the square of the total number of photons in the cavity and can be made arbitrary large. Such large magnetic fields are required for realizing fractional quantum Hall phases and the Hofstadter butterfly. This scheme might open up the possibility for realizing these phases in cavity QED environments.

By extending this single-atom cavity QED scheme to many bosons in the weak atom-photon coupling regime, I have showed that in addition to inducing SO coupling for the individual atoms the cavity fields also mediate infinite-ranged interactions between atoms, whose strengths and signs can readily be tuned experimentally. The ground state and collective behaviour of the system is governed by the interplay between these cavity-mediated long-ranged and the two-body contact interactions. In the stripe phase, atoms condense in both minima of the single-particle energy dispersion, and consequently the translational symmetry is spontaneously broken and the total density exhibits fringes. This is in contrast to the plane-wave phase where all atoms Bose condense into a single minimum of the single-particle energy dispersion. The positive cavity-mediated interactions favor the stripe phase. Furthermore, appropriately tuned cavity-mediated long-ranged interactions can stabilize an attractive Bose condensate which otherwise is unstable and collapses. Thus, the ring-cavity environment provides an experimentally convenient framework for exploring exotic ground states of SO-coupled Bose condensates. This might have possible applications when the common Feshbach resonance techniques for tuning the two-body interactions are impractical to implement due to the drastic atom losses from the trap or not feasible at all.

When an external optical lattice is imposed inside the cavity in this many-body scheme, the two-body contact and cavity-mediated long-ranged interactions result in on-site and off-site interactions between atoms, respectively. The SO-coupling modifies the tunnelling

amplitude matrix according to the the Peierls substitution [188]. The cavity-mediated interactions are long range and are the same for any pair of lattice sites, regardless of their distance from each other. Like continuum, they might give rise to interesting phenomena in the presence of the optical lattice. A mean-field theory may be then used to describe this system accurately, since mean-field theories become more accurate in higher spatial dimensions or when interactions are long range [189]. I used a mean-field theory to decouple these long-ranged interactions in the weak atom-photon coupling limit. The resultant Hamiltonian then resembles an SO-coupled extended Bose-Hubbard model, where there is nearest-neighbour interactions between atoms in adjacent sites, in addition to the on-site interactions. The (single-component) extended Bose-Hubbard model exhibits rich phases. In addition to superfluid and Mott-insulator phases, there exist two extra phases associated with the extended Bose-Hubbard model: density-wave and supersolid states [190]. Although, the (single-component) extended Bose-Hubbard model has been the subject of intense studies in the past, to the best of my knowledge, an SO-coupled extended Bose-Hubbard model has not been studied yet. Motivated by these, I have started to study a one-dimensional SO-coupled extended Bose-Hubbard model, with some preliminary results presented in the following.

The one-dimensional SO-coupled extended Bose-Hubbard (eBH) model is described by,

$$H_{\mathrm{eBH}} = H_{\mathrm{hop}} + H_{\mathrm{int}} + h_z \sum_j \hat{s}_{z,j} - \sum_{j,\tau} \mu_\tau \hat{N}_{j,\tau}, \tag{5.1}$$

with

$$H_{\mathrm{hop}} = -\sum_{\langle j,j' \rangle} \left(\hat{B}_j^\dagger \check{J}_{j,j'} \hat{B}_{j'} + \mathrm{H.c.} \right), \tag{5.2}$$

$$H_{\mathrm{int}} = \frac{1}{2} \sum_{j,\tau} U_\tau \hat{N}_{j,\tau} (\hat{N}_{j,\tau} - 1) + U_{12} \sum_j \hat{N}_{j,1} \hat{N}_{j,2} + V \sum_{\langle j,j' \rangle} \hat{N}_j \hat{N}_{j'}, \tag{5.3}$$

where H.c. stands for Hermitian conjugate, $\langle \cdots \rangle$ for the nearest neighbours, and $\tau = \{1, 2\}$ represents the pseudospin states. The bosonic annihilation and creation operators satisfy the

usual bosonic commutation relation $[\hat{b}_{j,\tau}, \hat{b}^{\dagger}_{j',\tau'}] = \delta_{j,j'}\delta_{\tau,\tau'}$, $\hat{B}_j = (\hat{b}_{j,1}, \hat{b}_{j,2})^{\mathsf{T}}$, $\hat{N}_{j,\tau} = \hat{b}^{\dagger}_{j,\tau}\hat{b}_{j,\tau}$ is the particle number operator for pseudospin state τ in site j, $\hat{s}_{z,j} = \hat{N}_{j,1} - \hat{N}_{j,2}$, and $\hat{N}_j = \sum_{\tau=1,2}\hat{N}_{j,\tau}$. Here, $\check{J}_{j,j'}$ and V are, respectively, the SO-coupled tunnelling-amplitude matrix and the strength of species-independent interaction between nearest-neighbour sites j and j', U_τ (U_{12}) is the on-site intra-species (inter-species) interaction, $h_z = \hbar\Omega_R/2$ is the Raman-Rabi energy, and μ_τ is the chemical potential. For the equal Rashba-Dresselhaus SO coupling, the tunnelling amplitude matrix is given by [188],

$$\check{J}_{j,j\pm1} = \begin{pmatrix} J & \mp J' \\ \pm J' & J \end{pmatrix}, \tag{5.4}$$

where $J \equiv \tilde{J}\cos\gamma$ and $J' \equiv \tilde{J}\sin\gamma$. Here, $\tilde{J}$ is the species-independent tunnelling amplitude in the absence of the SO coupling and γ is related to the strength of the SO coupling.

In the atomic limit $\tilde{J} = 0$, the particle number operator $\hat{N}_{j,\tau}$ commutes with the Hamiltonian H_{eBH}, implying that the number of particles in each pseudospin τ and lattice site j is conserved. The ground state of the system can then be obtained by minimizing the energy functional $E = \langle H_{\mathrm{int}} + h_z\sum_j \hat{s}_{z,j} - \sum_{j,\tau}\mu_\tau\hat{N}_{j,\tau}\rangle$ for given parameters, which is either a Mott-insulator (MI) state or a density-wave (DW) state. In the MI state, there is an equal, integer number of atoms in each lattice site. In the DW state, the lattice is divided into two sub-lattices where the number of atoms in each sub-lattice is conceivably different. The phase diagrams are depicted in Fig. 5.1 for $h_z/U = 0$ and -0.5, where $U \equiv U_1 = U_2$ and $\mu \equiv \mu_1 = \mu_2$. The inter-species interaction is fixed at $U_{12}/U = 0.6$ and $z = 2$ is the number of nearest neighbours. A Mott-insulator state is specified by the number of atoms in both pseudospin states in one lattice site, denoted as $\mathrm{MI}(N_1, N_2)$. A density-wave state is specified by the number of atoms in both pseudospin states in two lattice sites, denoted as $\mathrm{DW}(N_{A,1}, N_{A,2}; N_{B,1}, N_{B,2})$ where A and B indicate the two sub-lattices.

When the tunnelling amplitude is non-zero $\tilde{J} \neq 0$, one must then exactly diagonalize the Hamiltonian H_{eBH}, Eq. (5.1), over the whole lattice. That said, a mean-field theory can

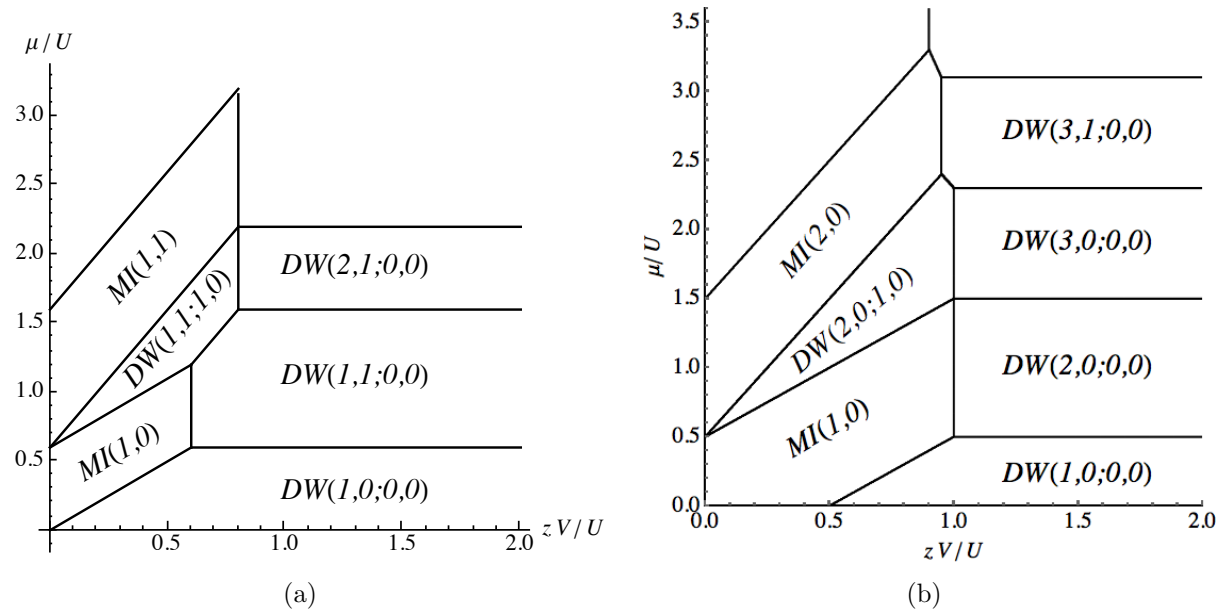

Figure 5.1: Atomic limit phase diagrams for (a) $h_z/U = 0$ and (b) $h_z/U = -0.5$. The other parameters are $U \equiv U_1 = U_2$, $\mu \equiv \mu_1 = \mu_2$, and $U_{12}/U = 0.6$. Here, $z = 2$ is the number of nearest neighbours.

be exploited to decouple the nearest-neighbour hopping terms (5.2) and therefore allow an analytical approach [191, 192]. To this end, the annihilation operator is replaced by $\hat{b}_{j,\tau} = \beta_{j,\tau} + \delta\hat{b}_{j,\tau}$ in the nearest-neighbour hopping terms, where $\beta_{j,\tau} \equiv \langle \hat{b}_{j,\tau} \rangle$ is the expectation value of the annihilation operator and $\delta\hat{b}_{j,\tau} \equiv \hat{b}_{j,\tau} - \langle \hat{b}_{j,\tau} \rangle$. $\beta_{j,\tau}$ is the superfluid (SF) order parameter of component τ, since it vanishes identically in the MI and DW phases and takes non-zero values in the SF state. This stems from the fact that in the MI and DW phases all lattice sites have definite (integer) particle number; hence the expectation value of the annihilation operator is identically zero. While in the SF phase, the particle number in a single lattice site is not fixed and $\beta_{j,\tau}$ can therefore be non-zero. Calculating $\beta_{j,\tau} = \langle \hat{b}_{j,\tau} \rangle = \mathrm{Tr}(\hat{b}_{j,\tau}\hat{\rho})$ yields phase boundaries for both MI-SF and DW-SF phase transitions [193]. Here, $\hat{\rho} = \frac{1}{Z} \exp\left(-H^{\mathrm{MF}}_{\mathrm{eBH}}/k_B T\right)$ is the density matrix operator, where $H^{\mathrm{MF}}_{\mathrm{eBH}}$ is the mean-field decoupled Hamiltonian, T is the temperature, and $Z = \mathrm{Tr}(e^{-H^{\mathrm{MF}}_{\mathrm{eBH}}/k_B T})$ is the partition function.

In the atomic limit $\tilde{J} = 0$, the SO-coupling has basically no effect in the system. That said, the system even in the atomic limit exhibit very rich quantum phase transitions be-

tween the MI and DW states. This stems from the interplay between the on-site intra- and inter-species interactions, the nearest-neighbour interaction, and the Raman-Rabi energy (which is like an out-of-plane magnetic field for pseudospins). Such interesting and complicated quantum phase transitions do not exist in the one-component extended Bose-Hubbard model [190]. When the tunnelling amplitude is non-zero $\tilde{J} \neq 0$, more intriguing quantum phase transitions are even expected. In this regime, the SO-coupling affects properties of the system and is expected to give rise to twisted SF states [194, 195]. Quantum phase transitions obtained for a non-zero tunnelling amplitude in the SO-coupled extended Bose-Hubbard model are under examination and will be published elsewhere [196].

The gauge potentials in condensed matter systems are normally static. That is, they are background gauge potentials where electron fields couple to them without affecting them. Analogously, most of the proposed and all of the realized artificial gauge potentials for ultracold neutral atoms are of this type. The static gauge potentials are in sharp contrast to dynamic gauge potentials, encountered usually in quantum gauge theories such as QED, quantum chromodynamics, the Standard Model of elementary particles, etc. The dynamic gauge potentials are not background potentials but rather evolve over time. There exist a few schemes to induce dynamic gauge potentials in ultracold neutral atoms [197, 198, 199, 200, 201]; they are, however, experimentally very challenging. For instance, the proposal of Ref. [197] relies on one fermionic and three distinct bosonic species, three interpenetrating lattices, fine detuning of many parameters, etc., which are difficult to achieve experimentally. Another alternative, natural route to induce dynamic gauge potentials in ultracold neutral atoms can be the cavity QED setting.

Let me briefly outline how QED might be simulated in a cavity QED setting. Consider ultracold fermions tapped in a honeycomb optical lattice located inside a cavity; see Fig. 5.2. The fermions move around the lattice due to their kinetic energy, resulting in a band structure which in some points of the quasi-momentum space is linear and mimics the energy dispersion

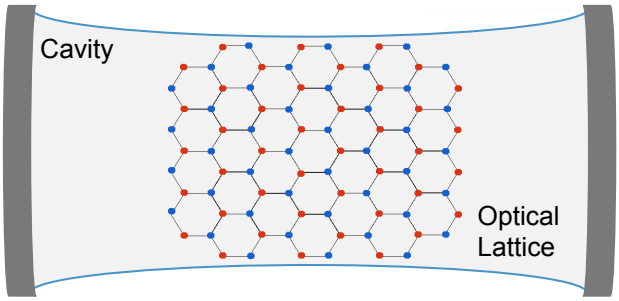

Figure 5.2: Ultracold fermions trapped in a honeycomb optical lattice located inside a cavity.

of the relativistic Dirac equations. With a proper fermionic filling factor (a half filling, to be precise) this provides the first constituent of QED, the relativistic fermionic field. On the other hand, the cavity-QED field provides naturally the second component of QED, the dynamic gauge potential. The last element of QED, coupling of the relativistic particle to the dynamic gauge potential should be synthesized, since the atoms are charge neutral and do not couple to the gauge potential. This can be achieved by employing Berry's geometric phase. One possible implementation of the Berry phase is exploiting the two-photon Raman scheme in conjunction with an external bias field, which I have developed in Chapter 3 for the cavity QED environment.

Therefore, cavity QED environments might open a new avenue for simulating dynamic gauge potentials in ultracold atomic systems. My work along with those of others might serve as the starting point of this research direction and may facilitate further theoretical studies for extending these schemes to simulate dynamic gauge field theories, such as QED (which is outlined above) and quantum chromodynamics, in cavity QED environments. These may finally allow one to address many open questions regarding elementary particle physics in the framework of ultracold atoms and cavity QED.

Appendix A

Adiabatic Theorem and Berry Phase

In this Appendix, I review the the Adiabatic Theorem and the concept of the Berry phase. Then I apply the concept of adiabatic passage and adiabatic elimination to a two-level atom interacting with an electromagnetic field.

The Adiabatic Theorem. Let the given system be initially in an eigenstate $|n\rangle_0$ *of the Hamiltonian* H_0 *at time* t_0*. If the Hamiltonian is changed very slowly and continuously (referred to as an adiabatic passage) into* H_1 *at later time* t_1*, such that* $\tau = t_1 - t_0 \to \infty$*, then the system remains in the instantaneous eigenstate* $|n\rangle_1$ *of the Hamiltonian* H_1 [202].

I now consider this theorem in detail and derive the exact condition under which the Adiabatic Theorem holds. Consider the Schrödinger equation,

$$H(X)\,|n(X)\rangle = \varepsilon_n(X)\,|n(X)\rangle\,, \tag{A.1}$$

where $|n\rangle$ is an eigenstate of the Hamiltonian H with the corresponding eigenenergy ε_n. Here, $X(t)$ is a parameter which depends on time, and in turn the Hamiltonian $H(X)$, eigenenergies $\{\varepsilon_n(X)\}$, and eigenstates $\{|n(X)\rangle\}$ all depend on $X(t)$. An arbitrary state vector of the system can be expressed in terms of the complete basis set $\{|n(X)\rangle\}$ as,

$$|\psi(t)\rangle = \sum_n c_n(t)\,|n(X(t))\rangle\,. \tag{A.2}$$

Substituting Eq. (A.2) into the time-dependent Schrödinger equation,

$$i\hbar\partial_t\,|\psi(t)\rangle = H(X)\,|\psi(t)\rangle\,, \tag{A.3}$$

and multiplying by $\langle n|$ from left yields

$$\partial_t c_n = -\frac{i\varepsilon_n}{\hbar}c_n - \dot{X}\sum_m \langle n\,|\partial_X m\rangle\, c_m, \tag{A.4}$$

where $\dot{X} = \partial_t X$ and $\partial_X = \partial/\partial_X$. Here I have suppressed all the t and X dependence for simplicity of the notation.

Note that $\langle n\,|\partial_X m\rangle = -\langle \partial_X n\,|m\rangle$, which can be readily obtained by taking the derivative of $\langle n\,|m\rangle = \delta_{n,m}$ with respect to X. This implies that $\langle n\,|\partial_X m\rangle$ is anti-Hermitian. Defining a new Hermitian matrix $\boldsymbol{\mathcal{A}}$ with elements

$$\mathcal{A}_{nm} \equiv i\,\langle n|\,\partial_X m\rangle\,, \tag{A.5}$$

Eq. (A.4) can be re-expressed as,

$$\partial_t c_n = -\frac{i\varepsilon_n}{\hbar}c_n + i\dot{X}\sum_m \mathcal{A}_{nm}c_m = -i\left(\frac{\varepsilon_n}{\hbar} - \dot{X}\mathcal{A}_n\right)c_n + i\dot{X}\sum_{m\neq n}\mathcal{A}_{nm}c_m, \tag{A.6}$$

where $\mathcal{A}_n \equiv \mathcal{A}_{n,n}$. The last term in Eq. (A.6) represents a perturbation due to the change in the system, whose strength is proportional to $\dot{X}$, and mixes different eigenstates. It can be recast in a more useful form by noting that $\partial_X \langle n|\,H\,|m\rangle = 0$ for any $n \neq m$,

$$\langle \partial_X n|\,H\,|m\rangle + \langle n|\,\partial_X H\,|m\rangle + \langle n|\,H\,|\partial_X m\rangle = 0. \tag{A.7}$$

A simple re-arrangement yields

$$\mathcal{A}_{nm} = i\,\langle n|\,\partial_X m\rangle = -i\frac{\langle n|\,\partial_X H\,|m\rangle}{\varepsilon_n - \varepsilon_m}. \tag{A.8}$$

By substituting $\mathcal{A}_{nm}$ (A.8) in Eq. (A.6), one obtains

$$\partial_t c_n = -i\left(\frac{\varepsilon_n}{\hbar} - \dot{X}\mathcal{A}_n\right)c_n + \dot{X}\sum_{m\neq n}\left(\frac{\langle n|\,\partial_X H\,|m\rangle}{\varepsilon_n - \varepsilon_m}\right)c_m. \tag{A.9}$$

Assuming that the system was initially in state $|n(X_0)\rangle$, the Adiabatic Theorem states that if the change in the system, proportional to $\dot{X}$, is sufficiently slow, then the system remains in its instantaneous eigenstate $|n(X)\rangle$, that is, $|c_n(t)|^2 \simeq$ const. This implies that the perturbation in Eq. (A.9) must be negligible compared to energy difference between the levels. Since the largest contribution to the perturbation comes from the transition into a

level, denoted by n', with closest energy to that of n, the adiabatic condition can then be expressed as,

$$\dot{X} \ll \frac{(\varepsilon_n - \varepsilon_{n'})^2}{\hbar \langle n| \partial_X H |n'\rangle}. \tag{A.10}$$

Omitting the perturbation term, Eq. (A.9) can be integrated to yield

$$c_n(t) = c_n(0) e^{-\frac{i}{\hbar}\int_0^t \varepsilon_n(t')dt'} e^{i\gamma_n}, \tag{A.11}$$

where the accumulated phase has an extra geometric contribution

$$\gamma_n = \int_0^t \dot{X}(t')\mathcal{A}_n(t')dt' = \int_{X_0}^{X(t)} \mathcal{A}_n(X')dX', \tag{A.12}$$

in addition to the dynamical phase. If the system changes in a cyclic manner, that is, $X_0 = X_1$, then the geometric phase,

$$\gamma_n = \oint \mathcal{A}_n(X)dX = i \oint \langle n(X)| \partial_X n(X)\rangle \, dX, \tag{A.13}$$

is independent of the time and solely depends on the path taken by the system [62]. This is the Berry phase, with $\mathcal{A}_n(X)$ referred to as the Berry connection [61].

A.1 Adiabatic Elimination: An Example

In order to illustrate the notion of the adiabatic elimination, consider a two-level atom with atomic transition frequency ω_0 coupled to a monochromatic electromagnetic field with frequency ω, $\mathbf{E}(\mathbf{r}, t) = [E_+(\mathbf{r})e^{-i\omega t} + E_-(\mathbf{r})e^{i\omega t}]\mathbf{e}$, where $\mathbf{e}$ is the polarization vector. The atom-field Hamiltonian density in the $\mathbf{d} \cdot \mathbf{E}$ picture and the rotating-wave approximation reads [149]

$$\mathcal{H} = \frac{\mathbf{P}^2}{2M} + \hbar\omega_0\sigma_{ee} + \frac{\hbar}{2}\Big[\Omega(\mathbf{r})e^{-i\omega t}\sigma_{eg} + \text{H.c.}\Big], \tag{A.14}$$

where $\Omega = \Omega(\mathbf{r}) = E_+(\mathbf{r}) \langle g| \mathbf{d} \cdot \mathbf{e} |e\rangle / \hbar$ is the Rabi frequency of the corresponding transition $g \leftrightarrow e$. Here, $\mathbf{P}$ is the center-of-mass momentum of the atom, M the mass of the atom, and

$\sigma_{\tau\tau'} = |\tau\rangle\langle\tau'|$. The time-dependence of the Hamiltonian can be removed by transferring to the rotating frame of the laser. This is accomplished by applying the unitary transformation $\mathscr{U} = e^{i\omega t\sigma_{ee}}$,

$$\tilde{\mathcal{H}} = \mathscr{U}\mathcal{H}\mathscr{U}^\dagger + i\hbar(\partial_t\mathscr{U})\mathscr{U}^\dagger = \frac{\mathbf{P}^2}{2M} - \hbar\Delta\sigma_{ee} + \frac{\hbar}{2}\Big[\Omega(\mathbf{r})\sigma_{eg} + \text{H.c.}\Big], \tag{A.15}$$

where $\Delta = \omega - \omega_0$.

Let me consider condition(s) under which the atom adiabatically follows its ground state $|g\rangle$ and remains in it, and as a consequence the atomic excited state $|e\rangle$ can be eliminated. The first approach is to diagonalize $\tilde{\mathcal{H}}$. Omitting the kinetic energy term, the Hamiltonian (A.15) can be readily diagonalized to yield the dressed states

$$\begin{aligned} |+\rangle &= \sin\theta\,|g\rangle + \cos\theta\,|e\rangle\,, \\ |-\rangle &= \cos\theta\,|g\rangle - \sin\theta\,|e\rangle\,, \end{aligned} \tag{A.16}$$

and dressed energies

$$\epsilon_\pm = -\frac{\hbar\Delta}{2} \pm \frac{\hbar\tilde{\Omega}}{2}, \tag{A.17}$$

where $\tan 2\theta = -\Omega/\Delta$ and $\tilde{\Omega} = \tilde{\Omega}(\mathbf{r}) = \sqrt{|\Omega|^2 + \Delta^2}$ is the generalized Rabi frequency. Note that there is an avoided crossing in the dressed-energy spectrum due to the coupling to the field through Ω. Consider a case where $|\Delta| \gg |\Omega|$, then $|-\rangle \simeq |g\rangle$ and $|+\rangle \simeq |e\rangle$ with the large energy gap $\Delta\epsilon = -\hbar\Delta$ between the two dressed states. This implies that if the atom is in $|-\rangle \simeq |g\rangle$, then it will always remain in this state with the corresponding energy $\epsilon_- \simeq \hbar|\Omega|^2/4\Delta$, provided that $|\Delta| \gg |\Omega|$. This is exactly the adiabatic condition.

There is yet another way to obtain the adiabatic condition and that is to look at equations of motion. An arbitrary state vector $|\psi\rangle$ can be decomposed as the product of the internal and external states as [149],

$$|\psi(t)\rangle = |\psi_g(t)\rangle\,|g\rangle + |\psi_e(t)\rangle\,|e\rangle\,, \tag{A.18}$$

where $|\psi_\tau(t)\rangle$ are the corresponding center-of-mass states. Defining the wavefunctions $\psi_\tau(\mathbf{r},t) = \langle \mathbf{r}|\,\psi_\tau(t)\rangle$, the time-dependent Schrödinger equation $i\hbar\partial_t\psi = \tilde{\mathcal{H}}\psi$ yields

$$i\hbar\left(\partial_t\psi_g\,|g\rangle + \partial_t\psi_e\,|e\rangle\right) = \frac{\mathbf{P}^2}{2M}\left(\psi_g\,|g\rangle + \psi_e\,|e\rangle\right) - \hbar\Delta\psi_e\,|e\rangle + \frac{\hbar}{2}\Big[\Omega(\mathbf{r})\psi_g\,|e\rangle + \Omega^*(\mathbf{r})\psi_e\,|g\rangle\Big]. \tag{A.19}$$

Separating the coefficients of $|g\rangle$ and $|e\rangle$, one obtains a set of coupled equations

$$\begin{aligned} i\hbar\partial_t\psi_g &= \frac{\mathbf{P}^2}{2M}\psi_g + \frac{1}{2}\hbar\Omega^*(\mathbf{r})\psi_e, \\ i\hbar\partial_t\psi_e &= \frac{\mathbf{P}^2}{2M}\psi_e + \frac{1}{2}\hbar\Omega(\mathbf{r})\psi_g - \hbar\Delta\psi_e, \end{aligned} \tag{A.20}$$

for ψ_g and ψ_e.

There are different time scales associated with this system, as can be seen from Eq. (A.20). The time scale associated with the free time evolution of the atomic excited state is $T_{\text{free}} \sim 1/\Delta$ (note the atomic ground state carries no free time evolution), while the time scale associated with its decay is in order of $T_{\text{dec}} \sim 1/\Gamma$, where Γ is the decay rate of the excited state. Atom-field coupling induces motion in a time scale corresponding to the Rabi frequency $T_{\text{R}} \sim 1/\Omega$, which together with the free time evolution induce internal atomic oscillation in a time scale of the generalized Rabi frequency $T_{\text{int}} \sim 1/\tilde{\Omega}$. Finally, the centre-of-motion is associated with motion in a time scale of order $T_{\text{c.m.}} \sim 2\pi/\omega_{\text{c.m.}}$, where $\omega_{\text{c.m.}} = \langle P\rangle^2/2\hbar M$. In a typical experimental situation, $\omega_{\text{c.m.}} \sim$ kHz, $\Gamma \sim$ MHz for alkali atoms, $\Omega \sim 0 - 100$ MHz, and $\Delta \sim 1 - 100$ GHz, implying that $\tilde{\Omega} \sim \Delta$. The corresponding time scales then are $T_{\text{c.m.}} \gg T_{\text{dec}} \gg T_{\text{int}}$. When one is interested in a time scale on the order of $T_{\text{c.m.}}$, it is a good approximation to assume that the excited state has damped out and reached its steady-state when $\hbar\Delta$ is the dominant energy scale in the system. One can then set $\partial_t\psi_e = 0$ in the time-evolution equations (A.20) and obtain

$$\psi_e \simeq \frac{\Omega}{2\Delta}\psi_g, \tag{A.21}$$

where use has been made of the fact that the kinetic energy $P^2/2M$ is negligible in comparison

to $\hbar\Delta$. Substituting Eq. (A.21) into the first equation of (A.20) yields

$$i\hbar\partial_t\psi_g = \frac{\mathbf{P}^2}{2M}\psi_g + \frac{\hbar|\Omega(\mathbf{r})|^2}{4\Delta}\psi_g, \tag{A.22}$$

where one can ready obtain the corresponding effective Hamiltonian for the ground state,

$$\mathcal{H}_{\text{eff}} = \frac{\mathbf{P}^2}{2M} + \frac{\hbar|\Omega(\mathbf{r})|^2}{4\Delta}. \tag{A.23}$$

Appendix B

Adiabatic Elimination of the Atomic Excited State: Strong-Coupling Regime

The procedure to adiabatically eliminate the atomic excited state in the three-level Hamiltonian, Eq. (3.1), is given in Ref. [164] and the derivation below follows this with some generalizations. The Heisenberg equations of motion for the atomic transition operators are given by

$$\begin{aligned} i\hbar\dot{\sigma}_{ae} &= \varepsilon_{ea}\sigma_{ae} + \hbar\mathscr{G}_{ae}(z)\hat{A}_1\sigma_z^{ae} + \hbar\mathscr{G}_{be}(z)\hat{A}_2\sigma_{ab}; \\ i\hbar\dot{\sigma}_{be} &= \varepsilon_{eb}\sigma_{be} + \hbar\mathscr{G}_{be}(z)\hat{A}_2\sigma_z^{be} + \hbar\mathscr{G}_{ae}(z)\hat{A}_1\sigma_{ba}; \end{aligned} \tag{B.1}$$

where $\sigma_z^{\tau\tau'} \equiv \sigma_{\tau\tau} - \sigma_{\tau'\tau'} = |\tau\rangle\langle\tau| - |\tau'\rangle\langle\tau'|$. Note that $\sigma_{\tau\tau'}^\dagger = \sigma_{\tau'\tau}$ so equations of motion for these operators follow directly from those above. Defining new variables $\sigma_{ae}(t) \equiv \tilde{\sigma}_{ae}(t)e^{-i\omega_1 t}$, $\sigma_{be}(t) \equiv \tilde{\sigma}_{be}(t)e^{-i\omega_2 t}$, $\hat{A}_1(t) \equiv \hat{\tilde{A}}_1(t)e^{-i\omega_1 t}$, $\hat{A}_2(t) \equiv \hat{\tilde{A}}_2(t)e^{-i\omega_2 t}$, and $\sigma_{ab}(t) = \sigma_{ae}(t)\sigma_{eb}(t) \equiv \tilde{\sigma}_{ab}(t)e^{i(\omega_2-\omega_1)t}$, with $\tilde{\sigma}_{ab} = \tilde{\sigma}_{ae}\tilde{\sigma}_{eb}$, the Heisenberg equation of motions (B.1) take the form

$$\begin{aligned} i\dot{\tilde{\sigma}}_{ae} &= -\Delta_1\tilde{\sigma}_{ae} + \mathscr{G}_{be}(z)\hat{\tilde{A}}_2\tilde{\sigma}_{ab} + \mathscr{G}_{ae}(z)\hat{\tilde{A}}_1\sigma_z^{ae}; \\ i\dot{\tilde{\sigma}}_{be} &= -\Delta_2\tilde{\sigma}_{be} + \mathscr{G}_{ae}(z)\hat{\tilde{A}}_1\tilde{\sigma}_{ba} + \mathscr{G}_{be}(z)\hat{\tilde{A}}_2\sigma_z^{be}; \end{aligned} \tag{B.2}$$

where $\Delta_1 = \omega_1 - \varepsilon_{ea}/\hbar$ and $\Delta_2 = \omega_2 - \varepsilon_{eb}/\hbar$. The adiabatic condition $\hbar\Delta_j \gg \varepsilon_{ba}$ implies that the time-dependence of all atomic transition operators involving the excited state is vanishingly small; that is, $\dot{\tilde{\sigma}}_{ae} = \dot{\tilde{\sigma}}_{ea} = \dot{\tilde{\sigma}}_{be} = \dot{\tilde{\sigma}}_{eb} \approx 0$. This yields

$$\begin{aligned} \tilde{\sigma}_{ae} &\approx \frac{1}{\Delta_1}\left[\mathscr{G}_{be}(z)\hat{\tilde{A}}_2\tilde{\sigma}_{ab} + \mathscr{G}_{ae}(z)\hat{\tilde{A}}_1\tilde{\sigma}_z^{ae}\right]; \\ \tilde{\sigma}_{be} &\approx \frac{1}{\Delta_2}\left[\mathscr{G}_{ae}(z)\hat{\tilde{A}}_1\tilde{\sigma}_{ba} + \mathscr{G}_{be}(z)\hat{\tilde{A}}_2\tilde{\sigma}_z^{be}\right]. \end{aligned} \tag{B.3}$$

Because $\tilde{\sigma}_{ee} = \tilde{\sigma}_{ea}\tilde{\sigma}_{ae} = \tilde{\sigma}_{eb}\tilde{\sigma}_{be} \propto |g|^2/\Delta^2 \ll 1$ by assumption, all terms involving only the excited state can be neglected; thus $\tilde{\sigma}_z^{ae} \approx \tilde{\sigma}_{aa}$ and $\tilde{\sigma}_z^{be} \approx \tilde{\sigma}_{bb}$. The excited state of the atom

is therefore decoupled from the other degrees of freedom in the Hamiltonian. Substituting Eq. (B.3) into Eq. (3.1) gives

$$H_{\text{eff}} \approx \frac{\hbar^2 q_z^2}{2m} I_{2\times 2} + \left[\varepsilon_a + \frac{\hbar|\mathscr{G}_{ae}|^2}{\Delta_1}\left(\hat{\tilde{A}}_1\hat{\tilde{A}}_1^\dagger + \hat{\tilde{A}}_1^\dagger\hat{\tilde{A}}_1\right)\right]\tilde{\sigma}_{aa} + \left[\varepsilon_b + \frac{\hbar|\mathscr{G}_{be}|^2}{\Delta_2}\left(\hat{\tilde{A}}_2\hat{\tilde{A}}_2^\dagger + \hat{\tilde{A}}_2^\dagger\hat{\tilde{A}}_2\right)\right]\tilde{\sigma}_{bb}$$
$$+ \hbar\left(\omega_1\hat{\tilde{A}}_1^\dagger\hat{\tilde{A}}_1 + \omega_2\hat{\tilde{A}}_2^\dagger\hat{\tilde{A}}_2\right) + \left[\hbar\mathscr{G}_{ae}^*(z)\mathscr{G}_{be}(z)\left(\frac{1}{\Delta_1}+\frac{1}{\Delta_2}\right)\hat{\tilde{A}}_1^\dagger\hat{\tilde{A}}_2\tilde{\sigma}_{ab} + \text{H.c.}\right], \tag{B.4}$$

where the Hamiltonian for the excited state is completely ignored. Defining the ac Stark-shifted energies

$$\tilde{\varepsilon}_a \equiv \varepsilon_a + \frac{2\hbar\,|\mathscr{G}_{ae}|^2}{\Delta_1}\left(\hat{\tilde{A}}_1^\dagger\hat{\tilde{A}}_1 + \frac{1}{2}\right);$$
$$\tilde{\varepsilon}_b \equiv \varepsilon_b + \frac{2\hbar\,|\mathscr{G}_{be}|^2}{\Delta_2}\left(\hat{\tilde{A}}_2^\dagger\hat{\tilde{A}}_2 + \frac{1}{2}\right), \tag{B.5}$$

and the two-photon Rabi frequency

$$\Omega_R \equiv \mathscr{G}_{ae}\mathscr{G}_{be}\frac{\Delta_1+\Delta_2}{\Delta_1\Delta_2}, \tag{B.6}$$

where $\{\mathscr{G}_{ae}, \mathscr{G}_{be}\} \in \mathbb{R}$, the adiabatically-eliminated Hamiltonian is

$$H_{\text{eff}} = \frac{\hbar^2 q_z^2}{2m} I_{2\times 2} + \tilde{\varepsilon}_a\tilde{\sigma}_{aa} + \tilde{\varepsilon}_b\tilde{\sigma}_{bb} + \hbar\left(\omega_1\hat{\tilde{A}}_1^\dagger\hat{\tilde{A}}_1 + \omega_2\hat{\tilde{A}}_2^\dagger\hat{\tilde{A}}_2\right) + \hbar\Omega_R\left[e^{i(k_1+k_2)z}\hat{\tilde{A}}_2^\dagger\hat{\tilde{A}}_1\tilde{\sigma}_{ba} + \text{H.c.}\right]. \tag{B.7}$$

Defining $\hbar\tilde{\omega}_0 \equiv \tilde{\varepsilon}_b - \tilde{\varepsilon}_a$ and $\hbar\overline{\omega} \equiv (\tilde{\varepsilon}_a + \tilde{\varepsilon}_b)/2$, then the Hamiltonian becomes

$$H_{\text{eff}} = \frac{\hbar^2 q_z^2}{2m} I_{2\times 2} + \frac{1}{2}\hbar\tilde{\omega}_0\tilde{\sigma}_z^{ba} + \hbar\left(\omega_1\hat{\tilde{A}}_1^\dagger\hat{\tilde{A}}_1 + \omega_2\hat{\tilde{A}}_2^\dagger\hat{\tilde{A}}_2\right) + \hbar\Omega_R\left[e^{i(k_1+k_2)z}\hat{\tilde{A}}_2^\dagger\hat{\tilde{A}}_1\tilde{\sigma}_{ba} + \text{H.c.}\right], \tag{B.8}$$

where the constant term $\hbar\overline{\omega}\,(\tilde{\sigma}_{aa} + \tilde{\sigma}_{bb}) = \hbar\overline{\omega}I_{2\times 2}$ has no effect on the dynamics and is therefore neglected. Because the frequency-dependent exponential factors all cancel, one can replace $\tilde{\sigma} \to \sigma$ and $\hat{\tilde{A}} \to \hat{A}$ without loss of generality, and this yields the effective Hamiltonian (3.2).

Appendix C

Adiabatic Elimination of the Atomic Excited State: Weak-Coupling Regime

We first express the single-particle Hamiltonian density $\mathcal{H}^{(1)}$, Eq. (4.1), in the rotating frame of pump lasers [178] by applying the unitary transformation

$$\mathscr{U}_1 = \exp\left\{ i \left[\left(\hat{A}_1^\dagger \hat{A}_1 - \sigma_{aa} \right) \omega_{\mathrm{p}1} + \left(\hat{A}_2^\dagger \hat{A}_2 - \sigma_{bb} \right) \omega_{\mathrm{p}2} \right] t \right\}, \tag{C.1}$$

to obtain

$$\begin{aligned} \mathcal{H}'^{(1)} = {} & \left[\frac{\mathbf{p}^2}{2m} + V_{\mathrm{ext}}(\mathbf{r}) \right] I_{3\times 3} + \frac{\hbar\delta'}{2} \left(\sigma_{aa} - \sigma_{bb} \right) - \frac{\hbar}{2} \left(\Delta_{\mathrm{a}1} + \Delta_{\mathrm{a}2} \right) \sigma_{ee} - \hbar \big(\Delta_{\mathrm{c}1} \hat{A}_1^\dagger \hat{A}_1 + \Delta_{\mathrm{c}2} \hat{A}_2^\dagger \hat{A}_2 \big) \\ & + i\hbar \left[\left(\eta_1 \hat{A}_1^\dagger + \eta_2 \hat{A}_2^\dagger \right) - \mathrm{H.c.} \right] + \hbar \left[\left(\mathscr{G}_{ae} e^{ik_R z} \hat{A}_1 \sigma_{ea} + \mathscr{G}_{be} e^{-ik_R z} \hat{A}_2 \sigma_{eb} \right) + \mathrm{H.c.} \right], \end{aligned} \tag{C.2}$$

where we have defined the atomic and the two-photon (or relative-atomic) detunings

$$\begin{aligned} \Delta_{\mathrm{a}1} = \omega_{\mathrm{p}1} - \frac{1}{\hbar}(\varepsilon_e - \varepsilon_a), \qquad \Delta_{\mathrm{a}2} = \omega_{\mathrm{p}2} - \frac{1}{\hbar}(\varepsilon_e - \varepsilon_b), \\ \delta' = (\omega_{\mathrm{p}1} - \omega_{\mathrm{p}2}) - \frac{1}{\hbar}(\varepsilon_b - \varepsilon_a) = \Delta_{\mathrm{a}1} - \Delta_{\mathrm{a}2}, \end{aligned} \tag{C.3a}$$

and cavity detunings

$$\Delta_{\mathrm{c}j} = \omega_{\mathrm{p}j} - \omega_j, \qquad j = 1, 2, \tag{C.3b}$$

with respect to the pump lasers. Let us now assume that the detunings $\Delta_1 = \omega_1 - \varepsilon_{ea}/\hbar = -\Delta_{\mathrm{c}1} + \Delta_{\mathrm{a}1}$ and $\Delta_2 = \omega_2 - \varepsilon_{eb}/\hbar = -\Delta_{\mathrm{c}2} + \Delta_{\mathrm{a}2}$ are large compared to $\varepsilon_{ba}/\hbar = (\varepsilon_b - \varepsilon_a)/\hbar$ so that we can adiabatically eliminate the dynamic of the atomic excited state $|e\rangle$ from the Hamiltonian (C.2) and obtain an effective Hamiltonian for the ground pseudospins $\{1, 2\} \equiv \{b, a\}$. Following the standard adiabatic elimination procedure [164, 116] outlined in the preceding appendix, we first find the Heisenberg equations of motion $i\hbar\dot{\sigma}_{e\tau} = [\sigma_{e\tau}, \mathcal{H}'^{(1)}]$

for $\dot{\sigma}_{ea}$ and $\dot{\sigma}_{eb}$, and then (after transferring to slowly rotating variables) set them equal to zero to find the steady-state solutions $\sigma_{ea}^{(\mathrm{ss})}$ and $\sigma_{eb}^{(\mathrm{ss})}$. After substituting these steady-state solutions back in $\mathcal{H}'^{(1)}$ (C.2) and dropping terms diagonal in σ_{ee}, we arrive at the single-particle Hamiltonian density for pseudospins

$$\mathcal{H}_{\mathrm{SO}}'^{(1)} = \left[\frac{\mathbf{p}^2}{2m} + V_{\mathrm{ext}}(\mathbf{r})\right]\mathbb{I} + \sum_{\tau=1,2}\hat{\varepsilon}_\tau\sigma_{\tau\tau} + H'_{\mathrm{cav}} + \hbar\Omega'_R\Big(e^{2ik_Rz}\hat{A}_2^\dagger\hat{A}_1\sigma_{12} + e^{-2ik_Rz}\hat{A}_1^\dagger\hat{A}_2\sigma_{21}\Big), \tag{C.4}$$

where

$$H'_{\mathrm{cav}} = -\hbar\big(\Delta_{\mathrm{c}1}\hat{A}_1^\dagger\hat{A}_1 + \Delta_{\mathrm{c}2}\hat{A}_2^\dagger\hat{A}_2\big) + i\hbar\left[\Big(\eta_1\hat{A}_1^\dagger + \eta_2\hat{A}_2^\dagger\Big) - \mathrm{H.c.}\right], \tag{C.5}$$

and

$$\hat{\varepsilon}_1 = -\frac{\hbar\delta'}{2} + \frac{2\hbar\mathscr{G}_{be}^2}{\Delta_2}(\hat{A}_2^\dagger\hat{A}_2 + \frac{1}{2}); \qquad \hat{\varepsilon}_2 = \frac{\hbar\delta'}{2} + \frac{2\hbar\mathscr{G}_{ae}^2}{\Delta_1}(\hat{A}_1^\dagger\hat{A}_1 + \frac{1}{2}). \tag{C.6}$$

Here, $\Omega'_R = \frac{\Delta_1+\Delta_2}{\Delta_1\Delta_2}\mathscr{G}_{ae}\mathscr{G}_{be}$ is the two-photon Rabi frequency and $\mathbb{I} \equiv I_{2\times2}$ is the identity matrix in the pseudospin space. Note the hat on $\hat{\varepsilon}_\tau$, implying that it depends on the cavity field operators. After transferring to the co-moving frame of the cavity modes by applying the unitary transformation $\mathscr{U}_2 = e^{-ik_R(\sigma_{11}-\sigma_{22})z}$ to the Hamiltonian density (C.4), we obtain the SO-coupled single-particle Hamiltonian density

$$\begin{aligned}\mathcal{H}_{\mathrm{SO}}''^{(1)} = {}& \frac{1}{2m}\left\{p_\perp^2\mathbb{I} + \big[p_z\mathbb{I} - \hbar k_R(\sigma_{22}-\sigma_{11})\big]^2\right\} + V_{\mathrm{ext}}(\mathbf{r})\mathbb{I} + \sum_{\tau=1,2}\hat{\varepsilon}_\tau\sigma_{\tau\tau} + H'_{\mathrm{cav}} \\ & + \hbar\Omega'_R\Big(\hat{A}_2^\dagger\hat{A}_1\sigma_{12} + \hat{A}_1^\dagger\hat{A}_2\sigma_{21}\Big).\end{aligned} \tag{C.7}$$

One can identify $\hbar k_R(\sigma_{22}-\sigma_{11})$ with $q^*\check{\mathcal{A}}_z$ as in the minimal coupling Hamiltonian, that is, $q^*\check{\mathcal{A}}_z \equiv \hbar k_R(\sigma_{22}-\sigma_{11}) = -\hbar k_R\check{\sigma}_z$, where $\check{\sigma}_z = \sigma_{11}-\sigma_{22}$ is the third Pauli matrix. Nonetheless, we emphasis that here $\check{\mathcal{A}}_z$ is a matrix acting in the internal pseudospin states, in contrast to the ordinary vector potential whose components are scaler fields. Then the

single-particle Hamiltonian reads

$$H''^{(1)}_{\mathrm{SO}} = \frac{1}{2m}\int \hat{\mathbf{\Psi}}^{\dagger}\left[p_{\perp}^{2}\mathbb{I} + (p_z\mathbb{I} + \hbar k_R \check{\sigma}_z)^2 + V_{\mathrm{ext}}(\mathbf{r})\mathbb{I}\right]\hat{\mathbf{\Psi}}d^3r + \sum_{\tau=1,2}\hat{\varepsilon}_{\tau}\hat{N}_{\tau} + H'_{\mathrm{cav}}$$
$$+ \hbar\Omega'_R\Big(\hat{A}_2^{\dagger}\hat{A}_1\hat{S}_+ + \hat{A}_1^{\dagger}\hat{A}_2\hat{S}_-\Big), \tag{C.8}$$

where $\hat{\mathbf{\Psi}}(\mathbf{r}) = (\hat{\psi}_1(\mathbf{r}), \hat{\psi}_2(\mathbf{r}))^{\mathsf{T}}$ are the bosonic field operators, $\hat{N}_{\tau} = \int \hat{\psi}_{\tau}^{\dagger}(\mathbf{r})\hat{\psi}_{\tau}(\mathbf{r})d^3r$ is the total atomic number operator for pseudospin τ, $\hat{N} = \hat{N}_1 + \hat{N}_2$ is the total atomic number operator, and $\hat{S}_+ = \hat{S}_-^{\dagger} = \int \hat{\psi}_1^{\dagger}(\mathbf{r})\hat{\psi}_2(\mathbf{r})d^3r$ are the collective pseudospin raising and lowering operators.

Appendix D

Adiabatic Elimination of the Cavity Fields: Weak-Coupling Regime

By noting that the cavity field operator commutes with the atomic interaction Hamiltonian $[\hat{A}_j, H_{\rm int}] = 0$, then the Heisenberg equations of motion of the cavity field operators are determined by the single-particle Hamiltonian $H_{\rm SO}^{\prime\prime(1)}$, Eq. (C.8): $\partial_t \hat{A}_j = -i[\hat{A}_j, H_{\rm SO}^{\prime\prime(1)}]/\hbar - \kappa \hat{A}_j$, where the cavity-mode decay $-\kappa \hat{A}_j$ is included phenomenologically. They can be recast in the matrix form,

$$\frac{d}{dt}\begin{pmatrix} \hat{A}_1 \\ \hat{A}_2 \end{pmatrix} = i \begin{pmatrix} \hat{\alpha}_{11} & -\hat{\alpha}_{12} \\ -\hat{\alpha}_{21} & \hat{\alpha}_{22} \end{pmatrix} \begin{pmatrix} \hat{A}_1 \\ \hat{A}_2 \end{pmatrix} + \begin{pmatrix} \eta_1 \\ \eta_2 \end{pmatrix}, \tag{D.1}$$

where the elements of the "operator" matrix $\hat{\boldsymbol{\alpha}}$ are given by

$$\hat{\alpha}_{11} = (\Delta_{\rm c1} + i\kappa) - \frac{2\mathscr{G}_{ae}^2}{\Delta_1}\hat{N}_2, \qquad \hat{\alpha}_{22} = (\Delta_{\rm c2} + i\kappa) - \frac{2\mathscr{G}_{be}^2}{\Delta_2}\hat{N}_1, \qquad \hat{\alpha}_{12} = \hat{\alpha}_{21}^\dagger = \Omega_R' \hat{S}_-. \tag{D.2}$$

The $2\mathscr{G}_{ae}^2\hat{N}_2/\Delta_1$ and $2\mathscr{G}_{be}^2\hat{N}_1/\Delta_2$ terms are the light shifts induced by the backaction of the atoms, and they lower the bare cavity frequencies $\Delta_{{\rm c}j}$, while the terms $\Omega_R'\hat{S}_+$ and $\Omega_R'\hat{S}_-$ couple the two cavity modes.

If the cavity decay rate κ is large, then the cavity fields reach steady states very quickly. By setting $\partial_t \hat{A}_1 = \partial_t \hat{A}_2 = 0$ in Eq. (D.1), one can simultaneously solve the two equations of motion to obtain formal expressions for the steady-state field amplitudes $\hat{A}_{{\rm ss}j}$. However, one should take special care in solving these equations since the cavity fields and atomic fields commute with one another and this can give rise to ambiguities in solving these equations. In order to avoid such ambiguities, we symmetrize the equations of motion and exercise symmetrization procedure in all results following from the equations of motion. Thus, after

setting $\partial_t \hat{A}_1 = \partial_t \hat{A}_2 = 0$ in Eq. (D.1), we re-express equations of motion as

$$\begin{aligned}
&\frac{i}{2}\left(\hat{\alpha}_{11}\hat{A}_{\rm ss1} + \hat{A}_{\rm ss1}\hat{\alpha}_{11}\right) - \frac{i}{2}\left(\hat{\alpha}_{12}\hat{A}_{\rm ss2} + \hat{A}_{\rm ss2}\hat{\alpha}_{12}\right) + \eta_1 = 0, \\
&\frac{i}{2}\left(\hat{\alpha}_{22}\hat{A}_{\rm ss2} + \hat{A}_{\rm ss2}\hat{\alpha}_{22}\right) - \frac{i}{2}\left(\hat{\alpha}_{21}\hat{A}_{\rm ss1} + \hat{A}_{\rm ss1}\hat{\alpha}_{21}\right) + \eta_2 = 0.
\end{aligned} \tag{D.3}$$

Equation (D.3) can then be rearranged

$$\hat{A}_{\rm ss1} = \frac{1}{4}\left[\left(\hat{\alpha}_{11}^{-1}\hat{\alpha}_{12} + \hat{\alpha}_{12}\hat{\alpha}_{11}^{-1}\right)\hat{A}_{\rm ss2} + \hat{A}_{\rm ss2}\left(\hat{\alpha}_{11}^{-1}\hat{\alpha}_{12} + \hat{\alpha}_{12}\hat{\alpha}_{11}^{-1}\right)\right] + i\hat{\alpha}_{11}^{-1}\eta_1, \tag{D.4a}$$

$$\hat{A}_{\rm ss2} = \frac{1}{4}\left[\left(\hat{\alpha}_{22}^{-1}\hat{\alpha}_{21} + \hat{\alpha}_{21}\hat{\alpha}_{22}^{-1}\right)\hat{A}_{\rm ss1} + \hat{A}_{\rm ss1}\left(\hat{\alpha}_{22}^{-1}\hat{\alpha}_{21} + \hat{\alpha}_{21}\hat{\alpha}_{22}^{-1}\right)\right] + i\hat{\alpha}_{22}^{-1}\eta_2, \tag{D.4b}$$

where $\hat{\alpha}_{11}^{-1}$ and $\hat{\alpha}_{22}^{-1}$ are the inverse operators of $\hat{\alpha}_{11}$ and $\hat{\alpha}_{22}$, respectively, such that $\hat{\alpha}_{11}\hat{\alpha}_{11}^{-1} = \hat{\alpha}_{11}^{-1}\hat{\alpha}_{11} = \hat{1}$ and $\hat{\alpha}_{22}\hat{\alpha}_{22}^{-1} = \hat{\alpha}_{22}^{-1}\hat{\alpha}_{22} = \hat{1}$. In order to make the subsequent analyses somewhat easier and trackable, we assume that all dual variables (except η_j at this moment) are equal, namely, $\Delta_1 = \Delta_2 \equiv \Delta$, $\Delta_{\rm c1} = \Delta_{\rm c2} \equiv \Delta_{\rm c}$, and $\mathscr{G}_{ae} = \mathscr{G}_{be} \equiv \mathscr{G}_0$. We also introduce $\tilde{\Delta}_{\rm c} \equiv \Delta_{\rm c} + i\kappa$ for a shorthand. We expand the inverse operators to the second order in a small unitless parameter $\xi \equiv 2\mathscr{G}_0^2/\Delta\tilde{\Delta}_{\rm c} \ll 1$ (and with $\langle\hat{N}_\tau\rangle \sim 10^5$ one still has $\xi\langle\hat{N}_\tau\rangle \sim 10^{-2} \ll 1$, see Sec. 4.2 for more details),

$$\begin{aligned}
\hat{\alpha}_{11}^{-1} &= \left(\tilde{\Delta}_{\rm c} - \frac{2\mathscr{G}_0^2}{\Delta}\hat{N}_2\right)^{-1} \simeq \tilde{\Delta}_{\rm c}^{-1}\left(1 + \frac{2\mathscr{G}_0^2}{\Delta\tilde{\Delta}_{\rm c}}\hat{N}_2 + \frac{4\mathscr{G}_0^4}{\Delta^2\tilde{\Delta}_{\rm c}^2}\hat{N}_2^2\right), \\
\hat{\alpha}_{22}^{-1} &= \left(\tilde{\Delta}_{\rm c} - \frac{2\mathscr{G}_0^2}{\Delta}\hat{N}_1\right)^{-1} \simeq \tilde{\Delta}_{\rm c}^{-1}\left(1 + \frac{2\mathscr{G}_0^2}{\Delta\tilde{\Delta}_{\rm c}}\hat{N}_1 + \frac{4\mathscr{G}_0^4}{\Delta^2\tilde{\Delta}_{\rm c}^2}\hat{N}_1^2\right),
\end{aligned} \tag{D.5}$$

such that $\hat{\alpha}_{11}\hat{\alpha}_{11}^{-1} = \hat{\alpha}_{11}^{-1}\hat{\alpha}_{11} = \hat{\alpha}_{22}\hat{\alpha}_{22}^{-1} = \hat{\alpha}_{22}^{-1}\hat{\alpha}_{22} = \hat{1} + \mathcal{O}(\xi^3)$. Note that the error in symmetrizing Eq. (D.4) is also of order $\mathcal{O}(\xi^3)$. This can be easily checked by substituting, say, Eq. (D.4a) in the first equation of (D.3). Equations (D.4a) and (D.4b) can now be simultaneously solved, yielding

$$\begin{aligned}
\hat{A}_{\rm ss1} &= i\hat{\Gamma}^{-1}\left[\eta_1\hat{\alpha}_{11}^{-1} + \frac{\eta_2}{4}\left(\hat{\alpha}_{11}^{-1}\hat{\alpha}_{12}\hat{\alpha}_{22}^{-1} + \hat{\alpha}_{12}\hat{\alpha}_{11}^{-1}\hat{\alpha}_{22}^{-1} + \hat{\alpha}_{22}^{-1}\hat{\alpha}_{11}^{-1}\hat{\alpha}_{12} + \hat{\alpha}_{22}^{-1}\hat{\alpha}_{12}\hat{\alpha}_{11}^{-1}\right)\right], \\
\hat{A}_{\rm ss2} &= i\hat{\Gamma}^{-1}\left[\eta_2\hat{\alpha}_{22}^{-1} + \frac{\eta_1}{4}\left(\hat{\alpha}_{22}^{-1}\hat{\alpha}_{21}\hat{\alpha}_{11}^{-1} + \hat{\alpha}_{21}\hat{\alpha}_{22}^{-1}\hat{\alpha}_{11}^{-1} + \hat{\alpha}_{11}^{-1}\hat{\alpha}_{22}^{-1}\hat{\alpha}_{21} + \hat{\alpha}_{11}^{-1}\hat{\alpha}_{21}\hat{\alpha}_{22}^{-1}\right)\right],
\end{aligned} \tag{D.6}$$

where $\hat{\Gamma} = \left[1 - \frac{1}{2\tilde{\Delta}_{\rm c}^2}\left(\hat{\alpha}_{12}\hat{\alpha}_{21} + \hat{\alpha}_{21}\hat{\alpha}_{12}\right)\right]$ up to ξ^2, by noting $\hat{\alpha}_{12} = \hat{\alpha}_{21}^\dagger \propto \Omega_R' = 2\mathcal{G}_0^2/\Delta$ and

(D.5). We then have

$$\hat{\Gamma}^{-1} \simeq 1 + \frac{1}{2\tilde{\Delta}_{\rm c}^2}\left(\hat{\alpha}_{12}\hat{\alpha}_{21} + \hat{\alpha}_{21}\hat{\alpha}_{12}\right) = 1 + \frac{2\mathscr{G}_0^4}{\Delta^2\tilde{\Delta}_{\rm c}^2}\left(\hat{S}_+\hat{S}_- + \hat{S}_-\hat{S}_+\right), \tag{D.7}$$

up to $\mathcal{O}(\xi^3)$. Using Eqs. (D.2), (D.5)-(D.7), and retaining terms up to ξ^2, we obtain

$$\begin{aligned}
\hat{A}_{\rm ss1} &= \frac{i}{\tilde{\Delta}_{\rm c}}\left\{\eta_1 + \frac{2\mathscr{G}_0^2}{\Delta\tilde{\Delta}_{\rm c}}\left(\eta_1\hat{N}_2 + \eta_2\hat{S}_-\right) + \frac{4\mathscr{G}_0^4}{\Delta^2\tilde{\Delta}_{\rm c}^2}\left[\eta_1\hat{N}_2^2 + \frac{\eta_1}{2}\left(\hat{S}_+\hat{S}_- + \hat{S}_-\hat{S}_+\right) + \eta_2\hat{N}\hat{S}_-\right]\right\}, \\
\hat{A}_{\rm ss2} &= \frac{i}{\tilde{\Delta}_{\rm c}}\left\{\eta_2 + \frac{2\mathscr{G}_0^2}{\Delta\tilde{\Delta}_{\rm c}}\left(\eta_2\hat{N}_1 + \eta_1\hat{S}_+\right) + \frac{4\mathscr{G}_0^4}{\Delta^2\tilde{\Delta}_{\rm c}^2}\left[\eta_2\hat{N}_1^2 + \frac{\eta_2}{2}\left(\hat{S}_+\hat{S}_- + \hat{S}_-\hat{S}_+\right) + \eta_1\hat{N}\hat{S}_+\right]\right\}.
\end{aligned} \tag{D.8}$$

By substituting steady-state solutions (D.8) and their Hermitian conjugates in the Hamiltonian $H_{\rm SO}^{\prime\prime(1)}$, Eq. (C.8), exercising symmetrization procedure again and retaining terms up to ξ^2, we can find an effective Hamiltonian which depends solely on the atomic operators. After some tedious though straightforward algebra, we obtain the cavity-field-eliminated effective many-body Hamiltonian

$$\begin{aligned}
H_{\rm eff} = &\int d^3r\left(\hat{\mathbf{\Psi}}^\dagger\mathcal{H}_{\rm SO}^{(1)}\hat{\mathbf{\Psi}} + \frac{1}{2}g_1\hat{n}_1^2 + \frac{1}{2}g_2\hat{n}_2^2 + g_{12}\hat{n}_1\hat{n}_2\right) \\
&+ \sum_{\tau=1,2}U_\tau\hat{N}_\tau^2 + \left(U_\pm\hat{S}_+\hat{S}_- + U_\mp\hat{S}_-\hat{S}_+\right) + 2U_{\rm ds}\hat{N}\hat{S}_x,
\end{aligned} \tag{D.9}$$

where the cavity-field-eliminated, effective single-particle Hamiltonian density takes the familiar form

$$\mathcal{H}_{\rm SO}^{(1)} = -\frac{\hbar^2}{2m}[\nabla_\perp^2 - (-i\partial_z + k_R\check{\sigma}_z)^2] + V_{\rm ext}(\mathbf{r}) + \frac{1}{2}\hbar\delta\check{\sigma}_z + \hbar\Omega_R\check{\sigma}_x, \tag{D.10}$$

with effective two-photon detuning and Raman coupling given by

$$\begin{aligned}
\delta &\equiv \frac{2\mathscr{G}_0^2(\Delta_{\rm c}^2 - \kappa^2)}{\Delta(\Delta_{\rm c}^2 + \kappa^2)^2}(\eta_2^2 - \eta_1^2), \\
\Omega_R &= \frac{2\mathscr{G}_0^2}{\Delta(\Delta_{\rm c}^2 + \kappa^2)^2}\left(\Delta_{\rm c}^2 - \kappa^2 - \frac{2\mathscr{G}_0^2\Delta_{\rm c}}{\Delta}\right)\eta_1\eta_2 = \frac{\Omega_R'}{(\Delta_{\rm c}^2 + \kappa^2)^2}\left(\Delta_{\rm c}^2 - \kappa^2 - \frac{2\mathscr{G}_0^2\Delta_{\rm c}}{\Delta}\right)\eta_1\eta_2.
\end{aligned} \tag{D.11}$$

(Note that $\delta' = 0$, since we have assumed $\Delta_{\mathrm{a}1} = \Delta_{\mathrm{a}2} \equiv \Delta_{\mathrm{a}}$; cf. Eqs. (C.3) and (C.6).) The coefficients of the cavity-mediated long-range interactions are found to be

$$U_1 = \frac{4\hbar\mathscr{G}_0^4\Delta_{\mathrm{c}}(\Delta_{\mathrm{c}}^2 - 3\kappa^2)}{\Delta^2(\Delta_{\mathrm{c}}^2+\kappa^2)^3}\eta_2^2, \quad U_2 = \frac{4\hbar\mathscr{G}_0^4\Delta_{\mathrm{c}}(\Delta_{\mathrm{c}}^2 - 3\kappa^2)}{\Delta^2(\Delta_{\mathrm{c}}^2+\kappa^2)^3}\eta_1^2, \quad U_{\mathrm{ds}} = \frac{4\hbar\mathscr{G}_0^4\Delta_{\mathrm{c}}\,(\Delta_{\mathrm{c}}^2 - 3\kappa^2)}{\Delta^2(\Delta_{\mathrm{c}}^2+\kappa^2)^3}\eta_1\eta_2,$$
$$U_{\pm} = \frac{4\hbar\mathscr{G}_0^4\Delta_{\mathrm{c}}}{\Delta^2(\Delta_{\mathrm{c}}^2+\kappa^2)^3}\left[\Delta_{\mathrm{c}}^2\eta_1^2 - (\eta_1^2+2\eta_2^2)\kappa^2\right], \quad U_{\mp} = \frac{4\hbar\mathscr{G}_0^4\Delta_{\mathrm{c}}}{\Delta^2(\Delta_{\mathrm{c}}^2+\kappa^2)^3}\left[\Delta_{\mathrm{c}}^2\eta_2^2 - (\eta_2^2+2\eta_1^2)\kappa^2\right]. \tag{D.12}$$

The terms with coefficients $U_{1/2}$, $U_{\pm/\mp}$, and U_{ds} in the effective Hamiltonian (D.9) are the cavity-mediated long-range interactions. Note that in the special case of $\eta_1 = \eta_2 \equiv \eta$, one has $\delta = 0$ and $U_1 = U_2 = U_{\pm} = U_{\mp} = U_{\mathrm{ds}} \equiv U$.

Bibliography

[1] R. Feynman, Int. J. Theor. Phys. **21**, 467 (1982).

[2] S. Bose, Z. Phys. **26**, 178 (1924).

[3] O. Theimer and B. Ram, Am. J. Phys. **44**, 1056 (1976).

[4] A. Einstein, Sitzungsber. K. Preuss. Akad. Wiss., Phys. Math. Kl. **261** (1924).

[5] A. Einstein, Sitzungsber. K. Preuss. Akad. Wiss., Phys. Math. Kl. **3** (1925).

[6] D. K. Buchwald, J. Illy, Z. Rosenkranz, T. Sauer, and O. Moses, editors, *The Collected Papers of Albert Einstein, Volume 14: The Berlin Years: Writings & Correspondence, April 1923-May 1925*, Princeton Univeristy Press, 2015.

[7] C. J. Pethick and H. Smith, *Bose-Einstein Condensation in Dilute Gases*, Cambridge University Press, New York, 2nd ed. edition, 2008.

[8] F. London, Nature (London) **141**, 643 (1938).

[9] N. N. Bogoliubov, J. Phys. **11**, 23 (1947).

[10] E. P. Gross, Nuovo Cimento **20**, 454 (1961).

[11] L. P. Pitaevskii, Zh. Eksp. Teor. Fiz. **40**, 646 (1961).

[12] E. P. Gross, J. Math. Phys. **4**, 195 (1963).

[13] S. Chu, Rev. Mod. Phys. **70**, 685 (1998).

[14] C. N. Cohen-Tannoudji, Rev. Mod. Phys. **70**, 707 (1998).

[15] W. D. Phillips, Rev. Mod. Phys. **70**, 721 (1998).

[16] G. Grynberg and R. Stora, editors, *New Trends in Atomic Physics*, North Holland, Amsterdam, 1984.

[17] M. H. Anderson, J. R. Ensher, M. R. Matthews, C. E. Wieman, and E. A. Cornell, Science **269**, 198 (1995).

[18] K. Davis et al., Phys. Rev. Lett. **75**, 3969 (1995).

[19] F. Dalfovo, S. Giorgini, L. P. Pitaevskii, and S. Stringari, Rev. Mod. Phys. **71**, 463 (1999).

[20] A. J. Leggett, Rev. Mod. Phys. **73**, 307 (2001).

[21] C. Bradley, C. A. Sackett, J. J. Tollett, and R. G. Hulet, Phys. Rev. Lett. **75**, 1687 (1995).

[22] E. Cornell, J. Res. Natl. Inst. Stand. Technol. **101**, 419 (1996).

[23] J. R. Anglin and W. Ketterle, Nature **416**, 211 (2002).

[24] A. Fetter and J. D. Walecka, *Quantum Theory of Many-Particle Systems*, McGraw-Hill, New York, 1971.

[25] D. I. Khomskii, *Basic Aspects of the Quantum Theory of Solids: Order and Elementary Excitations*, Cambridge University Press, 2010.

[26] A. Griffin, T. Nikuni, and E. Zaremba, *Bose-Condensed Gases at Finite Temperatures*, Cambridge University Press, 2009.

[27] L. Tisza, C. R. Acad. Sci. **207**, 1035 (1938).

[28] L. Tisza, C. R. Acad. Sci. **207**, 1186 (1938).

[29] P. A. Martin and F. Rothen, *Many-Body Problems and Quantum Field Theory: An Introduction*, Springer, 2004.

[30] L. Landau, J. Phys. (USSR) **5**, 71 (1941).

[31] L. Landau, J. Phys. (USSR) **11**, 91 (1947).

[32] H. T. C. Stoof, K. B. Gubbels, and D. B. M. Dickerscheid, *Ultracold Quantum Fields*, Springer, 2009.

[33] D. M. Stamper-Kurn et al., Phys. Rev. Lett. **80**, 2027 (1998).

[34] J. Stenger et al., Nature **396**, 345 (1998).

[35] Y. Kawaguchia and M. Ueda, Physics Reports **520**, 253 (2012).

[36] D. M. Stamper-Kurn and M. Ueda, Rev. Mod. Phys. **85**, 1191 (2013).

[37] C. J. Myatt, E. A. Burt, R. W. Ghrist, E. A. Cornell, and C. E. Wieman, Phys. Rev. Lett. **78**, 586 (1997).

[38] D. Jaksch and P. Zoller, Ann. Phys. **315**, 52 (2005).

[39] M. Lewenstein et al., Adv. Phys. **56**, 243 (2007).

[40] I. Bloch, J. Dalibard, and W. Zwerger, Rev. Mod. Phys. **80**, 885 (2008).

[41] V. I. Yukalov, Laser Physics **19**, 1 (2009).

[42] J. Hubbard, Proceedings of the Royal Society of London. Series A, Mathematical and Physical Sciences **276**, 238 (1963).

[43] M. Greiner, O. Mandel, T. Esslinger, T. W. Hänsch, and I. Bloch, Nature **415**, 39 (2002).

[44] J. Struck et al., Nature Physics **9**, 738 (2013).

[45] R. A. Hart et al., Nature **519**, 211 (2015).

[46] D. R. Yennie, Rev. Mod. Phys. **59**, 781 (1987).

[47] M. Z. Hasan and C. L. Kane, Rev. Mod. Phys. **82**, 3045 (2010).

[48] X.-L. Qi and S.-C. Zhang, Rev. Mod. Phys. **83**, 1057 (2011).

[49] K. Klitzing, G. Dorda, and M. Pepper, Phys. Rev. Lett. **45**, 494 (1980).

[50] R. B. Laughlin, Phys. Rev. B **23**, 5632 (1981).

[51] C. L. Kane and E. J. Mele, Phys. Rev. Lett. **95**, 146802 (2005).

[52] C. L. Kane and E. J. Mele, Phys. Rev. Lett. **95**, 226801 (2005).

[53] B. A. Bernevig, T. L. Hughes, and S.-C. Zhang, Science **314**, 1757 (2006).

[54] M. König et al., Science **318**, 766 (2007).

[55] E. Rashba, Fiz. Tverd. Tela **2**, 1224 (1960).

[56] G. Dresselhaus, Phys. Rev. **100**, 580 (1955).

[57] N. Goldman, G. Juzeliūnas, P. Öhberg, and I. B. Spielman, Rep. Prog. Phys. **77**, 126401 (2014).

[58] C. Nayak, S. H. Simon, A. Stern, M. Freedman, and S. D. Sarma, Rev. Mod. Phys. **80**, 1083 (2008).

[59] J. Dalibard, F. Gerbier, G. Juzeliūnas, and P. Öhberg, Rev. Mod. Phys. **83**, 1523 (2011).

[60] K. Madison, K. Bongs, L. D. Carr, A. M. Rey, and H. Zhai, editors, *Annual Review of Cold Atoms and Molecules: Volume 3*, World Scientific, 2015.

[61] M. Berry, Proceedings of the Royal Society A **392**, 45 (1984).

[62] B. Holstein, Am. J. Phys. **57**, 1079 (1989).

[63] M. Nakahara, *Geometry, Topology, and Physics*, IOP Publishing Ltd, 2003.

[64] R. Dum and M. Olshanii, Phys. Rev. Lett. **76**, 1788 (1996).

[65] Y.-J. Lin, R. L. Compton, K. Jiménez-García, J. V. Porto, and I. B. Spielman, Nature **462**, 628 (2009).

[66] Y.-J. Lin et al., Nature Physics **7**, 531 (2011).

[67] Y.-J. Lin, K. Jiménez-Garcia, and I. B. Spielman, Nature **471**, 83 (2011).

[68] M. C. Beeler et al., Nature **498**, 201 (2013).

[69] X. Zhou, Y. Li, Z. Cai, and C. Wu, J. Phys. B: At. Mol. Opt. Phys. **46**, 134001 (2013).

[70] D. R. Hofstadter, Phys. Rev. B **14**, 2239 (1976).

[71] M. Aidelsburger et al., Phys. Rev. Lett. **111**, 185301 (2013).

[72] H. Miyake, G. A. Siviloglou, C. J. Kennedy, W. C. Burton, and W. Ketterle, Phys. Rev. Lett. **111**, 185302 (2013).

[73] C. J. Kennedy, W. C. Burton, W. C. Chung, and W. Ketterle, Nature Physics **11**, 859 (2015).

[74] C. Wang, C. Gao, C.-M. Jian, and H. Zhai, Phys. Rev. Lett. **105**, 160403 (2010).

[75] T.-L. Ho and S. Zhang, Phys. Rev. Lett. **107**, 150403 (2011).

[76] Y. Li, L. P. Pitaevskii, and S. Stringari, Phys. Rev. Lett. **108**, 225301 (2012).

[77] W. Zheng and Z. Li, Phys. Rev. A **85**, 053607 (2012).

[78] Q.-Q. Lü and D. E. Sheehy, Phys. Rev. A **88**, 043645 (2013).

[79] W. S. Cole, S. Zhang, A. Paramekanti, and N. Trivedi, Phys. Rev. Lett. **109**, 085302 (2012).

[80] J. Radić, A. D. Ciolo, K. Sun, and V. Galitski, Phys. Rev. Lett. **109**, 085303 (2012).

[81] Z. Cai, X. Zhou, and C. Wu, Phys. Rev. A **85**, 061605(R) (2012).

[82] T. Graß, K. Saha, K. Sengupta, and M. Lewenstein, Phys. Rev. A **84**, 053632 (2011).

[83] W. Greiner, *Quantum Mechanics: An Introduction*, Springer, 2001.

[84] D. F. Walls and G. J. Milburn, *Quantum Optics*, Springer, 1994.

[85] G. N. Lewis, Nature **118**, 874 (1926).

[86] P. A. M. Dirac, Proc. Royal Soc. (London) **114**, 243 (1927).

[87] M. Scully and M. S. Zubairy, *Quantum Optics*, Cambridge University Press, 1997.

[88] B. E. A. Saleh and M. C. Teich, *Fundamentals of Photonics*, John Wiley & Sons, Inc., 2007.

[89] W. Greiner, *Classical Electrodynamics*, Springer, 1998.

[90] A. Yariv, *Quanum Electronics*, John Wiley & Sons, Inc., 1989.

[91] H. J. Kimble, Physica Scripta **T76**, 127 (1998).

[92] E. M. Purcell, Phys. Rev. **69**, 681 (1946).

[93] E. Jaynes and F. Cummings, Proc. IEEE **51**, 89 (1963).

[94] Z. Bialynicka-Birula, Acta Physica Polonica B **27**, 2409 (1996).

[95] I. R. Kenyon, *The Light Fantastic: A Modern Introduction to Classical and Quantum Optics*, Oxford University Press, 2008.

[96] P. Münstermann, T. Fischer, P. Maunz, P. H. Pinkse, and G. Rempe, Phys. Rev. Lett. **84**, 4068 (2000).

[97] F. Brennecke et al., Nature **450**, 268 (2007).

[98] J. M. Raimond, M. Brune, and S. Haroche, Rev. Mod. Phys. **73**, 565 (2001).

[99] H. Walther, B. T. H. Varcoe, B.-G. Englert, and T. Becker, Rep. Prog. Phys. **69**, 1325 (2006).

[100] J. J. Sanchez-Mondragon, N. B. Narozhny, and J. H. Eberly, Phys. Rev. Lett. **51**, 550 (1983).

[101] G. S. Agarwal, J. Opt. Soc. Am. B **2**, 480 (1985).

[102] M. Brune et al., Phys. Rev. Lett. **76**, 1800 (1996).

[103] M. Nielsen and I. Chuang, *Quantum computation and quantum information*, Cambridge University Press, 2000.

[104] E. S. Shuman, J. F. Barry, and D. DeMille, Nature **467**, 820 (2010).

[105] P. W. H. Pinkse, T. Fischer, P. Maunz, and G. Rempe, Nature **404**, 365 (2000).

[106] P. Maunz et al., Nature **428**, 50 (2004).

[107] H. Ritsch, P. Domokos, F. Brennecke, and T. Esslinger, Rev. Mod. Phys. **85**, 553 (2013).

[108] P. Horak, S. M. Barnett, and H. Ritsch, Phys. Rev. A **61**, 033609 (2000).

[109] D. Nagy, G. Szirmaia, and P. Domokos, Eur. Phys. J. D **48**, 127 (2008).

[110] K. Baumann, C. Guerlin, F. Brennecke, and T. Esslinger, Nature **464**, 1301 (2010).

[111] K. Baumann, R. Mottl, F. Brennecke, and T. Esslinger, Phys. Rev. Lett. **107**, 140402 (2011).

[112] P. Domokos and H. Ritsch, Phys. Rev. Lett. **89**, 253003 (2002).

[113] D. Kruse, C. von Cube, C. Zimmermann, and P. W. Courteille, Phys. Rev. Lett. **91**, 183601 (2003).

[114] C. von Cube et al., Phys. Rev. Lett. **93**, 083601 (2004).

[115] S. Slama, S. Bux, G. Krenz, C. Zimmermann, and P. W. Courteille, Phys. Rev. Lett. **98**, 053603 (2007).

[116] F. Mivehvar and D. L. Feder, Phys. Rev. A **89**, 013803 (2014).

[117] F. Mivehvar and D. L. Feder, Phys. Rev. A **92**, 023611 (2015).

[118] S. Inouye et al., Nature **392**, 151 (1998).

[119] J. Stenger et al., Phys. Rev. Lett. **82**, 2422 (1999).

[120] V. A. Yurovsky, A. Ben-Reuven, P. S. Julienne, and C. J. Williams, Phys. Rev. A **60**, R765(R) (1999).

[121] S. L. Cornish, N. R. Claussen, J. L. Roberts, E. A. Cornell, and C. E. Wieman, Phys. Rev. Lett. **85**, 1795 (2000).

[122] T. Köhler, K. Góral, and T. Gasenzer, Phys. Rev. A **70**, 023613 (2004).

[123] L. Dong, L. Zhou, B. Wu, B. Ramachandhran, and H. Pu, Phys. Rev. A **89**, 011602(R) (2014).

[124] Y. Deng, J. Cheng, H. Jing, , and S. Yi, Phys. Rev. Lett. **112**, 143007 (2014).

[125] L. Dong, C. Zhu, and H. Pu, Atoms **3**, 182 (2015).

[126] B. Padhi and S. Ghosh, Phys. Rev. A **90**, 023627 (2014).

[127] M. Kardar, *Statistical Physics of Particles*, Cambridge University Press, New York, 2007.

[128] W. Greiner, *Quantum Mechanics: Special Chapters*, Springer, 1998.

[129] J. D. Jackson, *Classical Electrodynamics*, Wiley, 1999.

[130] D. J. Griffiths, *Introduction to Electrodynamics*, Prentice Hall, 1999.

[131] B. Berche and E. Medina, Eur. J. Phys. **34**, 161 (2013).

[132] E. Merzbacher, *Quantum Mechanics*, John Wiley & Sons, Inc., 1998.

[133] A. Salam and J. C. Ward, Il Nuovo Cimento **19**, 165 (1961).

[134] W. Greiner and J. Reinhardt, *Field Quantization*, Springer, 1996.

[135] W. Greiner, S. Schramm, and E. Stein, *Quantum Chromodynamics*, Springer, 2007.

[136] M. E. Peskin and D. V. Schroeder, *An Introduction to Quantum Field Theory*, Perseus Books Publishing, L.L.C., 1995.

[137] C. N. Yang and R. L. Mills, Phys. Rev. **96**, 191 (1954).

[138] T. Fujita, M. B. A. Jalil, S. G. Tan, and S. Murakami, J. Appl. Phys. **110**, 121301 (2011).

[139] J. J. Sakurai, *Modern Quantum Mechanics*, Addison Wesley, 1994.

[140] R. Winkler, *Spin-Orbit Coupling Effects in Two-Dimensional Electron and Hole Systems*, Springer, 2003.

[141] J. J. Sakurai, *Advanced Quantum Mechanics*, Addison-Wesley, 1967.

[142] F. Schwable, *Advanced Quantum Mechanics*, Springer, 2008.

[143] G. Grynberg, A. Aspect, and C. Fabre, *Introduction to Quantum Optics: From the Semi-classical Approach to Quantized Light*, Cambridge University Press, New York, 2010.

[144] G. Compagno, R. Passante, and F. Persico, *Atom-Field Interactions and Dressed Atoms*, Cambridge University Press, 1995.

[145] K. Gottfried and T.-M. Yan, *Quantum Mechanics: Fundamentals*, Springer, 2003.

[146] C. Gerry and P. Knight, *Introductory Quantum Optics*, Cambridge University Press, 2005.

[147] W. Greiner and B. Müller, *Quantum Mechanics: Symmetries*, Springer, 1994.

[148] C. Cohen-Tannoudji, J. Dupont-Roc, and G. Grynberg, *Atom-Photon Interactions: Basic Processes and Applications*, Wiley-VCH Verlag GmbH & Co. KGaA, 2004.

[149] D. A. Steck, *Quantum and Atom Optics*, available online at http://steck.us/teaching, 2015.

[150] Y. A. Bychkov and E. I. Rashba, J. Phys. C **17**, 6039 (1984).

[151] A. P. Schnyder, S. Ryu, A. Furusaki, and A. W. W. Ludwig, Phys. Rev. B **78**, 195125 (2008).

[152] X.-G. Wen, Phys. Rev. B **85**, 085103 (2012).

[153] R.-J. Slager, A. Mesaros, V. Juričić, and J. Zaanen, Nature Phys. **9**, 98 (2013).

[154] N. Hatano, R. Shirasaki, and H. Nakamura, Phys. Rev. A **75**, 032107 (2007).

[155] G. Moller and N. R. Cooper, Phys. Rev. Lett. **108**, 045306 (2012).

[156] S. K. Baur and N. R. Cooper, Phys. Rev. Lett. **109**, 265301 (2012).

[157] N. R. Cooper and J. Dalibard, Phys. Rev. Lett. **110**, 185301 (2013).

[158] Y. Colombe et al., Nature **450**, 272 (2007).

[159] S. Slama, G. Krenz, S. Bux, C. Zimmermann, and P. W. Courteille, Phys. Rev. A **75**, 063620 (2007).

[160] S. Brattke, B. T. H. Varcoe, and H. Walther, Phys. Rev. Lett. **86**, 3534 (2001).

[161] J. McKeever et al., Science **33**, 1992 (2004).

[162] M. Keller, B. Lange, K. Hayasaka, W. Lange, and H. Walther, Nature **431**, 1075 (2004).

[163] M. Cooper, L. J. Wright, C. Söller, and B. J. Smith, Opt. Express **21**, 5309 (2013).

[164] C. C. Gerry and J. H. Eberly, Phys. Rev. A **42**, 6805 (1990).

[165] B. Shore and P. Knight, J. Mod. Opt. **40**, 1195 (1993).

[166] L. C. Biedenharn and H. V. Dam, editors, *Quantum Theory of Angular Momentum*, Academic Press, 1965.

[167] D. G. Angelakis, M. F. Santos, , and S. Bose, Phys. Rev. A **76**, 031805 (2007).

[168] J. Koch and K. L. Hur, Phys. Rev. A **80**, 023811 (2009).

[169] N. Brahms, T. P. Purdy, D. W. C. Brooks, T. Botter, and D. M. Stamper-Kurn, Nat. Phys. **7**, 604 (2011).

[170] M. P. A. Fisher and E. Fradkin, Nuclear Physics B **251**, 457 (1985).

[171] S. E. Sebastian et al., Phys. Rev. Lett. **108**, 196403 (2012).

[172] I. B. Spielman, Phys. Rev. A **79**, 063613 (2009).

[173] A. S. Parkins, P. Marte, P. Zoller, and H. J. Kimble, Phys. Rev. Lett. **71**, 3095 (1993).

[174] A. S. Parkins, P. Marte, P. Zoller, O. Carnal, and H. J. Kimble, Phys. Rev. A **51**, 1578 (1995).

[175] A. Gogyan, S. Guérin, C. Leroy, and Y. Malakyan, Phys. Rev. A **86**, 063801 (2012).

[176] P. Meystre and M. Sargent, *Elements of Quantum Optics, 3rd. ed.*, Springer, Berlin, Berlin, 1999.

[177] T. Kaplan, Z. Phys. B **49**, 313 (1983).

[178] C. Maschler, I. B. Mekhov, and H. Ritsch, Eur. Phys. J. D **46**, 545 (2008).

[179] M. Müller, P. Strack, and S. Sachdev, Phys. Rev. A **86**, 023604 (2012).

[180] R. Liao, O. Fialko, J. Brand, and U. Zülicke, Phys. Rev. A **92**, 043633 (2015).

[181] J. Dalibard and C. Cohen-Tannoudji, J. Opt. Soc. Am. B **6**, 2023 (1989).

[182] P. J. Ungar, D. S. Weiss, E. Riis, and S. Chu, J. Opt. Soc. Am. B **6**, 2058 (1989).

[183] T. P. Meyrath, F. Schreck, J. L. Hanssen, C.-S. Chuu, and M. G. Raizen, Phys. Rev. A **71**, 041604 (2005).

[184] A. L. Gaunt, T. F. Schmidutz, I. Gotlibovych, R. P. Smith, and Z. Hadzibabic, Phys. Rev. Lett. **110**, 200406 (2013).

[185] I. Gotlibovych et al., Phys. Rev. A **89**, 061604 (2014).

[186] T. Elsässer, B. Nagorny, and A. Hemmerich, Phys. Rev. A **69**, 033403 (2004).

[187] T. D. Stanescu, B. Anderson, and V. Galitski, Phys. Rev. A **78**, 023616 (2008).

[188] K. Jiménez-García et al., Phys. Rev. Lett. **108**, 225303 (2012).

[189] H. E. Stanley, *Introduction to Phase Transitions and Critical Phenomena*, Oxford University Press, 1971.

[190] M. Iskin, Phys. Rev. A **83**, 051606(R) (2011).

[191] K. Sheshadri, H. R. Krishnamurthy, R. Pandit, and T. V. Ramakrishnan, Europhys. Lett. **22**, 257 (1993).

[192] J. M. Kurdestany, R. V. Pai, , and R. Pandit, Ann. Phys. (Berlin) **524**, 234 (2012).

[193] C. Trefzger, C. Menotti, and M. Lewenstein, Phys. Rev. A **78**, 043604 (2008).

[194] S. Mandal, K. Saha, and K. Sengupta, Phys. Rev. B **86**, 155101 (2012).

[195] A. T. Bolukbasi and M. Iskin, Phys. Rev. A **89**, 043603 (2014).

[196] F. Mivehvar and D. L. Feder, "Quantum phase transitions in the spin-orbit-coupled extended Bose-Hubbard model", in preparation.

[197] E. Kapit and E. Mueller, Phys. Rev. A **83**, 033625 (2011).

[198] D. Banerjee et al., Phys. Rev. Lett. **109**, 175302 (2012).

[199] D. Banerjee et al., Phys. Rev. Lett. **110**, 125303 (2013).

[200] M. J. Edmonds, M. Valiente, G. Juzeliūnas, L. Santos, and P. Öhberg, Phys. Rev. L **110**, 085301 (2013).

[201] L. Tagliacozzo, A. Celi, A. Zamora, and M. Lewenstein, Annals of Physics **330**, 160 (2013).

[202] A. Messiah, *Quantum Mechanics: Volume II*, North Holland Publishing Company, 1963.